

NON-PERTURBATIVE STUDIES IN QUANTUM CHROMODYNAMICS

**THESIS SUBMITTED TO
JADAVPUR UNIVERSITY
FOR THE DEGREE OF
DOCTOR OF PHILOSOPHY (SCIENCE)**

By

DIPANKAR CHAKRAVORTY
SAHA INSTITUTE OF NUCLEAR PHYSICS
KOLKATA

2003

ACKNOWLEDGEMENTS

It gives me great pleasure to acknowledge my sincere gratitude to my supervisor Prof. A. Harindranath for providing me all the inspiration, encouragement and guidance to carry out my research work and for his prompt and sincere help whenever I needed it most. I thank him for his constant endeavor to show me what is happening and what can happen in the present and future “light cone”.

I would also like to thank my collaborators Prof. Asit K. De and Prof. James P. Vary for their active participation and illuminating discussions that I had with them. I am thankful to Rajen Kundu and Asmita Mukherjee for their ungrudging cooperation at different levels of my research program.

It is a mammoth task to individually mention the names of my numerous friends whose friendship I cherish. I would like to thank them all, both in and outside of Saha Institute, for their cooperation and help whenever I approached them, whether it be academic or nonacademic. Last, but not the least, I would like to thank the members of my extended family, especially my parents who stood by me all along my voyage to this point.

Bidhan Nagar,
November, 2003

Dipankar Chakrabarti
Theory Group, SINP

TABLE OF CONTENTS

	Page
List of Figures	vii
List of Tables	ix
 Chapters:	
1. Introduction	1
1.1 Motivation	1
1.2 Organization of the thesis	6
Bibliography	9
 2. Some Basic Features of Light-Front Field Theory	 10
2.0.1 LF dispersion relation	11
2.0.2 The light-front vacuum	12
2.0.3 Poincare generators in light-front	13
2.0.4 Basic strategy for bound state problem	15
2.0.5 Renormalization aspects	16
Bibliography	18
 3. Bloch Effective Hamiltonian and Bound State Problem in $(2 + 1)$ -Dimensional Light-Front QCD	 19
3.1 Introduction	19
3.2 Canonical Hamiltonian	24
3.3 Bloch effective Hamiltonian in the meson sector and the bound state equation	26
3.4 Divergence Structure	30
3.4.1 Ultraviolet Divergences	30
3.4.2 Infrared Divergences	31
3.5 Numerical study of the bound state equation	33

3.6	Reduced Model	36
3.6.1	Numerical study of the reduced model	37
3.7	Summary	40
	Bibliography	41
4.	Similarity Renormalization Group Approach to Meson Sector in $(2 + 1)$ Dimensions	43
4.1	A Brief Review of Renormalization Group Approach	43
4.2	Effective bound state equation in the $q\bar{q}$ sector in SRG scheme	47
4.3	Similarity factors	49
4.3.1	Parameterization I	49
4.3.2	Parameterization II	50
4.3.3	Parameterization III	50
4.4	Analytical calculations with the step function similarity factor	51
4.4.1	Self energy contributions	51
4.4.2	Gluon exchange contributions	53
4.5	Numerical studies	57
4.6	Summary and Discussion	65
	Bibliography	69
5.	Fermion Formulation on a Light-Front Transverse Lattice	71
5.1	Introduction	71
5.2	Hamiltonian with forward and backward derivatives	73
5.2.1	Construction	73
5.2.2	Absence of doubling	76
5.2.3	Numerical Investigation	78
5.3	Hamiltonian with symmetric derivative	82
5.3.1	Construction	82
5.3.2	Fermion doubling	83
5.3.3	Numerical Investigation	84
5.4	Staggered fermion on the light-front transverse lattice	87
5.5	Wilson fermion on the light-front transverse lattice	92
5.5.1	Numerical Investigation	95
5.6	Doubling and symmetries on the light front transverse lattice	96
5.7	Summary	98
	Bibliography	100
6.	Meson Bound States in Transverse Lattice QCD	101
6.1	Introduction	101
6.2	Gauge field part of the Lagrangian density	102

6.3	Effective Hamiltonian	106
6.3.1	Hamiltonian with forward and backward derivatives	106
6.3.2	Hamiltonian with the Wilson term	107
6.4	Meson bound state in one link approximation	109
6.4.1	Relevant interactions	109
6.4.2	Comparison with one gluon exchange in the continuum	109
6.4.3	Longitudinal dynamics and effects of transverse hopping	110
6.4.4	Singularities, divergence and counterterms	111
6.5	Numerical Results	112
6.5.1	$q\bar{q}$ at the same transverse location	114
6.5.2	Results of the one link approximation	115
6.6	Summary and Discussion	117
	Bibliography	120
7.	Summary, Conclusions and Future Outlook	121
Appendices:		
A.	Notations and Conventions	124
B.	Bloch Perturbation Theory for Effective Hamiltonian	127
C.	Details of Numerical Procedure to Diagonalize the Effective Hamiltonian	131
D.	Nonrelativistic Bound State Equation	133
E.	Similarity Renormalization Theory for the Effective Hamiltonian	135
E.1	Głazek-Wilson Formalism	137
E.2	Wegner Formalism	139
F.	Violations of Hypercubic Symmetry on Transverse Lattice	141
G.	Fermions With Forward-Backward Derivatives in Conventional Lattice Theory	142
H.	Mixed Covariant Derivative	144

I.	Transverse Gauge Invariance	145
J.	Hamiltonian Matrix Elements in One Link Approximation	148
J.1	Structure of terms in DLCQ	148
J.2	States in DLCQ	150
J.3	Forward-backward derivatives: Matrix Elements in DLCQ	151
J.3.1	Transitions from two particle state	151
J.3.2	Transitions from three particle ($q \bar{q}$ link) state $ 3a\rangle$	153
J.3.3	Transitions from three particle ($q \bar{q}$ link) state $ 3b\rangle$	155
J.4	Symmetric derivatives and Wilson term: Matrix elements in DLCQ	156
J.4.1	Transitions from the two particle state	156
J.4.2	Transitions from three particle state $ 3a\rangle$ to two particle state	158
J.4.3	Transitions from three particle state $ 3b\rangle$ to two particle state	159
J.5	Self energy counterterms	160

LIST OF FIGURES

Figure	Page
3.1 x^+ -ordered Hamiltonian diagrams for self energy and vertex corrections.	21
3.2 Cancellation of infrared divergences in Bloch effective Hamiltonian	34
3.3 The wavefunctions corresponding to the lowest four eigenvalues of the reduced model as a function of x and k	39
4.1 Structure of the effective Hamiltonian matrix as the cutoff is lowered.	45
4.2 The ground state wavefunction for different choices of the similarity factor. . .	59
4.3 The wavefunctions corresponding to the lowest four eigenvalues as a function of x and k with parametrization II.	61
4.4 Same as in FIG. 4.3 but with $8m^2$ subtracted from ΣM_{ij}^2	62
4.5 The wavefunctions corresponding to the lowest four eigenvalues as a function of x and k with parametrization II for large fermion mass.	63
5.1 Convergence of ground state eigenvalue (of forward-backward Hamiltonian) versus n ($m = 1.0$).	80
5.2 Eigenfunctions of first three states of the spin nonflip Hamiltonian (H_0) with forward and backward lattice derivatives	81
5.3 Spin splitting of the ground state caused by the spin dependent interaction as a function of n	82
5.4 First four eigenvalues of Hamiltonian with symmetric derivative as a function of n	86
5.5 Eigenfunctions of first four (degenerate) states for the case of fermion doubling with symmetric lattice derivative.	87

5.6	Eigenfunction corresponding to the fifth state.	88
5.7	Staggered lattice.	89
6.1	Effect of counterterm on the ground state eigenvalue. (a) With and without the counterterm in the $q\bar{q}$ sector for $m_f = 0.3$. (b) With and without the counterterm in the $q\bar{q}$ link sector for $m_f = 0.3$ and $\mu_b = 0.2$	113
6.2	Quark distribution function $ \psi(x) ^2$ of the ground state in the $q\bar{q}$ approximation for three choices of quark masses with coupling constant $g = 1.0$	115
6.3	Effect of self energy counterterms on the ground state eigenvalue in the case of (a) symmetric derivative with $\tilde{C}_2 = 0.4$, $\tilde{C}_3 = 0.1$ and (b) forward-backward derivative with $C_2 = 0.4$, $C_3 = 0.01$. $m_f = 0.3$, $\mu_b = 0.2$ for both cases.	116
6.4	(a) Quark distribution function $ \psi(x) ^2$ of the ground state in the one link approximation, (b) $q\bar{q}$ contribution to the ground state, (c) $q\bar{q}$ link contribution to the ground state. (d) Quark distribution function $ \psi(x) ^2$ of the fifth eigenstate in the one link approximation, (e) $q\bar{q}$ contribution to the fifth eigenstate, (f) $q\bar{q}$ link contribution to the fifth eigenstate. The parameters are $m_f = 0.3$, $\mu_b = 0.2$, $C_2 = 0.4$, $C_3 = 0.01$ and $K = 30$	118
6.5	Without the fermion - link instantaneous interaction: (a) Quark distribution function $ \psi(x) ^2$ of the ground state in the one link approximation, (b) $q\bar{q}$ contribution to the ground state, (c) $q\bar{q}$ link contribution to the ground state. (d) Quark distribution function $ \psi(x) ^2$ of the fifth eigenstate in the one link approximation, (e) $q\bar{q}$ contribution to the fifth eigenstate multiplied by 10^4 , (f) $q\bar{q}$ link contribution to the fifth eigenstate. Parameters are the same as in Fig. 6.4.	119

LIST OF TABLES

Table	Page
3.1 Variation with δ of the full Bloch effective Hamiltonian.	36
3.2 Convergence of eigenvalue with n_1 and n_2 (reduced model).	37
3.3 Comparison of reduced model results with other work.	38
3.4 First few eigenvalues of reduced model with large coupling.	38
4.1 Variation of first five eigenvalues of the full Hamiltonian with δ	58
4.2 Convergence of eigenvalues with n_1 and n_2 for different similarity factors.	60
4.3 Variation with σ of the full SRG Hamiltonian for $g = 0.2$ and $k = \frac{1}{\kappa} \tan(q\pi/2)$	64
4.4 Variation with σ of the full SRG Hamiltonian for $g = 0.6$ and $k = \frac{q\Delta m}{(1-q^2)\Lambda+m}$	65
4.5 Variation with σ of the full Hamiltonian (excluding the imaginary term) after subtracting $8m^2$ from ΣM_{ij}^2 in the definition of $u_{\sigma ij}$ and $n_g = 2$	66
4.6 Variation with σ of the full Hamiltonian(excluding the imaginary term) after subtracting the $8m^2$ term from ΣM_{ij}^2 in the definition of $u_{\sigma ij}$ and $n_g = 1$	66
4.7 Variation with u_0 of the full Hamiltonian after subtracting the $8m^2$ term from ΣM_{ij}^2 in the definition of $u_{\sigma ij}$	67
6.1 Ground state eigenvalue (in units of G^2) for $q\bar{q}$ sitting at the same transverse location.	114
6.2 Lowest four eigenvalues (in units of G^2) in one link approximation.	117

CHAPTER 1

Introduction

1.1 Motivation

Four types of force govern the universe, namely, Strong, Electromagnetic, Weak and Gravitation. One of the most challenging and least understood problems in modern particle physics is the dynamics of the fundamental particles responsible for the strong interactions. Quantum Chromodynamics (QCD), the SU(3) color gauge theory provides the theory of strong interactions. But even after more than thirty years of the formulation of QCD, it is not well understood and not yet solved. The fundamental particles of this theory are called *quarks*. They can appear in six flavors *up, down, strange, charm, bottom and top* and in three colors, say, *red, green and blue*. The quanta of the non-Abelian gauge field in QCD, called *gluon*, mediates color interactions between quarks. Gluons are flavor blind but carry color charges and hence interact among themselves. This can be contrasted with the Abelian gauge theory, Quantum Electrodynamics (QED), which describes the theory of electromagnetic interactions. Photons which mediate electromagnetic interactions between charged particles in QED do not have any electric charge and hence cannot interact among themselves. This non-Abelian property of the gauge fields in QCD makes the game completely different from QED. Again as the interactions are "strong" in QCD (the relative strengths of the four types of interaction at hadronic scale are 1, 10^{-2} , 10^{-7} and 10^{-39}), the perturbative treatment which is very successful to solve QED, is not applicable to solve the theory for strong interaction. The most important and challenging part of QCD is to understand and solve the low energy or large distance physics where it shows "confinement" and is completely nonperturbative in nature as discussed below.

In nature, quarks can only be found in colorless bound states, mesons and baryons which are combinedly called hadrons. The color symmetry imposed on QCD says that only colorless

states can be physically realized and hence a free quark which carries color charge cannot be observed. According to this postulate all hadrons are required to be in the singlet of color SU(3). It is just a kinematical constraint to eliminate non-singlet (colored) states. However, it is believed that the quark confinement is a dynamical consequence of QCD and thus it requires more attention and investigations. Owing to the non-Abelian nature of gluons QCD possesses an interesting property called "asymptotic freedom" [1] according to which the interactions between quarks become weak at very high energy (or at short distance). Thus, QCD enjoys asymptotic freedom at short distances while shows confinement at large distances (of the order of hadronic length scale). One can address the scattering experiments at very high energy (such as Deeply Inelastic Scattering (DIS), Deeply Virtual Compton Scattering (DVCS), etc) through perturbative QCD. But, investigation of low energy (or long distance) physics (such as hadronic bound state problem, nucleon-nucleon interactions), where the coupling strength become large, is not possible by perturbative theory and one needs a non-perturbative tool to compute the QCD bound state spectrum. It is also desirable to have informations about the hadronic wavefunctions which are essential to calculate the QCD observables such as form factors, structure functions, distribution functions, decay rates etc. We do not know how to exactly solve QCD. So, various approximations go into QCD calculations. But, no approximation is valid for all length scales of QCD. For example, perturbation theory which is applicable in high energy domain is not at all applicable for low energy calculations and low energy models assume dominance of few particle states. Again, the issues of confinement and hadronic bound states are much more difficult to be addressed with proper confidence due to the lack of adequate nonperturbative methods. To have control over realistic QCD calculations it is desirable to assess different nonperturbative methods in terms of their strengths and weaknesses. In this thesis, we will mainly concentrate on this aspect for different nonperturbative methods.

Till date, the most practiced non-perturbative method is the lattice gauge theory [2]. But lattice gauge theory has its own difficulties and limitations. In this method, without fixing any particular gauge, one calculates different n-point Green functions by path integral formalism in Euclidean space, but can not have any firsthand knowledge about the bound state wavefunctions. To explore the structure of hadrons (baryons or mesons) in terms of their constituent degrees

of freedom, a straightforward way is to solve the Hamiltonian eigenvalue equation

$$H | \Psi \rangle = E | \Psi \rangle \quad (1.1)$$

expanding the eigenstate into multiparticle Fock states. The conventional Fock state expansion becomes intractable in equal-time framework (by equal-time framework we refer to the *instant form* of Hamiltonian dynamics with quantization surface given by $x^0 = 0$ [3]) due to the complicated vacuum of the relativistic quantum field theory. Again in the equal-time framework the square root operator in $E = \sqrt{\vec{P}^2 + M^2}$ brings in severe mathematical difficulties. Even if one can solve these problems once, the eigensolutions are found in the rest frame, finding the solutions in a moving frame is highly nontrivial. This is because boosts are interaction dependent (dynamical) operators and boosting the system is as complicated as solving the theory.

An elegant way to avoid all the difficulties mentioned above is to choose the light-front (also called light-cone) framework [3] where the quantization surface is chosen to be the tangential plane to the light-cone. The light-cone or light-front coordinates are defined as

$$x^\pm = x^0 \pm x^3, \quad x^\perp = \{x^1, x^2\}$$

and the quantization surface is now chosen to be light-front time $x^+ = 0$ instead of $x^0 = 0$ in equal-time. The operator conjugate to x^+ is the light-front Hamiltonian P^- and P^+ which is conjugate to x^- is the light-front longitudinal momentum. (The detail of light-front coordinate system will be discussed in the next chapter.) The eigenvalue E in Eq. (1.1) does not involve any square root operator and takes the form $E = \frac{P^\perp{}^2 + M^2}{P^+}$, the vacuum structure is relatively simple and the boosts are interaction independent (kinematical) operators. Thus, unlike the usual equal-time Hamiltonian formalism, it is possible to have a frame independent (boost invariant) description of the bound state wavefunctions in the light-front Hamiltonian approach. Since the vacuum state of the free Hamiltonian is also an eigenstate of the full QCD Hamiltonian, the Fock space expansion on this vacuum provides a complete relativistic many-body basis for diagonalization of the full QCD Hamiltonian. Again, as the many-body states are also high energy states (see the discussion on light-front in Chapter 2), one can hope to have few body description of the bound states and can reconcile relativistic field theory like QCD in one hand with constituent quark model (CQM) in the other hand. [The CQM was motivated by the hadron

spectroscopy. According to CQM, mesons are made of a quark and an antiquark and baryons are made of three quarks or three antiquarks bounded by some empirical (phenomenological) potential.]

Two light-front non-perturbative methods that one can take up to address the QCD bound state problem are Similarity Renormalization Group (SRG) approach [4, 5] to construct an effective theory with few constituents and the light-front transverse lattice (LFTL) approach [6] which is a clever combination of lattice gauge theory and light-front Hamiltonian formalism. We will devote this thesis to investigate these two non-perturbative methods in the context of meson bound state problem.

In (3+1) dimensions, Euclidean lattice gauge theory predicts linear confinement for quarks while the lowest order calculation in SRG scheme produces logarithmic confinement which again violates rotational symmetry. Automatically, questions come. *Is the confinement produced by SRG an artifact of the scheme? What type of confinement does it produce in (2+1) dimensions? Does that also violate rotational symmetry?* In light-front field theory ultraviolet (UV) divergence issue is complicated due to different power counting rule on the light-front. In (2+1) dimensions this issue becomes simplified due to the absence of ultraviolet divergences except in mass corrections. Since in (2+1) dimensions QCD is superrenormalizable, the coupling does not run and one can keep the coupling arbitrarily small and study the structure of the bound states in a weakly coupled theory. In (2+1) dimensions one component of the gauge field remains dynamical and one can systematically study the effects of dynamical gluons without additional complications of (3+1) dimensions. One can also hope to enlarge the Fock space sector and investigate their effect on restoring Lorentz invariance. It is expected that such investigations are more viable in (2+1) dimensions compared to (3+1) dimensions due to less severe demand on computational resources. A major part of this work is devoted to understand these issues in (2+1) dimensional QCD using SRG scheme. SRG is a modification over Bloch effective theory [7]. A study of meson bound state problem using Bloch effective Hamiltonian can serve as benchmark to assess the strengths and weaknesses of SRG approach.

As we have already mentioned, another nonperturbative approach in light-front framework is the light-front transverse lattice formalism. In this approach, one keeps the light-front time (x^+) and longitudinal direction (x^-) continuous while the transverse plane ($x^\perp = (x^1, x^2)$) is

discretized on a square lattice. In the light-front field theories, UV divergences come only from small transverse separations. Lattice provides the gauge invariant UV cutoff on the transverse space. Thus, in the light-cone gauge $A^+ = 0$, one can still preserve x^- independent residual gauge invariance on the transverse plane. In this approach one avails the advantages of gauge invariant UV cutoff coming from the lattice on the transverse plane and the beautiful features of light-front framework. But, it is well known that formulation of fermions on a lattice is complicated due to the notorious problem of species doubling. In the usual (Euclidean or Minkowski) lattice gauge theory extra species of fermions are generated from the corners of the Brillouin zone. *Is there any fermion doubling on light-front transverse lattice? If yes, do they also come from the corners of the Brillouin zone as usual lattice? What are the possible ways to remove the doublers on the transverse lattice?* In usual lattice gauge theory there are rigorous theorems and anomaly arguments regarding fermion doubling. In standard lattice gauge theory, some chiral symmetry needs to be broken in the kinetic part of the action to avoid the doublers. In the light-front chirality is the same as helicity even for a massive fermion. The constraint equation for fermion in the light-front field theory violates the usual chiral symmetry. Here one should ask the question, *is it still possible to relate light-front chirality and fermion doubling on the transverse lattice? Since the notion of light-front chirality is different from usual chirality, is there any way of formulating fermions on a light-front transverse lattice without generating extra species of fermions?* There are many such questions one has to answer in order to use this method as a practical tool for QCD calculations. Our work shows that one can exploit the constraint equation for the fermionic field to formulate fermions in two different ways on the transverse lattice. In one formulation where we use forward and backward lattice derivatives without spoiling the Hermiticity of the Hamiltonian doublers do not appear. In the other way of formulating fermions people use symmetric lattice derivatives and encounters doublers. We have investigated both ways of formulating fermions on the transverse lattice and tried to understand the origin of doublers, possible ways to remove them and the symmetry relevant for doubling. Only when one understands the properties of fermions on the transverse lattice, realistic QCD calculations become viable.

Since we have two possible ways of formulating fermions on a light-front transverse lattice (a) with forward and backward lattice derivatives and (b) with symmetric lattice derivative, we need a comparative study of these two approaches in order to decide which one is best suited for QCD calculations. We take meson bound state problem in (3+1) dimensions for this purpose. Again we focus on the comparative analysis of the strengths and weaknesses of the different fermion formulations to deal with different QCD interactions rather than fitting data.

One important issue in nonperturbative analysis is the numerical procedure. Since analytic solutions of the nonperturbative bound state equations are not possible, one needs to solve them numerically. In Hamiltonian formalism, we need to diagonalize the Hamiltonian numerically in a suitable basis. There are several numerical procedures to diagonalize a matrix. When one deals with a theory like QCD, several complicated interactions come with different ultraviolet and infrared singularities. It is very important to know the efficiency of the numerical procedures in handling singular interactions. In the meson bound state problem using SRG approach we use Gauss Quadrature method to convert the integral equations into a matrix eigenvalue problem and discuss the efficiency of this method in handling different infrared singular terms. Due to longitudinal dynamics, in the bound state equation for transverse lattice Hamiltonian, linear light-front infrared divergences and logarithmic infrared divergences in self energy diagrams arise and one need to add counterterms to cancel them on the computer. We also discuss the efficiency of counterterms to cancel the divergences on a computer.

1.2 Organization of the thesis

The main objective of our work is to assess different nonperturbative approaches in the light-front formalism. It is very important to know the strengths and weaknesses of different approaches when one wants to do any nonperturbative QCD calculation. We investigate the meson bound state problem in light-front QCD using different nonperturbative methods. Whenever it is possible, we make comparative studies of different approaches. We should again emphasize that our main aim is not to fit data but to assess the different nonperturbative approaches in terms of their strengths and weaknesses to have control over the QCD calculations.

In Chapter 2, we discuss the basic features of light-front field theory which will heavily be used in this thesis. Then, we embark on detailed investigations of the meson bound state

problem in light-front QCD. We can broadly categorize the thesis into two parts, namely, (1) SRG approach and (2) transverse lattice formalism.

In the SRG scheme, starting from a bare cutoff Hamiltonian and by some similarity transformations one arrives at a low energy effective Hamiltonian which is band diagonal in Fock basis. The effective Hamiltonian is then diagonalized nonperturbatively. We have already mentioned that SRG is a modification over Bloch effective theory and a study of Bloch theory can serve as a benchmark to assess the SRG approach. In Chapter 3, we investigate the meson bound state problem with Bloch effective Hamiltonian in (2+1) dimensions. We start with a brief discussion on the basic ideas about the effective field theory (EFT). We observe that Bloch theory is infected with infrared divergences in (2+1) dimensions and as one cranks up the strength of the coupling constant eigenvalues diverge bringing instability in the system. Thus we define a reduced model which is free from the divergences but still has confinement in the lowest non-trivial order of the expansion in coupling constant. This allows us the opportunity to study the manifestation and possible violation of rotational symmetry in the context of light-front field theory.

After having the knowledge of difficulties and shortcomings of Bloch effective theory in the context of (2+1) dimensional meson bound state problem, we investigate the same meson bound state problem using similarity renormalization approach in Chapter 4. After a brief review of renormalization approach of constructing a low energy effective theory, we move on to the detailed analysis of SRG scheme. We immediately see the improvements due to SRG over Bloch effective theory. The bound state integral equation is converted into a matrix diagonalization problem by Gauss Quadrature method. The Gauss Quadrature method is quite efficient in handling divergences. We find that SRG produces linear confinement in transverse direction but only square root potential in the longitudinal direction. Thus, it severely violates the rotational symmetry. Our results show that higher order calculations are essential to investigate whether rotational invariance can be restored or not. By tuning the similarity cutoff and the quark mass we also study the interplay between SRG generated confining interaction and the Coulomb interaction which in (2+1) dimensions gives rotationally invariant logarithmic confinement.

In Chapter 5, we introduce the other promising nonperturbative approach in the light-front framework, namely, light-front transverse lattice (LFTL). We have already emphasized the

problem of fermion doubling in usual lattice gauge theory and the relevant questions on the transverse lattice one should ask. In this chapter, we propose a new method of putting fermions on a light-front transverse lattice which is free from fermion doubling. In this approach we use forward and backward lattice derivative in such a way that the Hermiticity of the action is not spoiled. In that case an irrelevant helicity flip interaction survives in the free field limit. We also discuss the violation of rotational symmetry on the transverse lattice. Then we discuss the transverse lattice Hamiltonian with symmetric lattice derivative where one encounters doublers. Our results show that the origin of doublers on the transverse lattice is not the same as usual lattice gauge theory. Here, the doublers appear due to decoupling of even and odd sub-lattices. The removal of doublers by two different ways, namely staggered fermion formulation and Wilson fermion formulation are discussed. We identify an even-odd helicity flip symmetry on the transverse lattice relevant for fermion doubling.

Once we understand the properties of fermions, in Chapter 6 we investigate the meson bound state problem in (3+1) dimensions with fermions formulated with forward and backward lattice derivatives and fermions formulated with symmetric lattice derivative. In the case of symmetric lattice derivative, we add a Wilson term to remove the doublers. In our investigation we use one link approximation, i.e., quark and antiquark at most can sit one lattice spacing apart on the transverse plane. We compare and contrast the two ways of fermion formulation in the context of meson bound state problem. The major difference between the two approaches is that, with forward and backward lattice derivatives, hopping of quark (or antiquark) in the transverse plane with helicity flip interferes with helicity non flip hopping, while there is no such interference with symmetric lattice derivatives. The consequence of this interference in the spectrum is also studied.

Summary and conclusions are given in Chapter 7. To ease the reading, we provide references at the end of each chapter. Several appendices are provided to clarify the notations and formalisms used and also to elucidate different intermediate steps.

BIBLIOGRAPHY

- [1] G. 't Hooft, *unpublished*, comments made at the *Colloquium on Renormalization of Yang-Mills Fields and Applications to Particle Physics*, Marseilles, 1972; D. J. Gross and F. Wilczek, Phys. Rev. Lett. **30**, 1343 (1973); H. D. Politzer, Phys. Rev. Lett. **30**, 1346 (1973); V. S. Vanyashin and M. V. Terentev, JETP (*Sov. Phys.*) **21**, 375 (1965).
- [2] K. G. Wilson, Phys. Rev. D **10**, 2445 (1974).
- [3] P. A. M. Dirac, Rev. Mod. Phys. **21**, 392 (1949).
- [4] S. D. Głazek and K. G. Wilson, Phys. Rev. D **48**, 5863 (1993); **49**, 4214 (1994); K. G. Wilson, T. S. Walhout, A. Harindranath, W. Zhang, R. J. Perry and S. D. Głazek, Phys. Rev. D **49**, 6720 (1994), hep-th/9401153.
- [5] F. Wegner, Ann. Phys. (Leipzig) **3**, 77 (1994).
- [6] W. A. Bardeen and R. B. Pearson, Phys. Rev. D **14**, 547 (1976); W. A. Bardeen, R. B. Pearson and E. Rabinovici, Phys. Rev. D **21**, 1037 (1980).
- [7] C. Bloch, Nucl. Phys. **6**, 329 (1958); K. G. Wilson, Phys. Rev. D **2**, 1438 (1970).

CHAPTER 2

Some Basic Features of Light-Front Field Theory

In this Chapter, we introduce the basic features of light-front field theory, in the context of light-front QCD (LFQCD). Since in the next few chapters we will heavily use the light-front coordinates and the features of field theory in this formalism, it is instructive to discuss its advantages and the problems that one must understand for a successful practical application of the theory. As, in Chapter 1, we have already emphasized the advantages of using Hamiltonian formalism to investigate the hadronic bound state problem and as we will perform all our investigations in the light-front Hamiltonian approach, here we shall only be concerned with the Hamiltonian formulation of LFQCD.

In 1949, Dirac [1] showed that there are three independent parametrizations of the space and time that can not be mapped on each other by a Lorentz transformations and discussed three forms of Hamiltonian dynamics. In the equal-time Hamiltonian formulation of field theory, quantization conditions in the form of commutator (or anticommutator) of dynamical fields and their conjugate momenta are specified on the space-like hypersurface $x^0 = 0$ and the Hamiltonian generates the time-evolution of the system (Dirac called it *instant form* as the kinematical part of the Lorentz group leaves the instant invariant). In the *front form*, the quantization conditions are specified on a light-like hypersurface $x^+ = x^0 + x^3 = 0$ (called a light-front) and the light-front Hamiltonian generates the evolution for a new time (x^+). This formulation is known as the light-front Hamiltonian field theory. Another form that Dirac mentioned is the *point form* of Hamiltonian dynamics where the quantization hypersurface is given by the hyperboloid $x^\mu x_\mu = \kappa^2$ with $x^0 > 0$ and $\kappa^2 > 0$, and the Lorentz group leaves a point invariant. However, later on two more possibilities of parametrization of the space and time were found [2]. The quantization hypersurfaces for these two parametrizations are given by $x_0^2 - x_1^2 - x_2^2 = \kappa^2 > 0$ with $x_0 > 0$ and $x_0^2 - x_3^2 = \kappa^2 > 0$ with $x_0 > 0$. Among all the parametrizations, the front form

has the largest stability group, the subgroup of the Poincare group that maps the quantization hypersurface onto itself.

There is no well defined guideline to decide which parametrization one should use. High energy experiments (e.g., deep inelastic scattering) probe the hadrons near the light-cone. It motivates people to use light-front parametrization of space and time to explore the QCD observables. One may hope that for highly relativistic systems in which cases the world-line lies very close to the light-cone, physics will be more transparent and it will be relatively easy to extract them if one uses light-front field theory.

In the context of current algebra, Fubini and Furlan [3] introduced another notion of Lorentz frame known as *Infinite-Momentum Frame (IMF)* as a limit of a reference frame moving with almost the speed of light. Weinberg [4] using old-fashioned perturbation theory for scalar meson showed that vacuum structures become simplified in the infinite-momentum limit. Later, Susskind [5] established that although the Lorentz transformation required to arrive at IMF is evidently singular ($\gamma = 1/\sqrt{1 - v^2/c^2} \rightarrow \infty$ as $v \rightarrow c$), the singularity cancels in the calculation of physical objects (like Poincare generators) and results in an effective coordinate change given by

$$x^\pm = x^0 \pm x^3, \quad \mathbf{x}^\perp = \{x^1, x^2\}, \quad (2.1)$$

same as the light-front coordinate we defined in Chapter 1. Thus, one can see the fact that what one obtains after going through singular limiting procedure in IMF is built in quite naturally in the light front field theory. That is why, light-front field theories are also sometimes referred as field theories in the infinite-momentum frame. But, we should reemphasize that the formulation here is as prescribed by Dirac and has no connection with any singular limiting procedure. For a review and exhaustive list of references on light-front field theories see Ref. [6].

2.0.1 LF dispersion relation

The inner product between two four-vectors is defined on the light front as

$$x \cdot y = \frac{1}{2}x^+y^- + \frac{1}{2}x^-y^+ - x^\perp \cdot y^\perp. \quad (2.2)$$

In analogy with the light-front space-time variables, the light-front four momenta are defined as

$$k^\pm = k^0 \pm k^3, \quad \mathbf{k}^\perp = \{k^1, k^2\}, \quad (2.3)$$

where k^- being conjugate to x^+ is the light front energy and k^+ which is conjugate to x^- is the light-front longitudinal momentum. With the above definitions, the dispersion relation, i.e., the relation between light-front energy k^- and the spatial components of momenta (k^+, \mathbf{k}^\perp) , for an on mass-shell particle of mass m , is given by,

$$k^- = \frac{k_\perp^2 + m^2}{k^+}. \quad (2.4)$$

One of the remarkable features of this relativistic dispersion relation is that there is no square root involved in contrast to the relativistic equal-time dispersion relation $E = \sqrt{\vec{k}^2 + m^2}$. This provide great simplification when one tries to solve eigenvalue equation which we have already emphasized in chapter 1. Secondly, the numerator in Eq. (2.4) being always positive implies that the particles with positive light-front energy (k^-) always carry positive longitudinal momentum ($k^+ \geq 0$). As usual, the particles with negative k^- which must have negative k^+ are mapped to antiparticles with positive k^- and k^+ . As a consequence, we always have $k^+ \geq 0$ for real particles. Thirdly, k^- becomes large for the large value of k^\perp as well as very small values of k^+ . This makes light front renormalization aspects very different from the usual one. Lastly, the dependence on the transverse momenta k_\perp is just like a nonrelativistic dispersion relation. We shall see later in this Chapter the crucial implications of these novel features of the light-front dispersion relation in the light-front field theory.

2.0.2 The light-front vacuum

The above dispersion relation has profound consequence in the vacuum structure of light-front field theory. Vacuum state is always an eigenstate of the longitudinal momentum $\hat{P}^+ | 0 \rangle = 0$. The positivity condition of k^+ ($k^+ \geq 0$) implies that the vacuum $| 0 \rangle$ is either a no particle state or, at most can have particles with longitudinal momenta exactly equal to zero. Now, if we consider a cut-off theory where longitudinal momentum is restricted to be $k^+ \geq \varepsilon$, the vacuum state $| 0 \rangle$ becomes completely devoid of any particle and therefore, an eigenstate of the full interacting Hamiltonian with zero eigenvalue. Thus, the light-front vacuum becomes *trivial*. It should be contrasted with equal-time case where the vacuum has highly complicated structure. In equal-time case, vacuum can contain infinite number of particles moving with positive and negative momenta adding up to zero. Another aspect of the cutoff $k^+ \geq \varepsilon$ is that

it automatically puts a restriction on the number of constituent particles a state with finite P^+ can have. A composite state with total longitudinal momentum P^+ now can have at most P^+/ε constituents. This again simplifies the Fock space expansion for the hadronic bound states. Again, as small k^+ means high energy (large k^-), one can hope to have a few body description for the low lying hadron states and reconcile QCD with CQM which is beyond hope in equal-time formalism.

On the other hand, a complicated vacuum structure is supposed to be responsible for spontaneous chiral symmetry breaking or confinement in QCD. It seems that with the trivial vacuum structure in light-front theory after removing the zero modes ($k^+ = 0$), we may lose these important aspects in our theory. It should be emphasized that we have not simply removed the zero modes from our theory. The longitudinal momentum cut-off (ε) should be removed from the theory at the end of any calculation by adding necessary counter terms in the effective Hamiltonian to render the observables independent of ε . Thus, we expect to get back all the effects of zero mode as an effective interaction in the Hamiltonian through renormalization.

2.0.3 Poincare generators in light-front

In equal-time theory, out of the ten Poincare generators (Hamiltonian (P^0), *three* linear momenta (\vec{P}), *three* angular momenta (\vec{J}) and *three* boosts (\vec{K})) *six* are kinematical $\{\vec{P}, \vec{J}\}$, i.e., they do not depend on the dynamics (interactions) and other *four* are dynamical $\{P^0, \vec{K}\}$.

In light-front, Poincare generators can be constructed in the same way as in equal-time case. Starting from Lagrangian density we construct the energy momentum stress tensor $T^{\mu\nu}$ and from the stress tensor we construct the four-momentum P^μ and the generalized angular momentum $M^{\mu\nu}$ defined in the following way.

$$P^\mu = \frac{1}{2} \int dx^- d^2x^\perp T^{+\mu}, \quad (2.5)$$

$$M^{\mu\nu} = \frac{1}{2} \int dx^- d^2x^\perp [x^\nu T^{+\mu} - x^\mu T^{+\nu}]. \quad (2.6)$$

In light-front dynamics P^- is the Hamiltonian and P^+ and P^i with ($i = 1, 2$) are the longitudinal and transverse momenta. $M^{+-} = 2K^3$ and $M^{+i} = E^i$ are the boost operators and $M^{12} = J^3$ and $M^{-i} = F^i$ are generators for rotations. In light-front theory, boost operators (K^3 and E^i) are kinematical. Longitudinal boost is like a scale transformation and the transverse boosts behave

like Gallilean boosts in the nonrelativistic theory. To elucidate it further let us consider the boost along the 3-axis (K^3) as an example. In equal-time, K^3 transforms the time (x^0) and the 3-axis (x^3) but leaves the transverse space invariant.

$$\tilde{x}^0 = \gamma(x^0 - \beta x^3), \quad \tilde{x}^3 = \gamma(x^3 - \beta x^0), \quad \tilde{x}^{1,2} = x^{1,2}, \quad (2.7)$$

where $\beta = \frac{v}{c}$ and $\gamma = \frac{1}{\sqrt{1-\beta^2}}$. From the above equations we see that K^3 changes the quantization surface $x^0 = 0$ and hence, K^3 is a dynamical generator in equal-time theory. Introducing the parameter ϕ such that $\gamma = \cosh \phi$ and $\beta\gamma = \sinh \phi$, we see that, in the light-front

$$\tilde{x}^+ = \tilde{x}^0 + \tilde{x}^3 = e^{-\phi} x^+, \quad \tilde{x}^- = \tilde{x}^0 - \tilde{x}^3 = e^{\phi} x^-, \quad \tilde{x}^{1,2} = x^{1,2}. \quad (2.8)$$

It clearly shows that K^3 , which is known as generator of longitudinal boost in light-front, behaves like a scale transformation. In particular, it keeps the quantization surface $x^+ = 0$ invariant. Therefore, it is a kinematical generator in light-front theory. On the other hand, two rotations about transverse axes (F^1 and F^2) which are kinematical in equal-time case become dynamical in light-front theory. Thus, in the light-front theory, we have *seven* kinematical (3 boosts, 3 translations and rotation about 3-axis), and *three* dynamical (Hamiltonian and two rotations about the transverse axes) generators.

Notice that the boost generators form a closed algebra among themselves which is similar to the generators of non-relativistic dynamics:

$$[E^1, E^2] = 0, \quad [K^3, E^i] = iE^i, \quad (2.9)$$

and

$$[J^3, E^i] = i\epsilon^{ij}E^j, \quad (2.10)$$

where $\epsilon^{12} = -\epsilon^{21} = 1$ and $\epsilon^{11} = \epsilon^{22} = 0$. Also, F^1 , F^2 and J^3 form a closed algebra.

$$[F^1, F^2] = 0, \quad [J^3, F^i] = i\epsilon^{ij}F^j. \quad (2.11)$$

For more details of the Poincare algebra in light-front see Ref. [6].

Since the kinematical subgroup of the Poincare group enlarges and contains seven generators in light-front theory, it is expected that defining a system will be easier in the light-front

theory as we can fix more variables of the system irrespective of its dynamics. Moreover, since different set of generators are kinematical in light-front compared to the equal-time theory, it is worth pursuing this theory, for certain things difficult to study in equal-time may just become simpler here. One such example is the feasibility of representing the QCD-bound states in terms of just a few boost invariant multi-particle wave-functions in the Fock-space expansion, which we discuss next.

2.0.4 Basic strategy for bound state problem

The starting point is the Hamiltonian eigenvalue equation

$$P^- |\Psi\rangle = \frac{P_\perp^2 + \mathcal{M}^2}{P^+} |\Psi\rangle \quad (2.12)$$

where \mathcal{M}^2 is the invariant mass-squared of the state $|\Psi\rangle$. As it is mentioned already, trivial structure of light-front vacuum makes it feasible to study the hadronic bound states in Fock language. Since the Fock-states form a complete basis, any state vector, in principle, can be expanded in terms of that basis introducing corresponding amplitude for each Fock-basis. The bound state of a hadron on light-front can be simply expanded in terms of the Fock states as

$$|\Psi\rangle = \sum_{n, \lambda_i} \int' dx_i d^2 \kappa_{\perp i} |n, x_i, x_i P_\perp + \kappa_{\perp i}, \lambda_i\rangle \Phi_n(x_i, \kappa_{\perp i}, \lambda_i), \quad (2.13)$$

where n represents n constituents contained in the Fock state $|n, x_i, x_i P_\perp + \kappa_{\perp i}, \lambda_i\rangle$, λ_i is the helicity of the i -th constituent, x_i is the fraction of the total longitudinal momentum carried by the i -th constituent, and $\kappa_{\perp i}$ is its relative transverse momentum with respect to the center of mass frame.

$$x_i = \frac{p_i^+}{P^+}, \quad \kappa_{\perp i} = p_{i\perp} - x_i P_\perp, \quad (2.14)$$

with p_i^+ , $p_{i\perp}$ being the longitudinal and transverse momenta of the i -th constituent

$$\sum_i x_i = 1, \quad \text{and} \quad \sum_i \kappa_{\perp i} = 0 \quad (2.15)$$

and \int' denotes the integral over the space. $\Phi_n(x_i, \kappa_{\perp i}, \lambda_i)$ is the amplitude of the Fock state $|n, x_i, x_i P_\perp + \kappa_{\perp i}, \lambda_i\rangle$, i.e., the *multi-parton wave function*, which is boost invariant and satisfies

the normalization condition:

$$\sum_{n, \lambda_i} \int' dx_i d^2 \kappa_{\perp i} |\Phi_n(x_i, \kappa_{\perp i}, \lambda_i)|^2 = 1. \quad (2.16)$$

For example, if we consider the meson bound state problem, then after expanding the eigenstate in the basis of Fock states, the light-front bound state equation can be written as,

$$\left(\mathcal{M}^2 - \sum_{i=1}^n \frac{\kappa_{i\perp}^2 + m_i^2}{x_i} \right) \begin{bmatrix} \Phi_{q\bar{q}} \\ \Phi_{q\bar{q}g} \\ \vdots \end{bmatrix} = \begin{bmatrix} \langle q\bar{q} | H_{int} | q\bar{q} \rangle & \langle q\bar{q} | H_{int} | q\bar{q}g \rangle & \cdots \\ \langle q\bar{q}g | H_{int} | q\bar{q} \rangle & \cdots & \\ \vdots & \ddots & \end{bmatrix} \begin{bmatrix} \Phi_{q\bar{q}} \\ \Phi_{q\bar{q}g} \\ \vdots \end{bmatrix}. \quad (2.17)$$

Here H_{int} is the interaction part of the light-front QCD Hamiltonian.

The expansion has infinite number of terms and it is impossible to solve the bound state equation, Eq. (2.17), which is an infinite dimensional coupled equation. To make any practical calculation viable using Fock-expansion, one needs to truncate the expansion at a suitable maximum particle number with the hope that a first few terms in the expansion may give useful information. We know two important informations from the light-front dispersion relation, one is that longitudinal momentum p^+ is always positive and secondly, states with small p^+ are high energy states (large p^-). Since p^+ is always positive, constituents of a many particles state with a fixed longitudinal momentum P^+ carry only small amounts of p_i^+ and hence the state is of high energy. Since high energy states are weakly coupled one can hope that the dynamics of the bound states is dominated by few particle states and multiparticle states can be considered in a bound state perturbation theory in a consistent manner.

The situation should again be contrasted with equal-time approach. As each Fock-state is obtained by operating various creation operator(s) on the vacuum of the theory, if the vacuum already has a complicated structure (as is the case in equal-time theory), which may contain arbitrary number of particles and thereby, the vacuum itself needs a Fock-expansion. This, in effect, render the Fock-expansion in equal-time theory meaningless for any practical application. This is not the case in light-front theory due to the simplicity of the vacuum.

2.0.5 Renormalization aspects

In light-front field theory in the Hamiltonian framework, the renormalization is a more complicated issue mainly due to the noncovariant structure of the theory and is quite different compared to the usual covariant one. This is due to the fact that the *power counting in light front*

is very different. For a detailed discussion on light-front power counting, see the Ref. [7]. Here we notice the fact that only transverse directions x^\perp carry the mass dimension, while the longitudinal direction x^- has no mass dimension. Thus, one has to treat transverse and longitudinal directions separately in determining the superficial degree of divergence of a divergent integral by power counting, in contrast to the covariant case where all the space-time directions are treated democratically. This is also evident in the single particle dispersion relation $k^- = \frac{(k^\perp)^2 + m^2}{k^+}$, which shows that there are two sources of divergences: $k^+ \rightarrow 0+$ and $k^\perp \rightarrow \infty$. The divergence coming from $k^+ \rightarrow 0+$ is referred as infrared (IR) divergence, whereas $k^\perp \rightarrow \infty$ is known as the ultraviolet divergence (UV) in light-front theory.

For the above reason, dimensional regularization, which is so elegant and commonly used in covariant perturbation theory, is of very little importance in light-front theory. Only in the transverse direction, one may use dimensional regularization. Since we know that the lattice gauge theory provides gauge invariant UV cutoff, another way to regulate the UV divergences is to discretize the transverse plane on a square lattice [8]. IR divergences are also regularized by putting a small longitudinal momentum cut-off, which is equivalent to using principal value prescription for the integration over longitudinal momenta. Also the fact that the light-front theory being gauge fixed and noncovariant, leads to new type of divergences like quadratic divergences (if we are using cut-off instead of transverse dimensional regularization) in mass renormalization or mixed divergences involving both IR and UV ones. To remove these divergences one has to add counter terms to the canonical Hamiltonian, which are often nonlocal and help to restore the invariance of the theory that might be broken in the process of manipulation. For detailed discussion on this subject, see the Refs. [7, 9, 10, 11]. Another method specially designed to address the bound state problem in light-front, is that of *similarity renormalization* introduced by Glazek and Wilson [12] and Wegner [13], where first an effective Hamiltonian is obtained perturbatively, by performing a similarity transformation on the bare UV cutoff Hamiltonian. Similarity renormalization approach will be discussed in detail in Chapter 4 and in Appendix E. Notations and conventions are given in Appendix A.

BIBLIOGRAPHY

- [1] P. A. M. Dirac, Rev. Mod. Phys. **21**, 392 (1949).
- [2] H. Leutwyler and J. Stern, Ann. Phys. **112**, 94 (1978).
- [3] S. Fubini and G. Furlan, Physics, **1**, 229 (1965).
- [4] S. Weinberg, Phys. Rev. **150**, 1313 (1966).
- [5] L. Susskind, Phys. Rev. **165**, 1535 (1968).
- [6] A. Harindranath, An Introduction to Light-Front Dynamics for Pedestrians in *Light-Front Quantization and Non-Perturbative QCD*, edited by J.P. Vary and F. Wolz (IITAP, Ames, Iowa, USA, 1997), hep-ph/9612244.
An exhaustive reference of light-front literature can also be found at <http://theory.saha.ernet.in/~hari/light/light.html>.
- [7] K.G. Wilson, T.S. Walhout, A. Harindranath, W.M. Zhang, R.J. Perry, and St.D. Głazek , Phys. Rev. D **49**, 6720 (1994);
- [8] W. A. Bardeen and R. B. Pearson, Phys. Rev. D **14**, 547 (1976); W. A. Bardeen, R. B. Pearson and E. Rabinovici, Phys. Rev. D **21**, 1037 (1980).
- [9] W.M. Zhang and A. Harindranath, Phys. Rev. D **48**, 4881 (1993).
- [10] A. Harindranath and W.M. Zhang, Phys. Rev. D **48**, 4903 (1993).
- [11] R.J. Perry, Ann. Phys., **232**, 116 (1994).
- [12] S. D. Głazek and K.G. Wilson, Phys. Rev. D **48**, 5863 (1993); D **49**, 4214 (1994).
- [13] F. Wegner, Ann. Phys. (Leipzig) **3**, 77 (1994).

CHAPTER 3

Bloch Effective Hamiltonian and Bound State Problem in (2 + 1)-Dimensional Light-Front QCD

3.1 Introduction

One of the very well known techniques to extract relativistic bound state solutions is the Bethe-Salpeter formalism [1]. Though Bethe-Salpeter equation is formally an exact equation for bound state problem, provides a covariant formalism and successful in quantitative understanding of bound states in different models [2] and positronium bound states in QED [3], the calculations in this approach are very complicated and almost out of control beyond the ladder approximation (for a review in the context of QCD see [4]).

The straightforward way to extract the relativistic and nonperturbative wavefunctions is the Hamiltonian approach where one solves the eigenvalue equation $H|\Psi\rangle = E|\Psi\rangle$. But the straightforward diagonalization of the Hamiltonian has two major problems namely (1) *it involves infinitely many energy scales* and (2) *the rapid growth of the dimension of the Hamiltonian matrix with particle number*. In the spirit to diagonalize the Hamiltonian in a single step, one may implement Discretized Light Cone Quantization (DLCQ) [5]. DLCQ has been quite successful in two dimensional models, but for QCD this approach may be quite ambitious. Typical Hamiltonians of interest couple low energy scales with high energy scales which results in ultraviolet divergences. Furthermore, Hamiltonian couples every particle number sector allowed by symmetries and at strong coupling, brute force particle truncation can fail miserably. An alternative approach will be to use an effective Hamiltonian that operates in a few particle basis.

Effective field theory (EFT) [6] relies on the assumption that physics at a low energy scale is insensitive to the microscopic details of the underlying physics at a high energy scale. EFT provides a powerful framework to study low-energy phenomena where one can replace the

microscopic degrees of freedom and their interactions by effective macroscopic degrees of freedom and their effective interactions. The basic procedure of EFT is to separate out the important field components and redefine the theory with those fields within a certain range of energy and momentum, so that, acting on a limited Hilbert space it produces the same result as the original theory. In other words, to construct a low energy effective theory one needs to “integrate out” the high energy degrees of freedom (degrees of freedom above the scale considered) from the theory. The effective interactions are renormalized accordingly to incorporate the effects of the degrees of freedom above the cutoff. An effective theory describes the main features of the original theory below the scale one considers in a simpler way. Effective field theory has wide applications in different wings of physics such as condense matter physics, nuclear physics, high energy physics, etc.

The strength or validity of an effective theory depends on how accurately the effective interactions mimic the effects of the degrees of freedom thrown out from the theory. There are many approaches to construct the effective Hamiltonian which acts on few particle states. It is also well known that there are some or the other drawbacks in all effective Hamiltonians. As the light-front framework is very much suitable for Hamiltonian formalism and due to triviality of the vacuum one can expand the bound states in Fock basis states, several attempts have been made for nonperturbative diagonalization of the light-front Hamiltonian for relativistic bound states (for a review see, Ref. [5]). One of the first attempt was to implement the Tamm-Dancoff truncation [7] or Bloch-Horowitz effective Hamiltonian [8]. Though Tamm-Dancoff was successful in tackling (1+1) dimensional gauge theories, its deficiencies become apparent when attempts were made in (3+1) dimensions. First and foremost is the lack of confinement in the case of QCD in the first non-trivial order. Second is the appearance of the bound state eigenvalue in the energy denominators. This has two undesirable consequences. Firstly, a light-front singularity of the type $\frac{1}{k^+}$, where k^+ is the light front longitudinal momentum of the exchanged gluon, remains in the bound state equation, which would have canceled if free energies appeared in the energy denominators. Secondly, for example, consider the meson bound state problem and truncate the Fock space with $q\bar{q}$ and $q\bar{q}g$ states. From the fermion self energy contribution (Fig.3.1(a)), in addition to the mass divergence another ultraviolet divergence appears (for an example in the context of (3+1) dimensional Yukawa model see Ref. [9]) which contributes

to the renormalization of the coupling. This contribution is also infrared divergent and can be identified as arising from fermion wave function renormalization (Z_2). It is the Fock space truncation that has produced this unphysical divergence which would otherwise have been canceled by vertex renormalization (Z_1) (Fig.3.1(b) and (c)) in a strict order by order perturbative calculation. Thus, it severely violates the gauge invariance (gauge invariance demands $Z_1 = Z_2$) and one has to abandon the Tamm-Dancoff formalism in more than $(1 + 1)$ dimensions. Another ap-

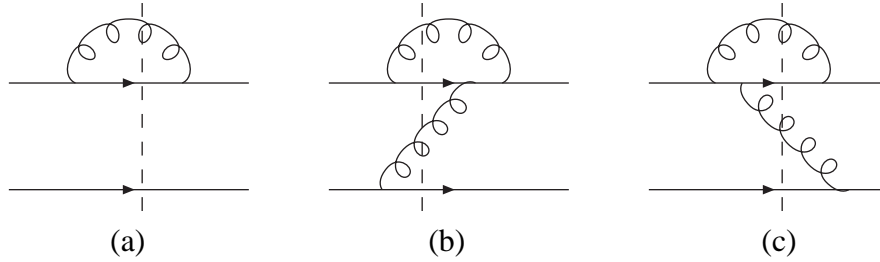


Figure 3.1: x^+ -ordered Hamiltonian diagrams for (a) self energy, (b) and (c) vertex correction. Diagrams (b) and (c) are not allowed by Tamm-Dancoff truncation as they involve two gluons in the intermediate state (shown by dashed lines).

proach mentioned above is the Bloch-Horowitz effective Hamiltonian approach. But one of the major drawbacks of Bloch-Horowitz formula for effective Hamiltonian is that the transformation rule does not preserve the ortho-normalization condition of the wavefunctions which is very much important for observable calculations. Bloch effective Hamiltonian [10](also reinvented by Wilson [11] in the context of renormalization group) is a modification of Bloch-Horowitz Hamiltonian and some of the deficiencies of the Bloch-Horowitz formalism are absent in the Bloch effective Hamiltonian (for a review see [12]).

Bloch Hamiltonian has two desired properties, namely, the effective Hamiltonian is (1) *Hermitian* and (2) *involves only unperturbed energies in the energy denominator*. The basic formalism of calculating Bloch effective Hamiltonian is discussed in Appendix B. Use of Bloch effective Hamiltonian eliminates two major problems of the Tamm-Dancoff approach to gauge

theories mentioned above. However, Bloch effective Hamiltonian involves the undesirable vanishing energy denominators. To the best of our knowledge, Bloch effective Hamiltonian was never assessed in terms of its strengths and weaknesses in the study of bound state problems in field theory. We first explore the Bloch effective Hamiltonian in the context of meson bound states in $(2 + 1)$ dimensional light-front QCD.

A major feature of gauge theories on the light-front is severe light-front infrared divergence of the type $\frac{1}{(k^+)^2}$ where k^+ is the exchanged gluon longitudinal momentum which appears in instantaneous four-fermion, two-fermion two-gluon, and four-gluon interactions. In old-fashioned perturbation theory these divergences are canceled by transverse gluon interactions. In similarity perturbation theory [13] which is considered in the next Chapter, the cancellation is only partial and singular interactions survive. Before embarking on a detailed study of effective Hamiltonian in the similarity renormalization approach which is a modification of the Bloch effective Hamiltonian, it is quite instructive to study the Bloch effective Hamiltonian itself. The result of such a study serves as benchmark against which one can evaluate the merits of similarity renormalization scheme. This also provides us quantitative measures on the strengths and weaknesses of numerical procedures in handling singular interactions (in the context of light-front field theory) on the computer. It is crucial to have such quantitative measures in order to study the effects of similarity cutoff factors on the nature of the spectrum.

Just as the Tamm-Dancoff or the Bloch-Horowitz formalism, Bloch effective Hamiltonian of QCD in the first non-trivial order also does not exhibit confinement in $(3+1)$ dimensions. Since one of our major concerns is the study of spectra for confining interactions, we go to $(2+1)$ dimensions. In this case, in the limit of heavy fermion mass, a logarithmic confining potential emerges. There are several other reasons also to study light-front QCD in $(2+1)$ dimensions. They arise from both theoretical and computational issues which we discuss next.

First of all, issues related to ultraviolet divergence become more complicated in the light-front approach since power counting is different [14] on the light front. We get products of ultraviolet and infrared divergent factors which complicate the renormalization problem. Going to two space one time dimensions greatly simplifies this issue due to the absence of ultraviolet divergences except in mass corrections. An extra complication is that Fock space truncation introduces extra ultraviolet divergences which complicate the situation in non-perturbative bound

state computations [9]. Such special divergences do not occur in (2+1) dimensions. A third complication one faces in (3+1) dimensions is that on enlarging the Fock space in a bound state calculation, one soon faces the running of the coupling constant. At low energy scales, the effective coupling grows resulting in a strongly coupled theory [15] making the weak coupling approach with a perturbatively determined Hamiltonian unsuitable or making it mandatory to invent mechanisms like non-zero gluon mass to stop the drastic growth [14]. In (2+1) dimensional QCD we do not face this problem since the coupling constant is dimensionful in this superrenormalizable field theory and does not run due to ultraviolet divergence. We *can keep* the coupling arbitrarily small and study the structure of the bound states in a weakly coupled theory.

Secondly, in (1+1) dimensions, in the gauge $A^+ = 0$, dynamical gluons are absent and their effect is felt only through instantaneous interactions between fermions. Further, recall that in light front theory, vacuum is trivial. As a result, the Fock space structure of the bound states are remarkably simple. For example, the ground state meson is just a $q\bar{q}$ pair both at weak and strong couplings. In contrast, in (2+1) dimensions, one component of the gauge field remains dynamical and one can systematically study the effects of dynamical gluons. Also note that (2+1) dimensions are the lowest dimensions where glueball states are possible and offer an opportunity to study their structure in the Fock space language without additional complications of (3+1) dimensions.

A third reason deals with aspects of rotational symmetry. (2+1) dimensions offer the first opportunity to investigate violations of Lorentz invariance introduced by various cutoffs (momenta and/or particle number) in the context of bound state calculations. This is to be contrasted with (1+1) dimensions where the sole Lorentz generator, namely boost, is kinematical in light-front field theory. Since in (2+1) dimensions we have a superrenormalizable field theory, violations introduced by transverse momentum cutoffs are minimal. Thus in contrast to (3+1) dimensions, one can study the violations caused by truncation of particle number alone and longitudinal momentum cutoffs. It is also conceivable that one can enlarge the Fock space sector and investigate their effect on restoring Lorentz invariance. It is expected that such investigations are more viable in (2+1) dimensions compared to (3+1) dimensions due to less severe demand on computational resources.

A fourth reason concerns similarity renormalization approach. In (3+1) dimensions it has been shown that similarity renormalization group approach [13] to effective Hamiltonian in QCD leads to logarithmic confining interaction [16]. It is of interest to investigate corresponding effective Hamiltonian in (2+1) dimensions especially since the canonical Hamiltonian already leads to logarithmic confinement in the nonrelativistic limit in this case. It is also known that in (3+1) dimensions the confining part of the effective Hamiltonian violates rotational symmetry. Does the violation of rotational symmetry occur also in (2+1) dimensions? If so, how does it manifest itself?

In [17] we initiated a systematic study of light-front QCD in (2+1) dimensions to investigate the various issues discussed above.

3.2 Canonical Hamiltonian

In this section we present the canonical light front Hamiltonian of (2+1) dimensional QCD. The Lagrangian density is given by

$$\mathcal{L} = \left[-\frac{1}{4}(F_{\lambda\sigma a})^2 + \bar{\Psi}(\gamma^\lambda(i\partial_\lambda + gA_\lambda) - m)\Psi \right] \quad (3.1)$$

with

$$F^{\mu\lambda a} = \partial^\mu A^{\lambda a} - \partial^\lambda A^{\mu a} + gf^{abc}A^{\mu b}A^{\lambda c}. \quad (3.2)$$

We have the equations of motion,

$$\left[i\gamma^\mu \partial_\mu + g\gamma^\mu A_\mu - m \right] \Psi = 0, \quad (3.3)$$

$$\partial_\mu F^{\mu\nu a} + gf^{abc}A_{\mu b}F_c^{\mu\nu} + g\bar{\Psi}\gamma^\nu T^a \Psi = 0. \quad (3.4)$$

Because we are in (2+1) dimensions, we immediately face an ambiguity since there are no γ matrices in (2+1) dimensions. In the literature both two component [18] and four component representation [19] have been in use. For simplicity, we pick the two component representation. Explicitly,

$$\gamma^0 = \sigma_2 = \begin{pmatrix} 0 & -i \\ i & 0 \end{pmatrix}, \quad \gamma^1 = i\sigma_3 = \begin{pmatrix} i & 0 \\ 0 & -i \end{pmatrix}, \quad \gamma^2 = i\sigma_1 = \begin{pmatrix} 0 & i \\ i & 0 \end{pmatrix}. \quad (3.5)$$

$$\gamma^\pm = \gamma^0 \pm \gamma^2, \quad \gamma^+ = \begin{pmatrix} 0 & 0 \\ 2i & 0 \end{pmatrix}, \quad \gamma^- = \begin{pmatrix} 0 & -2i \\ 0 & 0 \end{pmatrix}. \quad (3.6)$$

$$\Lambda^\pm = \frac{1}{4} \gamma^\mp \gamma^\pm, \quad \Lambda^+ = \begin{pmatrix} 1 & 0 \\ 0 & 0 \end{pmatrix}, \quad \Lambda^- = \begin{pmatrix} 0 & 0 \\ 0 & 1 \end{pmatrix}. \quad (3.7)$$

Fermion field operator $\psi^\pm = \Lambda^\pm \psi$. We have

$$\psi^+ = \begin{pmatrix} \eta \\ 0 \end{pmatrix}, \quad \psi^- = \begin{pmatrix} 0 \\ \xi \end{pmatrix} \quad (3.8)$$

where ξ and η are one component fields. We choose the light front gauge $A^{+a} = 0$. From the equation of motion, we get the equation of constraint for fermion

$$i\partial^+ \psi^- = \left[\alpha^1 (i\partial^1 + gA^1) + \gamma^0 m \right] \psi^+. \quad (3.9)$$

Thus the fermion constrained field

$$\xi = \frac{1}{\partial^+} \left[-(i\partial^1 + gA^1) + im \right] \eta. \quad (3.10)$$

The equation of constraint for the gauge fields is

$$-\frac{1}{2} (\partial^+)^2 A^{-a} = -\partial^1 \partial^+ A^{1a} - g f^{abc} A^{1b} \partial^+ A^{1c} - 2g \eta^\dagger T^a \eta. \quad (3.11)$$

Using these equations of constraint, we eliminate ψ^- and A^- in favor of dynamical field ψ^+ and A^1 and arrive at the canonical Hamiltonian given by

$$H = H_0 + H_{int} = \int dx^- dx^1 (\mathcal{H}_0 + \mathcal{H}_{int}). \quad (3.12)$$

The free Hamiltonian density is given by

$$\mathcal{H}_0 = \eta^\dagger \frac{-(\partial^1)^2 + m^2}{i\partial^+} \eta + \frac{1}{2} \partial^1 A^{1a} \partial^1 A^{1a}. \quad (3.13)$$

The interaction Hamiltonian density is given by

$$\mathcal{H}_{int} = \mathcal{H}_1 + \mathcal{H}_2 \quad (3.14)$$

with

$$\begin{aligned} \mathcal{H}_1 &= g \eta^\dagger A^1 \frac{\partial^1}{\partial^+} \eta + g \eta^\dagger \frac{\partial^1}{\partial^+} (A^1 \eta) \\ &\quad - g m \eta^\dagger A^1 \frac{1}{\partial^+} \eta + g m \eta^\dagger \frac{1}{\partial^+} (A^1 \eta) \\ &\quad - 2g \frac{1}{\partial^+} (\partial^1 A^{1a}) \eta^\dagger T^a \eta + g f^{abc} \partial^1 A^{1a} \frac{1}{\partial^+} (A^{1b} \partial^+ A^{1c}) \end{aligned} \quad (3.15)$$

and

$$\begin{aligned}
\mathcal{H}_2 = & -2g^2 \eta^\dagger T^a \eta \left(\frac{1}{\partial^+} \right)^2 \eta^\dagger T^a \eta + g^2 \eta^\dagger A^1 \frac{1}{\partial^+} (A^1 \eta) \\
& + 2g^2 f^{abc} \frac{1}{\partial^+} (\eta^\dagger T^a \eta) \frac{1}{\partial^+} (A^{1b} \partial^+ A^{1c}) \\
& + \frac{1}{2} g^2 f^{abc} f^{ade} \frac{1}{\partial^+} (A^{1b} \partial^+ A^{1c}) \frac{1}{\partial^+} (A^{1d} \partial^+ A^{1e}).
\end{aligned} \tag{3.16}$$

The one component fermion field is given by

$$\eta(x^+ = 0, x^-, x^1) = \int \frac{dk^+ dk^1}{2(2\pi)^2 \sqrt{k^+}} \left[b(k) e^{-ik \cdot x} + d^\dagger(k) e^{ik \cdot x} \right]. \tag{3.17}$$

The Fock operators obey the anti commutation relation

$$\{b(k), b^\dagger(q)\} = 2(2\pi)^2 k^+ \delta^2(k - q), \quad \{d(k), d^\dagger(q)\} = 2(2\pi)^2 k^+ \delta^2(k - q), \tag{3.18}$$

other anti commutators being zero. Note that in two component representation, light front fermions do not carry helicity in (2+1) dimensions.

In free field theory, the equation of motion of the dynamical field A^1 is the same as that of a free massless scalar field [20] and hence we can write

$$A^1(x^+ = 0, x^-, x^1) = \int \frac{dk^+ dk^1}{2(2\pi)^2 k^+} \left[a(k) e^{-ik \cdot x} + a^\dagger(k) e^{-ik \cdot x} \right]. \tag{3.19}$$

The Fock operators obey the commutation relation

$$[a(k), a^\dagger(q)] = 2(2\pi)^2 k^+ \delta^2(k - q), \tag{3.20}$$

other commutators being zero.

We substitute the Fock expansions, Eqs. (3.17) and (3.19) into the Hamiltonian and treat all the terms to be normal ordered. Thus we arrive at the canonical Hamiltonian in the Fock basis.

3.3 Bloch effective Hamiltonian in the meson sector and the bound state equation

In this section we evaluate the Bloch effective Hamiltonian to the lowest non-trivial order for a meson state and derive the effective bound state equation. We define the P space to be $q\bar{q}$

sector of the Fock space and Q space to be the rest of the space (see Appendix B for details). In the lowest non-trivial order, the Bloch effective Hamiltonian is given by

$$\begin{aligned} \langle a | H_{eff} | b \rangle &= \langle a | (H_0 + H_{int}) | b \rangle \\ &+ \frac{1}{2} \sum_k \langle a | H_{int} | k \rangle \langle k | H_{int} | b \rangle \left[\frac{1}{\varepsilon_a - \varepsilon_k} + \frac{1}{\varepsilon_b - \varepsilon_k} \right]. \end{aligned} \quad (3.21)$$

The states $|a\rangle$ and $|b\rangle$ are, explicitly,

$$\begin{aligned} |a\rangle &= b^\dagger(p_1, \alpha) d^\dagger(p_2, \alpha) |0\rangle, \\ |b\rangle &= b^\dagger(p_3, \beta) d^\dagger(p_4, \beta) |0\rangle, \end{aligned} \quad (3.22)$$

where p_1, p_2 denote momenta and α, β denote color which is summed over. Explicitly, $p_1 = (p_1^+, p_1^\perp)$ etc., where p_1^+ is the longitudinal component and p_1^\perp is the transverse component. For simplicity of notation, we will denote the transverse component of momenta without the superscript 1.

The free part of the Hamiltonian leads to the matrix element

$$\langle a | H | b \rangle = \left[\frac{m^2 + p_1^2}{p_1^+} + \frac{m^2 + p_2^2}{p_2^+} \right] 2(2\pi)^2 p_1^+ \delta^2(p_1 - p_3) 2(2\pi)^2 p_2^+ \delta^2(p_2 - p_4) \delta_{\alpha\beta}. \quad (3.23)$$

From the four fermion interaction, we get the contribution

$$-4g^2 (T^a T^a)_{\alpha\alpha} \frac{1}{(p_1^+ - p_3^+)^2} 2(2\pi)^2 \sqrt{p_1^+ p_2^+ p_3^+ p_4^+} \delta^2(p_1 + p_2 - p_3 - p_4) \delta_{\alpha\beta}. \quad (3.24)$$

Next we evaluate the contribution from the second order term. The intermediate state $|k\rangle$ is any state in higher Fock space, e.g., $q\bar{q}g, q\bar{q}gg, q\bar{q}q\bar{q}$, and so on. In the lowest nontrivial order we take $|k\rangle$ a quark, anti-quark, gluon ($q\bar{q}g$) state. This intermediate state gives rise to both self energy and gluon exchange contributions.

The self energy contributions are

$$\begin{aligned} &g^2 C_f \delta_{\alpha\beta} p_1^+ 2(2\pi)^2 \delta^2(p_1 - p_3) p_2^+ 2(2\pi)^2 \delta^2(p_2 - p_4) \\ &\int \frac{dk_1^+ dk_1}{2(2\pi)^2 (p_1^+ - k_1^+)} \left\{ -2 \frac{(p_1 - k_1)}{(p_1^+ - k_1^+)} + \frac{k_1}{k_1^+} + \frac{p_1}{p_1^+} - i \frac{m}{k_1^+} + i \frac{m}{p_1^+} \right\} \frac{1}{\mathcal{E}_1} \\ &\left\{ -2 \frac{(p_1 - k_1)}{(p_1^+ - k_1^+)} + \frac{k_1}{k_1^+} + \frac{p_1}{p_1^+} + i \frac{m}{k_1^+} - i \frac{m}{p_1^+} \right\} \\ &+ g^2 C_f \delta_{\alpha\beta} p_1^+ 2(2\pi)^2 \delta^2(p_1 - p_3) p_2^+ 2(2\pi)^2 \delta^2(p_2 - p_4) \end{aligned}$$

$$\int \frac{dk_2^+ dk_2^-}{2(2\pi)^2(p_2^+ - k_2^+)} \left\{ -2 \frac{(p_2 - k_2)}{(p_2^+ - k_2^+)} + \frac{k_2}{k_2^+} + \frac{p_2}{p_2^+} - i \frac{m}{k_2^+} + i \frac{m}{p_2^+} \right\} \frac{1}{\mathcal{E}_2} \left\{ -2 \frac{(p_2 - k_2)}{(p_2^+ - k_2^+)} + \frac{k_2}{k_2^+} + \frac{p_2}{p_2^+} + i \frac{m}{k_2^+} - i \frac{m}{p_2^+} \right\}, \quad (3.25)$$

with

$$\begin{aligned} \mathcal{E}_1 &= \frac{p_1^2 + m^2}{p_1^+} - \frac{m^2 + k_1^2}{k_1^+} - \frac{(p_1 - k_1)^2}{(p_1^+ - k_1^+)}, \\ \mathcal{E}_2 &= \frac{p_2^2 + m^2}{p_2^+} - \frac{m^2 + k_2^2}{k_2^+} - \frac{(p_2 - k_2)^2}{(p_2^+ - k_2^+)}, \end{aligned} \quad (3.26)$$

and the color factor $C_f = (T^a T^a) = \frac{N^2 - 1}{2N}$ for N number of colors. The gluon exchange contributions are

$$\begin{aligned} &-g^2 C_f 2(2\pi)^2 \delta^2(p_1 + p_2 - p_3 - p_4) \sqrt{p_1^+ p_2^+ p_3^+ p_4^+} \\ &\left\{ -2 \frac{(p_1 - p_3)}{(p_1^+ - p_3^+)} + \frac{p_3}{p_3^+} + \frac{p_1}{p_1^+} - i \frac{m}{p_3^+} + i \frac{m}{p_1^+} \right\} \left\{ -2 \frac{(p_1 - p_3)}{(p_1^+ - p_3^+)} + \frac{p_2}{p_2^+} + \frac{p_4}{p_4^+} + i \frac{m}{p_2^+} - i \frac{m}{p_4^+} \right\} \\ &\frac{1}{2} \frac{\theta(p_1^+ - p_3^+)}{(p_1^+ - p_3^+)} \left\{ \frac{1}{\frac{m^2 + p_4^2}{p_4^+} - \frac{(p_1 - p_3)^2}{(p_1^+ - p_3^+)} - \frac{m^2 + p_2^2}{p_2^+}} + \frac{1}{\frac{m^2 + p_1^2}{p_1^+} - \frac{(p_1 - p_3)^2}{(p_1^+ - p_3^+)} - \frac{m^2 + p_3^2}{p_3^+}} \right\} \\ &-g^2 C_f 2(2\pi)^2 \delta^2(p_1 + p_2 - p_3 - p_4) \sqrt{p_1^+ p_2^+ p_3^+ p_4^+} \\ &\left\{ -2 \frac{(p_3 - p_1)}{(p_3^+ - p_1^+)} + \frac{p_3}{p_3^+} + \frac{p_1}{p_1^+} - i \frac{m}{p_3^+} + i \frac{m}{p_1^+} \right\} \left\{ -2 \frac{(p_3 - p_1)}{(p_3^+ - p_1^+)} + \frac{p_2}{p_2^+} + \frac{p_4}{p_4^+} + i \frac{m}{p_2^+} - i \frac{m}{p_4^+} \right\} \\ &\frac{1}{2} \frac{\theta(p_3^+ - p_1^+)}{(p_3^+ - p_1^+)} \left\{ \frac{1}{\frac{m^2 + p_2^2}{p_2^+} - \frac{(p_3 - p_1)^2}{(p_3^+ - p_1^+)} - \frac{m^2 + p_4^2}{p_4^+}} + \frac{1}{\frac{m^2 + p_3^2}{p_3^+} - \frac{(p_3 - p_1)^2}{(p_3^+ - p_1^+)} - \frac{m^2 + p_1^2}{p_1^+}} \right\}. \end{aligned} \quad (3.27)$$

After the construction of H_{eff} in the two particle space, we proceed as follows. Consider the bound state equation

$$H_{eff} |\Psi\rangle = \frac{M^2 + P^2}{P^+} |\Psi\rangle \quad (3.28)$$

where P^+ , P , and M are the longitudinal momentum, the transverse momentum and the invariant mass of the state respectively. The two particle $(q\bar{q})$ bound state $|\Psi\rangle$ is given by

$$|\Psi\rangle = \sum_{\beta} \int \frac{dp_3^+ dp_3}{\sqrt{2(2\pi)^2 p_3^+}} \int \frac{dp_4^+ dp_4}{\sqrt{2(2\pi)^2 p_4^+}} \phi_2(P; p_3, p_4) b^\dagger(p_3, \beta) d^\dagger(p_4, \beta) |0\rangle$$

$$\sqrt{2(2\pi)^2 P^+} \delta^2(P - p_3 - p_4) \quad (3.29)$$

with the normalization

$$\langle \Psi(Q) | \Psi(P) \rangle = 2(2\pi)^2 P^+ \delta^2(P - Q) \quad (3.30)$$

provided

$$\int \int dp_1^+ dp_1 | \phi_2(P; p_1, P - p_1) |^2 = 1. \quad (3.31)$$

We symbolically represent the above state as

$$|\Psi\rangle = \sum_j \phi_{2j} |j\rangle. \quad (3.32)$$

Taking projection with the state $\langle i | = \langle 0 | d(p_2, \alpha) b(p_1, \alpha)$, we get the effective bound state equation,

$$\frac{M^2 + P^2}{P^+} \phi_{2i} = H_{0i} \phi_{2i} + \sum_j \langle i | H_{Ieff} | j \rangle \phi_{2j}. \quad (3.33)$$

Introduce the internal momentum variables (x, k) and (y, q) via $p_1^+ = xP^+$, $p_1 = xP + k$, $p_2^+ = (1-x)P^+$, $p_2 = (1-x)P - k$, $p_3^+ = yP^+$, $p_3 = yP + q$, $p_4^+ = (1-y)P^+$, $p_4 = (1-y)P - q$ and the amplitude $\phi_2(P; p_1, p_2) = \frac{1}{\sqrt{P^+}} \psi_2(x, k)$.

The fermion momentum fractions x and y range from 0 to 1. To handle end point singularities, we introduce the cutoff $\varepsilon \leq x, y \leq 1$. This does not prevent the gluon longitudinal momentum fraction $(x - y)$ from becoming zero and we introduce the regulator δ such that $|x - y| \geq \delta$. To regulate ultraviolet divergences, we introduce the cutoff Λ on the relative transverse momenta k and q . We remind the reader that in the superrenormalizable field theory under study, only ultraviolet divergence is in the fermion self energy contribution which we remove by a counterterm before discretization.

The bound state equation is

$$\left[M^2 - \frac{m^2 + k^2}{x(1-x)} \right] \psi_2(x, k) = S \psi_2(x, k) - 4 \frac{g^2}{2(2\pi)^2} C_f \int dy dq \psi_2(y, q) \frac{1}{(x-y)^2}$$

$$-\frac{g^2}{2(2\pi)^2} C_f \int dy dq \psi_2(y, q) \frac{1}{2} \frac{\mathcal{V}}{\mathcal{E}}. \quad (3.34)$$

The self energy contribution

$$S = -\frac{g^2}{2(2\pi)^2} C_f \left[\int_0^x dy \int dq xy \frac{\left[\left(\frac{q}{y} + \frac{k}{x} - \frac{2(k-q)}{(x-y)} \right)^2 + \frac{m^2(x-y)^2}{x^2 y^2} \right]}{(ky - qx)^2 + m^2(x-y)^2} \right. \\ \left. + \int_x^1 dy \int dq (1-x)(1-y) \frac{\left[\left(\frac{q}{1-y} + \frac{k}{1-x} + \frac{2(q-k)}{(y-x)} \right)^2 + \frac{m^2(y-x)^2}{(1-x)^2(1-y)^2} \right]}{[k(1-y) - q(1-x)]^2 + m^2(x-y)^2} \right]. \quad (3.35)$$

The boson exchange contribution

$$\frac{\mathcal{V}}{\mathcal{E}} = \frac{\theta(x-y)}{(x-y)} \left[\frac{1}{\frac{m^2+q^2}{y} + \frac{(k-q)^2}{(x-y)} - \frac{m^2+k^2}{x}} + \frac{1}{\frac{m^2+k^2}{1-x} + \frac{(k-q)^2}{x-y} - \frac{m^2+q^2}{1-y}} \right] \\ \times [K(k, x, q, y) + iV_I] \\ + \frac{\theta(y-x)}{(y-x)} \left[\frac{1}{\frac{m^2+k^2}{x} + \frac{(q-k)^2}{(y-x)} - \frac{q^2+m^2}{y}} + \frac{1}{\frac{m^2+q^2}{1-y} + \frac{(q-k)^2}{y-x} - \frac{m^2+k^2}{1-x}} \right] \\ \times [K(q, y, k, x) + iV_I], \quad (3.36)$$

where

$$K(k, x, q, y) = \left(\frac{q}{y} + \frac{k}{x} - \frac{2(k-q)}{(x-y)} \right) \left(\frac{q}{1-y} + \frac{k}{1-x} + \frac{2(k-q)}{(x-y)} \right) - \frac{m^2(x-y)^2}{xy(1-x)(1-y)}, \quad (3.37)$$

$$V_I = -\frac{m}{xy(1-x)(1-y)} [q(2-y-3x) + k(3y+x-2)]. \quad (3.38)$$

3.4 Divergence Structure

Now, let us analyze the divergence structure of the effective bound state equation. We encounter both infrared and ultraviolet divergences.

3.4.1 Ultraviolet Divergences

First consider ultraviolet divergences. In the super renormalizable field theory under consideration, with the terms appearing in the canonical Hamiltonian as normal ordered, ultraviolet

divergence is encountered only in the self energy contributions. To isolate the ultraviolet divergence, we rewrite the self energy integrals as

$$\begin{aligned}
S = & -\frac{g^2}{2(2\pi)^2}C_f \int_0^x dy \int_{-\Lambda}^{+\Lambda} dq \left[\frac{(x+y)^2}{xy(x-y)^2} - \frac{4m^2}{(ky-qx)^2 + m^2(x-y)^2} \right] \\
& -\frac{g^2}{2(2\pi)^2}C_f \int_x^1 dy \int_{-\Lambda}^{+\Lambda} dq \\
& \left[\frac{(2-x-y)^2}{(y-x)^2(1-x)(1-y)} - \frac{4m^2}{[k(1-y)-q(1-x)]^2 + m^2(x-y)^2} \right]. \quad (3.39)
\end{aligned}$$

The first term inside the square brackets in the above equation is ultraviolet divergent, which we cancel by adding an ultraviolet counterterm given by

$$CT = +\frac{g^2}{2(2\pi)^2}C_f \int_{-\Lambda}^{+\Lambda} dq \left[\int_0^x dy \frac{(x+y)^2}{xy(x-y)^2} + \int_x^1 dy \frac{(2-x-y)^2}{(y-x)^2(1-x)(1-y)} \right]. \quad (3.40)$$

After the addition of this counterterm, the bound state equation is ultraviolet finite.

3.4.2 Infrared Divergences

The infrared divergences (IR) that appear in the bound state equation are of two types: (1) light front infrared divergences that arise from the gluon longitudinal momentum fraction $x_g = 0$, (2) true infrared divergences that arise from gluon transverse momentum $k_g = 0$ and gluon longitudinal momentum fraction $x_g = 0$. The IR divergences of type (1) are generated due to elimination of the constrained degrees of freedom.

Cancellation of Light-front Infrared Divergences in the Effective Bound State Equation

First consider light front infrared divergences. The effective bound state equation, Eq. (3.34), explicitly has a linear light front infrared divergent term $\frac{1}{(x-y)^2}$ coming from instantaneous gluon exchange. The most divergent part of the numerator of the transverse gluon exchange term in this equation is $-4\frac{(k-q)^2}{(x-y)^2}$. After combining the terms, the linear infrared divergent term is completely canceled and the resultant effective bound state equation takes the form

$$\begin{aligned}
\left[M^2 - \frac{m^2 + k^2}{x(1-x)} \right] \psi_2(x, k) = & S_1 \psi_2(x, k) - \frac{g^2}{2(2\pi)^2} C_f \int dy dq \psi_2(y, q) \\
& \times \frac{1}{2} \left[\frac{\tilde{V}_1}{E_1} + \frac{\tilde{V}_2}{E_2} + iV_I \left(\frac{1}{E_1} + \frac{1}{E_2} \right) \right]. \quad (3.41)
\end{aligned}$$

The self energy contribution, made ultraviolet finite by the addition of the counterterm is

$$S_1 = +\frac{g^2}{2(2\pi)^2}C_f \int_0^x dy \int_{-\Lambda}^{+\Lambda} dq \frac{4m^2}{(ky - qx)^2 + m^2(x-y)^2} \\ + \frac{g^2}{2(2\pi)^2}C_f \int_x^1 dy \int_{-\Lambda}^{+\Lambda} dq \frac{4m^2}{[k(1-y) - q(1-x)]^2 + m^2(x-y)^2}. \quad (3.42)$$

The energy denominator factors are

$$\frac{1}{E_1} = \frac{xy}{[ky - qx]^2 + m^2(x-y)^2}, \quad \frac{1}{E_2} = \frac{(1-x)(1-y)}{[k(1-y) - q(1-x)]^2 + m^2(x-y)^2}. \quad (3.43)$$

The vertex terms are

$$\tilde{V}_1 = \theta(x-y)\tilde{U}(k,x,q,y) + \theta(y-x)\tilde{U}(q,y,k,x), \quad (3.44)$$

$$\tilde{V}_2 = \theta(x-y)\tilde{U}(k,1-x,q,1-y) + \theta(y-x)\tilde{U}(q,1-y,k,1-x), \quad (3.45)$$

with

$$\tilde{U}(k,x,q,y) = 4\frac{m^2}{xy} - \frac{m^2(x-y)^2}{xy(1-x)(1-y)} \\ + \frac{q^2}{y(1-y)} + \frac{k^2}{x(1-x)} - 2\frac{k^2}{(x-y)}\frac{1}{x(1-x)} + 2\frac{q^2}{(x-y)}\frac{1}{y(1-y)} \\ + \frac{kq}{x(1-y)} + \frac{kq}{y(1-x)} + 2\frac{kq}{(x-y)}\left[\frac{1-2y}{y(1-y)} - \frac{1-2x}{x(1-x)}\right]. \quad (3.46)$$

In addition to the $\frac{1}{x_g^2}$ singularity which is canceled, transverse gluon exchange contributions also contain $\frac{1}{x_g}$ singularity which is removed by the principal value prescription. Cancellation of this singularity is an appealing feature of the Bloch effective Hamiltonian in contrast to the Tamm-Dancoff effective Hamiltonian where the singularity cancellation does not occur because of the presence of invariant mass in the energy denominator [21].

“True” infrared divergences

Next we consider true infrared divergences. Consider the self energy integrals. The energy denominators in these expressions vanish when $k = q$ and $x = y$ which correspond to vanishing gluon momentum. By carrying out the integrals explicitly, in the limit $\Lambda \rightarrow \infty$ we get,

$$S_1 = \frac{mg^2}{2\pi} C_f \left[\frac{1}{x} \ln \frac{x}{\delta} + \frac{1}{1-x} \ln \frac{1-x}{\delta} \right]. \quad (3.47)$$

Thus the singular part of self energy is

$$S_{1 \text{ singular}} = -\frac{mg^2}{2\pi} C_f \frac{1}{x(1-x)} \ln \delta. \quad (3.48)$$

The infrared divergent contribution from self energy gives a positive contribution to the fermion mass. It is important to note that the vanishing of energy denominator is possible also in (3+1) dimensions, but in that case we do not encounter any divergence. It is the peculiarity of (2+1) dimensions that the vanishing energy denominators cause a severe infrared divergence problem.

The same vanishing energy denominators occur also in the one gluon exchange contributions. Let us now consider various terms in the numerator separately. The terms proportional to $4m^2$ arose from the denominator of the transverse gluon exchange. A straightforward calculation shows that this term leads to both finite and infrared divergent contributions. The infrared divergent contribution is given by

$$\frac{mg^2}{2\pi} C_f \frac{1}{x(1-x)} \ln \delta \quad (3.49)$$

which exactly cancels the infrared divergent contribution from self energy. The finite part, in the nonrelativistic limit, can be shown to give rise to the logarithmically confining potential. Next we have to consider the remaining terms in the numerator. Rest of the terms proportional to m^2 are multiplied by $(x-y)^2$ so that they do not lead to an infrared divergence problem. The numerator of the imaginary part vanishes at $k = q$, and $x = y$ and hence is also infrared finite. It is easy to verify that the rest of the (transverse momentum dependent) terms in the numerator does not vanish when the denominator vanishes and hence the resulting bound state equation is inflicted with infrared divergences arising from the vanishing energy denominator. This problem was first noted in the context of QED in (2+1) dimensions by Tam, Hamer, and Yung [22] but was not investigated by these authors. We remind the reader that this is a peculiarity of (2+1) dimensions which provides us a unique opportunity to explore the consequences of the vanishing energy denominator problem.

3.5 Numerical study of the bound state equation

Once we derive the effective Hamiltonian, we need to diagonalize it nonperturbatively. For that, we convert the integral equation into a matrix equation with the use of Gaussian Quadrature. (For details of the numerical procedure see Appendix C.) The color factor C_f is set to 1 for

all the numerical calculations presented. As mentioned before, an important feature of gauge theories on the light-front is the presence of linear infrared divergences. They appear in the canonical Hamiltonian in instantaneous four fermion interaction term. When the $q\bar{q}g$ states are

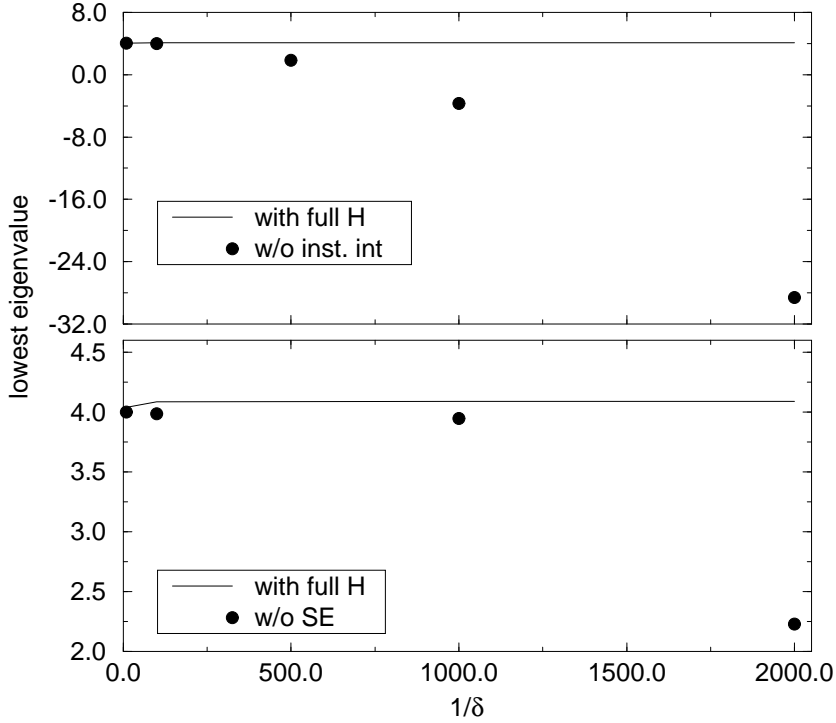


Figure 3.2: Cancellation of infrared divergence. Full line denotes the full Hamiltonian. (a) shows the cancellation of light-front infrared divergence by switching on and off the instantaneous interaction. Filled circles - without instantaneous interaction. (b) shows the cancellation of logarithmic infrared divergence by switching on and off the self energy term. Filled circles - without self energy. The parameters are $g = 0.2$, $\varepsilon = 0.00001$, $m = 1$, $\kappa = 20$, $n_1 = 40$, $n_2 = 50$.

integrated out *completely* in perturbation theory, they also appear in the effective four fermion interaction and cancel against each other. Non-cancellation of this divergence is a major feature of similarity renormalization approach. We first address the issue of how linear divergences manifest in the non-uniform grid of the Gaussian Quadrature and how well it can handle linear light front infrared divergence. We have studied numerically discretized versions of Eq. (3.34) where the divergences are present separately in the discretized version together with the

counterterm given in Eq. (3.40). For $g = 0.2$, we have calculated the eigenvalues with and without the instantaneous interaction. The result presented in Fig. 3.2(a) for the lowest eigenvalue shows that the Gaussian Quadrature can handle the cancellation very efficiently.

After the cancellation of linear light-front infrared divergence, a logarithmic infrared divergence which arises from the vanishing energy denominator survives in the bound state equation. Here we have to distinguish two types of terms. First type, where the coefficient of the logarithmic infrared divergence is independent of the fermion transverse momentum and the second type where the coefficient is dependent. Self energy and Coulomb interaction are of the first type. In the weak coupling limit, since the wavefunction is dominated by very low transverse momentum, we anticipate that contributions of the second type will be dynamically suppressed even though both are multiplied by the same coupling constant. This is especially true of any discrete grid which automatically imposes a lower limit on the smallest longitudinal momentum fraction allowed. Thus at weak coupling, even if there are uncanceled infrared divergences (divergences of the second type), they may not be significant numerically whereas divergences of the first type are significant. By switching the self energy contribution off and on, we have studied this interplay. The lowest eigenvalue with and without self energy contribution is plotted in Fig. 3.2(b). This shows the cancellation of the dominant logarithmic infrared divergence. Since there are still uncanceled infrared divergences in the bound state equation (with coefficient proportional to fermion transverse momenta) these figures further illustrate the fact that such divergences are *not* numerically significant at weak coupling.

As the strength of the interaction grows, wavefunction develops medium to large transverse momentum components and the infrared catastrophe triggered by the vanishing energy denominator becomes manifest numerically. This is illustrated in Table 3.1 where we present the variation with δ of the first five eigenvalues for two different choices of the coupling g . The table clearly shows that on a discrete grid, the uncanceled infrared divergences due to the vanishing energy denominator problem are not numerically significant at weak coupling but their effect is readily felt at a stronger coupling.

g	δ	eigenvalues (M^2)				
0.2	0.01	4.0870	4.0972	4.0972	4.0973	4.0973
	0.005	4.0901	4.1066	4.1099	4.1100	4.1112
	0.001	4.0913	4.1113	4.1122	4.1181	4.1209
	0.0001	4.0913	4.1113	4.1122	4.1181	4.1209
	0.00001	4.0913	4.1113	4.1122	4.1181	4.1209
0.6	0.01	4.5735	4.7337	4.7667	4.7832	4.8277
	0.005	1.9094	1.9415	3.1393	3.1399	4.5697
	0.001	-187230.4	-187225.4	-186664.9	-186664.8	-31506.9
	0.0001	-187230.4	-187225.4	-186664.9	-186664.8	-31506.9

Table 3.1: Variation with δ of the full Hamiltonian. The parameters are $n_1=40$, $n_2=50$, $\varepsilon=0.00001$, $\kappa=20.0$ in $k = \frac{1}{\kappa} \tan(\frac{u\pi}{2})$

3.6 Reduced Model

In this section we consider a model Hamiltonian free from infrared divergences constructed by dropping the transverse momentum dependent terms from the numerator of the effective Hamiltonian. For convenience, we further drop the terms proportional to $(x-y)^2$ and the imaginary part. This defines our reduced model which is also ultraviolet finite. The equation governing the model is given by

$$\left[M^2 - \frac{m^2 + k^2}{x(1-x)} \right] \psi_2(x, k) = S_1 \psi_2(x, k) + \mathcal{B}. \quad (3.50)$$

The self energy contribution S_1 is the same as given in Eq. (3.42). The boson exchange contribution \mathcal{B} is given by

$$\begin{aligned} \mathcal{B} = & -\frac{g^2}{4(2\pi)^2} C_f \int_0^1 dy \int_{-\Lambda}^{+\Lambda} dq \frac{4m^2}{(ky - qx)^2 + m^2(x-y)^2} \psi_2(y, q) \\ & -\frac{g^2}{4(2\pi)^2} C_f \int_0^1 dy \int_{-\Lambda}^{+\Lambda} dq \frac{4m^2}{[k(1-y) - q(1-x)]^2 + m^2(x-y)^2} \psi_2(y, q). \end{aligned} \quad (3.51)$$

Note that in the above approximations we dropped only the term sick with vanishing energy denominator and not so important imaginary terms and Eq. (3.50) still represents a *relativistic* bound state equation. Though the rotational symmetry is not manifest in this equation, Eq. (3.50) in the nonrelativistic limit reduces to a Schrödinger equation with explicit rotational

symmetry (see Appendix D). This model provides us an opportunity to study the simplest manifestation and possible violation of rotational symmetry in the context of light-front field theory.

3.6.1 Numerical study of the reduced model

Again we discretize the Eq. (3.50) by Gaussian Quadrature. The convergence of the eigenvalues as a function of the number of grid points is presented in Table 3.2. In this table we also present the (in)dependence of eigenvalues on the momentum cutoff.

n_1	n_2	eigenvalues (lowest five) ($\kappa=10.0$)				
20	20	4.08926	4.10605	4.10768	4.11061	4.11085
30	30	4.09045	4.10909	4.11038	4.11516	4.11699
40	30	4.09045	4.10913	4.11035	4.11524	4.11697
40	40	4.09102	4.11052	4.11154	4.11711	4.11951
40	50	4.09136	4.11133	4.11222	4.11811	4.12096
50	50	4.09136	4.11135	4.11219	4.11816	4.12095
50	60	4.09158	4.11188	4.11263	4.12189	4.12290
46	60	4.09158	4.11187	4.11264	4.11877	4.12189
46	66	4.09168	4.11212	4.11284	4.11905	4.12231
46	74	4.09179	4.11237	4.11305	4.11934	4.12276
n_1	n_2	eigenvalues (lowest five) ($\kappa=20.0$)				
46	74	4.09179	4.11240	4.11301	4.11940	4.12273

Table 3.2: Convergence of eigenvalue with n_1 and n_2 (reduced model). The parameters are $m=1.0$, $g=0.2$, $\varepsilon = 0.00001$.

(2+1) dimensions provide an opportunity to study the manifestation and violation of rotational symmetry in light front field theory in a simpler setting compared to (3+1) dimensions. The absence of spin further facilitates this study. Rotational symmetry in this case simply implies degeneracy with respect to the sign of the azimuthal quantum number l (see Appendix D). Thus we expect all $l \neq 0$ states to be two fold degenerate. By a suitable change of variables, one can easily show that our reduced model, in the nonrelativistic limit reduces to Schrödinger equation in two space dimensions with a logarithmic confining potential. In the weak coupling

g	eigenvalues			
0.2	This work	4.0918 (4.1227, 4.1235)	(4.1124, 4.1130) (4.1268, 4.1273)	4.1194 (4.1298, 4.1303)
	Koures (Ref. [23])	4.0925 ($l=0$) 4.1260 ($l=2$)	4.1144 ($l=1$) 4.1303 ($l=1$)	4.1214 ($l=0$) 4.1340 ($l=3$)
0.6	This work	4.5856 (4.8767, 4.8816)	(4.7741, 4.7821) (4.9094, 4.9184)	4.8390 (4.9458, 4.9481)
	Koures (Ref. [23])	4.5806 ($l=0$) 4.8827 ($l=2$)	4.7777 ($l=1$) 4.9205 ($l=1$)	4.8409 ($l=0$) 4.9545 ($l=3$)

Table 3.3: Reduced model. The parameters are $n_1=46$, $n_2=74$, $\varepsilon = 0.00001$, $m=1.0$. $k = \tan(q\pi/2)/\kappa$, $\kappa = 20.0$. Eigenvalues within () are $\pm l$ degenerate (broken) states.

	n_1	n_2	eigenvalues					
<i>I</i>	40	50	18.217	(30.702 33.499)	35.206	(39.955 41.159)	(41.332 43.271)	(44.134 45.272)
	46	70	18.276	(30.774 33.616)	35.318	(40.106 41.331)	(41.483 43.477)	(44.375 45.503)
<i>II</i>	40	50	18.980	(31.507 34.219)	35.826	(40.406 41.888)	(41.921 43.788)	(44.345 45.163)
	46	70	19.008	(31.542 34.319)	35.935	(40.626 42.031)	(42.088 44.010)	(44.647 45.780)

Table 3.4: First few eigenvalues in the reduced model. The parameters are $g=5.0$, $m=1.0$, $\varepsilon=0.00001$. (*I*) for the parametrization $k = u\Lambda m / ((1 - u^2)\Lambda + m)$, $\Lambda = 40.0$. (*II*) for the parametrization $k = \tan(u\pi/2)/\kappa$, $\kappa = 10.0$. Eigenvalues within () are $\pm l$ degenerate (broken) states.

limit, since C_f is set to 1, we can compare our results of the reduced model (where we do not make any nonrelativistic approximation) with the spectra obtained in nonrelativistic QED_{2+1} . Tam *et al.* [22] solved the radial Schrödinger equation in momentum space for $l=0$ states and Koures [23] solved the coordinate space radial Schrödinger equation for general l . Since we are solving the light front bound state equation, rotational symmetry is not at all manifest. However, at weak coupling we expect that the spectra exhibit rotational symmetry to a very good approximation. Our numerical results are compared with those of Koures in Table 3.3 for two values of the coupling. At $g = 0.2$ we find reasonable agreement with the degeneracy in

the spectrum. Even at $g = 0.6$ the violation of rotational symmetry is very small. Splitting of levels which are supposed to be degenerate become more visible at very strong coupling as can be seen from Table 3.4 for $g = 5.0$.

Along with the eigenvalues, the diagonalization process also yields wavefunctions. We have plotted the wavefunctions corresponding to the first four eigenvalues in Fig. 3.3 as a function of x and k . All wavefunctions are normalized to be $\int_0^1 dx \int dk \psi^2(x, k) = 1$. The lowest state

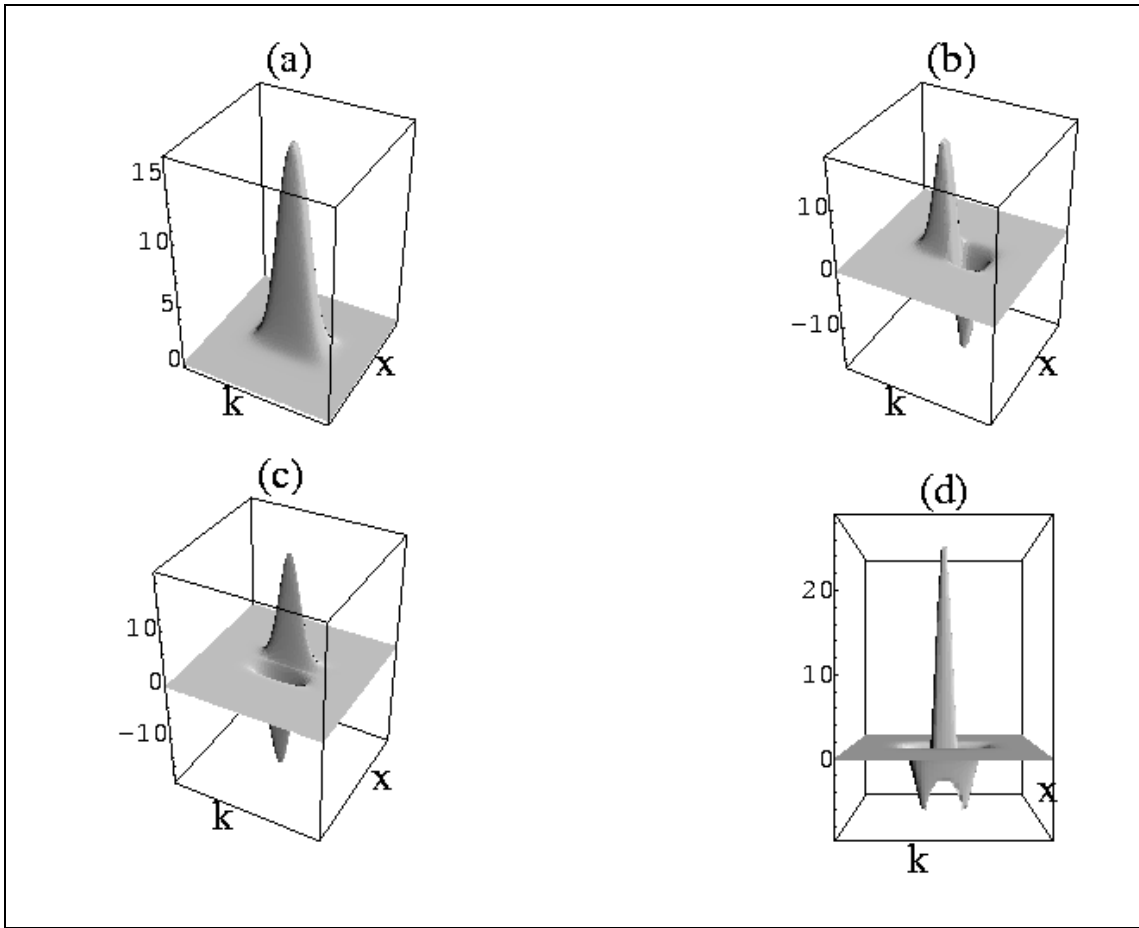


Figure 3.3: The wavefunctions corresponding to the lowest four eigenvalues of the reduced model as a function of x and k . The parameters are $g = .2$, $\varepsilon = 0.00001$, $m = 1$, $\kappa = 10$, $n_1 = 46$, $n_2 = 74$. (a) Lowest state, (b) first excited state, (c) second excited state, (d) third excited state. The first and second excited states should be degenerate in the absence of violation of rotational symmetry.

is nodeless and corresponds to $l = 0$. The next two states correspond to $l = 1$ and have one

node. It is interesting to note the way the node appears in the wavefunctions which correspond to degenerate levels. Since the rotational symmetry cannot be manifest in the variables x and k , how can the wavefunctions still indicate this? From Fig. 3.3, it is clear that the way this problem is resolved is by one wavefunction having a node in k and the other wavefunction having a node in x . Thus even if we did not know about the underlying symmetry from other means, the light-front wavefunctions have a subtle way of indicating the symmetry.

3.7 Summary

The numerical solutions of the bound state equations are performed by using the Gaussian Quadrature (GQ) which is a straightforward procedure to solve the integral equation by converting it into a matrix equation. The investigation shows the efficiency of the GQ method in handling linear and logarithmic light-front infrared divergences. The manifestation of rotational invariance in light-front framework is demonstrated very clearly in the reduced model. But, our study of the Bloch effective Hamiltonian indicates that in the context of Fock space based effective Hamiltonian methods to tackle gauge theories in (2+1) dimensions, approaches like similarity renormalization method are mandatory due to uncanceled infrared divergences caused by the vanishing energy denominator problem. It is important to recall that Bloch effective Hamiltonian is generated by completely integrating out the intermediate gluons irrespective of whether they are low energy or high energy which has no clear justification specially in a confining theory. Once we have obtained quantitative measures of the vanishing energy denominator problem and the nature of the spectra at weak coupling of the Bloch effective Hamiltonian, the next step is to study QCD₂₊₁ in the similarity renormalization approach which avoids the vanishing energy denominator problem. An important issue here is the nature of new effective interactions generated by the similarity approach. It has been shown that in (3+1) dimensions, similarity approach generates logarithmic confining interactions [16] which however breaks rotational symmetry. It is interesting to investigate the corresponding situation in (2+1) dimensions.

BIBLIOGRAPHY

- [1] E. E. Salpeter, H. A. Bethe, Phys. Rev. **84**, 1232 (1951).
- [2] For reviews and exhaustive list of references see N. Nakanishi, Prog. Theor. Phys. Suppl. **43**, 1 (1969); **95**, 1 (1988); N. Seto, Prog. Theor. Phys. Suppl. **95**, 25 (1988).
- [3] T. Murota, Prog. Theor. Phys. Suppl. **95**, 46 (1988).
- [4] W. Lucha, F. F. Schöberl and D. Gomes, Phys. Rep. **200**, 127 (1991).
- [5] T. Maskawa and K. Yamawaki, Prog. Theor. Phys. **56**, 270 (1976); A. Casher, Phys. Rev. D **14**, 452 (1976); C. B. Thorn, Phys. Rev. D **17**, 1073 (1978); H.C. Pauli and S.J. Brodsky, Phys. Rev. D **32**, 1993, (1985); *ibid.*, 2001 (1985). For a review, see, S. J. Brodsky, H. Pauli and S. S. Pinsky, Phys. Rep. **301**, 299 (1998), hep-ph/9705477. For recent work in Discrete Light Cone Quantization see J. Hiller, Int. J. Mod. Phys. A **16S1C**, 1213 (2001), hep-ph/0010061 and references therein.
- [6] Detailed discussions on effective field theory are available in H. Georgi, *Weak Interaction and Modern Particle Theory*, (Benjamin/Cummings, 1984); S. Weinberg, *Quantum Theory of Fields*, Vols. I and II, (Cambridge University Press, 1995).
- [7] R. J. Perry, A. Harindranath and K. G. Wilson, Phys. Rev. Lett. **65**, 2959 (1990).
- [8] C. Bloch, J. Horowitz, Nucl. Phys. **8**, 91 (1958).
- [9] S. Głazek, A. Harindranath, S. Pinsky, J. Shigemitsu and K. Wilson, Phys. Rev. D **47**, 1599 (1993).
- [10] C. Bloch, Nucl. Phys. **6**, 329 (1958).
- [11] K. G. Wilson, Phys. Rev. D **2**, 1438 (1970).
- [12] R. J. Perry, Ann. Phys. **232** (1994) 116, hep-th/9402015.
- [13] S. D. Głazek and K. G. Wilson, Phys. Rev. D **48**, 5863 (1993); **49**, 4214 (1994); Similar flow equations were proposed by F. Wegner, Ann. Phys. (Leipzig) **3**, 77 (1994).
- [14] K. G. Wilson, T. S. Walhout, A. Harindranath, W. Zhang, R. J. Perry and S. D. Głazek, Phys. Rev. D **49**, 6720 (1994), hep-th/9401153.
- [15] S. D. Głazek and K. G. Wilson, Phys. Rev. D **57**, 3558 (1998), hep-th/9707028.

- [16] R. J. Perry, Hamiltonian Light Front Field Theory and Quantum Chromodynamics, in *Hadron Physics '94: Topics on the Structure and Interaction of Hadron Systems*, Proceedings, Gramado, Brazil, edited by V. Hercovitz *et al.*, (World Scientific, Singapore 1995), hep-th/9407056.
- [17] D. Chakrabarti and A. Harindranath, Phys. Rev. D **64**, 105002 (2001), hep-th/0107188.
- [18] K. M. Bitar, Phys. Rev. D **7**, 1184 (1973).
- [19] M. Burkardt and A. Langnau, Phys. Rev. D **44**, 1187 (1991).
- [20] B. Binegar, J. Math. Phys. **23**, 1511 (1982).
- [21] M. Krautgartner, H. C. Pauli and F. Wolz, Phys. Rev. D **45**, 3755 (1992).
- [22] A. Tam, C. J. Hamer and C. M. Yung, J. Phys. **G21**, 1463 (1995).
- [23] V. G. Koures, J. Comp. Phys. **128**, 1 (1996), quant-ph/9510006.

CHAPTER 4

Similarity Renormalization Group Approach to Meson Sector in $(2 + 1)$ Dimensions

4.1 A Brief Review of Renormalization Group Approach

In the previous chapter we have studied the meson bound state problem in $(2+1)$ dimensional QCD with Bloch effective Hamiltonian where we encountered the problem of vanishing energy denominators. We also concluded that Similarity Renormalization Group (SRG) approach is mandatory to get rid of the problem. In this chapter we discuss the same bound state problem in SRG scheme. But before that, we recapitulate the basic concept of Renormalization Group and explain why SRG is preferred over original Wilsonian Renormalization Group approach.

It is well established that the most important tool to construct a low energy effective field theory is the Renormalization Group (RG). The concept of Renormalization Group was first introduced by Stueckelberg and Peterman [1] and Gell-Mann and Low [2] and further developed by Bogoliubov and Shirkov [3]. RG as a practical tool to construct effective theory was developed by K.G. Wilson [4, 5, 6]. The aim of RG is to simplify the problem with many energy (length) scales involving many degrees of freedom which are coupled through the interactions. In the Wilsonian approach the cutoff on energy is lowered and the number of degrees of freedom is reduced in an iterative way and in each step one has to construct the effective interactions for the effective degrees of freedom. The simplification of Renormalization Group lies in the hope that the effective interactions are local interactions i.e., only nearby degrees of freedom are directly coupled by the interactions which holds true for original local theories we normally deal with [5]. Construction of nondiagrammatic RG transformations enables one to solve them numerically in a computer and hence the problems which cannot be solved by Feynman diagrams can be solved by using RG.

The starting point of the RG transformations is a bare Hamiltonian H_0 with cutoff Λ_0 . The transformation τ converts H_0 to H_1 , H_1 to H_2 etc. as the cutoff is lowered $\Lambda_0 > \Lambda_1 > \Lambda_2$ in each step and thins the degrees of freedom. This transformation is to be iterated until one gets the effective Hamiltonian at the desired low energy scale λ . RG transformation is the evolution operator of the Hamiltonian as the cutoff changes. Here I should mention that the RG transformation is free of (UV or IR) divergences, since in each step, a momentum integral involves only a finite range of momentum. But the divergences occur as a result of many iterations of the RG transformation. The logic of RG transformation is best explained by the “*triangle of Renormalization*” [6]. Suppose one is interested to solve a theory at the energy scale 1 in some suitable unit. Consider, for example, that in each step we lower the cutoff by a factor of 1/2, i.e., we have a discrete set of cutoffs, $\Lambda = 2^N$ for $N = 1, 2, 3, 4, \dots, \infty$. For each N , we apply the RG transformation to produce a sequence of effective Hamiltonians $H_0^N, H_1^N, H_2^N, \dots$ until we reach H_N^N with cutoff $\Lambda = 1$. Thus the transformation produces a triangle.

$$\begin{array}{ccccccc}
 \Lambda_0 = 4 & \text{---} & H_0^2 & \cdots & H_{N-2}^N & & \\
 & & \downarrow \tau & & \downarrow \tau & & \\
 \Lambda_0 = 2 & \text{---} & H_0^1 & & H_1^2 & \cdots & H_{N-1}^N \\
 & & \downarrow \tau & & \downarrow \tau & & \downarrow \tau \\
 \Lambda_0 = 1 & \text{---} & H_0^0 & & H_1^1 & & H_2^2 \cdots H_N^N
 \end{array}$$

The $N \rightarrow \infty$ limit along any row produces the infinite cutoff limit or the renormalized Hamiltonian. For example, the $N \rightarrow \infty$ limit of $\Lambda_0 = 1$ row generates the Hamiltonian renormalized at the scale $\Lambda = 1$.

The fixed point of the transformation is defined by

$$\tau(H^*) = H^*. \tag{4.1}$$

The fixed point of a transformation is a property of τ and does not depend on the initial Hamiltonian H_0 .

But, this formalism to construct an effective low energy Hamiltonian acting on a limited Fock space is again plagued with the problem of vanishing energy denominator. If we view the Hamiltonian as a matrix, the energy cutoff limits the size of the matrix and as one lowers the

cutoff, the matrix size is also reduced as shown in Fig. 4.1(a) [7]. The matrix elements near the diagonal region (gray region in Fig.4.1(a)) involve states with almost same energy (nearly degenerate) and involve degenerate perturbation theory for calculation of the effective interactions. In nonperturbative theory like QCD we do not even know how to do that. To overcome

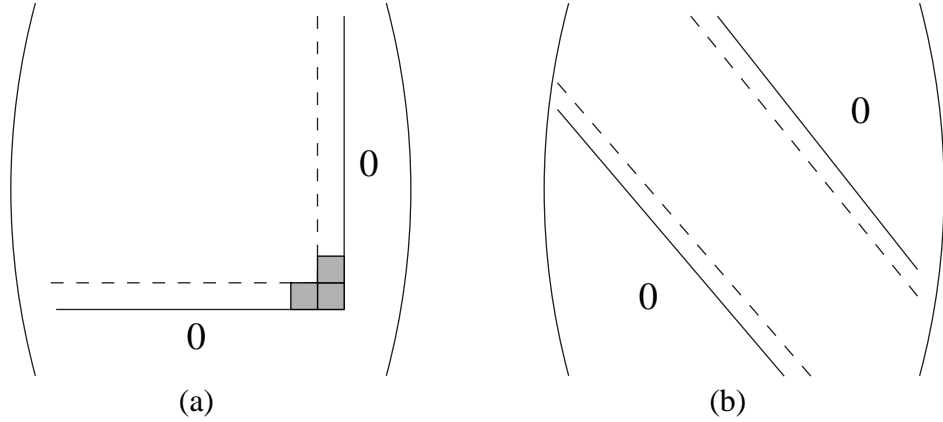


Figure 4.1: Effective Hamiltonian as the cutoff is lowered (solid to dashed line). (a) energy cutoff, (b) cutoff on energy difference.

this problem Głazek and Wilson [8] and Wegner [9] independently developed the similarity renormalization group (SRG) technique to calculate low energy effective Hamiltonian. In this approach the cutoff is not on the energy of the states but on the energy difference of the states. In place of removing the states, off-diagonal matrix elements involving large energy transfer are removed. If the free energy difference between two states is larger than the cutoff, interactions between those two states are then removed from the effective Hamiltonian. The working prescription for SRG is as the following. Again, as in the standard Wilsonian RG, the starting point is a finite and bare cutoff Hamiltonian H_B at some ultra-violet cutoff Λ . Define a similarity transformation that converts H_B into a band-diagonal H_{σ_1} as the energy scale is lowered to σ_1 and removes the coupling between the states with energy difference greater than σ_1 . This process should be repeated until one produces an effective Hamiltonian H_σ at a low energy scale σ . It can again be viewed as a new “triangle of renormalization” [10] as discussed above in the context of Wilsonian RG transformations. The way it works can be compared with the standard numerical algorithm for matrix diagonalization [11] where to keep control over the

complexities, the matrix is first brought to a tri-diagonal form which is then diagonalized. In the SRG approach the Hamiltonian is brought perturbatively into a band-diagonal form (see Fig. 4.1(b)) which is then diagonalized nonperturbatively. Since it does not involve any energy jump below the energy scale σ , the energy denominator cannot be smaller than σ and is free from the problem of vanishing energy denominator.

The diagonalization of the Hamiltonian using SRG is a two step process. In the first step, by removing any direct interactions between states with energy difference larger than the cutoff one arrives at an effective Hamiltonian which is in a band diagonal form. At this step, one can identify the ultraviolet divergent part of the counterterms needed to be added to the Hamiltonian to remove ultraviolet divergences. It is quite advantageous to treat the ultraviolet divergences perturbatively especially in gauge theories since one can avoid pitfalls of other effective Hamiltonian approaches. For example, it is well known that a simple truncation of the Fock space (like a Tamm-Dancoff truncation) leads to uncanceled divergences as a result of violations of gauge symmetry.

In the second step, the effective Hamiltonian is diagonalized exactly. It is important to note that in the process of removing the interactions with very large energy exchange we integrate out small x gluons, i.e., gluons having small longitudinal momentum fraction. Since the vacuum is trivial, it is hoped that, as a result of integrating out small x gluons which are sensitive to long distance physics on the light front, the effective Hamiltonian may contain interactions responsible for low energy properties of QCD. Indeed Perry [12] found a logarithmic confining interaction in the $q\bar{q}$ sector in the lowest order effective interaction.

Initial bound state studies in the similarity renormalization approach worked in either the non-relativistic limit [13] or in the heavy quark effective theory formalism [14] to investigate heavy-quark systems. Only in last few years, some works have been done [15] in the context of glueball spectrum to address many practical problems, especially the numerical ones that one faces in this approach. Since the conceptual and technical problems one encounters in QCD are numerous, we initiated a study of bound state problems in QCD in (2+1) dimensions [16, 17]. Our main motivation is not the fitting of data but a critical evaluation of the strengths and weaknesses of the various assumptions and approximations made in the similarity approach.

In the previous chapter we have discussed the meson sector of (2+1) dimensional light front QCD using a Bloch effective Hamiltonian [18] in the first non-trivial order. The resulting two dimensional integral equation was converted into a matrix equation and solved numerically. We have already discussed in detail the problem of vanishing energy denominator which leads to severe infrared divergences in (2+1) dimensions and came to the conclusion that in the context of Fock space based effective Hamiltonian methods to tackle gauge theories in (2+1) dimensions, approaches like similarity renormalization method is mandatory due to uncanceled infrared divergences caused by the vanishing energy denominator problem. Now, we discuss the similarity renormalization approach in the first non-trivial order to the same problem. The detail of similarity renormalization theory for the Effective Hamiltonian in both Głazek-Wilson and Wegner approaches is discussed in Appendix E.

4.2 Effective bound state equation in the $q\bar{q}$ sector in SRG scheme

In similarity renormalization approach due to Głazek and Wilson, to second order, the interacting part of the effective Hamiltonian at a scale σ is given by (see Appendix E for details)

$$H_{I\sigma ij}^{(2)} = - \sum_k H_{BIik} H_{BIkj} \left[\frac{g_{\sigma ijk}}{P_k^- - P_j^-} + \frac{g_{\sigma jik}}{P_k^- - P_i^-} \right], \quad (4.2)$$

where

$$\begin{aligned} g_{\sigma ijk} &= f_{\sigma ij} \int_{\sigma}^{\infty} d\sigma' f_{\sigma' ik} \frac{d}{d\sigma'} f_{\sigma' jk}, \\ g_{\sigma jik} &= f_{\sigma ij} \int_{\sigma}^{\infty} d\sigma' f_{\sigma' jk} \frac{d}{d\sigma'} f_{\sigma' ik}. \end{aligned} \quad (4.3)$$

. The similarity factor $f_{\sigma ij}(x)$ is such that

$$\begin{aligned} \text{when } \sigma^2 \gg \Delta M_{ij}^2, & \quad f(x) = 1 & \quad (\text{near diagonal region}); \\ \text{when } \sigma^2 \ll \Delta M_{ij}^2, & \quad f(x) = 0 & \quad (\text{far off diagonal region}); \\ \text{in between} & \quad f(x) & \quad \text{drops from 1 to 0} \quad (\text{transition region}). \end{aligned} \quad (4.4)$$

Here $\Delta M_{ij}^2 = (M_i^2 - M_j^2)$ denotes the difference of invariant masses of states i and j . We restrict ourselves to the $q\bar{q}$ sector. Then the states involved in the matrix elements i and j refer to $q\bar{q}$ states and k refer to $q\bar{q}g$ states.

Following the steps similar to the ones outlined in Chapter 3, we arrive at the bound state equation

$$\left[M^2 - \frac{m^2 + k^2}{x(1-x)} \right] \psi_2(x, k) = S \psi_2(x, k) - 4 \frac{g^2}{2(2\pi)^2} C_f \int dy \int dq f_{\sigma ij} \psi_2(y, q) \frac{1}{(x-y)^2} - \frac{g^2}{2(2\pi)^2} C_f \int dy \int dq \psi_2(y, q) \frac{\mathcal{V}}{\mathcal{E}}. \quad (4.5)$$

Here x and y are the longitudinal momentum fractions and k and q are the relative transverse momenta. We introduce the cutoff ε such that $\varepsilon \leq x, y \leq 1 - \varepsilon$. We further introduce the regulator δ such that $|x - y| \geq \delta$. Ultraviolet divergences are regulated by the introduction of the cutoff Λ on the relative transverse momenta k and q . The self energy contribution

$$S = -\frac{g^2}{2(2\pi)^2} C_f \int_0^1 dy \int dq \theta(x-y) [1 - f_{\sigma ik}^2] xy \frac{\left[\left(\frac{q}{y} + \frac{k}{x} - \frac{2(k-q)}{(x-y)} \right)^2 + \frac{m^2(x-y)^2}{x^2 y^2} \right]}{(ky - qx)^2 + m^2(x-y)^2} - \frac{g^2}{2(2\pi)^2} C_f \int_0^1 dy \int dq \theta(y-x) [1 - f_{\sigma ik}^2] (1-x)(1-y) \times \frac{\left[\left(\frac{q}{1-y} + \frac{k}{1-x} + \frac{2(q-k)}{(y-x)} \right)^2 + \frac{m^2(y-x)^2}{(1-x)^2(1-y)^2} \right]}{[k(1-y) - q(1-x)]^2 + m^2(x-y)^2}. \quad (4.6)$$

The boson exchange contribution

$$\frac{\mathcal{V}}{\mathcal{E}} = \frac{\theta(x-y)}{(x-y)} \left[\frac{g_{\sigma jik}}{\frac{m^2+q^2}{y} + \frac{(k-q)^2}{(x-y)} - \frac{m^2+k^2}{x}} + \frac{g_{\sigma ijk}}{\frac{m^2+k^2}{1-x} + \frac{(k-q)^2}{x-y} - \frac{m^2+q^2}{1-y}} \right] \times [K(k, x, q, y) + iV_I] + \frac{\theta(y-x)}{(y-x)} \left[\frac{g_{\sigma jik}}{\frac{m^2+k^2}{x} + \frac{(q-k)^2}{(y-x)} - \frac{q^2+m^2}{y}} + \frac{g_{\sigma ijk}}{\frac{m^2+q^2}{1-y} + \frac{(q-k)^2}{y-x} - \frac{m^2+k^2}{1-x}} \right] \times [K(q, y, k, x) + iV_I], \quad (4.7)$$

where

$$K(k, x, q, y) = \left(\frac{q}{y} + \frac{k}{x} - 2 \frac{(k-q)}{(x-y)} \right) \left(\frac{q}{1-y} + \frac{k}{1-x} + \frac{2(k-q)}{(x-y)} \right) - \frac{m^2(x-y)^2}{xy(1-x)(1-y)}, \quad (4.8)$$

$$V_I = -\frac{m}{xy(1-x)(1-y)} [q(2-y-3x) + k(3y+x-2)]. \quad (4.9)$$

For all the f and g factors,

$$M_i^2 = \frac{k^2 + m^2}{x(1-x)} \text{ and } M_j^2 = \frac{q^2 + m^2}{y(1-y)}. \quad (4.10)$$

$$\text{For } x > y, M_k^2 = \frac{(k-q)^2}{x-y} + \frac{q^2 + m^2}{y} + \frac{k^2 + m^2}{1-x} \quad (4.11)$$

and

$$\text{for } y > x, M_k^2 = \frac{(q-k)^2}{y-x} + \frac{q^2 + m^2}{1-y} + \frac{k^2 + m^2}{x}. \quad (4.12)$$

Before proceeding further, we perform the ultraviolet renormalization. The only ultraviolet divergence arises from the term involving the factor 1 inside the square bracket in Eq. (4.6). We isolate the ultraviolet divergent term which is given by

$$S_{divergent} = -\frac{g^2}{2(2\pi)^2} C_f \left[\int_0^{x-\delta} dy \int_{-\Lambda}^{+\Lambda} dq \frac{(x+y)^2}{xy(x-y)^2} + \int_{x+\delta}^1 dy \int_{-\Lambda}^{+\Lambda} dq \frac{(2-x-y)^2}{(1-x)(1-y)(x-y)^2} \right] \quad (4.13)$$

which is canceled by adding a counterterm.

4.3 Similarity factors

Up to this point, we have not chosen any particular form of the similarity factor $f(x)$. Any function that satisfies the criterion (4.4) is a suitable candidate for the similarity factor. Here we consider three possible choices of similarity factor for comparative studies in the context of meson bound state problem.

4.3.1 Parameterization I

In the SRG study of glueball [15], the following form for the similarity factor has been chosen:

$$f_{\sigma ij} = e^{-\frac{(\Delta M_{ij}^2)^2}{\sigma^4}} \quad (4.14)$$

with $\Delta M_{ij}^2 = M_i^2 - M_j^2$ where M_i^2 denotes the invariant mass of the state i , i.e., $M_i^2 = \Sigma_i \frac{(\kappa_i^\perp)^2 + m_i^2}{x_i}$.

Then

$$\begin{aligned} g_{\sigma ijk} &= f_{\sigma ij} \int_{\sigma}^{\infty} d\sigma' f_{\sigma' ik} \frac{d}{d\sigma'} f_{\sigma' jk} \\ &= e^{-\frac{(\Delta M_{ij}^2)^2}{\sigma^4}} \frac{(\Delta M_{jk}^2)^2}{(\Delta M_{ik}^2)^2 + (\Delta M_{jk}^2)^2} \left[1 - e^{-\frac{((\Delta M_{ik}^2)^2 + (\Delta M_{jk}^2)^2)}{\sigma^4}} \right]. \end{aligned} \quad (4.15)$$

For the self energy contribution, $i = j$ and we get

$$g_{\sigma ijk} = g_{\sigma jik} = g_{\sigma iik} = \frac{1}{2} \left[1 - e^{-\frac{2(\Delta M_{jk}^2)^2}{\sigma^4}} \right]. \quad (4.16)$$

Due to the sharp fall of f with σ , the effective Hamiltonian has a strong dependence on σ . Note that this parameterization emerges naturally in the Wegner formalism (see Appendix E).

4.3.2 Parameterization II

St. Głazek has proposed the following form [19] for $f_{\sigma ij}$.

$$f_{\sigma ij} = \frac{1}{\left[1 + \left(\frac{u_{\sigma ij}(1-u_0)}{u_0(1-u_{\sigma ij})} \right)^{2n_g} \right]} \quad (4.17)$$

with

$$u_{\sigma ij} = \frac{\Delta M_{ij}^2}{\Sigma M_{ij}^2 + \sigma^2}, \quad (4.18)$$

u_0 a small parameter, and n_g an integer. The *mass sum* $\Sigma M_{ij}^2 = M_i^2 + M_j^2$. The derivative

$$\frac{df_{\sigma ij}}{d\sigma} = 2^{n_g} \frac{2\sigma}{\Sigma M_{ij}^2 + \sigma^2} \left(\frac{u_{\sigma ij}}{u_0} \right)^{2n_g} \frac{(1-u_0)^{2n_g}}{(1-u_{\sigma ij})^{2n_g+1}} \frac{1}{\left[1 + \left(\frac{u_{\sigma ij}(1-u_0)}{u_0(1-u_{\sigma ij})} \right)^{2n_g} \right]^2}. \quad (4.19)$$

Note that for small u , both $1 - f(u)$ and $\frac{df}{d\sigma}$ vanish like u^{2n_g} .

4.3.3 Parameterization III

For analytical calculations it is convenient to choose [12] a step function cutoff for the similarity factor:

$$f_{\sigma ij} = \theta(\sigma^2 - \Delta M_{ij}^2). \quad (4.20)$$

Then

$$g_{\sigma_{ijk}} = \theta(\sigma^2 - \Delta M_{ij}^2) \theta(\Delta M_{jk}^2 - \sigma^2) \theta(\Delta M_{jk}^2 - \Delta M_{ik}^2). \quad (4.21)$$

It is the factor $\theta(\Delta M_{jk}^2 - \sigma^2)$ in $g_{\sigma_{ijk}}$ that prevents the energy denominator from becoming small.

4.4 Analytical calculations with the step function similarity factor

In this section we perform analytical calculations to understand the nature of the effective interactions generated by the similarity factor. The differences in the divergences at some places with those discussed in Chapter 3 come due to the similarity factors associated with different terms in SRG scheme. As we have already emphasized that SRG is a modification over Bloch perturbation theory, we will see here how the divergences are made softer and their consequences in similarity group transformed effective bound state equation. Since there are no divergences associated with ε and Λ , we suppress their presence in the limits of integration in the following equations.

4.4.1 Self energy contributions

Consider the self energy contributions to the bound state equation Eq. (4.6). Rewriting the energy denominators to expose the most singular terms, we have,

$$\begin{aligned} S = & -\frac{g^2}{2(2\pi)^2} C_f \int_0^1 dy \int dq \frac{\theta(x - \delta - y)}{x - y} \{1 - f_{\sigma_{ik}}^2\} \frac{\left[\left(\frac{q}{y} + \frac{k}{x} - \frac{2(k-q)}{(x-y)} \right)^2 + \frac{m^2(x-y)^2}{x^2 y^2} \right]}{\frac{(k-q)^2}{(x-y)} + \frac{q^2 + m^2}{y} - \frac{k^2 + m^2}{x}} \\ & -\frac{g^2}{2(2\pi)^2} C_f \int_0^1 dy \int dq \frac{\theta(y - x - \delta)}{y - x} \{1 - f_{\sigma_{ik}}^2\} \\ & \times \frac{\left[\left(\frac{q}{1-y} + \frac{k}{1-x} + \frac{2(q-k)}{(y-x)} \right)^2 + \frac{m^2(y-x)^2}{(1-x)^2(1-y)^2} \right]}{\frac{(q-k)^2}{y-x} + \frac{q^2 + m^2}{1-y} - \frac{k^2 + m^2}{1-x}}. \end{aligned} \quad (4.22)$$

The terms associated with 1 in the curly brackets are the same as in Bloch effective Hamiltonian and lead to ultraviolet linear divergent terms which we cancel by counterterms. They also lead to an infrared divergent term [16] which remains uncanceled. Explicitly this contribution is given by

$$4 \frac{g^2 m^2}{2(2\pi)^2} C_f \int_0^{x-\delta} dy \int dq \frac{1}{[ky - qx]^2 + m^2(x-y)^2}$$

$$+4 \frac{g^2 m^2}{2(2\pi)^2} C_f \int_{x+\delta}^1 dy \int dq \frac{1}{[k(1-y) - q(1-x)]^2 + m^2(x-y)^2}. \quad (4.23)$$

This is simply indicative of the fact that terms associated with 1 in the curly bracket still has a vanishing energy denominator problem. We will address the resolution of this problem shortly.

Let us next consider new infrared divergences that arise as a result of the modifications due to similarity factor.

Leading singular terms

Keeping only the most infrared singular terms in the numerators (i.e., for $x > y$, $4 \frac{(k-q)^2}{(x-y)^2}$ and for $y > x$, $4 \frac{(q-k)^2}{(y-x)^2}$) and denominators (i.e., for $x > y$, $\frac{(k-q)^2}{(x-y)^2}$ and for $y > x$, $\frac{(q-k)^2}{(y-x)^2}$), we have,

$$S_1 = \frac{g^2}{2(2\pi)^2} C_f \int_0^1 dy \int dq \theta(x - \delta - y) f_{\sigma ik}^2 4 \frac{1}{(x-y)^2} + \frac{g^2}{2(2\pi)^2} C_f \int_0^1 dy \int dq \theta(y - x - \delta) f_{\sigma ik}^2 4 \frac{1}{(y-x)^2}. \quad (4.24)$$

The integral with θ -function similarity factor is given by

$$\int dq \left[\int_0^{x-\delta} dy \frac{1}{(x-y)^2} \theta \left(\sigma^2 - \frac{(k-q)^2}{x-y} \right) + \int_{x+\delta}^1 dy \frac{1}{(y-x)^2} \theta \left(\sigma^2 - \frac{(k-q)^2}{y-x} \right) \right]. \quad (4.25)$$

We change the transverse momentum variable, $p = k - q$. For $x - \delta > y$, we set $x - y = z$ and for $y > x + \delta$ we set $y - x = z$. Then, we have,

$$4 \frac{g^2}{2(2\pi)^2} C_f \left[\int_{\delta}^x \frac{dz}{z^2} \int dp \theta \left(\sigma^2 - \frac{p^2}{z} \right) + \int_{\delta}^{1-x} \frac{dz}{z^2} \int dp \theta \left(\sigma^2 - \frac{p^2}{z} \right) \right] = \frac{16g^2}{2(2\pi)^2} C_f \sigma \left[\frac{2}{\sqrt{\delta}} - \frac{1}{\sqrt{x}} - \frac{1}{\sqrt{1-x}} \right]. \quad (4.26)$$

Sub-leading singular terms

Next we study sub-leading singular terms containing $\frac{1}{x-y}$ in self energy generated by the similarity transformation. They are given by

$$S_2 = -4 \frac{g^2}{2(2\pi)^2} C_f \left[\int_0^{x-\delta} dy \int dq \theta \left(\sigma^2 - \frac{(k-q)^2}{x-y} \right) \frac{1}{x-y} \left(\frac{k^2}{x} - \frac{q^2}{y} \right) \frac{1}{(k-q)^2} - \int_{x+\delta}^1 dy \int dq \theta \left(\sigma^2 - \frac{(q-k)^2}{y-x} \right) \frac{1}{y-x} \left(\frac{k^2}{1-x} - \frac{q^2}{1-y} \right) \frac{1}{(q-k)^2} \right] \quad (4.27)$$

where we have kept only $(k - q)^2$ term in the denominator since the rest vanish in the limit $x \rightarrow y$. As before, for $x - \delta > y$, we put $x - y = z$, $k - q = p$. With the symmetric integration in p , terms linear in p do not contribute. Only potential source of δ divergence is the p^2 term in the integrand. Since $p_{max} = \sigma\sqrt{z}$, after p integration $\frac{1}{z}$ is converted into $\frac{1}{\sqrt{z}}$ which is an integrable singularity. Same situation occurs for $y > x$. Thus there are no terms divergent in δ coming from sub-leading singular terms.

4.4.2 Gluon exchange contributions

Let us next consider the effect of similarity factors on gluon exchange terms.

Instantaneous gluon exchange

From instantaneous interaction we have,

$$V_{inst} = -4 \frac{g^2}{2(2\pi)^2} C_f \int dy \int dq \psi_2(y, q) f_{\sigma ij} \frac{1}{(x-y)^2}. \quad (4.28)$$

For the sake of clarity, it is convenient to rewrite this as

$$\begin{aligned} V_{inst} = & -4 \frac{g^2}{2(2\pi)^2} \frac{1}{2} C_f \int dy \int dq f_{\sigma ij} \psi_2(y, q) \\ & \left[\frac{\theta(x-y-\delta)}{x-y} \left\{ \frac{\frac{(k-q)^2}{x-y} + (\frac{q^2}{y} - \frac{k^2}{x}) + m^2(\frac{1}{y} - \frac{1}{x})}{(k-q)^2 + (\frac{q^2}{y} - \frac{k^2}{x})(x-y) + m^2(\frac{1}{y} - \frac{1}{x})(x-y)} \right. \right. \\ & + \left. \frac{\frac{(k-q)^2}{x-y} - (\frac{q^2}{1-y} - \frac{k^2}{1-x}) - m^2(\frac{1}{1-y} - \frac{1}{1-x})}{(k-q)^2 - (\frac{q^2}{1-y} - \frac{k^2}{1-x})(x-y) - m^2(\frac{1}{1-y} - \frac{1}{1-x})(x-y)} \right\} \\ & + \frac{\theta(y-x-\delta)}{y-x} \left\{ \frac{\frac{(q-k)^2}{y-x} - (\frac{q^2}{y} - \frac{k^2}{x}) + m^2(\frac{1}{x} - \frac{1}{y})}{(q-k)^2 - (\frac{q^2}{y} - \frac{k^2}{x})(y-x) + m^2(\frac{1}{x} - \frac{1}{y})(y-x)} \right. \\ & \left. \left. + \frac{\frac{(q-k)^2}{y-x} + (\frac{q^2}{1-y} - \frac{k^2}{1-x}) + m^2(\frac{1}{1-y} - \frac{1}{1-x})}{(q-k)^2 + (\frac{q^2}{1-y} - \frac{k^2}{1-x})(y-x) + m^2(\frac{1}{1-y} - \frac{1}{1-x})(y-x)} \right\} \right]. \quad (4.29) \end{aligned}$$

We have to separately analyze the three types of terms in the numerator.

First consider terms proportional to m^2 in the numerator. They are given by

$$\begin{aligned} & -4 \frac{g^2 m^2}{2(2\pi)^2} \frac{1}{2} C_f \int dy \int dq f_{\sigma ij} \psi_2(y, q) \\ & \times \left[\frac{1}{[ky - qx]^2 + m^2(x-y)^2} + \frac{1}{[k(1-y) - q(1-x)]^2 + m^2(x-y)^2} \right] \quad (4.30) \end{aligned}$$

which leads to the logarithmic confining interaction in the nonrelativistic limit. Note, however, that Eq. (4.30) is affected by a logarithmic infrared divergence arising from the vanishing energy denominator problem. The logarithmic infrared divergence is canceled by the self energy contribution, Eq. (4.23). Thus it explicitly shows that the logarithmically confining Coulomb interaction survives similarity transformation but the associated infrared divergence is canceled by self energy contribution.

Next we look at the most singular term in the numerator in the limit $x \rightarrow y$. In this limit we keep only the leading term in the denominator and we get

$$-4 \frac{g^2}{2(2\pi)^2} C_f \int dy \int dq \psi_2(y, q) f_{\sigma ij} \left\{ \frac{\theta(x-y)}{(x-y)^2} + \frac{\theta(y-x)}{(y-x)^2} \right\}. \quad (4.31)$$

Lastly we look at the rest of the terms in the instantaneous exchange. Since we are interested only in the singularity structure, we keep only the leading term in the denominator and we get

$$\begin{aligned} & -2 \frac{g^2}{2(2\pi)^2} C_f \int dy \int dq f_{\sigma ij} \frac{1}{(k-q)^2} \\ & \times \left[\frac{\theta(x-y)}{x-y} \left[\frac{q^2(1-2y)}{y(1-y)} - \frac{k^2(1-2x)}{x(1-x)} \right] + \frac{\theta(y-x)}{y-x} \left[\frac{k^2(1-2x)}{x(1-x)} - \frac{q^2(1-2y)}{y(1-y)} \right] \right]. \end{aligned} \quad (4.32)$$

Transverse gluon exchange

First, consider the most singular terms.

Keeping only the most singular terms, the gluon exchange contribution is

$$\begin{aligned} & -\frac{g^2}{2(2\pi)^2} C_f \int dy \int dq \psi_2(y, q) \times \\ & \left\{ \frac{\theta(x-\delta-y)}{x-y} \left[\frac{g_{\sigma jik} + g_{\sigma ijk}}{\frac{(k-q)^2}{(x-y)}} (-4) \frac{(k-q)^2}{(x-y)^2} \right] + \frac{\theta(y-x-\delta)}{y-x} \left[\frac{g_{\sigma jik} + g_{\sigma ijk}}{\frac{(q-k)^2}{(y-x)}} (-4) \frac{(q-k)^2}{(y-x)^2} \right] \right\} \\ & = -\frac{g^2}{2(2\pi)^2} C_f \int dy \int dq \psi_2(y, q) \times \\ & \left\{ \frac{\theta(x-\delta-y)}{(x-y)^2} \left[g_{\sigma jik} + g_{\sigma ijk} \right] + \frac{\theta(y-x-\delta)}{(y-x)^2} \left[g_{\sigma jik} + g_{\sigma ijk} \right] \right\}. \end{aligned} \quad (4.33)$$

Explicitly, for $x > y$,

$$\begin{aligned} g_{\sigma ijk} &= \theta(\sigma^2 - M_{ij}^2) \theta(M_{jk}^2 - M_{ik}^2) \theta(M_{jk}^2 - \sigma^2), \\ g_{\sigma jik} &= \theta(\sigma^2 - M_{ij}^2) \theta(M_{ik}^2 - M_{jk}^2) \theta(M_{ik}^2 - \sigma^2). \end{aligned} \quad (4.34)$$

We are interested in the situation x near y and i near j . Then $\theta(M_{jk}^2 - M_{ik}^2) = \frac{1}{2} = \theta(M_{ik}^2 - M_{jk}^2)$ and $\theta(\sigma^2 - M_{ij}^2) = 1$. Then the gluon exchange contribution is

$$4 \frac{g^2}{2(2\pi)^2} C_f \int dy \int dq \psi_2(y, q) \left[\frac{\theta(x - \delta - y)}{(x - y)^2} \left\{ 1 - \theta \left(\sigma^2 - \frac{(k - q)^2}{x - y} \right) \right\} + \frac{\theta(y - x - \delta)}{(y - x)^2} \left\{ 1 - \theta \left(\sigma^2 - \frac{(q - k)^2}{y - x} \right) \right\} \right] \quad (4.35)$$

where we have used $\theta(x) = 1 - \theta(-x)$. Combining with the most singular part of the instantaneous contribution given in Eq. (4.31) we arrive at

$$-4 \frac{g^2}{2(2\pi)^2} C_f \int dy \int dq \psi_2(y, q) \times \left[\frac{\theta(x - \delta - y)}{(x - y)^2} \theta \left(\sigma^2 - \frac{(k - q)^2}{x - y} \right) + \frac{\theta(y - x - \delta)}{(y - x)^2} \theta \left(\sigma^2 - \frac{(q - k)^2}{y - x} \right) \right]. \quad (4.36)$$

For convenience we change variables. For $x > y$, we put $x - y = \frac{p^+}{P^+}$ and $k - q = p^1$ and for $y > x$, we put $y - x = \frac{p^+}{P^+}$ and $q - k = p^1$ where P^+ is the total longitudinal momentum. Thus we arrive at

$$-4 \frac{g^2}{2(2\pi)^2} C_f P^+ \left[\int dp \int_{P^+\delta}^{P^+x} dp^+ \psi_2(x - \frac{p^+}{P^+}, k - p^1) \frac{1}{(p^+)^2} \theta \left(\sigma^2 - \frac{(p^1)^2 P^+}{p^+} \right) + \int dp \int_{P^+\delta}^{P^+(1-x)} dp^+ \psi_2(x + \frac{p^+}{P^+}, k + p^1) \frac{1}{(p^+)^2} \theta \left(\sigma^2 - \frac{(p^1)^2 P^+}{p^+} \right) \right]. \quad (4.37)$$

Consider the Fourier transform

$$V(x^-, x^\perp) = -4 \frac{g^2}{2(2\pi)^2} C_f P^+ \left[\int_{P^+\delta}^{P^+x} \frac{dp^+}{(p^+)^2} \int_{-p_{max}^1}^{+p_{max}^1} dp^1 e^{i\frac{1}{2}p^+x^- - ip^1x^1} \theta \left(\sigma^2 - \frac{(p^1)^2 P^+}{p^+} \right) + \int_{P^+\delta}^{P^+(1-x)} \frac{dp^+}{(p^+)^2} \int_{-p_{max}^1}^{+p_{max}^1} dp^1 e^{i\frac{1}{2}p^+x^- - ip^1x^1} \theta \left(\sigma^2 - \frac{(p^1)^2 P^+}{p^+} \right) \right] \quad (4.38)$$

where $p_{max}^1 = \sigma \sqrt{\frac{p^+}{P^+}}$. We are interested in the behavior of $V(x^-, x^\perp)$ for large x^-, x^\perp . For large x^- , nonnegligible contribution to the integral comes from the region $q^+ < \frac{1}{|x^-|}$. For large x^\perp , we need $p_{max}^1 x^\perp$ to be small, i.e., $(p_{max}^1)^2 < \frac{1}{(x^\perp)^2}$, i.e., $p^+ < \frac{P^+}{(x^\perp)^2 \sigma^2}$. Thus we have the requirements, $p^+ < \frac{1}{|x^-|}$, $p^+ < \frac{P^+}{(x^\perp)^2 \sigma^2}$. We make the approximations

$$\int_{-p_{max}^1}^{+p_{max}^1} dp^1 e^{-ip^1x^1} \approx 2p_{max}^1 \quad (4.39)$$

and $e^{\frac{i}{2}q^+x^-} \approx 1$.

For large x^- , we have $p^+ < \frac{1}{|x^-|} < \frac{P^+}{(x^1)^2\sigma^2}$, the upper limit of p^+ integral is cut off by $\frac{1}{|x^-|}$. Adding the contributions from both the integrals (which are equal), for large x^- , we have

$$V(x^-, x^1) \approx 32 \frac{g^2}{2(2\pi)^2} C_f \sigma \left[\sqrt{P^+ |x^-|} - \frac{1}{\sqrt{\delta}} \right]. \quad (4.40)$$

Thus for large x^- the similarity factors have produced a square root potential but it is also infrared singular.

For large x^1 the upper limit of p^+ integral is cut off by $\frac{P^+}{(x^1)^2\sigma^2}$ and we get,

$$V(x^-, x^1) \approx 32 \frac{g^2}{2(2\pi)^2} C_f \sigma \left[|x^1| \sigma - \frac{1}{\sqrt{\delta}} \right]. \quad (4.41)$$

For large x^1 , similarity factors have produced a linear confining potential which is also infrared singular. We note that the rotational symmetry is violated in the finite part of the potential. In both cases, however, the infrared singular part is $-32 \frac{g^2}{2(2\pi)^2} C_f \sigma \frac{1}{\sqrt{\delta}}$ which is exactly canceled by the infrared contribution generated by similarity transformation from self energy, Eq. (4.26).

Lastly, we consider the terms that go like $\frac{1}{x-y}$. Keeping only the leading term in the energy denominator, we have,

$$\begin{aligned} & -2 \frac{g^2}{2(2\pi)^2} C_f \int dy \int dq \psi_2(y, q) \times \\ & \left[\frac{\theta(x-y)}{x-y} \frac{g_{\sigma jik} + g_{\sigma ijk}}{(k-q)^2} \left[\frac{k^2(1-2x)}{x(1-x)} - \frac{q^2(1-2y)}{y(1-y)} \right] \right. \\ & \left. + \frac{\theta(y-x)}{y-x} \frac{g_{\sigma jik} + g_{\sigma ijk}}{(q-k)^2} \left[\frac{q^2(1-2y)}{y(1-y)} - \frac{k^2(1-2x)}{x(1-x)} \right] \right]. \quad (4.42) \end{aligned}$$

With the step function cut off we have

$$g_{\sigma jik} + g_{\sigma ijk} \approx f_{\sigma ij} \theta(\Delta M_{ik}^2 - \sigma^2). \quad (4.43)$$

Then, combining Eq. (4.32) and Eq. (4.42) for the sub-leading divergences, we get,

$$\begin{aligned} & -2 \frac{g^2}{2(2\pi)^2} C_f \int dy \int dq f_{\sigma ij} \psi_2(y, q) \times \\ & \left[\frac{\theta(x-y)}{x-y} \frac{1}{(k-q)^2} \theta \left(\sigma^2 - \frac{(k-q)^2}{x-y} \right) \left[\frac{k^2(1-2x)}{x(1-x)} - \frac{q^2(1-2y)}{y(1-y)} \right] \right. \\ & \left. + \frac{\theta(y-x)}{y-x} \frac{1}{(q-k)^2} \theta \left(\sigma^2 - \frac{(q-k)^2}{y-x} \right) \left[\frac{q^2(1-2y)}{y(1-y)} - \frac{k^2(1-2x)}{x(1-x)} \right] \right]. \quad (4.44) \end{aligned}$$

Taking the Fourier transform of this interaction, a straightforward calculation shows that no $\log \delta$ divergence arise from this term.

Summary of divergence analysis

The logarithmic confining Coulomb interaction of (2+1) dimensions is unaffected by similarity transformation and is still affected by a logarithmic divergence which is however canceled by a logarithmic divergence from self energy contribution. Similarity transformation leads to a non-cancellation of the most singular $(\frac{1}{(x-y)^2})$ term between instantaneous and transverse gluon interaction terms. This leads to a linear confining interaction for large transverse separations and a square root confining interaction for large longitudinal separations. The confining interactions generated by similarity transformations violates rotational symmetry in lowest order of perturbation theory and needs higher order calculations to see if restoration of the symmetry occurs. However, non-cancellation also leads to $\frac{1}{\sqrt{\delta}}$ divergences where δ is the cutoff on $|x-y|$. This divergence is cancelled by new contributions from self energy generated by similarity transformation. The subleading singular $\frac{1}{x-y}$ terms do not lead to any divergence in δ .

4.5 Numerical studies

The integral equation is converted in to a matrix equation using Gaussian Quadrature. The matrix is numerically diagonalized using standard LAPACK routines [20]. We follow the same procedure as what we adopted for study with Bloch effective theory (see Chapter 3) and the details of numerical procedure are discussed in Appendix C. With the exponential form and the step function form of the similarity factor, the integral over the scale in the definition of g_σ factors in Eq. (4.3) can be performed analytically as shown in Sec. 4.4. For parametrization II, we perform the integration numerically using n_s quadrature points.

The first question we address is the cancellation of divergences which are of two types: (1) the $\ln \delta$ divergence in the self energy and Coulomb interaction which has its source in the vanishing energy denominator problem that survives the similarity transformation and (2) $\frac{1}{\sqrt{\delta}}$ divergences in the self energy and gluon exchange generated by the similarity transformation. Here I should remind the reader once again that the main motivation of our work is not to fit data but to assess the strengths and weaknesses of SRG scheme over Bloch perturbation

theory and comparative study of different choices for similarity factor. In Table 4.1 we present

δ	Parametrization I				
0.1	4.89535	4.90359	4.90420	4.90420	4.90482
0.01	5.62612	6.38083	6.82963	7.20037	7.36414
0.001	5.68417	6.42147	6.90879	7.30609	7.64650
0.0001	5.68432	6.42148	6.90909	7.30611	7.64677
0.00001	5.68432	6.42148	6.90909	7.30611	7.64677
δ	Parametrization II				
0.1	4.55364	4.55668	4.55668	4.55668	4.55669
0.01	4.86066	5.33491	5.49693	5.59838	5.79111
0.001	4.87607	5.35671	5.59226	5.64476	5.88613
0.0001	4.87604	5.35671	5.59236	5.64477	5.88615
0.00001	4.87604	5.35671	5.59236	5.64477	5.88615
δ	Parametrization III				
0.1	5.12410	5.13039	5.13101	5.13101	5.13754
0.01	6.02600	6.94326	7.50445	7.98054	8.39927
0.001	6.00968	6.97160	7.55376	8.07749	8.49199
0.0001	5.96636	6.97160	7.51814	8.07751	8.46524
0.00001	5.96636	6.97160	7.51814	8.07751	8.46524

Table 4.1: Variation with δ of the first five eigenvalues of the full Hamiltonian (excluding the less significant imaginary term). The parameters are $m = 1.0$, $g = 0.6$, $n_1 = 58$, $n_2 = 58$, $\varepsilon = 0.00001$, $\Lambda = 20.0$, $\sigma = 4.0$, ($u_0 = 0.1$, $n_g = 2$ and $n_s = 500$ (for σ integration) in parametrization II)

the δ independence of the first five eigenvalues of the Hamiltonian for $g=0.6$. Results are presented for three parametrizations of the similarity factor, namely, the exponential form, the form proposed by St. Głazek and the step function form used in our analytical studies. It is clear that the Gaussian Quadrature effectively achieves the cancellation of δ divergences. Recall that in the study of the same problem using Bloch approach in Chapter 3, negative eigenvalues appeared for $g=0.6$ when δ was sufficiently small (for example, 0.001) which was caused by the vanishing energy denominator problem. Our results in the similarity approach for the same coupling shows that this problem is absent in the latter approach.

Next we study the convergence of eigenvalues with quadrature points. In Table 4.2 we present the results for all three parametrizations of the similarity factor for the coupling $g=0.2$

with the transverse space discretized using $k = \frac{1}{\kappa} \tan \frac{u\pi}{2}$ where u 's are the quadrature points (see Appendix C). The table show that for $m = 1$, convergence is rather slow for all three choices of the similarity factor compared to the results in Bloch approach. Among the three choices, parameterization II shows better convergence.

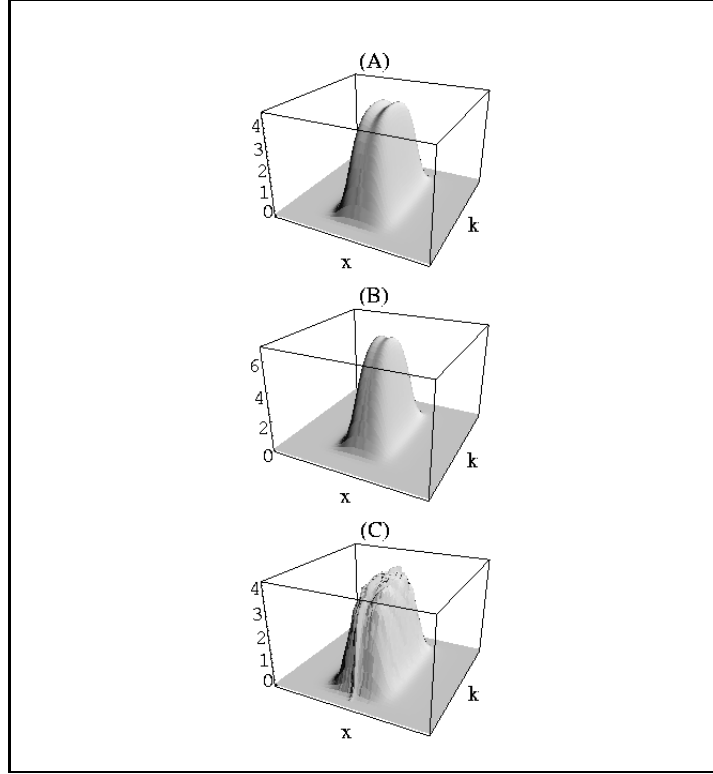


Figure 4.2: The ground state wavefunction for different choices of the similarity factor using the parametrization $k = \frac{1}{\kappa} \tan(q\pi/2)$ for transverse momentum grid and for $n_1 = 40$, $n_2 = 80$, $m=1.0$, $g = 0.2$, $\sigma = 4.0$ and $\varepsilon = \delta = 10^{-5}$, $\kappa = 10.0$ as a function of x and k . (A) Parametrization I, (B) Parametrization II with $n_g = 2$, $u_0 = 0.1$, $n_s = 500$, (C) Parametrization III.

Let us now discuss the nature of low lying levels and wavefunctions. First we show the ground state wavefunctions for all three similarity factors for a given choice of parameters in Fig. 4.2. As is anticipated, step function choice produces a non-smooth wavefunction. For parameterizations I and II, the wavefunctions show some structure near $x = 0.5$. From our previous experience with calculations in the Bloch formalism, we believe that the structures indicate poor convergence with the number of grid points.

n_1	n_2	Parametrization I				
10	10	4.320	4.353	4.357	4.357	4.361
20	20	4.375	4.442	4.484	4.484	4.485
20	30	4.398	4.482	4.546	4.583	4.610
20	40	4.411	4.502	4.570	4.615	4.656
30	40	4.412	4.503	4.570	4.615	4.655
40	50	4.420	4.515	4.585	4.634	4.678
40	60	4.426	4.524	4.594	4.645	4.692
40	80	4.434	4.535	4.607	4.661	4.709
n_1	n_2	Parametrization II				
10	10	4.163	4.194	4.194	4.194	4.203
20	20	4.186	4.244	4.276	4.276	4.277
20	30	4.192	4.256	4.296	4.323	4.329
20	40	4.195	4.262	4.304	4.335	4.344
30	40	4.195	4.262	4.304	4.335	4.344
40	50	4.197	4.266	4.308	4.341	4.353
40	60	4.199	4.268	4.311	4.345	4.359
40	80	4.201	4.272	4.315	4.350	4.367
n_1	n_2	Parametrization III				
10	10	4.360	4.379	4.381	4.381	4.391
20	20	4.469	4.533	4.572	4.572	4.572
20	30	4.503	4.604	4.674	4.721	4.749
20	40	4.520	4.632	4.703	4.768	4.810
30	40	4.528	4.636	4.714	4.768	4.811
40	50	4.542	4.657	4.736	4.797	4.848
40	60	4.548	4.668	4.748	4.813	4.866
40	80	4.556	4.683	4.764	4.833	4.889

Table 4.2: Convergence of eigenvalues with n_1 and n_2 for the parametrization $k = \frac{1}{\kappa} \tan(q\pi/2)$. The parameters are $m=1.0$, $g=0.2$, $\varepsilon = 0.00001$, $\delta = 0.00001$, $\kappa = 10.0$, $\sigma = 4.0$, $(u_0=0.1, n_g=2)$ and the number of quadrature points $n_s = 500$ for σ integration for parametrization II).

Now consider the structure of low lying levels. Recall that in the Bloch formalism discussed in the previous chapter, the ordering of levels was $l = 0, 1, 0, \dots$ corresponding to logarithmic potential in the nonrelativistic limit (see Appendix D). In the presence of effective interactions

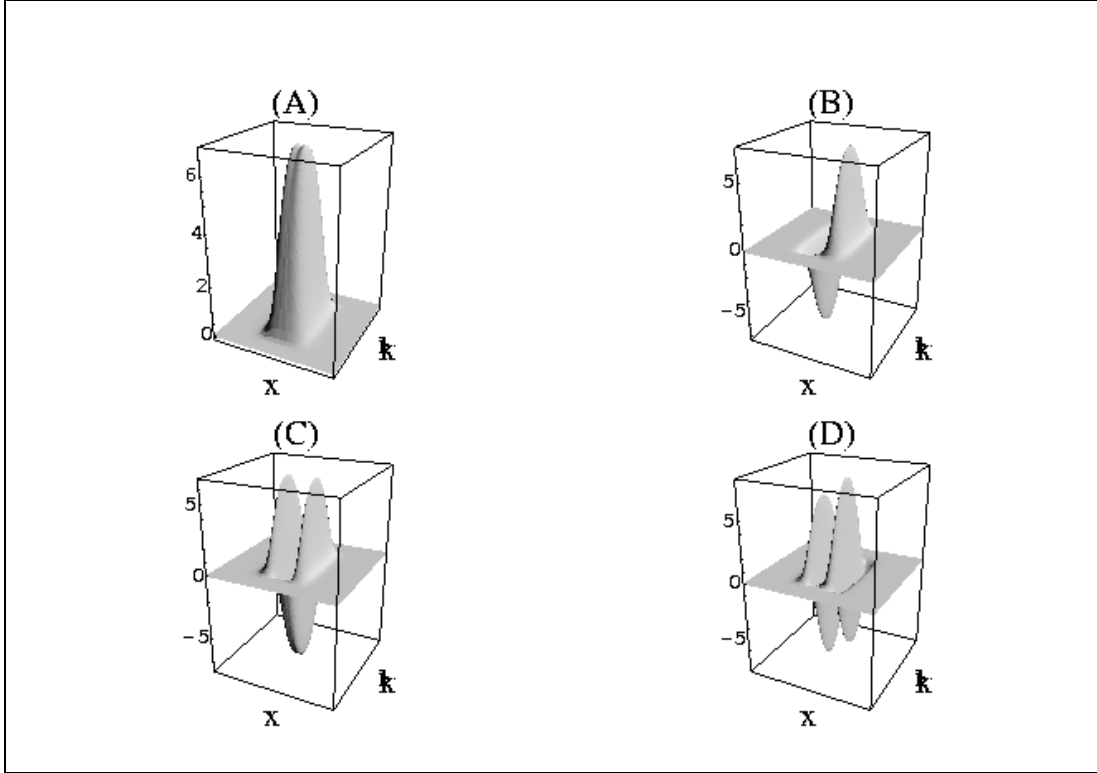


Figure 4.3: The wavefunctions corresponding to the lowest four eigenvalues as a function of x and k for parametrization II. The parameters are as in FIG. 4.2. (A) Lowest state, (B) first excited state, (C) second excited state, (D) third excited state.

generated by the similarity transformation, obviously the level ordering changes. Now we have additional confining interactions which, however, act differently in longitudinal and transverse directions. From our analytic calculation in Sec. 4.4 we know that the confining potential generated by similarity transformation is linear in x^1 and square root in x^- . Thus a node in x^1 costs more energy than a node in x^- and thus the states with nodes in x^1 (i.e., in k) will be of higher energy compared to states with nodes in x^- . This feature is well manifested in Fig. 4.3 where the wavefunctions for the first four low lying levels are presented for parametrization II.

There is extra freedom in parametrization II due to the presence of ΣM_{ij}^2 in the definition of $u_{\sigma ij}$, Eq. (4.18). For zero transverse momentum of constituents, ΣM_{ij}^2 has the minimum value $8m^2$. Thus relative insensitivity of parametrization to σ in parametrization II for small values of σ may be due to this factor. When we consider the heavy fermion mass limit, presence of $8m^2$ in $u_{\sigma ij}$ enhances the effect of similarity factor. In Fig. 4.4 we present the wavefunctions corresponding to first four levels for parametrization II with $8m^2$ subtracted from ΣM_{ij}^2 in $u_{\sigma ij}$. From Figs. 4.3 and 4.4, note that the fourth level is different for parametrization II with and without $8m^2$ in $u_{\sigma ij}$.

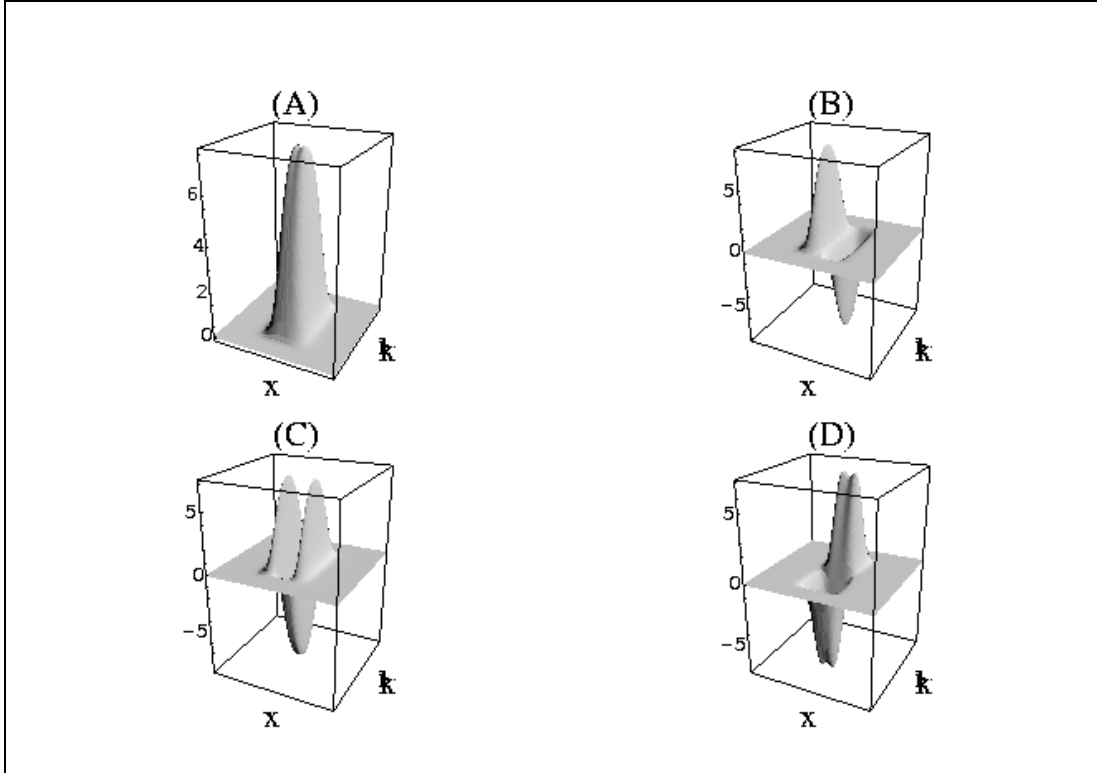


Figure 4.4: Same as in FIG. 4.3 but with $8m^2$ subtracted from ΣM_{ij}^2 .

By suitable choice of parameters we can study the interplay of rotationally symmetric logarithmically confining interaction and effective interactions generated by similarity transformation. Since for a given coupling constant g , strength of the logarithmic interaction and similarity generated interactions are determined by m and σ respectively, for $m \gg \sigma$ we should recover

the Bloch spectrum (Fig. 3.3). Upto what levels the recovery occurs, of course depends on the exact value of m and the energy scale σ at which the effective Hamiltonian is constructed. As we have already observed, for parametrization II this will happen only if $8m^2$ is subtracted from ΣM_{ij}^2 . For this case, we present the first four levels for $m = 10.0$ and $\sigma = 4.0$ in Fig. 4.5 which clearly shows the level spacing corresponding to the Bloch spectrum presented in Fig. 3.3.

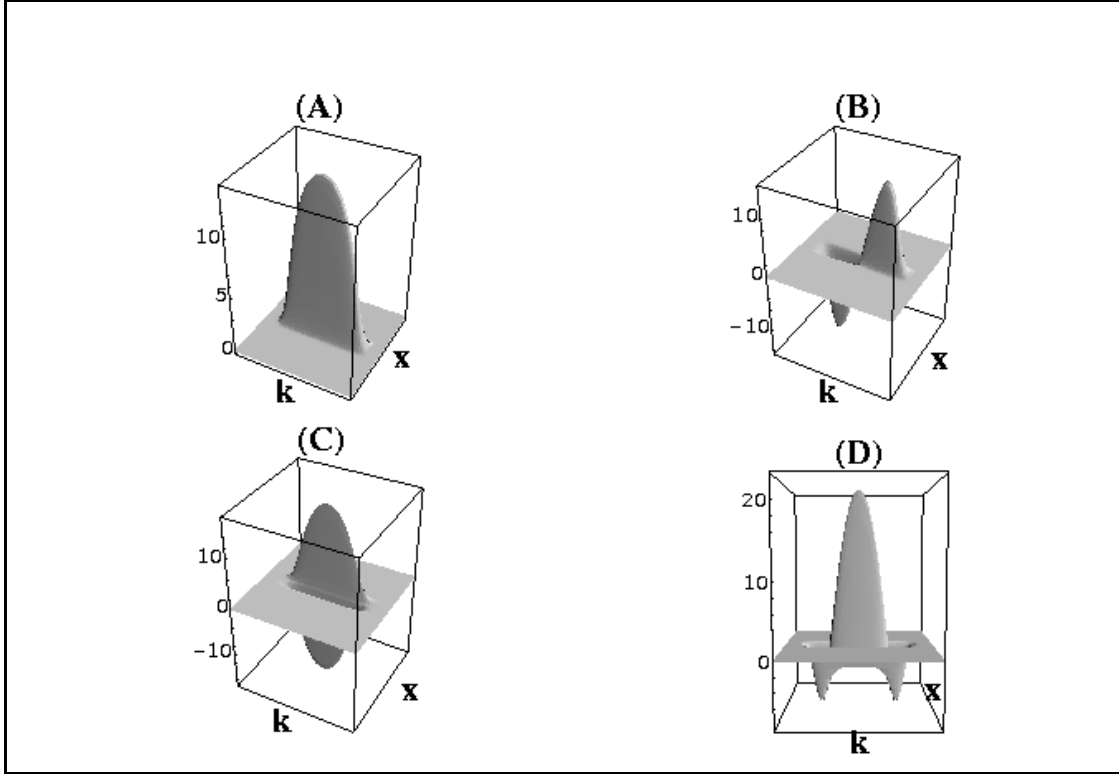


Figure 4.5: The wavefunctions corresponding to the lowest four eigenvalues as a function of x and k for large fermion mass with parametrization II with $8m^2$ subtracted from ΣM_{ij}^2 . The parameters are $m = 10.0$ $g = 0.2$, $\varepsilon = \delta = 0.00001$, $\kappa = 10.0$, $n_g = 2$, $u_0 = 0.1$, $n_1 = 40$, $n_2 = 80$. (A) Lowest state, (B) first excited state, (C) second excited state, (D) third excited state.

Finally, we discuss the sensitivity of the spectra to the similarity scale σ . Ideally the low lying energy levels should be insensitive to σ . However we have calculated the effective Hamiltonian to only order g^2 and we expect significant sensitivity to σ . In Tables 4.3 and 4.4 we present

Eigenvalues (M^2)					
σ	Parametrization I				
2.0	4.214	4.285	4.329	4.365	4.393
4.0	4.434	4.535	4.607	4.661	4.709
6.0	4.701	4.821	4.914	4.980	5.043
σ	Parametrization II				
2.0	4.157	4.214	4.248	4.260	4.276
4.0	4.201	4.272	4.315	4.350	4.367
6.0	4.266	4.350	4.404	4.446	4.483
σ	Parametrization III				
2.0	4.254	4.346	4.395	4.443	4.477
4.0	4.556	4.683	4.764	4.833	4.889
6.0	4.927	5.075	5.179	5.262	5.333

Table 4.3: Variation with σ of the full Hamiltonian (excluding the imaginary term). The parameters are $m = 1.0$, $g = 0.2$, $n_1 = 40$, $n_2 = 80$, $\varepsilon = 0.00001$, $\kappa = 10.0$, ($k = \frac{1}{\kappa} \tan(q\pi/2)$), $\delta = 0.00001$, ($u_0 = 0.1$, $n_g = 2$, and $n_s = 500$ for σ integration for parameterization II).

the lowest five eigenvalues for all three parametrizations of the similarity factor for $g = 0.2$ and $g = 0.6$ respectively. As expected σ dependence is greater for larger value of g .

Among the three parametrizations, the parametrization II is least sensitive to σ . In order to check whether this behaviour is due to the presence of $8m^2$ in ΣM_{ij}^2 in the definition of $u_{\sigma ij}$ we present the results in Table 4.5 for parametrization II with $8m^2$ subtracted from ΣM_{ij}^2 . It is clear that sensitivity to σ is still considerably less compared to the other two parametrizations. This may be due to the fact that ΣM_{ij}^2 is added to σ^2 in the definition of σ .

Note that in parametrization II sensitivity to σ is controlled also by additional parameters u_0 and n_g . The sharpness of the cutoff in this parametrization depends on n_g . The cutoff becomes sharper as one increases the value of n_g . σ dependence of the eigenvalues for two different n_g are presented in Tables 4.5 and 4.6. The other adjustable parameter u_0 is a small number ($u_0 \ll 1$) and the sensitivity to u_0 of the lowest five eigenvalue for the coupling $g = 0.6$ is presented in Table 4.7.

Eigenvalues (M^2)					
σ	Parametrization I				
2.0	4.941	5.418	5.708	5.713	5.950
4.0	5.684	6.421	6.909	7.306	7.647
6.0	6.678	7.617	8.274	8.801	9.267
σ	Parametrization II				
2.0	4.769	5.152	5.226	5.372	5.485
4.0	4.876	5.357	5.592	5.645	5.886
6.0	5.071	5.655	6.016	6.159	6.316
σ	Parametrization III				
2.0	4.888	5.589	5.882	6.120	6.263
4.0	5.966	6.972	7.518	8.077	8.465
6.0	7.359	8.603	9.360	10.083	10.621

Table 4.4: Variation with σ of the full hamiltonian (excluding the imaginary term). The parameters are $m = 1.0$, $g = 0.6$, $n_1 = 58$, $n_2 = 58$, $\varepsilon = 0.00001$, $\Lambda = 20.0$, ($k = \frac{q\Lambda m}{(1-q^2)\Lambda+m}$), $\delta = 0.00001$, ($u_0 = 0.1$, $n_g = 2$, and $n_s = 500$ for σ integration for parameterization II).

4.6 Summary and Discussion

From our results of Chapter 3, we know that the attempt to solve (2+1) dimensional gauge theories using the Bloch effective Hamiltonian is unseccessful due to problem of uncanceled infrared divergences. They arise out of vanishing energy denominators and a more sophisticated tool is necessary to handle the bound state problems in QCD. Similarity renormalization formalism attempts to solve the bound state problem in a two step process. At the first step, coupling between low and high energy degrees of freedom are integrated out and ultraviolet renormalization carried out perturbatively. In the second step, the effective Hamiltonian is diagonalized non-perturbatively.

Here I briefly summarize the main points addressed in this chapter. In order to have a better understanding of the numerical results, we have performed analytical calculations with step function form for the similarity factor. Many interesting results emerge from our analytical calculations. First of all, it is shown that due to the presence of instantaneous interactions in gauge theories on the light front, the logarithmic infrared divergence that appeared in the Bloch formalism persists in two places, namely a part of the self energy contribution and the Coloumb

		Eigenvalues (M^2)				
g	σ	Parametrization II				
0.2	2.0	4.126	4.166	4.176	4.189	4.201
	4.0	4.172	4.235	4.273	4.298	4.304
	6.0	4.241	4.321	4.371	4.411	4.445
0.6	2.0	4.739	5.003	5.020	5.134	5.193
	4.0	4.802	5.222	5.350	5.470	5.626
	6.0	4.993	5.541	5.876	5.940	6.156

Table 4.5: Variation with σ of the full Hamiltonian (excluding the imaginary term) after subtracting $8m^2$ from ΣM_{ij}^2 in the definition of $u_{\sigma ij}$. The parameters are $m = 1.0$, $\varepsilon = 0.00001$, $\delta = 0.00001$, $u_0 = 0.1$, $n_g = 2$, and $n_s = 500$

- 1) for $g = 0.2$, $k = \frac{1}{\kappa} \tan(q\pi/2)$ with $\kappa = 10.0$ and $n_1 = 40$, $n_2 = 80$
2) for $g = 0.6$, $k = \frac{q\Lambda m}{(1-q^2)\Lambda+m}$ with $\Lambda = 20.0$, and $n_1 = n_2 = 58$.

g	σ	M^2 (Parameterization II)				
0.6	2.0	4.781	5.049	5.051	5.161	5.221
	4.0	4.843	5.235	5.391	5.464	5.639
	6.0	5.030	5.538	5.848	5.956	6.106

Table 4.6: Variation with σ of the full Hamiltonian(excluding the imaginary term) after subtracting the $8m^2$ term from ΣM_{ij}^2 in the definition of $u_{\sigma ij}$. The parameters are $m = 1.0$, $\varepsilon = 0.00001$, $\delta = 0.00001$, $u_0 = 0.1$, $n_g = 1$, and $n_s = 500$ $g = 0.6$, $k = \frac{q\Lambda m}{(1-q^2)\Lambda+m}$ with $\Lambda = 20.0$, and $n_1 = n_2 = 58$.

interaction that gives rise to the logarithmically confining potential in the nonrelativistic limit. However the terms that persist are precisely those that produce a cancellation of resulting infrared divergences in the bound state equation. The rest of the infrared problem that appeared in the Bloch formalism due to the vanishing energy denominator problem is absent in the similarity formalism.

Similarity transformation however prevents the cancellation of the most severe $\frac{1}{(x-y)^2}$ singularity between instantaneous gluon exchange and transverse gluon exchange interactions and

g	u_0	M^2 (Parameterization II)				
0.6	0.2	4.990	5.548	5.887	5.969	6.171
	0.1	4.802	5.222	5.350	5.469	5.626
	0.05	4.746	5.076	5.091	5.253	5.313
	0.01	4.813	5.003	5.029	5.069	5.130

Table 4.7: Variation with u_0 of the full Hamiltonian(excluding the imaginary term) after subtracting the $8m^2$ term from ΣM_{ij}^2 in the definition of $u_{\sigma ij}$. The parameters are $m = 1.0$, $\varepsilon = 0.00001$, $\delta = 0.00001$, $\sigma = 4.0$, $n_g=2$, and $n_s = 500$ $g = 0.6$, $k = \frac{q\Lambda m}{(1-q^2)\Lambda+m}$ with $\Lambda = 20.0$, and $n1 = n2 = 58$.

produces $\frac{1}{\sqrt{\delta}}$ divergences in the self energy and gluon exchange contributions which cancel between the two in the bound state equation. The resulting effective interaction between the quark and antiquark grows linearly with large transverse separation but grows only with the square root of the longitudinal separation. This produces severe violations of rotational symmetry in the bound state spectrum. We have also verified that no $\ln \delta$ divergence results from the $\frac{1}{x-y}$ singularity in the self energy and gluon exchange contributions.

In the Głazek-Wilson formalism the exact form of the similarity factor f_σ is left unspecified. In the literature an exponential form has been used in numerical calculations [15]. For analytical calculations it is convenient to choose a step function even though it is well known that it is not suitable for quantitative calculations [5]. There is also a proposal due to Stan Głazek which has two extra free parameters. We have tested all three parametrizations. Our numerical results indeed show that step function choice always produces non-smooth wavefunctions. Parameterization II costs us an extra integration to be performed numerically but convergence is slightly better for small g compared to exponential form. All three parametrizations produce violations of rotational symmetry even for small g . When an exponential form is used in the Głazek-Wilson formalism, the resulting effective Hamiltonian differs from the Wegner form only by an overall factor that restricts large energy differences between initial and final states. Numerically we have found this factor to be insignificant.

We have studied the sensitivity of the low lying eigenvalues to the similarity scale σ . Since the effective Hamiltonian is calculated only to order g^2 results do show sensitivity to σ . Among

the three parametrizations the form II is least sensitive to σ due to the functional form chosen. We have also studied the sensitivity of eigenvalues to the parameters u_0 and n_g .

The bound state equation has three parameters m , g^2 and σ with dimension of mass. The strength of the logarithmically confining interaction is determined by m and the strength of the rotational symmetry violating effective interactions generated by similarity transformation is determined by σ . For a given g we expect the former to dominate over the latter for $m \gg \sigma$. An examination of low lying eigenvalues and corresponding wavefunctions show that this is borne out by our numerical calculations.

A major problem in the calculations is the slow convergence. Compared to the Bloch formalism, in calculations with the similarity formalism, various factors may contribute to this problem with the Gauss quadrature points. One important factor is the presence of linear and square root confining interactions generated by the similarity transformation. It is well known that such interactions are highly singular in momentum space. Another factor is the presence of $\frac{1}{\sqrt{\delta}}$ divergences, the cancellation of which is achieved numerically. It is of interest to carry out the same calculations with numerical procedures other than the Gauss quadrature. However, one should note that calculations in (3+1) dimensions employing basis functions and splines have also yielded [15] wavefunctions which show non-smooth structures.

An undesirable result of the similarity transformation carried out in perturbation theory is the violation of rotational symmetry. Our results show that this violation persists at all values of g for $m = 1$. Such a violation was also observed in (3+1) dimensions. In that case the functional form of the logarithmic potential generated by similarity transformation is the same in longitudinal and transverse directions but the coefficients differ by a factor of two. Same mechanism in (2+1) dimensions makes even the functional forms different. The important questions are whether the confining interactions generated by the similarity transformation are an artifact of the lowest order approximation and if they are not, then, whether the violation of rotational symmetry will diminish with higher order corrections to the effective Hamiltonian. Recall that matrix element between low and high energy degrees of freedom has been integrated out and the effective low energy Hamiltonian determined only to order g^2 . A clear answer will emerge only after the determination of the effective Hamiltonian to fourth order in the coupling.

BIBLIOGRAPHY

- [1] E. C. Stueckelberg and A. Petermann, *Helv. Phys. Acta* **26**, 499 (1953).
- [2] M. Gell-Mann and F. E. Low, *Phys. Rev.* **95**, 1300 (1954).
- [3] N. N. Bogoliubov and D. V. Shirkov, *Introduction to the Theory of Quantized Fields* (Interscience, New York, 1959).
- [4] K. G. Wilson, *Phys. Rev. B* **4**, 3174, 3184 (1971).
- [5] K. G. Wilson and J. Kogut, *Phys. Rep.* **12**, 75 (1974).
- [6] K. G. Wilson, *Rev Mod. Phys.* **47**, 773 (1975), *ibid.* **55**, 583 (1983).
- [7] R. J. Perry and S. Szpigel, The Similarity renormalization Group, in *Quantum Field Theory, A 20th Century Profile*, edited by A. N. Mitra, (Hindustan Book Agency and Indian National Science Academy, 2000), hep-ph/0009071.
- [8] S. D. Głazek and K. G. Wilson, *Phys. Rev. D* **48**, 5863 (1993); **49**, 4214 (1994).
- [9] F. Wegner, *Ann. Phys. (Leipzig)* **3**, 77 (1994).
- [10] K. G. Wilson, T. S. Walhout, A. Harindranath, W. Zhang, R. J. Perry and S. D. Głazek, *Phys. Rev. D* **49**, 6720 (1994), hep-th/9401153.
- [11] See for example, *Numerical Recipes in Fortran: The Art of Scientific Computing*, William H. Press, Saul A. Teukolsky, William T. Vetterling, and Brian P. Flannery, Second Edition, (Cambridge University Press, Cambridge, 1988).
- [12] R. J. Perry, Hamiltonian Light Front Field Theory and Quantum Chromodynamics, in *Hadron Physics '94: Topics on the Structure and Interaction of Hadron Systems*, Proceedings, Gramado, Brazil, edited by V. Hercovitz *et al.*, (World Scientific, Singapore 1995), hep-th/9407056.
- [13] M. Brisudova and R. Perry, *Phys. Rev. D* **54**, 1831 (1996), hep-ph/9511443; M. Brisudova, R. J. Perry and K. G. Wilson, *Phys. Rev. Lett.* **78**, 1227 (1997), hep-ph/9607280.
- [14] W. M. Zhang, *Phys. Rev. D* **56**, 1528 (1997), hep-ph/9705226.
- [15] B. H. Allen and R. J. Perry, *Phys. Rev. D* **62**, 025005 (2000), hep-th/9908124; R. D. Kylin, Ph. D. Thesis, hep-ph/0103129.
- [16] D. Chakrabarti and A. Harindranath, *Phys. Rev. D* **64**, 105002 (2001), hep-th/0107188.

- [17] D. Chakrabarti and A. Harindranath, Phys. Rev. D **65**, 045001 (2002), hep-th/0110156.
- [18] C. Bloch, Nucl. Phys. **6**, 329 (1958); K. G. Wilson, Phys. Rev. D **2**, 1438 (1970); R. J. Perry, Ann. Phys. **232**, 116 (1994), hep-th/9402015.
- [19] S. D. Głazek, Acta Phys. Polon. B **29**, 1979 (1998), hep-th/9712188.
- [20] E. Anderson *et al.*, *LAPACK Users' Guide*, third edition (Society for Industrial and Applied Mathematics, Philadelphia, 1999). Available on the internet at the URL: <http://www.netlib.org/lapack/lug/index.html>.

CHAPTER 5

Fermion Formulation on a Light-Front Transverse Lattice

5.1 Introduction

In the previous two chapters we have discussed the meson bound state problem in (2+1) dimensions in the light-front framework using Bloch and similarity effective Hamiltonians and have seen that light-front framework provides the opportunity for non-perturbative studies in Hamiltonian formalism. In this chapter we introduce another approach in light-front Hamiltonian framework.

Till date, the most practiced non-perturbative technique is the lattice gauge theory [1]. Using path integral formalism in Euclidean space, with no gauge fixing one calculates the n-point Green functions, but no direct informations about the bound state wavefunctions are accessible in this approach. Hamiltonian formalism provides bound state wavefunctions in a straightforward way. Since boosts are kinematical, one can have frame independent description of the bound state wavefunctions in light-front framework. One extra advantage of lattice gauge theory over light-front formalism is full gauge invariance. Light front Hamiltonian formulation of transverse lattice QCD [2, 3] is an optimum combination of lattice gauge theory and light-front QCD. It uses the power of light-front Hamiltonian formalism to produce the boost invariant wavefunctions and the advantage of having gauge invariant ultraviolet cutoff from lattice gauge theory. With the gauge choice $A^+ = A^0 + A^3 = 0$ and the elimination of the constrained variable $A^- = A^0 - A^3$, it uses minimal gauge degrees of freedom in a manifestly gauge invariant formulation exploiting the residual gauge symmetry in this gauge.

For Hamiltonian formalism light-front time (x^+) is kept continuous. Due to the constraint equations in fermion and gauge degrees of freedom in the light-front, non-locality comes in the longitudinal direction. Also there is no ultraviolet divergences coming from small x^- and hence

x^- is not latticized. Ultraviolet divergences come only from small transverse separations which we want to regulate with gauge invariant cutoff. Thus, the transverse plane ($x^\perp = (x^1, x^2)$) is discretized on a square lattice. This defines the light-front transverse lattice (LFTL) in (3+1) dimensions. It is a promising and developing tool for non-perturbative investigations of QCD. So far encouraging results have been obtained in the pure gauge sector [4] and in the meson sector with particle number truncation (for a recent review see, Ref. [5]).

It is well known that fermions on the lattice pose challenging problems due to the doubling phenomenon. Light-front formulation of field theory has its own peculiarities concerning fermions because of the presence of a constraint equation. As an example, the usual chiral transformation on the four component fermion field is incompatible with the constraint equation for nonzero fermion mass [6]. There have been previous studies of fermions on the transverse lattice [7, 8, 9, 10] in different contexts. But properties and origin of species doubling of fermion on light-front transverse lattice were not studied with proper care and desired details. So, before embarking on any QCD calculation on transverse lattice, it is better to understand the fermions on it in detail. I devote this chapter to discuss different ways of formulating fermion on a light-front transverse lattice and related issues such as absence or origin of doublers, different ways of removing doublers, relevant symmetry on light-front transverse lattice and so on [11].

As we shall see later in this chapter, the presence of the constraint equation in light front field theory allows different methods to put fermions on a transverse lattice. It is worthwhile to study all the different methods in order to examine their strengths and weaknesses. Here I should also mention two important points. One, our ultimate aim is to calculate QCD observables on LFTL where we deal with a Hamiltonian acting on a Fock space. For a reasonable size of Fock space, computing limitations will force us to be in a reasonably small lattice volume when we deal with realistic problems. The second point is that the currently practiced version of the transverse lattice gauge theory uses *linear* link variables [2, 3] justified on a coarse lattice and recovering continuum physics is nontrivial. Hence it is very important to carry out detailed numerical investigation of all the possible ways of formulating fermions on LFTL with proper attention to the finite volume effects.

In one of the approaches of treating fermions on the light front transverse lattice, we maintain as much transverse locality as possible on the lattice by using forward and backward lattice

derivatives without spoiling the hermiticity of the Hamiltonian. In this case doublers are not present and the helicity flip term proportional to the fermion mass in the full light front QCD becomes an irrelevant term in the free field limit. Thus in finite volume, depending on the boundary condition used, the two helicity states of the fermion may not be degenerate in the free field limit. However, we find that in the infinite volume limit the degeneracy is restored irrespective of the boundary condition.

In the second approach [8], symmetric derivatives are used which results in a Hamiltonian with only next to nearest neighbor interaction when we take the free field limit. As a consequence even and odd lattice sites decouple and the fermions live independently of each other on the two sets of sites. As a result we get four species of fermions on a two dimensional lattice as excitations around zero transverse momentum. Note that this is quite different from what one gets in the conventional Euclidean lattice theory when one uses symmetric derivatives. In that case, doublers have at least one momentum component near the edge of the Brillouin zone. The doublers can be removed in more than one way. We also study the staggered fermion formulation on the light front transverse lattice to eliminate two doublers and reinterpret the remaining two as two flavors. In this light front staggered fermion formulation, there is no flavor mixing in free field limit. But, in QCD, we get irrelevant flavor mixing terms. An alternative which removes doubling completely is to add the conventional Wilson term which generates many irrelevant interactions on the transverse lattice. Among them, the helicity flip interactions vanish but the helicity non flip interactions survive in the free field limit.

5.2 Hamiltonian with forward and backward derivatives

5.2.1 Construction

In this section we propose to use different lattice derivatives for dynamical and constrained fermion field components on the transverse lattice in such a way that sacred Hermiticity of the Hamiltonian is preserved. The starting point of our discussion is the fermionic part of the QCD Lagrangian density

$$\mathcal{L}_f = \bar{\psi}(i\gamma^\mu D_\mu - m)\psi \tag{5.1}$$

with $iD^\mu = i\partial^\mu - gA^\mu$. Since fermions on LFTL are our main concern in this chapter, we omit the pure gauge part from QCD Lagrangian.

Moving to the light front coordinates we impose the light-cone gauge $A^+ = 0$ and introduce the transverse lattice by discretizing the transverse plane on a square lattice with lattice spacing a . Now, \mathcal{L}_f on the LFTL can be written as

$$\begin{aligned}\mathcal{L}_f = & \psi^{+\dagger}(i\partial^- - gA^-)\psi^+ + \psi^{-\dagger}i\partial^+\psi^- \\ & - i\psi^{-\dagger}\alpha_r D_r^f \psi^+ - i\psi^{+\dagger}\alpha_r D_r^b \psi^- \\ & - m\psi^{-\dagger}\gamma^0\psi^+ - m\psi^{+\dagger}\gamma^0\psi^-.\end{aligned}\tag{5.2}$$

Here $r = 1, 2$ and $D_r^{f/b}$ is the forward/backward covariant lattice derivative defined as

$$D_r^f \eta(\mathbf{x}) = \frac{1}{a}[U_r(\mathbf{x})\eta(\mathbf{x} + a\hat{\mathbf{r}}) - \eta(\mathbf{x})]\tag{5.3}$$

and

$$D_r^b \eta(\mathbf{x}) = \frac{1}{a}[\eta(\mathbf{x}) - U_r^\dagger(\mathbf{x} - a\hat{\mathbf{r}})\eta(\mathbf{x} - a\hat{\mathbf{r}})],\tag{5.4}$$

where a is the lattice constant and $\hat{\mathbf{r}}$ is unit vector in the direction $r = 1, 2$ and $D_r^{f\dagger} = -D_r^b$. $U_r(\mathbf{x})$ is the group valued lattice gauge field with the property $U_r^\dagger(\mathbf{x}) = U_{-r}(\mathbf{x} + a\hat{\mathbf{r}})$. In the weak coupling limit

$$U_r(\mathbf{x}) \approx e^{igaA_r(\mathbf{x} + a\hat{\mathbf{r}}/2)}.\tag{5.5}$$

For notational convenience we suppress x^- in the arguments of the fields.

Our goal here is to write the most local lattice derivative. That is why, instead of using the symmetric lattice derivative, in the above we have used the forward and backward lattice derivatives. However, the Hermiticity of the Lagrangian (Hamiltonian) requires that if one of the covariant lattice derivatives appearing in Eq. (5.2) is the forward derivative, the other has to be the backward derivative or vice versa.

The constraint equation is

$$i\partial^+\psi^- = (i\alpha_r D_r^f + \gamma^0 m)\psi^+.\tag{5.6}$$

Eliminating the constrained field component ψ^- in terms of dynamical field ψ^+ , we obtain

$$\begin{aligned}
\mathcal{L}_f &= \psi^{+\dagger}(i\partial^- - gA^-)\psi^+ - m\psi^{+\dagger}\gamma^0\psi^- - i\psi^{+\dagger}\alpha_r D_r^b \psi^- \\
&= \psi^{+\dagger}(i\partial^- - gA^-)\psi^+ \\
&\quad - \psi^{+\dagger}[i\alpha_r D_r^b + \gamma^0 m] \frac{1}{i\partial^+} [i\alpha_s D_s^f + \gamma^0 m] \psi^+. \tag{5.7}
\end{aligned}$$

The dynamical field ψ^+ can essentially be represented by two components [12] such that

$$\psi^+(x^-, x^\perp) = \begin{bmatrix} \eta(x^-, x^\perp) \\ 0 \end{bmatrix}, \tag{5.8}$$

where η is a two component field. Finally going over to the two component fields η , the Lagrangian density can be written as

$$\begin{aligned}
\mathcal{L}_f &= \eta^\dagger(i\partial^- - gA^-)\eta \\
&\quad - \eta^\dagger[i\hat{\sigma}_r D_r^b - im] \frac{1}{i\partial^+} [i\hat{\sigma}_s D_s^f + im] \eta. \tag{5.9}
\end{aligned}$$

$\hat{\sigma}_1 = \sigma_2$ and $\hat{\sigma}_2 = -\sigma_1$ where σ_i are Pauli spin matrices. Writing explicitly in terms of the link variables, the Lagrangian density is

$$\begin{aligned}
\mathcal{L}_f &= \eta^\dagger(\mathbf{x})(i\partial^- - gA^-)\eta(\mathbf{x}) - m^2\eta^\dagger(\mathbf{x})\frac{1}{i\partial^+}\eta(\mathbf{x}) \\
&\quad - m\eta^\dagger(\mathbf{x})\sum_r \hat{\sigma}_r \frac{1}{a} \frac{1}{i\partial^+} [U_r(\mathbf{x})\eta(\mathbf{x} + a\hat{\mathbf{r}}) - \eta(\mathbf{x})] \\
&\quad - m\sum_r [\eta^\dagger(\mathbf{x} + a\hat{\mathbf{r}})U_r^\dagger(\mathbf{x}) - \eta^\dagger(\mathbf{x})] \hat{\sigma}_r \frac{1}{a} \frac{1}{i\partial^+} \eta(\mathbf{x}) \\
&\quad - \frac{1}{a^2} \sum_{r,s} [\eta^\dagger(\mathbf{x} + a\hat{\mathbf{r}})U_r^\dagger(\mathbf{x}) - \eta^\dagger(\mathbf{x})] \hat{\sigma}_r \frac{1}{i\partial^+} \hat{\sigma}_s [U_s(\mathbf{x})\eta(\mathbf{x} + a\hat{\mathbf{s}}) - \eta(\mathbf{x})]. \tag{5.10}
\end{aligned}$$

In the free limit the fermionic part of the Hamiltonian becomes

$$\begin{aligned}
P_{fb}^- &= \int dx^- a^2 \sum_{\mathbf{x}} \mathcal{H} \\
&= \int dx^- a^2 \sum_{\mathbf{x}} \left[m^2\eta^\dagger(\mathbf{x})\frac{1}{i\partial^+}\eta(\mathbf{x}) \right. \\
&\quad - \frac{1}{a^2}\eta^\dagger(\mathbf{x})\sum_r \frac{1}{i\partial^+} [\eta(\mathbf{x} + a\hat{\mathbf{r}}) - 2\eta(\mathbf{x}) + \eta(\mathbf{x} - a\hat{\mathbf{r}})] \\
&\quad \left. + \frac{1}{a^2}\eta^\dagger(\mathbf{x})\sum_r (am\hat{\sigma}_r) \frac{1}{i\partial^+} [\eta(\mathbf{x} + a\hat{\mathbf{r}}) - 2\eta(\mathbf{x}) + \eta(\mathbf{x} - a\hat{\mathbf{r}})] \right]. \tag{5.11}
\end{aligned}$$

In order to get Eq. (5.11), we have assumed infinite transverse lattice and accordingly have used shifting of lattice points which is equivalent of neglecting surface terms. The positive sign in front of the last term would change if we had switched forward and backward derivatives. One should note that the cross term coming from the last line of Eq. (5.10) survives in the free field limit. Explicitly, the term is

$$\frac{1}{a^2} \sum_{r \neq s} [\eta^\dagger(\mathbf{x} + a\hat{\mathbf{r}}) - \eta(\mathbf{x})] \hat{\sigma}_r \frac{1}{i\partial^+} \hat{\sigma}_s [\eta(\mathbf{x} + a\hat{\mathbf{s}}) - \eta(\mathbf{x})]. \quad (5.12)$$

It produces extra helicity nonflip hoppings in the transverse plane. In the continuum limit ($a \rightarrow 0$) this term does not survive and one can recover the right continuum limit without this cross term. If one demands hypercubic (square) symmetry of the transverse lattice, then this cross term (Eq. (5.12)) vanishes. More detailed discussion about this term is provided in Appendix F.

Because of the presence of $\hat{\sigma}_r$, the last term of Eq. (5.11) couples fermions of opposite helicities. Note that it is also linear in mass. Such a helicity flip linear mass term is typical in continuum light-front QCD. Here in free transverse lattice theory this term arises from the interference of the first order derivative term and the mass term, due to the constraint equation. This is in contrast to the conventional lattice (see Appendix G) where no helicity flip or chirality-mixing term arises in the free theory if we use forward and backward lattice derivatives.

5.2.2 Absence of doubling

Consider the Fourier transform in transverse space

$$\eta(x^-, \mathbf{x}) = \int \frac{d^2k}{(2\pi)^2} e^{i\mathbf{k}\cdot\mathbf{x}} \phi_{\mathbf{k}}(x^-) \quad (5.13)$$

where $-\frac{\pi}{a} \leq k_1, k_2 \leq +\frac{\pi}{a}$. Then the helicity nonflip part of Eq. (5.11) becomes

$$P_{nf}^- = \int dx^- \int \frac{d^2k}{(2\pi)^2} \int \frac{d^2p}{(2\pi)^2} \phi_{\mathbf{k}}^\dagger(x^-) \frac{1}{i\partial^+} \phi_{\mathbf{p}}(x^-) a^2 \sum_{\mathbf{x}} e^{-i(\mathbf{k}-\mathbf{p})\cdot\mathbf{x}} \left[m^2 - \sum_r \frac{1}{a^2} [e^{i\mathbf{p}\cdot a\hat{\mathbf{r}}} - 2 + e^{-i\mathbf{p}\cdot a\hat{\mathbf{r}}}] \right]. \quad (5.14)$$

Using

$$a^2 \sum_{\mathbf{x}} e^{i(\mathbf{k}-\mathbf{p})\cdot\mathbf{x}} = (2\pi)^2 \delta^2(\mathbf{k}-\mathbf{p}) \quad (5.15)$$

we get,

$$P_{nf}^- = \int dx^- \int \frac{d^2k}{(2\pi)^2} \phi_{\mathbf{k}}^\dagger(x^-) \frac{1}{i\partial^+} \phi_{\mathbf{k}}(x^-) \left[m^2 + \sum_r k_r^2 \left(\frac{\sin k_r a/2}{k_r a/2} \right)^2 \right] \quad (5.16)$$

where we have defined $k_r a = \mathbf{k} \cdot \hat{\mathbf{r}} a$. Note that the *sine* function vanishes at the origin $k_1, k_2 = 0$ but does not vanish at the edges of the Brillouin zone $k_1, k_2 = \pm \frac{\pi}{a}$.

Define $\tilde{k}_r = k_r \frac{\sin k_r a/2}{k_r a/2}$. In the naive continuum limit $\tilde{k}_r \rightarrow k_r$.

Now, let us consider the full Hamiltonian (Eq. 5.11) including the helicity flip term. In the helicity space we have the following matrix structure for $P^+ P^-$ (since P^- is inversely proportional to the total longitudinal momentum P^+ , we study the operator $P^+ P^-$)

$$\begin{pmatrix} m^2 + \frac{4}{a^2} \sum_r \sin^2 \frac{k_r a}{2} & -\frac{4m}{a} (i \sin^2 \frac{k_x a}{2} + \sin^2 \frac{k_y a}{2}) \\ \frac{4m}{a} (i \sin^2 \frac{k_x a}{2} - \sin^2 \frac{k_y a}{2}) & m^2 + \frac{4}{a^2} \sum_r \sin^2 \frac{k_r a}{2} \end{pmatrix} \quad (5.17)$$

which leads to the eigenvalue equation

$$\mathcal{M}^2 = m^2 + \frac{4}{a^2} \sum_r \sin^2 \frac{k_r a}{2} \pm \frac{4m}{a} \sqrt{\sum_r \sin^4 \frac{k_r a}{2}}. \quad (5.18)$$

Third term in the above equation comes from the linear mass helicity flip term. If the mass $m = 0$, then it is obvious from Eq. (5.18) that $\mathcal{M}^2 = 0$ if and only if $k_1 = k_2 = 0$. For nonzero m , one can also in general conclude that $\mathcal{M}^2 = m^2$ only for the case $k_1 = k_2 = 0$. Thus there are no fermion doublers in this case (for physical masses $am < 1$). In the following for specific choices of momenta we elaborate on this further.

If one component of the momentum vanishes, then

$$\mathcal{M}^2 = m^2 + \frac{4}{a} \left(\frac{1}{a} \pm m \right) \sin^2 \frac{ka}{2} \quad (5.19)$$

where k is the non-vanishing momentum component. Thus for $am = 1$, irrespective of the value of k we get $\mathcal{M}^2 = m^2$ which is unwanted. In general, for $am > 1$, \mathcal{M}^2 can become negative. It is important to recall that physical particles have $m < \frac{1}{a}$ (the lattice cutoff) and hence are free from the species doubling on the lattice. With periodic boundary condition (discussed in the next subsection), allowed k values are $k_q a = \pm \frac{2\pi q}{2n+1}$, with $q = 1, 2, 3, \dots, n$ for $2n+1$ lattice sites in each direction. Let $k_1 = 0$. For $ma = 1.0$, Eq. (5.19) with the minus sign within the bracket gives $\mathcal{M}^2 = m^2$ for all values of k_2 and we get $2(2n+1)$ -fold degenerate ground state with

eigenvalue m^2 .

The two spin states (spin up and down) are degenerate for $k_1 = k_2 = 0$. But if any one (or both) of the two transverse momenta is (are) nonzero then the degeneracy is broken on the lattice by the spin flip term proportional to m . So the total degeneracy of the lowest states for $ma = 1.0$ can be calculated in the following way: (a) $k_1 = k_2 = 0$: Number of states =2 (spin up and spin down), (b) $k_1 = 0, k_2 \neq 0$: Number of states = $2n$ and (c) $k_1 \neq 0, k_2 = 0$: Number of states = $2n$. Note that k_i can have $2n$ nonzero values and there is no spin degeneracy for any nonzero k_i . So, the total number of degenerate states = $2 + 2n + 2n = 2(2n + 1)$. But if $ma \neq 1$ we cannot have m^2 eigenvalue for nonzero k_i and we have only two (spin) degenerate states with eigenvalue m^2 . Again we see from Eq. (5.19) that if $ma > 1$, the kinetic energy term becomes negative and the eigenvalues go below m^2 . But $ma \geq 1$ means $m \geq \frac{1}{a}$ (ultra violet lattice cutoff) and hence unphysical.

5.2.3 Numerical Investigation

For numerical investigations we use Discretized Light Cone Quantization (DLCQ) [13] for the longitudinal direction ($-L \leq x^- \leq +L$) and implement antiperiodic boundary condition to avoid zero modes. Then,

$$\eta(x^-, \mathbf{x}) = \frac{1}{\sqrt{2L}} \sum_{\lambda} \chi_{\lambda} \sum_{l=1,3,5,\dots} [b(l, \mathbf{x}, \lambda) e^{-i\pi l x^- / (2L)} + d^{\dagger}(l, \mathbf{x}, -\lambda) e^{i\pi l x^- / (2L)}] \quad (5.20)$$

with

$$\{b(l, \mathbf{x}, \lambda), b^{\dagger}(l', \mathbf{x}', \lambda')\} = \{d(l, \mathbf{x}, \lambda), d^{\dagger}(l', \mathbf{x}', \lambda')\} = \delta_{ll'} \delta_{\mathbf{x}, \mathbf{x}'} \delta_{\lambda, \lambda'}. \quad (5.21)$$

In DLCQ with antiperiodic boundary condition, it is usual to multiply the Hamiltonian P^- by $\frac{\pi}{L}$, so that $H = \frac{\pi}{L} P^-$ has the dimension of mass squared.

In DLCQ the Hamiltonian (Eq. 5.11) can be written as,

$$H_{fb} = H_0 + H_{hf} \quad (5.22)$$

where, the helicity nonflip part

$$H_0 = \sum_{\mathbf{z}} \sum_{\lambda} \sum_l \frac{a^2 m^2}{l} \left[b^{\dagger}(l, \mathbf{z}, \lambda) b(l, \mathbf{z}, \lambda) + d^{\dagger}(l, \mathbf{z}, \lambda) d(l, \mathbf{z}, \lambda) \right]$$

$$\begin{aligned}
& - \sum_{\mathbf{z}} \sum_r \sum_{\lambda} \sum_{\lambda'} \sum_l \frac{1}{l} \chi_{\lambda'}^{\dagger} \chi_{\lambda} \left[b^{\dagger}(l, \mathbf{z}, \lambda') b(l, \mathbf{z} + a\hat{\mathbf{r}}, \lambda) - 2b^{\dagger}(l, \mathbf{z}, \lambda') b(l, \mathbf{z}, \lambda) \right. \\
& + b^{\dagger}(l, \mathbf{z}, \lambda') b(l, \mathbf{z} - a\hat{\mathbf{r}}, \lambda) + d^{\dagger}(l, \mathbf{z}, \lambda') d(l, \mathbf{z} + a\hat{\mathbf{r}}, \lambda) - 2d^{\dagger}(l, \mathbf{z}, \lambda') d(l, \mathbf{z}, \lambda) \\
& \left. + d^{\dagger}(l, \mathbf{z}, \lambda') d(l, \mathbf{z} - a\hat{\mathbf{r}}, \lambda) \right] \tag{5.23}
\end{aligned}$$

and helicity flip term

$$\begin{aligned}
H_{hf} = & \sum_{\mathbf{z}} \sum_r \sum_{\lambda} \sum_{\lambda'} \sum_l \frac{1}{l} \chi_{\lambda'}^{\dagger} [am\hat{\sigma}^r] \chi_{\lambda} \left[b^{\dagger}(l, \mathbf{z}, \lambda') b(l, \mathbf{z} + a\hat{\mathbf{r}}, \lambda) \right. \\
& - 2b^{\dagger}(l, \mathbf{z}, \lambda') b(l, \mathbf{z}, \lambda) + b^{\dagger}(l, \mathbf{z}, \lambda') b(l, \mathbf{z} - a\hat{\mathbf{r}}, \lambda) + d^{\dagger}(l, \mathbf{z}, \lambda') d(l, \mathbf{z} + a\hat{\mathbf{r}}, \lambda) \\
& \left. - 2d^{\dagger}(l, \mathbf{z}, \lambda') d(l, \mathbf{z}, \lambda) + d^{\dagger}(l, \mathbf{z}, \lambda') d(l, \mathbf{z} - a\hat{\mathbf{r}}, \lambda) \right]. \tag{5.24}
\end{aligned}$$

Let us now investigate the Hamiltonian (Eq. 5.22) with two types of boundary conditions on the transverse lattice: (1) fixed boundary condition and (2) periodic boundary condition. For each transverse direction, we choose $2n + 1$ lattice points ranging from $-n$ to $+n$ where fermions are allowed to hop. For the study of the fermion spectra on the transverse lattice, the longitudinal momentum plays a passive role and for the numerical studies we choose the dimensionless longitudinal momentum (l) to be unity which is kept fixed. For a given set of lattice points in the transverse space we diagonalize the Hamiltonian and compute both eigenvalues and eigenfunctions.

Boundary conditions

Fixed boundary condition: To implement fixed boundary condition we add two more points at the two ends and demand that the fermion remains fixed at these lattice points. Thus we consider $2n + 3$ lattice points. Let us denote the fermion wavefunction at the location s by $u(s)$. We have $u(s) \sim \sin(s - 1)ka$ with $u(1) = u(2n + 3) = 0$. Allowed values of k are $(2n + 2)k_p a = p\pi$ with $p = 1, 2, 3, \dots, 2n + 1$ and $k_p = \frac{\pi}{(2n+2)a}p$. Thus the minimum k_p allowed is $\frac{\pi}{a} \frac{1}{(2n+2)}$ and maximum k_p allowed is $\frac{\pi}{a} \frac{(2n+1)}{(2n+2)}$. For example, for $n = 1$ we have $k_1 = \frac{\pi}{4a}$, $k_2 = \frac{2\pi}{4a}$, $k_3 = \frac{3\pi}{4a}$, etc.

Periodic boundary condition: Periodic boundary condition identifies the $(2n + 2)^{th}$ lattice point with the first lattice point. In this case we have the fermion wavefunction $u(s) \sim e^{iska}$ with the condition $u(s) = u(s + L)$ where $L = 2n + 1$. Thus $(2n + 1)k_p a = \pm 2\pi p$ so that $k_p =$

$\pm \frac{2\pi}{(2n+1)a}p$, $p = 0, 1, 2, \dots, n$. Thus the minimum k_p allowed is 0 and the maximum k_p allowed is $\frac{2n\pi}{(2n+1)a}$. For $n = 1$, we have, $k_0 = 0, k_1 = \pm \frac{2\pi}{3a}$, etc.

Numerical results

First we discuss the results for H_0 given in Eq. (5.23). We diagonalize the Hamiltonian using basis states defined at each lattice point in a finite region in the transverse plane. Let us denote a general lattice point in the transverse plane by (x_i, y_i) . For each choice of n (measure of the linear lattice size), we have $-n \leq x_i, y_i \leq +n$. Thus for a given n , we have a $(2n+1) \times (2n+1)$ dimensional matrix for the Hamiltonian. The boundary conditions do have significant effects at

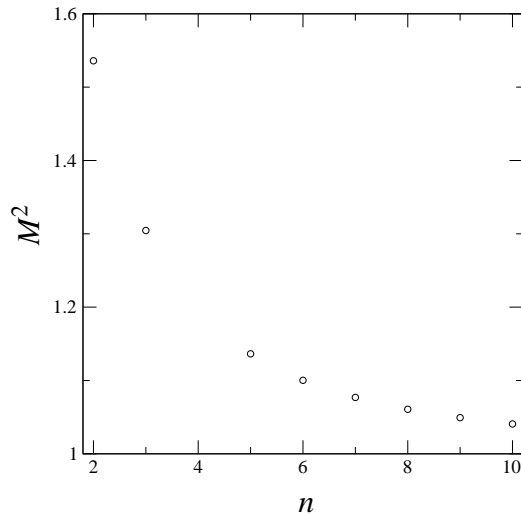


Figure 5.1: Convergence of ground state eigenvalue (of forward-backward Hamiltonian) versus n ($m = 1.0$).

small volumes. For example, a zero transverse momentum fermion at finite n is not allowed with fixed boundary condition. But with periodic boundary condition, we can have zero transverse momentum fermion for any finite n . With fixed boundary condition, in the infinite volume limit, we expect the lowest eigenstate to be the zero transverse momentum fermion with the eigenvalue m^2 . In Fig. 5.1 we show the convergence of the lowest eigenvalue as a function of n .

For a zero transverse momentum fermion, the probability amplitude to be at any transverse location should be independent of the transverse location. Thus we expect the eigenfunction

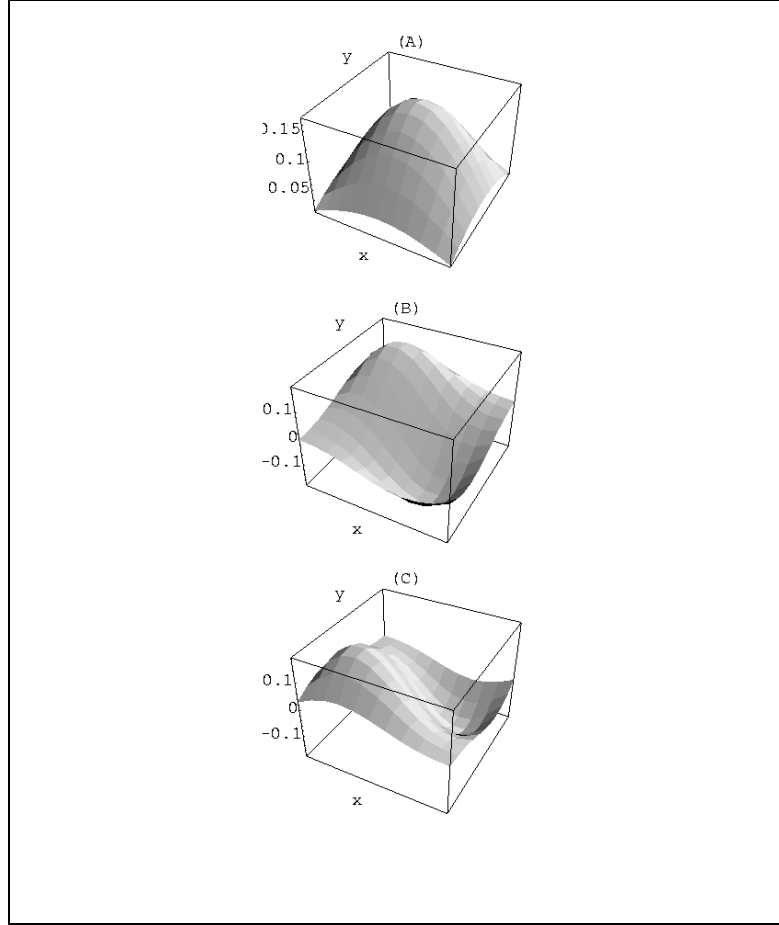


Figure 5.2: Eigenfunctions of first three states of the Hamiltonian H_0 with lattice points $n = 5$.

for such a particle to be a constant. At finite volume, with fixed boundary condition, we do get a nodeless wave function which nevertheless is not a constant since it carries some non-zero transverse momentum. All the excited states carry non-zero transverse momentum in the infinite volume limit. All of them have nodes characteristic of sine waves. The eigenfunctions corresponding to the first three eigenvalues are shown in Fig. 5.2 for the case of fixed boundary condition. With periodic boundary condition, for any n , we get a zero transverse momentum fermion with a flat wave function.

Now, we consider the effect of helicity flip term. With fixed boundary condition the lowest eigenstate has non vanishing transverse momentum in finite volume. In the absence of helicity flip term positive and negative helicity fermions are degenerate. The helicity flip term lifts the

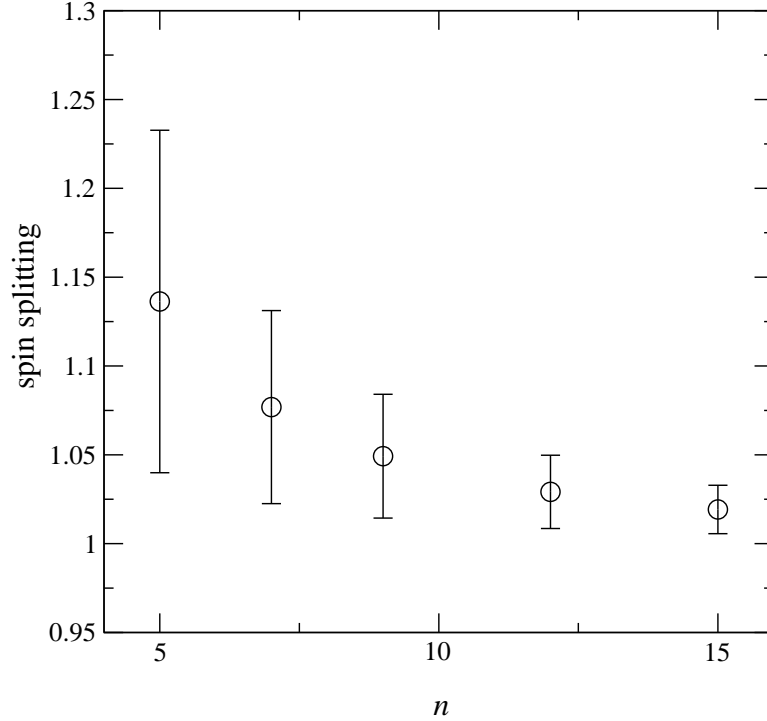


Figure 5.3: Spin splitting of the ground state caused by the spin dependent interaction as a function of n . Circles represent the eigenvalues without splitting and the vertical bars show the magnitude of splitting due to spin flip interaction.

degeneracy. The splitting is larger for larger transverse momentum. In Fig. 5.3 we present the level splitting for the helicity up and down fermions as a function of n . As expected, the level splitting vanishes and we get exact degeneracy in the infinite volume limit. For the periodic boundary condition, the lowest state has exactly zero transverse momentum and we get two degenerate fermions for all n .

5.3 Hamiltonian with symmetric derivative

5.3.1 Construction

Now, let us discuss the other way of putting fermions on a transverse lattice. Here we use the symmetric lattice derivative defined by

$$D_r \psi^\pm(\mathbf{x}) = \frac{1}{2a} [U_r(\mathbf{x}) \psi^\pm(\mathbf{x} + a\hat{\mathbf{r}}) - U_{-r}(\mathbf{x}) \psi^\pm(\mathbf{x} - a\hat{\mathbf{r}})]. \quad (5.25)$$

In place of using forward and backward derivatives in Eq. (5.2), we use the above symmetric derivative for all lattice derivatives. Proceeding as in Sec. 5.2, we arrive at the fermionic part of the QCD Hamiltonian

$$\begin{aligned}
P_{sd}^- &= \int dx^- a^2 \sum_{\mathbf{x}} m^2 \eta^\dagger(\mathbf{x}) \frac{1}{i\partial^+} \eta(\mathbf{x}) \\
&\quad - \int dx^- a^2 \sum_{\mathbf{x}} \left\{ m \frac{1}{2a} \eta^\dagger(\mathbf{x}) \sum_r \hat{\sigma}_r \frac{1}{i\partial^+} [U_r(\mathbf{x}) \eta(\mathbf{x} + a\hat{\mathbf{r}}) - U_{-r}(\mathbf{x}) \eta(\mathbf{x} - a\hat{\mathbf{r}})] \right. \\
&\quad \left. - m \frac{1}{2a} \sum_r \left[\eta^\dagger(\mathbf{x} - a\hat{\mathbf{r}}) \hat{\sigma}_r U_r(\mathbf{x} - a\hat{\mathbf{r}}) - \eta^\dagger(\mathbf{x} + a\hat{\mathbf{r}}) \hat{\sigma}_r U_{-r}(\mathbf{x} + a\hat{\mathbf{r}}) \right] \frac{1}{i\partial^+} \eta(\mathbf{x}) \right\} \\
&\quad - \int dx^- a^2 \sum_{\mathbf{x}} \frac{1}{4a^2} \sum_r \left[\eta^\dagger(\mathbf{x} - a\hat{\mathbf{r}}) U_r(\mathbf{x} - a\hat{\mathbf{r}}) - \eta^\dagger(\mathbf{x} + a\hat{\mathbf{r}}) U_{-r}(\mathbf{x} + a\hat{\mathbf{r}}) \right] \\
&\quad \frac{1}{i\partial^+} [U_r(\mathbf{x}) \eta(\mathbf{x} + a\hat{\mathbf{r}}) - U_{-r}(\mathbf{x}) \eta(\mathbf{x} - a\hat{\mathbf{r}})]. \tag{5.26}
\end{aligned}$$

In the free limit, the above Hamiltonian becomes

$$\begin{aligned}
P_{sd}^- &= \int dx^- a^2 \sum_{\mathbf{x}} \left\{ m^2 \eta^\dagger(\mathbf{x}) \frac{1}{i\partial^+} \eta(\mathbf{x}) \right. \\
&\quad \left. + \frac{1}{4a^2} \sum_r [\eta^\dagger(\mathbf{x} + a\hat{\mathbf{r}}) - \eta^\dagger(\mathbf{x} - a\hat{\mathbf{r}})] \frac{1}{i\partial^+} [\eta(\mathbf{x} + a\hat{\mathbf{r}}) - \eta(\mathbf{x} - a\hat{\mathbf{r}})] \right\}. \tag{5.27}
\end{aligned}$$

In the free field limit the two linear mass terms cancel with each other.

When we implement the constraint equation on the lattice and use symmetric definition of the lattice derivative, it is important to keep in mind that we have only *next to nearest neighbor* interactions which can easily be seen from Eq. (5.27). Thus in each transverse direction even and odd lattice points are decoupled and as a result we have four independent sub-lattices in two dimensional transverse plane connecting $(x^1 = \text{even}, x^2 = \text{even})$, $(x^1 = \text{even}, x^2 = \text{odd})$, $(x^1 = \text{odd}, x^2 = \text{even})$ and $(x^1 = \text{odd}, x^2 = \text{odd})$ lattice points.

Let us now address the nature of the spectrum and the presence and origin of doublers.

5.3.2 Fermion doubling

For clarity, the Hamiltonian (Eq. 5.27) can be rewritten as

$$\begin{aligned}
P_{sd}^- &= \int dx^- a^2 \left\{ \right. \\
&\quad \left. \sum_{x_e^1, x_e^2} \left[m^2 \eta^\dagger(\mathbf{x}) \frac{1}{i\partial^+} \eta(\mathbf{x}) - \frac{1}{4a^2} a^2 [\eta^\dagger(\mathbf{x}) \frac{1}{i\partial^+} \sum_r [\eta(\mathbf{x} + 2a\hat{\mathbf{r}}) + \eta(\mathbf{x} - 2a\hat{\mathbf{r}}) - 2\eta(\mathbf{x})] \right] \right\}
\end{aligned}$$

$$\begin{aligned}
& + \sum_{x_e^1, x_o^2} \left[m^2 \eta^\dagger(\mathbf{x}) \frac{1}{i\partial^+} \eta(\mathbf{x}) - \frac{1}{4a^2} a^2 [\eta^\dagger(\mathbf{x}) \frac{1}{i\partial^+} \sum_r [\eta(\mathbf{x} + 2a\hat{\mathbf{r}})] + \eta(\mathbf{x} - 2a\hat{\mathbf{r}}) - 2\eta(\mathbf{x})] \right] \\
& + \sum_{x_o^1, x_e^2} \left[m^2 \eta^\dagger(\mathbf{x}) \frac{1}{i\partial^+} \eta(\mathbf{x}) - \frac{1}{4a^2} a^2 [\eta^\dagger(\mathbf{x}) \frac{1}{i\partial^+} \sum_r [\eta(\mathbf{x} + 2a\hat{\mathbf{r}})] + \eta(\mathbf{x} - 2a\hat{\mathbf{r}}) - 2\eta(\mathbf{x})] \right] \\
& + \sum_{x_o^1, x_o^2} \left[m^2 \eta^\dagger(\mathbf{x}) \frac{1}{i\partial^+} \eta(\mathbf{x}) - \frac{1}{4a^2} a^2 [\eta^\dagger(\mathbf{x}) \frac{1}{i\partial^+} \sum_r [\eta(\mathbf{x} + 2a\hat{\mathbf{r}})] + \eta(\mathbf{x} - 2a\hat{\mathbf{r}}) - 2\eta(\mathbf{x})] \right] \Big\},
\end{aligned} \tag{5.28}$$

where x_e^i stands for $x^i = \text{even}$ and x_o^i stands for $x^i = \text{odd}$. Clearly the Hamiltonian is divided into four independent sub-lattices each with lattice constant $2a$. As a result, a momentum component in each sub-lattice is bounded by $\frac{\pi}{2a}$ in magnitude. Again, going through the Fourier transform in each sub-lattice of the transverse space, we arrive at the free particle dispersion relation for the light front energy in each sector

$$k_{\mathbf{k}}^- = \frac{1}{k^+} [m^2 + \frac{1}{a^2} \sum_r \sin^2 k_r a]. \tag{5.29}$$

For fixed k_r , in the limit $a \rightarrow 0$, $\frac{1}{a^2} \sin^2 k_r a \rightarrow k_r^2$ and we get the continuum dispersion relation

$$k_{\mathbf{k}}^- = \frac{m^2 + \mathbf{k}^2}{k^+}. \tag{5.30}$$

Because of the momentum bound of $\frac{\pi}{2a}$ doublers cannot arise from $ka = \pi$ in sharp contrast with Euclidean lattice gauge theory where doublers come from $ka = \pi$ [14]. However, because of the decoupling of odd and even lattices, one can get zero transverse momentum fermions one each from the four sub-lattices for a two dimensional transverse lattice. Thus we expect a four fold degeneracy of zero transverse momentum fermions.

5.3.3 Numerical Investigation

Using DLCQ for the longitudinal direction, Eq. (5.27) can be written as

$$P_{sd}^- = \frac{L}{\pi} H_{sd} \equiv \frac{L}{\pi} [H_m + H_k] \tag{5.31}$$

where

$$\begin{aligned}
H_m & = a^2 m^2 \sum_l \sum_\sigma \sum_{\mathbf{z}} \frac{1}{l} \\
& \quad [b^\dagger(l, \mathbf{z}, \sigma) b(l, \mathbf{z}, \sigma) + d^\dagger(l, \mathbf{z}, \sigma) d(l, \mathbf{z}, \sigma)]
\end{aligned} \tag{5.32}$$

and

$$\begin{aligned}
H_k = & \sum_l \sum_\sigma \sum_{\mathbf{z}} \sum_r \frac{1}{l} \\
& \left[b^\dagger(l, \mathbf{z} + a\hat{\mathbf{r}}, \sigma) b(l, \mathbf{z} + a\hat{\mathbf{r}}, \sigma) + b^\dagger(l, \mathbf{z} - a\hat{\mathbf{r}}, \sigma) b(l, \mathbf{z} - a\hat{\mathbf{r}}, \sigma) \right. \\
& - b^\dagger(l, \mathbf{z} + a\hat{\mathbf{r}}, \sigma) b(l, \mathbf{z} - a\hat{\mathbf{r}}, \sigma) - b^\dagger(l, \mathbf{z} - a\hat{\mathbf{r}}, \sigma) b(l, \mathbf{z} + a\hat{\mathbf{r}}, \sigma) \\
& + d^\dagger(l, \mathbf{z} + a\hat{\mathbf{r}}, \sigma) d(l, \mathbf{z} + a\hat{\mathbf{r}}, \sigma) + d^\dagger(l, \mathbf{z} - a\hat{\mathbf{r}}, \sigma) d(l, \mathbf{z} - a\hat{\mathbf{r}}, \sigma) \\
& \left. - d^\dagger(l, \mathbf{z} + a\hat{\mathbf{r}}, \sigma) d(l, \mathbf{z} - a\hat{\mathbf{r}}, \sigma) - d^\dagger(l, \mathbf{z} - a\hat{\mathbf{r}}, \sigma) d(l, \mathbf{z} + a\hat{\mathbf{r}}, \sigma) \right]. \quad (5.33)
\end{aligned}$$

For each transverse direction, we have $2n + 1$ lattice points where the fermions are allowed to hop. Since even and odd lattice points are decoupled we need to fix the boundary conditions separately for even and odd sub-lattices in each transverse direction.

Boundary conditions

Fixed boundary condition: To implement the fixed boundary condition, we need to consider $2n + 5$ lattice points. For one sub-lattice we have to fix particles at $s = 1$ and $s = 2n + 5$. We have, the wavefunction at location s , $u_s \sim \sin (s - 1)ka$ which gives $u_s = 0$ for $s = 1$. We also need $u_s = 0$ for $s = 2n + 5$. Thus $(2n + 4)k_p a = p\pi$, with $p = 1, 2, 3, \dots, n + 1$. For $n = 1$, allowed values of k_p are $k_p = \frac{\pi}{6a}, \frac{2\pi}{6a}$.

For the other sub-lattice, we fix the particles at $s = 2$ and $s = 2n + 4$. The wavefunction at location s , $u_s \sim \sin (s - 2)ka$. $u_s = 0$ for $s = 2$ and $s = 2n + 4$. Thus $(2n + 2)k_p a = p\pi$ with $p = 1, 2, 3, \dots, n$. For $n = 1$, only allowed value of k is $k = \frac{\pi}{4a}$.

Combining the two sub-lattices, for $n = 1$, the allowed values of k are $\frac{\pi}{6a}, \frac{\pi}{4a}$, and $\frac{2\pi}{6a}$.

Periodic boundary condition: To implement the periodic boundary condition, we need to consider $2n + 3$ lattice points when fermions can hop in $2n + 1$ lattice points. For one sub-lattice $(2n + 3)^{rd}$ lattice point is identified with the lattice point 1. For the other sub-lattice $(2n + 2)^{nd}$ lattice point is identified with the lattice point 2. Wavefunction at point s , $u_s \sim e^{iska}$. We require $e^{ika} = e^{i(2n+3)ka}$. Thus $k_p a = \pm \frac{2\pi p}{(2n+2)}$, $p = 0, 1, 2, \dots, \frac{n+1}{2}$. For $n = 1$, we have, $k_0 = 0, k_1 = \pm \frac{\pi}{2a}$.

For the other sub-lattice we require $e^{2ika} = e^{i(2n+2)ka}$. Thus the allowed values of momentum k_p are $k_p a = \pm \frac{\pi}{n} p$, $p = 0, 1, 2, \dots, \frac{n-1}{2}$. For $n = 1$, allowed value of $k = 0$. Thus for $n = 1$, taking the two sub-lattices together, the allowed values of k are $0, 0, \frac{\pi}{2a}$.

Numerical results

The results of matrix diagonalization in the case of the symmetric derivative with fixed boundary condition are presented in Figs. 5.4, 5.5 and 5.6. In Fig. 5.4 we present the lowest

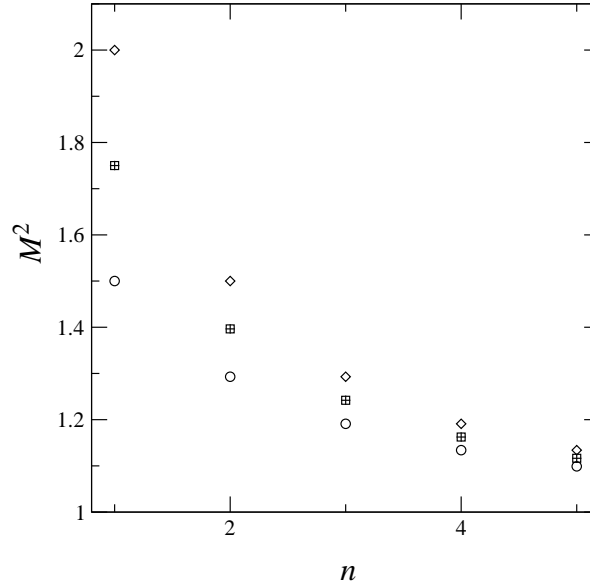


Figure 5.4: First four eigenvalues of Hamiltonian with symmetric derivative as a function of n .

four eigenvalues as a function of n . At finite volume, the four states do not appear exactly degenerate even though the even-odd and odd-even states are always degenerate because of the hypercubic (square) symmetry in the transverse plane. The four states become degenerate in the infinite volume limit. The eigenfunctions of the lowest four states are presented in Fig. 5.5 for $n = 5$ and fixed boundary condition. As they carry small nonzero transverse momenta they are not flat in the transverse plane. But, as they correspond to particle states, they are nodeless and same in shape and magnitude. All other states in the spectrum have one or more nodes. For example, in Fig. 5.6 we show the eigenfunction corresponding to the fifth eigenvalue for $n = 5$ which clearly exhibits the node structure.

With periodic boundary condition we can achieve exactly zero transverse momenta for any n and hence get four fold degenerate lowest eigenvalue corresponding to four zero transverse

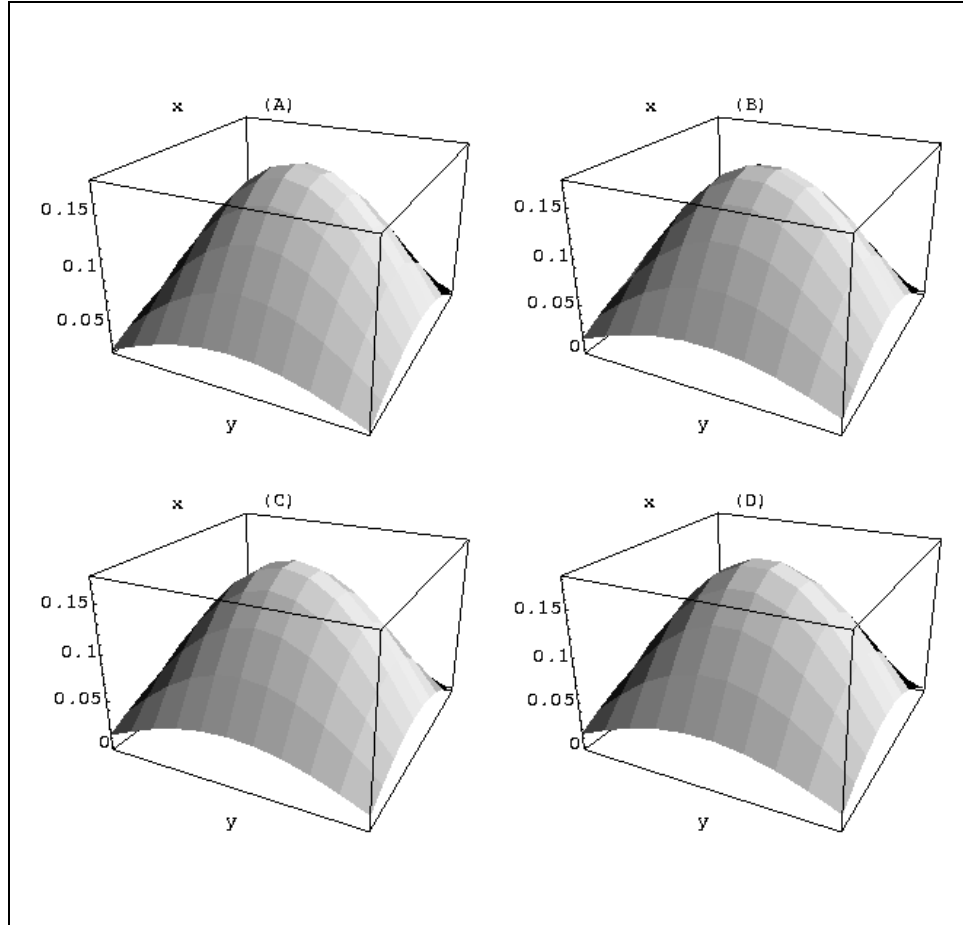


Figure 5.5: Eigenfunctions of first four (degenerate) states for the case of fermion doubling with symmetric lattice derivative.

momentum fermions. Corresponding wavefunctions are flat in transverse coordinate space and excited states (nonzero k states) show the expected node structures.

5.4 Staggered fermion on the light-front transverse lattice

As we have seen in the previous section that the method of symmetric derivatives results in fermion doublers, we now consider two approaches to remove the doublers. In this section we study an approach similar to the staggered fermions in conventional lattice gauge theory. In the next section we will take up the case of Wilson fermions.

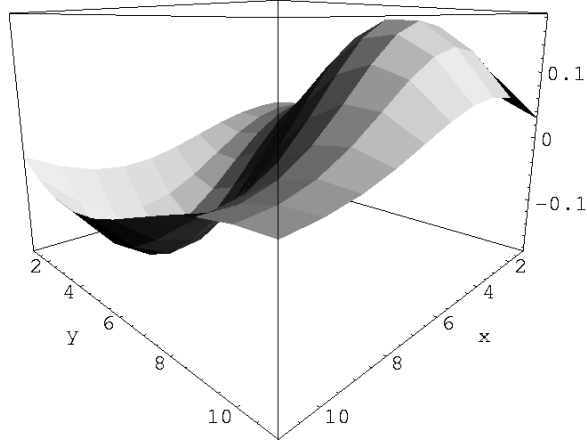


Figure 5.6: Eigenfunction corresponding to the fifth state.

In analogy with the Euclidean staggered formulation, define the spin diagonalization transformation

$$\eta(x_1, x_2) = (\hat{\sigma}^1)^{x_1} (\hat{\sigma}^2)^{x_2} \chi(x_1, x_2). \quad (5.34)$$

We see from the QCD Hamiltonian given in Eq. (5.26) with symmetric derivative that in the interacting theory (except for the linear mass term) and also in the free fermion limit, even and odd lattice sites are decoupled and the Hamiltonian is already spin diagonal. So, it is very natural to try staggered fermion formulation on the light front transverse lattice. In this section we shall follow the Kogut-Susskind formulation [15] and present an elementary configuration space analysis for two flavor interpretation. After the spin transformation the linear mass term in the Hamiltonian (Eq. 5.26) becomes:

$$\int dx^- a^2 \sum_{\mathbf{x}} \left\{ m \frac{1}{2a} \chi^\dagger(\mathbf{x}) \sum_r \phi(\mathbf{x}, r) \frac{1}{i\partial^+} [U_r(\mathbf{x}) \chi(\mathbf{x} + a\hat{\mathbf{r}}) - U_{-r}(\mathbf{x}) \chi(\mathbf{x} - a\hat{\mathbf{r}})] \right. \\ \left. - m \frac{1}{2a} \sum_r \left[\chi^\dagger(\mathbf{x} - a\hat{\mathbf{r}}) \phi(\mathbf{x}, r) U_r(\mathbf{x} - a\hat{\mathbf{r}}) - \chi^\dagger(\mathbf{x} + a\hat{\mathbf{r}}) \phi(\mathbf{x}, r) U_{-r}(\mathbf{x} + a\hat{\mathbf{r}}) \right] \frac{1}{i\partial^+} \chi(\mathbf{x}) \right\} \quad (5.35)$$

where, $\phi(\mathbf{x}, r) = 1$ for $r = 1$ and $\phi(\mathbf{x}, r) = (-1)^{x_1}$ for $r = 2$. After spin diagonalization, the full Hamiltonian in the free field limit becomes

$$\begin{aligned}
P_{sf}^- = & \int dx^- a^2 \sum_{\mathbf{x}} \left\{ m^2 \chi^\dagger(\mathbf{x}) \frac{1}{i\partial^+} \chi(\mathbf{x}) \right. \\
& + \frac{1}{4a^2} \sum_r [\chi^\dagger(\mathbf{x} + a\hat{\mathbf{r}}) - \chi^\dagger(\mathbf{x} - a\hat{\mathbf{r}})] \frac{1}{i\partial^+} [\chi(\mathbf{x} + a\hat{\mathbf{r}}) - \chi(\mathbf{x} - a\hat{\mathbf{r}})] \\
& - \frac{1}{2a} m \chi^\dagger(\mathbf{x}) \frac{1}{i\partial^+} \sum_r \phi(\mathbf{x}, r) [\chi(\mathbf{x} + a\hat{\mathbf{r}}) - \chi(\mathbf{x} - a\hat{\mathbf{r}})] \\
& \left. - \frac{1}{2a} m \sum_r [\chi^\dagger(\mathbf{x} + a\hat{\mathbf{r}}) - \chi^\dagger(\mathbf{x} - a\hat{\mathbf{r}})] \phi(\mathbf{x}, r) \frac{1}{i\partial^+} \chi(\mathbf{x}) \right\}. \quad (5.36)
\end{aligned}$$

The two linear mass terms cancel with each other in the free theory, but since they are present in the interacting theory we keep them to investigate the staggered fermions.

Since all the terms in Eq. (5.36) are spin diagonal, we can put only a single component field at each transverse site. From now on, all the χ 's and χ^\dagger 's appearing in Eq. (5.36) can be taken as single component fermion fields. Thus we have thinned the fermionic degrees of freedom by half. Without loss of generality, we keep the helicity up component of χ at each lattice point.

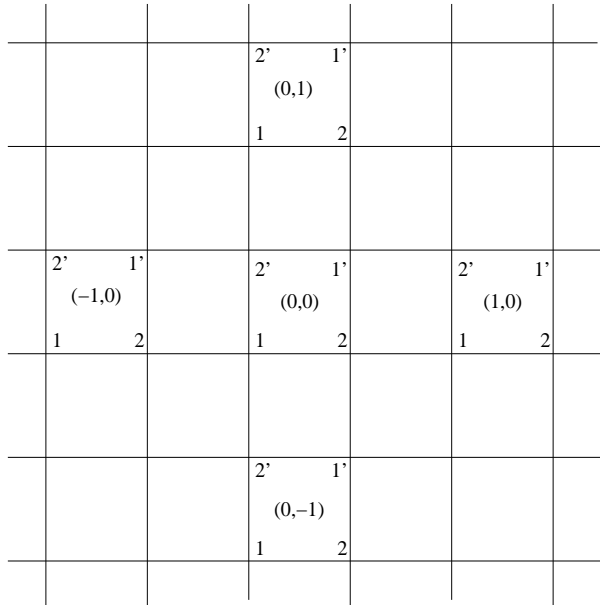


Figure 5.7: Staggered lattice.

Apart from the linear mass term in Eq. (5.36), all the other terms have the feature that fermion fields on the even and odd lattices do not mix. Let us denote (see Fig. 5.7) the even-even lattice points by 1, odd-odd lattice points by 1', odd-even lattice points by 2 and even-odd lattice points by 2', and the corresponding fields by χ_1 , $\chi_{1'}$, χ_2 and $\chi_{2'}$. Then the first of the linear mass terms

$$\sum_{\mathbf{x}} \chi^\dagger(\mathbf{x}) \frac{1}{i\partial^+} \sum_r \phi(\mathbf{x}, r) [\chi(\mathbf{x} + a\hat{\mathbf{r}}) - \chi(\mathbf{x} - a\hat{\mathbf{r}})] \quad (5.37)$$

can be rewritten as (suppressing factors of a from now on),

$$\begin{aligned} & \chi_1^\dagger \frac{1}{i\partial^+} (\nabla_1 \chi_2 + \nabla_2 \chi_{2'}) + \chi_2^\dagger \frac{1}{i\partial^+} (\nabla_1 \chi_1 - \nabla_2 \chi_{1'}) \\ & + \chi_{1'}^\dagger \frac{1}{i\partial^+} (\nabla_1 \chi_{2'} - \nabla_2 \chi_2) + \chi_{2'}^\dagger \frac{1}{i\partial^+} (\nabla_1 \chi_{1'} + \nabla_2 \chi_1) + B \end{aligned} \quad (5.38)$$

where ∇_1 and ∇_2 are the symmetric derivatives in the respective directions and B represents the contribution from other blocks. Looking at Fig. 5.7 it is apparent that these ∇_1 and ∇_2 can also be interpreted as a block derivative, i.e., finite differences between block variables. For example, $\nabla_1 \chi_1 = \chi_1(1, 0) - \chi_1(0, 0)$ where $(1, 0)$ and $(0, 0)$ are the block indices as shown in Fig. 5.7.

Using Eq. (5.34), in terms of the nonvanishing components of η , we have

$$\eta_1 = \chi_1, \quad \eta_2 = i\chi_2, \quad \eta_{1'} = i\chi_{1'}, \quad \eta_{2'} = -\chi_{2'}. \quad (5.39)$$

An interesting feature of lattice points 1 and 1' is that fermion fields η_1 and $\eta_{1'}$ have positive helicity. η_2 and $\eta_{2'}$ have negative helicity. In terms of η fields the expression given in Eq. (5.38) can be written as

$$\begin{aligned} & \eta_1^\dagger \frac{1}{i\partial^+} (-i\nabla_1 \eta_2 - \nabla_2 \eta_{2'}) + i\eta_2^\dagger \frac{1}{i\partial^+} (\nabla_1 \eta_1 + i\nabla_2 \eta_{1'}) \\ & + i\eta_{1'}^\dagger \frac{1}{i\partial^+} (-\nabla_1 \eta_{2'} + i\nabla_2 \eta_2) - \eta_{2'}^\dagger \frac{1}{i\partial^+} (-i\nabla_1 \eta_{1'} + \nabla_2 \eta_1) + B. \end{aligned} \quad (5.40)$$

Now,

$$\begin{aligned} \eta(1) - \eta(0) &= \frac{1}{2}(\eta(1) - \eta(-1)) + \frac{1}{2}(\eta(1) + \eta(-1) - 2\eta(0)) \\ &\equiv \hat{\nabla} \eta(0) + \frac{1}{2} \hat{\nabla}^2 \eta(0), \end{aligned} \quad (5.41)$$

$$\begin{aligned}
\eta(0) - \eta(-1) &= \frac{1}{2}(\eta(1) - \eta(-1)) - \frac{1}{2}(\eta(1) + \eta(-1) - 2\eta(0)) \\
&\equiv \hat{\nabla}\eta(0) - \frac{1}{2}\hat{\nabla}^2\eta(0)
\end{aligned} \tag{5.42}$$

where $\hat{\nabla}$ and $\hat{\nabla}^2$ are respectively first order and second order block derivatives. So, we can write the expression (5.40) as

$$\begin{aligned}
&\eta_1^\dagger \frac{1}{i\partial^+} \left\{ -i(\hat{\nabla}_1\eta_2 - \frac{1}{2}\hat{\nabla}_1^2\eta_2) - (\hat{\nabla}_2\eta_{2'} - \frac{1}{2}\hat{\nabla}_2^2\eta_{2'}) \right\} \\
&+ i\eta_2^\dagger \frac{1}{i\partial^+} \left\{ (\hat{\nabla}_1\eta_1 + \frac{1}{2}\hat{\nabla}_1^2\eta_1) + i(\hat{\nabla}_2\eta_{1'} - \frac{1}{2}\hat{\nabla}_2^2\eta_{1'}) \right\} \\
&+ i\eta_{1'}^\dagger \frac{1}{i\partial^+} \left\{ -(\hat{\nabla}_1\eta_{2'} + \frac{1}{2}\hat{\nabla}_1^2\eta_{2'}) + i(\hat{\nabla}_2\eta_2 + \frac{1}{2}\hat{\nabla}_2^2\eta_2) \right\} \\
&- \eta_{2'}^\dagger \frac{1}{i\partial^+} \left\{ -i(\hat{\nabla}_1\eta_{1'} - \frac{1}{2}\hat{\nabla}_1^2\eta_{1'}) + (\hat{\nabla}_2\eta_1 + \frac{1}{2}\hat{\nabla}_2^2\eta_1) \right\}.
\end{aligned} \tag{5.43}$$

Let us introduce the fields

$$\begin{aligned}
u_1 &= \frac{1}{\sqrt{2}}(\eta_1 + \eta_{1'}) \\
u_2 &= \frac{1}{\sqrt{2}}(\eta_2 + \eta_{2'}) \\
\tilde{d}_1 &= \frac{1}{\sqrt{2}}(\eta_1 - \eta_{1'}) \\
\tilde{d}_2 &= \frac{1}{\sqrt{2}}(\eta_2 - \eta_{2'}).
\end{aligned} \tag{5.44}$$

Then, the first order derivative term in Eq. (5.43) can be written as

$$u^\dagger \frac{1}{i\partial^+} \hat{\sigma}^r \hat{\nabla}_r u + d^\dagger \frac{1}{i\partial^+} \hat{\sigma}^r \hat{\nabla}_r d = f^\dagger \frac{1}{i\partial^+} \hat{\sigma}^r \hat{\nabla}_r f \tag{5.45}$$

where, $d = \hat{\sigma}^1 \tilde{d}$ and the flavor isospin doublet

$$f = \begin{bmatrix} u \\ d \end{bmatrix}. \tag{5.46}$$

Similarly, we can write the second order block derivative term in expression (5.43) as

$$\frac{1}{2} f^\dagger \frac{1}{i\partial^+} \sigma^3 T^r \hat{\nabla}_r^2 f \tag{5.47}$$

where, T^r 's are the matrices in the flavor space defined as

$$T^1 = -i\sigma^2, \quad T^2 = -i\sigma^1. \tag{5.48}$$

Similarly, the second term in Eq. (5.36)

$$\sum_r [\eta^\dagger(\mathbf{x} + a\hat{\mathbf{r}}) - \eta^\dagger(\mathbf{x} - a\hat{\mathbf{r}})] \frac{1}{i\partial^+} [\eta(\mathbf{x} + a\hat{\mathbf{r}}) - \eta(\mathbf{x} - a\hat{\mathbf{r}})] \quad (5.49)$$

reads as

$$\hat{\mathbf{V}}_r f^\dagger \frac{1}{i\partial^+} \hat{\mathbf{V}}_r f + \hat{\mathbf{V}}_r^2 f^\dagger \frac{1}{i\partial^+} \hat{\mathbf{V}}_r^2 f + \frac{i}{2} [\hat{\mathbf{V}}_r f^\dagger \frac{1}{i\partial^+} \sigma^r T^r \hat{\mathbf{V}}_r^2 f + \hat{\mathbf{V}}_r^2 f^\dagger \frac{1}{i\partial^+} \sigma^r T^r \hat{\mathbf{V}}_r f]. \quad (5.50)$$

The full Hamiltonian given in Eq. (5.36) can now be written in two flavor notation (restoring factors of a) as

$$P_{sf}^- = \int dx^- a^2 \sum_x \left\{ m^2 f^\dagger \frac{1}{i\partial^+} f + \frac{1}{4} [\hat{\mathbf{V}}_r f^\dagger \frac{1}{i\partial^+} \hat{\mathbf{V}}_r f + a^2 \hat{\mathbf{V}}_r^2 f^\dagger \frac{1}{i\partial^+} \hat{\mathbf{V}}_r^2 f + \frac{ia}{2} (\hat{\mathbf{V}}_r f^\dagger \frac{1}{i\partial^+} \sigma^r T^r \hat{\mathbf{V}}_r^2 f + \hat{\mathbf{V}}_r^2 f^\dagger \frac{1}{i\partial^+} \sigma^r T^r \hat{\mathbf{V}}_r f)] - \frac{1}{2} m (f^\dagger \frac{1}{i\partial^+} \hat{\sigma}^r \hat{\mathbf{V}}_r f + \frac{a}{2} f^\dagger \frac{1}{i\partial^+} \sigma^3 T^r \hat{\mathbf{V}}_r^2 f + h.c.) \right\}. \quad (5.51)$$

The above simple exercise shows that applying the spin diagonalization on the symmetric derivative method, the number of doublers on the transverse lattice can be reduced from four to two which can be reinterpreted as two flavors. Although in the free case given by Eq. (5.51) the second and third lines are separately zero identically, we have kept these terms because in QCD similar terms will survive. These terms exhibit flavor mixing and also helicity flipping. The flavor mixing terms are always irrelevant.

5.5 Wilson fermion on the light-front transverse lattice

Since doublers in the light front transverse lattice arise from the decoupling of even and odd lattice sites, a term that will couple these sites will remove the zero momentum doublers. However, conventional doublers now may arise from the edges of the Brillouin zone. A second derivative term couples the even and odd lattice sites and also removes the conventional doublers. Thus, the term originally proposed by Wilson to remove the doublers arising from $ka = \pi$ in the conventional lattice theory will do the job [8].

To remove doublers, add an irrelevant term to the Lagrangian density

$$\delta \mathcal{L}(\mathbf{x}) = \frac{\kappa}{a} \sum_r \bar{\psi}(\mathbf{x}) [U_r(\mathbf{x}) \psi(\mathbf{x} + a\hat{\mathbf{r}}) - 2\psi(\mathbf{x}) + U_{-r}(\mathbf{x}) \psi(\mathbf{x} - a\hat{\mathbf{r}})] \quad (5.52)$$

where κ is the Wilson parameter. The constraint equation for ψ^- in the presence of the Wilson term becomes

$$\begin{aligned}
i\partial^+ \psi^-(\mathbf{x}) &= m\gamma^0 \psi^+(\mathbf{x}) \\
&+ i\frac{\alpha_r}{2a} [U_r(\mathbf{x})\psi^+(\mathbf{x} + a\hat{\mathbf{r}}) - U_{-r}(\mathbf{x})\psi^+(\mathbf{x} - a\hat{\mathbf{r}})] \\
&- \frac{\kappa}{a} \gamma^0 [U_r(\mathbf{x})\psi^+(\mathbf{x} + a\hat{\mathbf{r}}) - 2\psi^+(\mathbf{x}) + U_{-r}(\mathbf{x})\psi^+(\mathbf{x} - a\hat{\mathbf{r}})]. \quad (5.53)
\end{aligned}$$

The Wilson term generates the following additional terms in the Hamiltonian (5.26):

$$\begin{aligned}
P_w^- &= - \int dx^- a^2 \sum_{\mathbf{x}} \left\{ 4\frac{\kappa}{a} \frac{1}{2a} \eta^\dagger(\mathbf{x}) \sum_r \hat{\sigma}_r \frac{1}{i\partial^+} [U_r(\mathbf{x})\eta(\mathbf{x} + a\hat{\mathbf{r}}) - U_{-r}(\mathbf{x})\eta(\mathbf{x} - a\hat{\mathbf{r}})] \right. \\
&- 4\frac{\kappa}{a} \frac{1}{2a} \sum_r \left[\eta^\dagger(\mathbf{x} - a\hat{\mathbf{r}}) \hat{\sigma}_r U_r(\mathbf{x} - a\hat{\mathbf{r}}) - \eta^\dagger(\mathbf{x} + a\hat{\mathbf{r}}) \hat{\sigma}_r U_{-r}(\mathbf{x} + a\hat{\mathbf{r}}) \right] \frac{1}{i\partial^+} \eta(\mathbf{x}) \left. \right\} \\
&+ \int dx^- a^2 \sum_{\mathbf{x}} \left\{ \frac{\kappa}{a} \frac{1}{2a} \sum_r \sum_s \left[\eta^\dagger(\mathbf{x} - a\hat{\mathbf{r}}) U_r(\mathbf{x} - a\hat{\mathbf{r}}) + \eta^\dagger(\mathbf{x} + a\hat{\mathbf{r}}) U_{-r}(\mathbf{x} + a\hat{\mathbf{r}}) \right] \right. \\
&\quad \frac{1}{i\partial^+} \hat{\sigma}_s \left[U_s(\mathbf{x})\eta(\mathbf{x} + a\hat{\mathbf{s}}) - U_{-s}(\mathbf{x})\eta(\mathbf{x} - a\hat{\mathbf{s}}) \right] \\
&- \frac{\kappa}{a} \frac{1}{2a} \sum_r \sum_s \left[\eta^\dagger(\mathbf{x} - a\hat{\mathbf{r}}) \hat{\sigma}_r U_r(\mathbf{x} - a\hat{\mathbf{r}}) - \eta^\dagger(\mathbf{x} + a\hat{\mathbf{r}}) \hat{\sigma}_r U_{-r}(\mathbf{x} + a\hat{\mathbf{r}}) \right] \\
&\quad \left. \frac{1}{i\partial^+} \left[U_s(\mathbf{x})\eta(\mathbf{x} + a\hat{\mathbf{s}}) + U_{-s}(\mathbf{x})\eta(\mathbf{x} - a\hat{\mathbf{s}}) \right] \right\} \\
&- \int dx^- a^2 \sum_{\mathbf{x}} \left\{ \mu \frac{\kappa}{a} \eta^\dagger(\mathbf{x}) \frac{1}{i\partial^+} \sum_r [U_r(\mathbf{x})\eta(\mathbf{x} + a\hat{\mathbf{r}}) + U_{-r}(\mathbf{x})\eta(\mathbf{x} - a\hat{\mathbf{r}})] \right. \\
&+ \mu \frac{\kappa}{a} \sum_r \left[\eta^\dagger(\mathbf{x} - a\hat{\mathbf{r}}) U_r(\mathbf{x} - a\hat{\mathbf{r}}) + \eta^\dagger(\mathbf{x} + a\hat{\mathbf{r}}) U_{-r}(\mathbf{x} + a\hat{\mathbf{r}}) \right] \frac{1}{i\partial^+} \eta(\mathbf{x}) \left. \right\} \\
&- \int dx^- a^2 \sum_{\mathbf{x}} \frac{\kappa^2}{a^2} \sum_r \sum_s \left[\eta^\dagger(\mathbf{x} - a\hat{\mathbf{r}}) U_r(\mathbf{x} - a\hat{\mathbf{r}}) + \eta^\dagger(\mathbf{x} + a\hat{\mathbf{r}}) U_{-r}(\mathbf{x} + a\hat{\mathbf{r}}) \right] \\
&\quad \frac{1}{i\partial^+} \left[U_s(\mathbf{x})\eta(\mathbf{x} + a\hat{\mathbf{s}}) + U_{-s}(\mathbf{x})\eta(\mathbf{x} - a\hat{\mathbf{s}}) \right]. \quad (5.54)
\end{aligned}$$

In addition, the factor m^2 in the free term in Eq. (5.26) gets replaced by $\mu^2 = (m + 4\frac{\kappa}{a})^2$.

In the free limit the resulting Hamiltonian goes over to

$$\begin{aligned}
P_w^- &= \int dx^- a^2 \sum_{\mathbf{x}} \left[\mu^2 \eta^\dagger(\mathbf{x}) \frac{1}{i\partial^+} \eta(\mathbf{x}) \right. \\
&\quad \left. + \frac{1}{2a} \sum_r [\eta^\dagger(\mathbf{x} + a\hat{\mathbf{r}}) - \eta^\dagger(\mathbf{x} - a\hat{\mathbf{r}})] \frac{1}{i\partial^+} \frac{1}{2a} [\eta(\mathbf{x} + a\hat{\mathbf{r}}) - \eta(\mathbf{x} - a\hat{\mathbf{r}})] \right]
\end{aligned}$$

$$\begin{aligned}
& + \frac{\kappa^2}{a^2} \sum_r [\eta^\dagger(\mathbf{x} + a\hat{\mathbf{r}}) - 2\eta^\dagger(\mathbf{x}) + \eta^\dagger(\mathbf{x} - a\hat{\mathbf{r}})] \frac{1}{i\partial^+} [\eta(\mathbf{x} + a\hat{\mathbf{r}}) - 2\eta(\mathbf{x}) + \eta(\mathbf{x} - a\hat{\mathbf{r}})] \\
& - 2\frac{\mu\kappa}{a} \sum_r \eta^\dagger(\mathbf{x}) \frac{1}{i\partial^+} [\eta(\mathbf{x} + a\hat{\mathbf{r}}) - 2\eta(\mathbf{x}) + \eta(\mathbf{x} - a\hat{\mathbf{r}})] \Big]. \tag{5.55}
\end{aligned}$$

We rewrite the free Hamiltonian (5.55) as

$$P_w^- = P_D^- + P_{OD1}^- + P_{OD2}^- . \tag{5.56}$$

The diagonal terms are

$$P_D^- = \int dx^- a^2 \sum_{\mathbf{x}} \eta^\dagger(\mathbf{x}) \frac{1}{i\partial^+} \eta(\mathbf{x}) \left[\mu^2 + \frac{1}{a^2} + 8\mu\kappa \frac{1}{a} + 12\kappa^2 \frac{1}{a^2} \right]. \tag{5.57}$$

The nearest neighbor interaction is

$$\begin{aligned}
P_{OD1}^- &= - \int dx^- a^2 \sum_{\mathbf{x}} \sum_{\hat{\mathbf{r}}} \\
& \left[(2\mu\kappa \frac{1}{a} + 4\frac{\kappa^2}{a^2}) \left[\eta^\dagger(\mathbf{x}) \frac{1}{i\partial^+} \eta(\mathbf{x} + a\hat{\mathbf{r}}) + \eta^\dagger(\mathbf{x}) \frac{1}{i\partial^+} \eta(\mathbf{x} - a\hat{\mathbf{r}}) \right] \right]. \tag{5.58}
\end{aligned}$$

The next to nearest neighbor interaction is

$$\begin{aligned}
P_{OD2}^- &= \int dx^- a^2 \sum_{\mathbf{x}} \sum_{\hat{\mathbf{r}}} \left\{ -\frac{1}{4a^2} + \frac{\kappa^2}{a^2} \right\} \\
& \left[\eta^\dagger(\mathbf{x} + a\hat{\mathbf{r}}) \frac{1}{i\partial^+} \eta(\mathbf{x} - a\hat{\mathbf{r}}) + \eta^\dagger(\mathbf{x} - a\hat{\mathbf{r}}) \frac{1}{i\partial^+} \eta(\mathbf{x} + a\hat{\mathbf{r}}) \right]. \tag{5.59}
\end{aligned}$$

Using the Fourier transform in the transverse space, we get,

$$\begin{aligned}
P_w^- &= \int dx^- \int \frac{d^2k}{(2\pi)^2} \phi_{\mathbf{k}}^\dagger(x^-) \frac{1}{i\partial^+} \phi_{\mathbf{k}}(x^-) \left[\mu^2 + \sum_r k_r^2 \left(\frac{\sin k_r a}{k_r a} \right)^2 \right. \\
& \left. + 2a\mu\kappa \sum_r k_r^2 \left(\frac{\sin k_r a/2}{k_r a/2} \right)^2 + a^2 \kappa^2 \sum_r k_r^4 \left(\frac{\sin k_r a/2}{k_r a/2} \right)^4 \right]. \tag{5.60}
\end{aligned}$$

Note that, as anticipated, Wilson term removes the doublers. Since the Wilson term introduces nearest neighbor interactions, the sub-lattices are now coupled to each other and we have only one transverse lattice. The lowest eigenvalue in Eq. (5.60) occurs only if all the k_r 's are zero and there are no more doublers in the theory.

5.5.1 Numerical Investigation

For our numerical investigation, we write the Hamiltonian (Eq. 5.56) in DLCQ as

$$H_w = H_D + H_{OD1} + H_{OD2} \quad (5.61)$$

with

$$H_D = [a^2\mu^2 + 1 + 8a\mu\kappa + 12\kappa^2] \sum_l \sum_\sigma \sum_{\mathbf{z}} \frac{1}{l} [b^\dagger(l, \mathbf{z}, \sigma)b(l, \mathbf{z}, \sigma) + d^\dagger(l, \mathbf{z}, \sigma)d(l, \mathbf{z}, \sigma)], \quad (5.62)$$

$$H_{OD1} = -[2\kappa a\mu + 4\kappa^2] \sum_l \sum_\sigma \sum_{\mathbf{z}} \sum_r \frac{1}{l} \left[b^\dagger(l, \mathbf{z}, \sigma)b(l, \mathbf{z} + a\hat{\mathbf{r}}, \sigma) + b^\dagger(l, \mathbf{z}, \sigma)b(l, \mathbf{z} - a\hat{\mathbf{r}}, \sigma) + d^\dagger(l, \mathbf{z}, \sigma)d(l, \mathbf{z} + a\hat{\mathbf{r}}, \sigma) + d^\dagger(l, \mathbf{z}, \sigma)d(l, \mathbf{z} - a\hat{\mathbf{r}}, \sigma) \right] \quad (5.63)$$

and

$$H_{OD2} = -\left[\frac{1}{4} - \kappa^2\right] \sum_l \sum_\sigma \sum_{\mathbf{z}} \sum_r \frac{1}{l} \left[b^\dagger(l, \mathbf{z} + a\hat{\mathbf{r}}, \sigma)b(l, \mathbf{z} - a\hat{\mathbf{r}}, \sigma) + b^\dagger(l, \mathbf{z} - a\hat{\mathbf{r}}, \sigma)b(l, \mathbf{z} + a\hat{\mathbf{r}}, \sigma) + d^\dagger(l, \mathbf{z} + a\hat{\mathbf{r}}, \sigma)d(l, \mathbf{z} - a\hat{\mathbf{r}}, \sigma) + d^\dagger(l, \mathbf{z} - a\hat{\mathbf{r}}, \sigma)d(l, \mathbf{z} + a\hat{\mathbf{r}}, \sigma) \right]. \quad (5.64)$$

Boundary condition

With the Wilson term added, we do not have decoupled sub-lattices. We have both nearest neighbor and next-to-nearest neighbor interactions. Since with fixed boundary condition, the lowest four eigenvalues are not exactly degenerate in finite volume, it is difficult to investigate the removal of degeneracy by the addition of Wilson term. With periodic boundary condition, for a lattice with $2n + 1$ lattice points in each transverse direction, we identify the $(2n + 2)^{th}$ lattice site with the first lattice site. Then for the Hamiltonian matrix we get the following

additional contributions.

$$H = \begin{pmatrix} \cdot & \cdot & \cdot & \cdot & \dots & \cdot & \cdot & NN & N \\ \cdot & \cdot & \cdot & \cdot & \dots & \cdot & \cdot & 0 & NN \\ \cdot & \cdot & \cdot & \cdot & \dots & \cdot & \cdot & \cdot & \cdot \\ \dots & & & & & & & & \\ \dots & & & & & & & & \\ \cdot & \cdot & \cdot & \cdot & \dots & \cdot & \cdot & \cdot & \cdot \\ NN & 0 & \cdot & \cdot & \dots & \cdot & \cdot & \cdot & \cdot \\ N & NN & \cdot & \cdot & \dots & \cdot & \cdot & \cdot & \cdot \end{pmatrix} \quad (5.65)$$

The matrix elements $NN = -\frac{1}{4} + \kappa^2$ and $N = -2a\mu\kappa - 4\kappa^2$. For a given n , the allowed values of k are $k_p a = \pm \frac{2\pi p}{2n+1}$, $p = 0, 1, 2, \dots$. Thus for $n = 3$, we expect multiples of $\frac{2\pi}{7}$ apart from 0. For $n = 5$, apart from 0, allowed values of k are multiples of $\frac{2\pi}{11}$.

Numerical results

Since the Wilson term connects even and odd lattices, the extra fermions that appear at zero transverse momentum are removed once Wilson term is added as we now have nearest and next to nearest neighbor interactions. For large n , we get the expected spectra but, numerical results suggest that the finite volume effect is larger for small κ which is obvious because κ is a mass-like parameter. For small κ the wavefunctions become fat and requires larger lattice to fit into. For example, with periodic boundary condition, for $n = 3$, for $\kappa = 1.0, 0.5, 0.4$, we get the expected harmonics but not for $\kappa = 0.1$. The situation is similar for $n = 5$. For $n = 10$, expected harmonics emerge even for $\kappa = 0.1$ but not for $\kappa = 0.01$. Since all realistic calculations are done in a small lattice, it is desirable to have the Wilson parameter κ not too small.

5.6 Doubling and symmetries on the light front transverse lattice

Let us now try to understand the fermion doubling in terms of the symmetries of the transverse lattice Hamiltonians. We are aware that there are rigorous theorems and anomaly arguments in the conventional lattice gauge theories [16] regarding presence of fermion doublers. In standard lattice gauge theory, some chiral symmetry needs to be broken in the kinetic part of the action to avoid the doublers. On the light-front, chirality means helicity. For example, a standard Wilson term which is not invariant under chiral transformations in the conventional lattice gauge theory, is chirally invariant on the light-front in the free field limit. The question

is then why the Wilson term removes the doublers on the light-front transverse lattice. The argument that there is nonlocality in the longitudinal direction cannot hold because, in the first place, having nonlocality is not a guarantee for removing doublers and secondly, there is no nonlocality on the transverse lattice. One, therefore needs to find a reasoning that involves the helicity in some way.

Because of the constraint equation which is inconsistent with the equal time chiral transformation in the presence of massive fermions, we should distinguish between chiral symmetry in the equal time formalism and in the light-front formalism. For example, the free massive light-front Lagrangian involving only the dynamical degrees of freedom is invariant under γ_5 transformation. On the light-front, helicity takes over the notion of chirality even in presence of fermion mass which can be understood in the following way.

In the two component representation [12] in the light-front formalism, let us look at the objects ψ_L^+ and ψ_R^+ . We have

$$\psi^+(x) = \begin{pmatrix} \eta(x) \\ 0 \end{pmatrix} \quad (5.66)$$

with

$$\eta(x) = \begin{pmatrix} \eta_1(x) \\ \eta_2(x) \end{pmatrix} \quad (5.67)$$

The projection operators are $P_R = \frac{1}{2}(1 + \gamma^5)$ and $P_L = \frac{1}{2}(1 - \gamma^5)$ with

$$\gamma^5 = \begin{pmatrix} \sigma^3 & 0 \\ 0 & -\sigma^3 \end{pmatrix}. \quad (5.68)$$

Then

$$\psi_R^+ = P_R \psi^+ = \begin{pmatrix} \eta_1 \\ 0 \\ 0 \\ 0 \end{pmatrix} \quad (5.69)$$

and

$$\psi_L^+ = P_L \psi^+ = \begin{pmatrix} 0 \\ \eta_2 \\ 0 \\ 0 \end{pmatrix}. \quad (5.70)$$

Thus $\psi_R^+ = P_R \psi^+$ represents a positive helicity fermion and $\psi_L^+ = P_L \psi^+$ represents a negative helicity fermion, even when the fermion is *massive*. This makes sense since chirality *is* helicity

even for a massive fermion in front form. This is again to be contrasted with the instant form. In that case the right handed and left handed fields defined by $\psi_R = P_R \psi = \frac{1}{2}(1 + \gamma^5)\psi$ and $\psi_L = P_L \psi = \frac{1}{2}(1 - \gamma^5)\psi$ contain both positive helicity and negative helicity states. Only in the massless limit or in the infinite momentum limit, ψ_R becomes the positive helicity state and ψ_L becomes the negative helicity state.

As a passing remark, we would like to mention that in continuum light front QCD there is a linear mass term that allows for helicity flip interaction.

In lattice gauge theory in the Euclidean or equal time formalism, because of reasons connected to anomalies (the standard ABJ anomaly in vector-like gauge theories), there has to be explicit chiral symmetry breaking in the kinetic part of the action or Hamiltonian. Translated to the light front transverse lattice formalism, this would then require helicity flip in the kinetic part. A careful observation of all the above methods that get rid of fermion doublers on the light front transverse lattice reveals that this is indeed true.

In particular, we draw attention to the even-odd helicity flip transformation

$$\eta(x_1, x_2) \rightarrow (\hat{\sigma}_1)^{x_1} (\hat{\sigma}_2)^{x_2} \eta(x_1, x_2) \quad (5.71)$$

that was used in Sec. 5.4 for spin diagonalization. It should also be clear that the form of the above transformation is not unique in the sense that one could exchange $\hat{\sigma}_1$ and $\hat{\sigma}_2$ and their exponents x_1 and x_2 could be changed by ± 1 .

Note that the Hamiltonians P_{fb}^- given in Eq. (5.11) and P_w^- given in Eq. (5.55) that do not exhibit fermion doubling are not invariant under the transformation Eq. (5.71). On the other hand the Hamiltonian P_{sd}^- given by Eq. (5.27) that exhibits fermion doubling is invariant under this transformation.

5.7 Summary

The presence of the constraint equation for fermions on the light front gives rise to interesting possibilities of formulating fermions on a transverse lattice. We have discussed in detail the transverse lattice Hamiltonians resulting from different approaches in two different boundary conditions.

In the first approach, we have proposed to use forward and backward lattice derivatives respectively for ψ^+ and ψ^- (or vice versa) so that the resulting Hamiltonian is Hermitian. There is no fermion doubling. The helicity flip (chiral symmetry breaking) term proportional to the fermion mass in the full light front QCD becomes an irrelevant term in the free field limit. With periodic boundary condition one can get the helicity up and helicity down fermions to be degenerate for any transverse lattice size n . With fixed boundary condition, there is a splitting between the two states at any n but the splitting vanishes in the large volume limit.

In the second approach, symmetric derivatives are used for both ψ^+ and ψ^- . This results in four fermion species. This is a consequence of the fact that the resulting free Hamiltonian has only next to nearest neighbor interactions and as a result even and odd lattice sites get decoupled. One way to remove doublers is to reinterpret them as flavors using staggered fermion formulation on the light front. In QCD Hamiltonian, it generates irrelevant flavor mixing interactions. However, in the free field limit, there is no flavor mixing. Another way to remove the doublers is to add a Wilson term which generates many extra terms in the Hamiltonian. In the free field limit, only the helicity nonflip terms survive. The Wilson term couples even and odd sites and removes the doublers. Numerically, we found that in small lattice volumes it is preferable to have not too small values of the Wilson mass κ/a .

Chiral symmetry in light-front is different from the chiral symmetry in equal time formalism. So, fermion doubling on LFTL should be related with the *chiral symmetry on the light-front*. Light-front chirality is equivalent to helicity even for massive fermions. We have identified an even-odd helicity flip symmetry of the light front transverse lattice Hamiltonian, absence of which means removal of doublers in all the cases we have studied.

BIBLIOGRAPHY

- [1] K. G. Wilson, Phys. Rev. D **10**, 2445 (1974).
- [2] W. A. Bardeen and R. B. Pearson, Phys. Rev. D **14**, 547 (1976).
- [3] W. A. Bardeen, R. B. Pearson and E. Rabinovici, Phys. Rev. D **21**, 1037 (1980).
- [4] S. Dalley and B. van de Sande, Phys. Rev. Lett. **82**, 1088 (1999), hep-th/9810236.
- [5] M. Burkardt and S. Dalley, Prog. Part. Nucl. Phys. **48**, 317 (2002), hep-ph/0112007.
- [6] K. G. Wilson, T. S. Walhout, A. Harindranath, W. M. Zhang, R. J. Perry and S. D. Glazek, Phys. Rev. D **49**, 6720 (1994), hep-th/9401153.
- [7] P. A. Griffin, Phys. Rev. D **47**, 3530 (1993), hep-th/9207083.
- [8] M. Burkardt and H. El-Khozondar, Phys. Rev. D **60**, 054504 (1999), hep-ph/9805495.
- [9] S. Dalley, Phys. Rev. D **64**, 036006 (2001), hep-ph/0101318.
- [10] M. Burkardt and S.K. Seal, Phys. Rev. D **65**, 034501 (2002), hep-ph/0102245; M. Burkardt and S. K. Seal, Phys. Rev. D **64**, 111501 (2001), hep-ph/0105109.
- [11] D. Chakrabarti, A. K. De and A. Harindranath, Phys. Rev. D **67**, 076004 (2003), hep-th/0211145.
- [12] W. M. Zhang and A. Harindranath, Phys. Rev. D **48**, 4881 (1993), W. M. Zhang, Phys. Rev. D **56**, 1528 (1997), hep-ph/9705226.
- [13] T. Maskawa and K. Yamawaki, Prog. Theor. Phys. **56**, 270 (1976); A. Casher, Phys. Rev. D **14**, 452 (1976); C. B. Thorn, Phys. Rev. D **17**, 1073 (1978); H.C. Pauli and S.J. Brodsky, Phys. Rev. D **32**, 1993, (1985); *ibid.*, 2001 (1985). For a review, see, S. J. Brodsky, H. C. Pauli and S. S. Pinsky, Phys. Rept. **301**, 299 (1998), hep-ph/9705477.
- [14] I. Montvay and G. Münster, *Quantum Fields on a Lattice* (Cambridge University Press, 1994); H. J. Rothe, *Lattice Gauge Theory - An Introduction* (World Scientific lecture notes in physics, Vol - 43, 1992).
- [15] J. B. Kogut and L. Susskind, Phys. Rev. D **11**, 395 (1975), L. Susskind, Phys. Rev. D **16**, 3031 (1977), J. B. Kogut, Rev. Mod. Phys. **55**, 775 (1983).
- [16] H. B. Nielsen and M. Ninomiya, Nucl. Phys. B **185**, 20 (1981) [Erratum-*ibid.* B **195**, 541 (1982)].

CHAPTER 6

Meson Bound States in Transverse Lattice QCD

6.1 Introduction

In the previous chapter we have discussed different ways of formulating fermions on a light-front transverse lattice. We have also discussed the advantages and disadvantages of all the methods in free field limit. But, the true testing ground for the strengths and weaknesses of different methods is the full QCD. To complete this comparative study, in this chapter we consider the meson bound state problem in (3+1) dimensional light-front QCD with two transverse directions (x^1, x^2) discretized on a square lattice.

In this chapter we make a detailed comparison of two different light-front QCD Hamiltonians. One is the Hamiltonian with fermions formulated using forward and backward lattice derivatives and the other Hamiltonian with fermions formulated with symmetric lattice derivative with Wilson term [1] to get rid of doublers on the transverse lattice. Light-front staggered lattice formalism [2, 3] to remove doublers in case of symmetric lattice derivative that we have discussed in the previous Chapter is a different game altogether and will not be further investigated in this work. For our calculation, we adopt the *one link approximation* in the meson sector which has been widely used in the literature [4, 5, 6]. (Only very recently, the effect of additional links in the meson sector has been investigated [7]). One link approximation is too crude to reproduce physical observables. So, rather than fitting the parameters to reproduce any physical observable we concentrate here to investigate the effects of various coupling strengths on the low-lying spectra and wave functions and compare two different formulations.

We use Discretized Light Cone Quantization (DLCQ) [8] to address longitudinal dynamics. Because of the presence of severe light-front infrared divergences, a major concern here is the reliability of DLCQ results when calculations are done at finite resolution K and results are

extrapolated to the continuum ($K \rightarrow \infty$). In meson calculations so far, $K \leq 20$ have been chosen. We perform a detailed study of the continuum limit of DLCQ by performing calculations at larger values of K [9].

In the meson sector, in the zero link approximation, at each transverse location we have a two-dimensional field theory which in the large N_c limit (where N_c is the number of colors) is nothing but the 't Hooft model. In this well-studied model, excited states are simply excitations of the $q\bar{q}$ pair, which contain nodes in the wavefunctions. The picture changes when one link is included thereby allowing fermions to hop. The admixture of $q\bar{q}$ link states with $q\bar{q}$ states is controlled by the strengths of the particle number changing interactions and the mass of the link field. One link approximation is a priori justified for very massive links and/or weak particle changing interaction since in this case low lying excited states are also $q\bar{q}$ excitations. Likewise, for large particle changing interaction strength and/or light link mass, low lying excited states are $q\bar{q}$ link states. We explore the spectra and wavefunctions resulting from the choice of various regions of parameter space.

Details of the derivation of the fermionic part of the Hamiltonian are already discussed in the previous chapter. Here we give the details of the gauge field part of the QCD Hamiltonian. Non-linear constraints on the unitary link variables make it difficult to perform canonical quantization. We also present the effective Hamiltonian when non-linear unitary variables are replaced by linear variables.

6.2 Gauge field part of the Lagrangian density

The gauge field part of the Lagrangian density in the continuum is

$$\mathcal{L}_G = \frac{1}{2g^2} \text{Tr} F_{\rho\sigma} F^{\rho\sigma} \quad (6.1)$$

where $F^{\rho\sigma} = \partial^\rho A^\sigma - \partial^\sigma A^\rho + [A^\rho, A^\sigma]$ with $A^\rho = igA^{\rho\alpha} T^\alpha$. Here $\rho, \sigma = 0, 1, 2, 3$ and $\alpha = 1, 2, \dots, 8$. For ease of notation we suppress the dependence of field variables on the longitudinal coordinate in this section. With the gauge choice $A^+ = 0$, the Lagrangian density can be separated into three parts,

$$\mathcal{L}_G = \mathcal{L}_T + \mathcal{L}_L + \mathcal{L}_{LT}. \quad (6.2)$$

Here \mathcal{L}_T depends entirely on the lattice gauge field $U_r(\mathbf{x})$.

$$\mathcal{L}_T = \frac{1}{g^2 a^4} \sum_{r \neq s} \left\{ \text{Tr} \left[U_r(\mathbf{x}) U_s(\mathbf{x} + a\hat{\mathbf{r}}) U_{-r}(\mathbf{x} + a\hat{\mathbf{r}} + a\hat{\mathbf{s}}) U_{-s}(\mathbf{x} + a\hat{\mathbf{s}}) - 1 \right] \right\}, \quad (6.3)$$

$r, s = 1, 2$. The purely longitudinal part \mathcal{L}_L depends on the constrained gauge field A^- ,

$$\mathcal{L}_L = \frac{1}{8} (\partial^+ A^{-\alpha})^2 \quad (6.4)$$

and the mixed part \mathcal{L}_{LT} depends both on lattice gauge field and the constrained gauge field.

$$\begin{aligned} \mathcal{L}_{LT} &= \frac{1}{2g^2} \text{Tr} [F_{\mu r} F^{\mu r}] = \frac{1}{g^2 a^2} \text{Tr} [D_\mu U_r(\mathbf{x}) (D^\mu U_r(\mathbf{x}))^\dagger] \\ &= \frac{1}{g^2 a^2} \text{Tr} \left[\partial_\mu U_r(\mathbf{x}) \partial^\mu U_r^\dagger(\mathbf{x}) + A_\mu(\mathbf{x}) [U_r(\mathbf{x}) \overset{\leftrightarrow}{\partial}^\mu U_r^\dagger(\mathbf{x})] \right. \\ &\quad \left. + A_\mu(\mathbf{x} + a\hat{\mathbf{r}}) [U_r^\dagger(\mathbf{x}) \overset{\leftrightarrow}{\partial}^\mu U_r(\mathbf{x})] \right] \end{aligned} \quad (6.5)$$

where $\mu = +, -$ only and the mixed covariant derivatives of the link variables are defined by (see Appendix H for the derivation)

$$D_\mu U_r(\mathbf{x}) = \partial_\mu U_r(\mathbf{x}) + A_\mu U_r(\mathbf{x}) - U_r(\mathbf{x}) A_\mu(\mathbf{x} + a\hat{\mathbf{r}}). \quad (6.6)$$

In the $A^+ = 0$ gauge, we can write \mathcal{L}_{LT} as

$$\mathcal{L}_{LT} = \frac{1}{g^2 a^2} \text{Tr} [\partial_\mu U_r(\mathbf{x}) \partial^\mu U_r^\dagger(\mathbf{x})] + \frac{1}{2a^2} g A^{-\alpha} J_{LINK}^{+\alpha}. \quad (6.7)$$

Here the link current

$$J_{LINK}^{+\alpha}(\mathbf{x}) = \sum_r \frac{1}{g^2} \text{Tr} \left\{ T^\alpha [U_r(\mathbf{x}) i \overset{\leftrightarrow}{\partial}^+ U_r^\dagger(\mathbf{x}) + U_r^\dagger(\mathbf{x} - a\hat{\mathbf{r}}) i \overset{\leftrightarrow}{\partial}^+ U_r(\mathbf{x} - a\hat{\mathbf{r}})] \right\}. \quad (6.8)$$

Substituting back the expression for $A^{-\alpha}$ from the constraint equation

$$(\partial^+)^2 A^{-\alpha} = \frac{2g}{a^2} (J_{LINK}^{+\alpha} - J_q^{+\alpha}) \quad (6.9)$$

with

$$J_q^{+\alpha}(\mathbf{x}) = 2\eta^\dagger(\mathbf{x}) T^\alpha \eta(\mathbf{x}) \quad (6.10)$$

where η is the dimensionless two-component lattice fermion field, in the $A^{-\alpha}$ dependent terms in the Lagrangian density, namely,

$$-\frac{1}{2} \frac{g}{a^2} A^{-\alpha} J_q^{+\alpha} + \frac{1}{8} (\partial^+ A^{-\alpha})^2 + \frac{1}{2} \frac{g}{a^2} A^{-\alpha} J_{LINK}^{+\alpha} \quad (6.11)$$

we generate the terms

$$\frac{g^2}{2a^4} J_{LINK}^{+\alpha} \left(\frac{1}{\partial^+} \right)^2 J_{LINK}^{+\alpha} + \frac{g^2}{2a^4} \eta^\dagger T^\alpha \eta \left(\frac{1}{\partial^+} \right)^2 \eta^\dagger T^\alpha \eta - \frac{g^2}{a^4} J_{LINK}^{+\alpha} \left(\frac{1}{\partial^+} \right)^2 \eta^\dagger T^\alpha \eta. \quad (6.12)$$

Collecting all the terms, the canonical Lagrangian density for transverse lattice QCD is

$$\begin{aligned} \mathcal{L} = & \mathcal{L}_f + \frac{1}{a^4 g^2} Tr[\partial_\mu U_r(\mathbf{x}) \partial^\mu U_r^\dagger(\mathbf{x})] \\ & + \frac{1}{a^4 g^2} \sum_{r \neq s} \left\{ Tr \left[U_r(\mathbf{x}) U_s(\mathbf{x} + a\hat{\mathbf{r}}) U_{-r}(\mathbf{x} + a\hat{\mathbf{r}} + a\hat{\mathbf{s}}) U_{-s}(\mathbf{x} + a\hat{\mathbf{s}}) - 1 \right] \right\} \\ & + \frac{g^2}{2a^4} J_{LINK}^{+\alpha} \left(\frac{1}{\partial^+} \right)^2 J_{LINK}^{+\alpha} + \frac{1}{2a^4} g^2 J_q^{+\alpha} \left(\frac{1}{\partial^+} \right)^2 J_q^{+\alpha} \\ & - \frac{g^2}{a^4} J_{LINK}^{+\alpha} \left(\frac{1}{\partial^+} \right)^2 J_q^{+\alpha}, \end{aligned} \quad (6.13)$$

where \mathcal{L}_f is the fermionic part of the QCD Lagrangian density with forward and backward lattice derivatives given by

$$\begin{aligned} \mathcal{L}_f = & \frac{1}{a^2} \eta^\dagger(\mathbf{x}) i \partial^- \eta(\mathbf{x}) - \frac{m^2}{a^2} \eta^\dagger(\mathbf{x}) \frac{1}{i \partial^+} \eta(\mathbf{x}) \\ & + im \frac{1}{a^2} \eta^\dagger(\mathbf{x}) \hat{\sigma}_s \frac{1}{a} \frac{1}{\partial^+} \left[U_s(\mathbf{x}) \eta(\mathbf{x} + a\hat{\mathbf{s}}) - \eta(\mathbf{x}) \right] \\ & + im \frac{1}{a^2} \left[\eta^\dagger(\mathbf{x} + a\hat{\mathbf{r}}) U_r^\dagger(\mathbf{x}) - \eta^\dagger(\mathbf{x}) \right] \hat{\sigma}_r \frac{1}{a} \frac{1}{\partial^+} \eta(\mathbf{x}) \\ & - \frac{1}{a^4} \left[\eta^\dagger(\mathbf{x} + a\hat{\mathbf{r}}) U_r^\dagger(\mathbf{x}) - \eta^\dagger(\mathbf{x}) \right] \hat{\sigma}_r \frac{1}{i \partial^+} \hat{\sigma}_s \left[U_s(\mathbf{x}) \eta(\mathbf{x} + a\hat{\mathbf{s}}) - \eta(\mathbf{x}) \right], \end{aligned} \quad (6.14)$$

or with symmetric lattice derivative with Wilson term given by

$$\begin{aligned} \mathcal{L}_f = & \frac{1}{a^2} \eta^\dagger(\mathbf{x}) i \partial^- \eta(\mathbf{x}) - \frac{1}{a^2} \left(m + 4 \frac{\kappa}{a} \right)^2 \eta^\dagger(\mathbf{x}) \frac{1}{i \partial^+} \eta(\mathbf{x}) \\ & + \frac{1}{a^2} \left(m + 4 \frac{\kappa}{a} \right) \frac{1}{2a} \left\{ \eta^\dagger(\mathbf{x}) \sum_r \hat{\sigma}_r \frac{1}{i \partial^+} \left[U_r(\mathbf{x}) \eta(\mathbf{x} + a\hat{\mathbf{r}}) - U_{-r}(\mathbf{x}) \eta(\mathbf{x} - a\hat{\mathbf{r}}) \right] \right. \\ & \left. - \sum_r \left[\eta^\dagger(\mathbf{x} - a\hat{\mathbf{r}}) \hat{\sigma}_r U_r(\mathbf{x} - a\hat{\mathbf{r}}) - \eta^\dagger(\mathbf{x} + a\hat{\mathbf{r}}) \hat{\sigma}_r U_{-r}(\mathbf{x} + a\hat{\mathbf{r}}) \right] \frac{1}{i \partial^+} \eta(\mathbf{x}) \right\}. \\ & - \frac{1}{a^2} \left\{ \frac{\kappa}{a} \frac{1}{2a} \sum_r \sum_s \left[\eta^\dagger(\mathbf{x} - a\hat{\mathbf{r}}) U_r(\mathbf{x} - a\hat{\mathbf{r}}) + \eta^\dagger(\mathbf{x} + a\hat{\mathbf{r}}) U_{-r}(\mathbf{x} + a\hat{\mathbf{r}}) \right] \right. \\ & \left. \frac{1}{i \partial^+} \hat{\sigma}_s \left[U_s(\mathbf{x}) \eta(\mathbf{x} + a\hat{\mathbf{s}}) - U_{-s}(\mathbf{x}) \eta(\mathbf{x} - a\hat{\mathbf{s}}) \right] \right. \\ & \left. - \frac{\kappa}{a} \frac{1}{2a} \sum_r \sum_s \left[\eta^\dagger(\mathbf{x} - a\hat{\mathbf{r}}) \hat{\sigma}_r U_r(\mathbf{x} - a\hat{\mathbf{r}}) - \eta^\dagger(\mathbf{x} + a\hat{\mathbf{r}}) \hat{\sigma}_r U_{-r}(\mathbf{x} + a\hat{\mathbf{r}}) \right] \right\}. \end{aligned}$$

$$\begin{aligned}
& \left. \frac{1}{i\partial^+} \left[U_s(\mathbf{x})\eta(\mathbf{x} + a\hat{\mathbf{s}}) + U_{-s}(\mathbf{x})\eta(\mathbf{x} - a\hat{\mathbf{s}}) \right] \right\} \\
& + \frac{1}{a^2} \frac{1}{4a^2} \sum_r \sum_s \left[\eta^\dagger(\mathbf{x} - a\hat{\mathbf{r}}) \hat{\sigma}_r U_r(\mathbf{x} - a\hat{\mathbf{r}}) - \eta^\dagger(\mathbf{x} + a\hat{\mathbf{r}}) \hat{\sigma}_r U_{-r}(\mathbf{x} + a\hat{\mathbf{r}}) \right] \\
& \frac{1}{i\partial^+} \hat{\sigma}_s \left[U_s(\mathbf{x})\eta(\mathbf{x} + a\hat{\mathbf{s}}) - U_{-s}(\mathbf{x})\eta(\mathbf{x} - a\hat{\mathbf{s}}) \right] \\
& + \frac{1}{a^2} \left(m + 4\frac{\kappa}{a} \right) \frac{\kappa}{a} \left\{ \eta^\dagger(\mathbf{x}) \frac{1}{i\partial^+} \sum_r \left[U_r(\mathbf{x})\eta(\mathbf{x} + a\hat{\mathbf{r}}) + U_{-r}(\mathbf{x})\eta(\mathbf{x} - a\hat{\mathbf{r}}) \right] \right. \\
& \left. + \sum_r \left[\eta^\dagger(\mathbf{x} - a\hat{\mathbf{r}}) U_r(\mathbf{x} - a\hat{\mathbf{r}}) + \eta^\dagger(\mathbf{x} + a\hat{\mathbf{r}}) U_{-r}(\mathbf{x} + a\hat{\mathbf{r}}) \right] \frac{1}{i\partial^+} \eta(\mathbf{x}) \right\} \\
& + \frac{1}{a^2} \frac{\kappa^2}{a^2} \sum_r \sum_s \left[\eta^\dagger(\mathbf{x} - a\hat{\mathbf{r}}) U_r(\mathbf{x} - a\hat{\mathbf{r}}) + \eta^\dagger(\mathbf{x} + a\hat{\mathbf{r}}) U_{-r}(\mathbf{x} + a\hat{\mathbf{r}}) \right] \\
& \frac{1}{i\partial^+} \left[U_s(\mathbf{x})\eta(\mathbf{x} + a\hat{\mathbf{s}}) + U_{-s}(\mathbf{x})\eta(\mathbf{x} - a\hat{\mathbf{s}}) \right]. \tag{6.15}
\end{aligned}$$

Here we use the two-component representation [10] for the dynamical fermion field

$$\psi^+(x^-, x^\perp) = \begin{bmatrix} \frac{1}{a} \eta(x^-, x^\perp) \\ 0 \end{bmatrix} \tag{6.16}$$

where η is the dimensionless two component lattice fermion field and $\hat{\sigma}_1 = \sigma_2$, $\hat{\sigma}_2 = -\sigma_1$.

Linearization of the link fields

Because of the nonlinear constraints $U^\dagger U = 1$, $\det U = 1$, it is highly nontrivial to quantize the system. Hence Bardeen and Pearson [11] and Bardeen, Pearson, and Rabinovici [12] proposed to replace the nonlinear variables U by *linear* variables M where M belongs to $GL(N, \mathcal{C})$, i.e., we replace $\frac{1}{g} U_r(\mathbf{x}) \rightarrow M_r(\mathbf{x})$. This linearized approximation is somewhat meaningful only on a coarse lattice. Justification may come from the fact that particle structure of a hadron is a long-distance property which can be described by some effective variables without any explicit details of the microscopic variables [12]. The x^- independent residual gauge invariance on the transverse plane is still preserved with the linear gauge fields (see Appendix I for details). Once we replace U by M , many more terms are allowed in the Hamiltonian. Thus one needs to add an effective potential V_{eff} to the Lagrangian density

$$V_{eff} = -\frac{\mu^2}{a^2} Tr(M^\dagger M) + \lambda_1 Tr[(M^\dagger M)^2] + \lambda_2 [\det M + H.c.] + \dots \tag{6.17}$$

6.3 Effective Hamiltonian

6.3.1 Hamiltonian with forward and backward derivatives

Once we replace the nonlinear link fields by linear link field by including the effective potential, we perform canonical quantization and construct the effective Hamiltonian for transverse lattice QCD.

Thus, the effective Hamiltonian for QCD on the transverse lattice, when fermions are put in with forward and backward lattice derivatives, becomes

$$\begin{aligned} P_{fb}^- &= P_{f\ free}^- + P_V^- + P_{fhf}^- + P_{hfh}^- + P_{chnf}^- \\ &\quad + P_{qqc}^- + P_{ggc}^- + P_{qgc}^- + P_p^-. \end{aligned} \quad (6.18)$$

The free fermion part is

$$P_{f\ free}^- = \int dx^- \sum_{\mathbf{x}} (m^2 + \frac{2}{a^2}) \eta^\dagger(\mathbf{x}) \frac{1}{i\partial^+} \eta(\mathbf{x}). \quad (6.19)$$

The effective potential part is

$$P_V^- = \int dx^- a^2 \sum_{\mathbf{x}} \left(\frac{\mu^2}{a^2} Tr(M^\dagger M) - \lambda_1 Tr[(M^\dagger M)^2] - \lambda_2 [det M + H.c.] + \dots \right). \quad (6.20)$$

The free helicity-flip part is

$$P_{fhf}^- = 2im \int dx^- \sum_{\mathbf{x}} \sum_s \eta^\dagger(\mathbf{x}) \hat{\sigma}_s \frac{1}{a} \frac{1}{\partial^+} \eta(\mathbf{x}). \quad (6.21)$$

Helicity flip associated with the fermion hop is

$$\begin{aligned} P_{hfh}^- &= -img \int dx^- \sum_{\mathbf{x}} \sum_s \eta^\dagger(\mathbf{x}) \hat{\sigma}_s \frac{1}{a} \frac{1}{\partial^+} \left[M_s(\mathbf{x}) \eta(\mathbf{x} + a\hat{\mathbf{s}}) \right] \\ &\quad -img \int dx^- \sum_{\mathbf{x}} \sum_r \left[\eta^\dagger(\mathbf{x} + a\hat{\mathbf{r}}) M_r^\dagger(\mathbf{x}) \right] \hat{\sigma}_r \frac{1}{a} \frac{1}{\partial^+} \eta(\mathbf{x}). \end{aligned} \quad (6.22)$$

Canonical helicity non-flip terms are

$$\begin{aligned} P_{chnf}^- &= -\frac{g}{a^4} \int dx^- a^2 \sum_{\mathbf{x}} \sum_{rs} [\eta^\dagger(\mathbf{x} + a\hat{\mathbf{r}}) M_r^\dagger(\mathbf{x})] \hat{\sigma}_r \frac{1}{i\partial^+} \hat{\sigma}_s [\eta(\mathbf{x})] \\ &\quad -\frac{g}{a^4} \int dx^- a^2 \sum_{\mathbf{x}} \sum_{rs} [\eta^\dagger(\mathbf{x})] \hat{\sigma}_r \frac{1}{i\partial^+} \hat{\sigma}_s [M_s(\mathbf{x}) \eta(\mathbf{x} + a\hat{\mathbf{s}})] \\ &\quad -\frac{g^2}{a^4} \int dx^- a^2 \sum_{\mathbf{x}} \sum_{rs} [\eta^\dagger(\mathbf{x} + a\hat{\mathbf{r}}) M_r^\dagger(\mathbf{x})] \hat{\sigma}_r \frac{1}{i\partial^+} \hat{\sigma}_s [M_s(\mathbf{x}) \eta(\mathbf{x} + a\hat{\mathbf{s}})]. \end{aligned} \quad (6.23)$$

The four-fermion instantaneous term is

$$P_{qqc}^- = -2\frac{g^2}{a^2} \int dx^- \sum_{\mathbf{x}} \eta^\dagger(\mathbf{x}) T^a \eta(\mathbf{x}) \frac{1}{(\partial^+)^2} \eta^\dagger(\mathbf{x}) T^a \eta(\mathbf{x}). \quad (6.24)$$

The four link instantaneous term is

$$P_{ggc}^- = -\frac{1}{2} \frac{g^2}{a^2} \int dx^- \sum_{\mathbf{x}} J_{LINK}^{+a}(\mathbf{x}) \frac{1}{(\partial^+)^2} J_{LINK}^{+a}(\mathbf{x}). \quad (6.25)$$

The fermion - link instantaneous term is

$$P_{qgc}^- = 2\frac{g^2}{a^2} \int dx^- \sum_{\mathbf{x}} J_{LINK}^{+a}(\mathbf{x}) \frac{1}{(\partial^+)^2} \eta^\dagger(\mathbf{x}) T^a \eta(\mathbf{x}). \quad (6.26)$$

The plaquette term is

$$P_p^- = -\frac{g^2}{a^4} \int dx^- a^2 \sum_{\mathbf{x}} \sum_{r \neq s} \left\{ Tr \left[M_r(\mathbf{x}) M_s(\mathbf{x} + a\hat{r}) M_{-r}(\mathbf{x} + a\hat{r} + a\hat{s}) M_{-s}(\mathbf{x} + a\hat{s}) - 1 \right] \right\}. \quad (6.27)$$

Here

$$J_{LINK}^{+\alpha}(\mathbf{x}) = \sum_r Tr \left\{ T^\alpha [M_r(\mathbf{x}) i \overset{\leftrightarrow}{\partial}^+ M_r^\dagger(\mathbf{x}) + M_r^\dagger(\mathbf{x} - a\hat{r}) i \overset{\leftrightarrow}{\partial}^+ M_r(\mathbf{x} - a\hat{r})] \right\}. \quad (6.28)$$

6.3.2 Hamiltonian with the Wilson term

When one uses symmetric derivatives for the fermion fields, doublers arise as a result of the decoupling of even and odd lattice sites. Here we use the Wilson term to remove the doublers. In this subsection, the details of the structure of the Hamiltonian resulting with the modification of the Wilson term are presented.

The effective Hamiltonian for this case can be written as

$$\begin{aligned} P^- &= P_{f\ free}^- + P_V^- + P_{hf}^- + P_{whf}^- \\ &\quad + P_{chnf}^- + P_{wnf1}^- + P_{wnf2}^- \\ &\quad + P_{qqc}^- + P_{ggc}^- + P_{qgc}^- + P_p^-. \end{aligned} \quad (6.29)$$

The free fermion part is

$$P_{f\ free}^- = \int dx^- a^2 \sum_{\mathbf{x}} \frac{1}{a^2} \left(m + 4\frac{\mathbf{K}}{a} \right)^2 \eta^\dagger(\mathbf{x}) \frac{1}{i\partial^+} \eta(\mathbf{x}). \quad (6.30)$$

The helicity flip part is

$$\begin{aligned}
P_{hf}^- &= -g \int dx^- \sum_{\mathbf{x}} \left\{ \left(m + 4 \frac{\kappa}{a} \right) \frac{1}{2a} \eta^\dagger(\mathbf{x}) \sum_r \hat{\sigma}_r \frac{1}{i\partial^+} [M_r(\mathbf{x}) \eta(\mathbf{x} + a\hat{\mathbf{r}}) - M_{-r}(\mathbf{x}) \eta(\mathbf{x} - a\hat{\mathbf{r}})] \right. \\
&\quad \left. - \left(m + 4 \frac{\kappa}{a} \right) \frac{1}{2a} \sum_r \left[\eta^\dagger(\mathbf{x} - a\hat{\mathbf{r}}) \hat{\sigma}_r M_r(\mathbf{x} - a\hat{\mathbf{r}}) - \eta^\dagger(\mathbf{x} + a\hat{\mathbf{r}}) \hat{\sigma}_r M_{-r}(\mathbf{x} + a\hat{\mathbf{r}}) \right] \frac{1}{i\partial^+} \eta(\mathbf{x}) \right\}.
\end{aligned} \tag{6.31}$$

The Wilson term induced helicity flip part

$$\begin{aligned}
P_{whf}^- &= g^2 \int dx^- \sum_{\mathbf{x}} \left\{ \frac{\kappa}{a} \frac{1}{2a} \sum_r \sum_s \left[\eta^\dagger(\mathbf{x} - a\hat{\mathbf{r}}) M_r(\mathbf{x} - a\hat{\mathbf{r}}) + \eta^\dagger(\mathbf{x} + a\hat{\mathbf{r}}) M_{-r}(\mathbf{x} + a\hat{\mathbf{r}}) \right] \right. \\
&\quad \frac{1}{i\partial^+} \hat{\sigma}_s \left[M_s(\mathbf{x}) \eta(\mathbf{x} + a\hat{\mathbf{s}}) - M_{-s}(\mathbf{x}) \eta(\mathbf{x} - a\hat{\mathbf{s}}) \right] \\
&\quad - \frac{\kappa}{a} \frac{1}{2a} \sum_r \sum_s \left[\eta^\dagger(\mathbf{x} - a\hat{\mathbf{r}}) \hat{\sigma}_r M_r(\mathbf{x} - a\hat{\mathbf{r}}) - \eta^\dagger(\mathbf{x} + a\hat{\mathbf{r}}) \hat{\sigma}_r M_{-r}(\mathbf{x} + a\hat{\mathbf{r}}) \right] \\
&\quad \left. \frac{1}{i\partial^+} \left[M_s(\mathbf{x}) \eta(\mathbf{x} + a\hat{\mathbf{s}}) + M_{-s}(\mathbf{x}) \eta(\mathbf{x} - a\hat{\mathbf{s}}) \right] \right\}.
\end{aligned} \tag{6.32}$$

The canonical helicity non-flip term arising from fermion constraint is

$$\begin{aligned}
P_{chnf}^- &= -g^2 \int dx^- \sum_{\mathbf{x}} \frac{1}{4a^2} \sum_r \sum_s \left[\eta^\dagger(\mathbf{x} - a\hat{\mathbf{r}}) \hat{\sigma}_r M_r(\mathbf{x} - a\hat{\mathbf{r}}) - \eta^\dagger(\mathbf{x} + a\hat{\mathbf{r}}) \hat{\sigma}_r M_{-r}(\mathbf{x} + a\hat{\mathbf{r}}) \right] \\
&\quad \frac{1}{i\partial^+} \hat{\sigma}_s \left[M_s(\mathbf{x}) \eta(\mathbf{x} + a\hat{\mathbf{s}}) - M_{-s}(\mathbf{x}) \eta(\mathbf{x} - a\hat{\mathbf{s}}) \right].
\end{aligned} \tag{6.33}$$

The Wilson term induced helicity non flip terms are

$$\begin{aligned}
P_{wnf1}^- &= -g \int dx^- \sum_{\mathbf{x}} \left\{ \left(m + 4 \frac{\kappa}{a} \right) \frac{\kappa}{a} \eta^\dagger(\mathbf{x}) \frac{1}{i\partial^+} \sum_r \left[M_r(\mathbf{x}) \eta(\mathbf{x} + a\hat{\mathbf{r}}) + M_{-r}(\mathbf{x}) \eta(\mathbf{x} - a\hat{\mathbf{r}}) \right] \right. \\
&\quad \left. + \left(m + 4 \frac{\kappa}{a} \right) \frac{\kappa}{a} \sum_r \left[\eta^\dagger(\mathbf{x} - a\hat{\mathbf{r}}) M_r(\mathbf{x} - a\hat{\mathbf{r}}) + \eta^\dagger(\mathbf{x} + a\hat{\mathbf{r}}) M_{-r}(\mathbf{x} + a\hat{\mathbf{r}}) \right] \frac{1}{i\partial^+} \eta(\mathbf{x}) \right\}.
\end{aligned} \tag{6.34}$$

and

$$\begin{aligned}
P_{wnf2}^- &= -g^2 \int dx^- \sum_{\mathbf{x}} \frac{\kappa^2}{a^2} \sum_r \sum_s \left[\eta^\dagger(\mathbf{x} - a\hat{\mathbf{r}}) M_r(\mathbf{x} - a\hat{\mathbf{r}}) + \eta^\dagger(\mathbf{x} + a\hat{\mathbf{r}}) M_{-r}(\mathbf{x} + a\hat{\mathbf{r}}) \right] \\
&\quad \frac{1}{i\partial^+} \left[M_s(\mathbf{x}) \eta(\mathbf{x} + a\hat{\mathbf{s}}) + M_{-s}(\mathbf{x}) \eta(\mathbf{x} - a\hat{\mathbf{s}}) \right].
\end{aligned} \tag{6.35}$$

Comparing the Hamiltonians with a) forward-backward derivative and b) symmetric derivative with the Wilson term we notice that the only differences are in the particle number changing interactions, namely, helicity flip and helicity non-flip terms.

6.4 Meson bound state in one link approximation

6.4.1 Relevant interactions

In one link approximation, for either Hamiltonian, the four link instantaneous term and the plaquette term do not contribute and only the link mass term of the effective potential contributes. Further, in the case of the forward-backward Hamiltonian, the helicity non-flip part proportional to g^2 does not contribute. For the Wilson term modified Hamiltonian, the Wilson term induced helicity flip part P_{whf}^- , the canonical helicity non-flip term P_{cnhf}^- and the term proportional to κ^2 in the Wilson term induced helicity non-flip part do not contribute. Thus in the case of the Wilson term modified Hamiltonian the entire fermion hopping with no helicity flip arises from the Wilson term. In the case of forward and backward derivatives, terms are also present in one link approximation which violate hypercubic symmetry on the transverse lattice (see Appendix F). They become irrelevant in the continuum limit when the linear variables M are replaced by non-linear variables U . We have removed them entirely from the Hamiltonian in the present investigation. The Hamiltonian matrix elements in DLCQ for both forward-backward and symmetric derivative with Wilson term are explicitly given in Appendix J.

6.4.2 Comparison with one gluon exchange in the continuum

It is interesting to compare the one link approximation on the transverse lattice with the one gluon exchange approximation in the continuum. In the latter, a major source of singularity is the $\frac{k^\perp}{k^+}$ term in the quark - gluon vertex where k^\perp (k^+) is the gluon transverse (longitudinal) momentum. This originates from the $A^- J_q^+$ interaction term in the Hamiltonian via $\frac{1}{\partial^+} \partial^\perp \cdot A^\perp$ contribution to the constrained field A^- . This term gives rise to quadratic ultraviolet divergence in the transverse plane accompanied by linear divergence in the longitudinal direction in fermion self energy. On the transverse lattice, $\partial^+ A^- \propto \frac{1}{\partial^+} J_{LINK}^+$ so that $A^- J_q^+ \rightarrow J_{LINK}^+ \frac{1}{(\partial^+)^2} J_q^+$. Thus a term which gives rise to severe divergence structure in the continuum gets buried in the fermion-link instantaneous interaction term which gives rise to a term in the gauge boson fermion vertex in the continuum in Abelian theory. In the non-Abelian gauge theory this gives rise to a term in the quark-gluon vertex and also to the instantaneous quark-gluon interaction in the continuum.

The transfer of the troublesome term from quark-gluon vertex in the continuum theory to quark - link instantaneous interaction term in the lattice theory has an interesting consequence. In the continuum theory, the addition of a gluon mass term by hand spoils the cancellation of the light front singularity between one gluon exchange and the instantaneous four - fermion interaction. On the transverse lattice, this cancellation is absent anyway with or without a link mass term.

6.4.3 Longitudinal dynamics and effects of transverse hopping

We first consider the dynamics in the absence of any link. In this case, fermions cannot hop, and at each transverse location we have (1+1) dimensional light front QCD which reduces to the 't Hooft model in the large N_c limit. In this case quark and antiquark at the same transverse position interact via the spin independent instantaneous interaction which, in the non-relativistic limit reduces to the linear potential in the longitudinal direction. The only parameters in the theory are the dimensionless fermion mass $m_f = am$ and the gauge coupling g . The spectrum consists of a ground state and a tower of excited states corresponding to the excitations of the $q\bar{q}$ pair.

Next consider the inclusion of the $q\bar{q}$ link states. There are four independent amplitudes corresponding to whether the quark is on the left or right of the antiquark or, above or below the antiquark. With non-zero mass of the link, these states lie above the ground state of pure quark - antiquark system. Further the q , \bar{q} and link (which are frozen at their transverse positions) undergo fermion - link instantaneous interactions in the longitudinal direction which further increases the mass of $q\bar{q}$ link states. Now the quark or antiquark can hop via helicity flip or helicity non-flip. Here we find a major difference between the Hamiltonians resulting from forward-backward derivative and symmetric derivative. Let us first consider the helicity flip hopping term in the forward-backward case

$$P_{hf}^- = -img \int dx^- \sum_{\mathbf{x}} \sum_r \left[\eta^\dagger(\mathbf{x}) \hat{\sigma}_r \frac{1}{a} \frac{1}{\partial^+} \eta(\mathbf{x} + a\hat{\mathbf{r}}) + \eta^\dagger(\mathbf{x} + a\hat{\mathbf{r}}) M_r^\dagger(\mathbf{x}) \hat{\sigma}_r \frac{1}{a} \frac{1}{\partial^+} \eta(\mathbf{x}) \right]. \quad (6.36)$$

If we consider transition from two particle to three particle state by a quark hop, then the first term in Eq. (6.36) corresponds to $|2\rangle \rightarrow |3a\rangle$ and the second term corresponds to $|2\rangle \rightarrow |3b\rangle$.

The helicity flip term in symmetric derivative case, after making some shifts in lattice points, can be written as

$$\begin{aligned}
P_{hf}^- &= -g \left(m + 4 \frac{\kappa}{a} \right) \frac{1}{2a} \int dx^- \sum_{\mathbf{x}} \sum_r \left[\left\{ \eta^\dagger(\mathbf{x}) \hat{\sigma}_r \frac{1}{i\partial^+} M_r(\mathbf{x}) \eta(\mathbf{x} + a\hat{\mathbf{r}}) - \eta^\dagger(\mathbf{x}) \hat{\sigma}_r M_r(\mathbf{x}) \frac{1}{i\partial^+} \eta(\mathbf{x} + a\hat{\mathbf{r}}) \right\} \right. \\
&\quad \left. - \left\{ \eta^\dagger(\mathbf{x}) \hat{\sigma}_r \frac{1}{i\partial^+} M_{-r}(\mathbf{x}) \eta(\mathbf{x} - a\hat{\mathbf{r}}) - \eta^\dagger(\mathbf{x}) \hat{\sigma}_r M_{-r}(\mathbf{x}) \frac{1}{i\partial^+} \eta(\mathbf{x} - a\hat{\mathbf{r}}) \right\} \right]. \quad (6.37)
\end{aligned}$$

For the Hamiltonian with symmetric derivative, a quark or antiquark hopping accompanied by helicity flip has opposite signs for forward and backward hops. On the other hand, hopping accompanied by helicity non-flip have the same signs. As a result, there is no interference between helicity flip and helicity non-flip interactions [1]. In the case of the Hamiltonian with forward-backward derivative, quark or antiquark hopping accompanied by helicity flip has the same sign for forward and backward hops. As a consequence the helicity non-flip hop can interfere with the helicity flip hop. This has immediate consequences for the spectrum. In the case with symmetric derivative, in lowest order perturbation theory, the helicity zero states mix with each other which causes a splitting in their eigenvalues resulting in the singlet state lower than the triplet state. On the other hand, helicity plus or minus one states do not mix with each other or with helicity zero states resulting in a two fold degeneracy. In the case with forward and backward derivatives all helicity states mix with each other resulting in the complete absence of degeneracy. Obviously, one has the freedom to tune the free parameters to minimize the splitting.

6.4.4 Singularities, divergence and counterterms

Since the transverse lattice serves as an ultraviolet regulator, we need to worry about only light front longitudinal momentum singularities.

Tree level

We take all the terms in the Hamiltonian to be normal ordered. At tree level this leaves us with singular factors of the form $\frac{1}{(k)^2}$ in the normal ordered four fermion and fermion link instantaneous interactions. The singularities are removed by adding the counterterms used in

the previous work [4] on transverse lattice. The explicit forms of the counterterms are given in Appendix J.3 in the appropriate places.

Self energy corrections

In the one link approximation, a quark can make a forward (backward) hop followed by a backward (forward) hop resulting in self energy corrections. In a single hop, helicity flip or non-flip can occur. In the case of symmetric derivatives, helicity flip cannot interfere with helicity non-flip, and as a consequence, self energy corrections are diagonal in helicity space. In the case of forward and backward derivatives, the interference is nonzero resulting in self energy corrections, both diagonal and off-diagonal in the helicity space. Similar self energy corrections are generated for an antiquark also. These self energy corrections contain a logarithmic light front infrared divergence which must be removed by counterterms. In Appendix J.5 we present the explicit form of counterterms in the two cases separately. In previous works on one link approximation [1, 4, 5], these counterterms were not implemented. For low K values one may not feel the divergence, but as one increases K the need of self energy counterterms are readily felt.

6.5 Numerical Results

We diagonalize the dimensionless matrix $a^2 P^-$. We further divide the matrix elements by $g^2 C_f$ which is the strength of the matrix elements for four fermion and fermion - link instantaneous interactions. Now, define the constant G with dimension of mass by $G^2 = \frac{g^2}{a^2} C_f$. DLCQ yields the eigenvalue $\mathcal{M}^2 = \frac{M^2}{G^2}$.

The dimensionless couplings are introduced [4] as follows. Fermion mass $m_f = m/G$, link mass $\mu_b = \mu/G$, particle number conserving helicity flip coupling $m_f/(aG) = m_f C_1$, particle number non-conserving helicity flip $\sqrt{N} g m_f / (aG) = m_f C_2$, and particle number non-conserving helicity non-flip $\sqrt{N} g / (a^2 G^2) = C_3$. In the case of the Wilson term modified Hamiltonian, we have fermion mass term $m_f = (m + 4\kappa/a)/G$, helicity-flip coupling $\sqrt{N} g m_f / (2aG) = m_f \tilde{C}_2$, and helicity non-flip coupling $\sqrt{N} g m_f \kappa / (aG) = m_f \tilde{C}_3$.

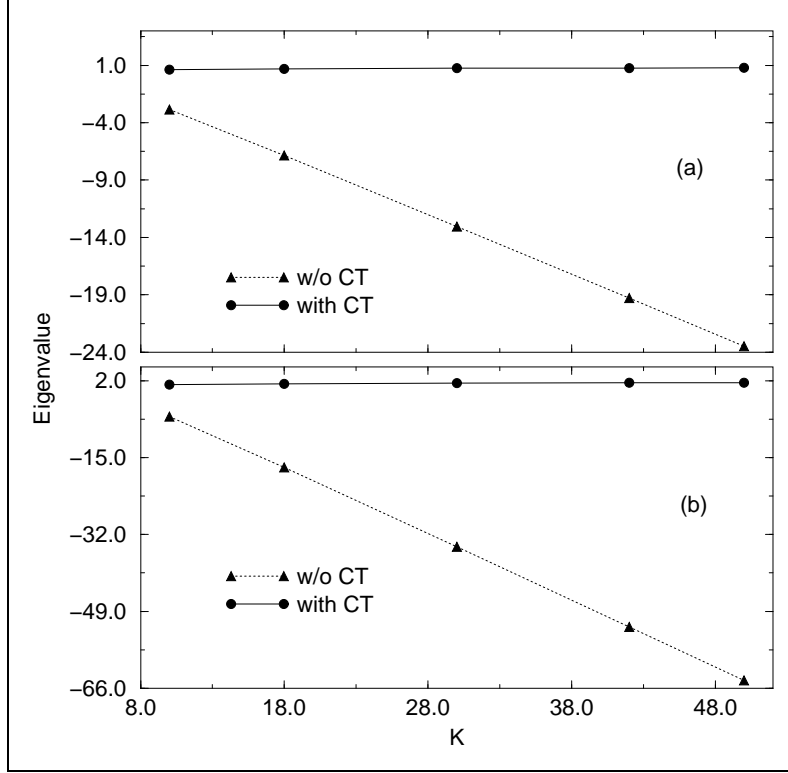


Figure 6.1: Effect of counterterm on the ground state eigenvalue. (a) With and without the counterterm in the $q\bar{q}$ sector for $m_f = 0.3$. (b) With and without the counterterm in the $q\bar{q}$ link sector for $m_f = 0.3$ and $\mu_b = 0.2$.

All the results presented here were obtained on a small cluster of computers using the Many Fermion Dynamics (MFD) code [13] implementing the Lanczos diagonalization method in parallel environment. For low K values, the results were checked against an independent code running on a single processor.

Cancellation of divergences

As we already mentioned, we encounter $\frac{1}{(k^+)^2}$ singularities with instantaneous four fermion and instantaneous fermion - link interactions which give rise to linear divergences. We remove the divergences by adding appropriately chosen counterterms. We have numerically checked the removal of linear divergence by counterterms in DLCQ. First we consider only $q\bar{q}$ states with instantaneous interaction. We study the ground state eigenvalue as a function of K with and without the counterterm. Results are presented in Fig. 6.1 (a). Next we consider only $q\bar{q}$

link states with fermion-link instantaneous interaction with and without the counterterms. The behavior of ground state eigenvalue as a function of K is presented in Fig. 6.1 (b). In both cases, it is evident that the counterterms are efficient in removing the divergence.

6.5.1 $q\bar{q}$ at the same transverse location

Next we study the spectrum of the Hamiltonian in the absence of any links. Since, in this case, the Hamiltonian depends only on the dimensionless ratio $\frac{m_f}{g}$ we fix $g = 1$ and vary m_f to study the spectra. The Hamiltonian matrix is diagonalized for various values of K . The convergence of the ground state eigenvalue as a function of K is presented in Table 6.1.

K	Eigenvalue (\mathcal{M}^2)		
	$m_f = 0.3$	$m_f = 0.9$	$m_f = 3.0$
10	0.620	4.547	39.233
18	0.693	4.664	39.861
30	0.745	4.724	40.053
50	0.788	4.762	40.163
78	0.819	4.783	40.220
98	0.832	4.791	40.241
$K \rightarrow \infty$	0.869	4.820	40.285

Table 6.1: Ground state eigenvalue (in units of G^2) for $q\bar{q}$ sitting at the same transverse location.

The ground state wavefunction squared as a function of the longitudinal momentum fraction x is plotted in Fig. 6.2. The convergence of the wavefunction has a very different behavior as a function of fermion mass m_f . As can be seen from this figure, the convergence in K is from above for heavy m_f and from below for light m_f . As a consequence the wavefunction is almost independent of K when m_f is of order g .

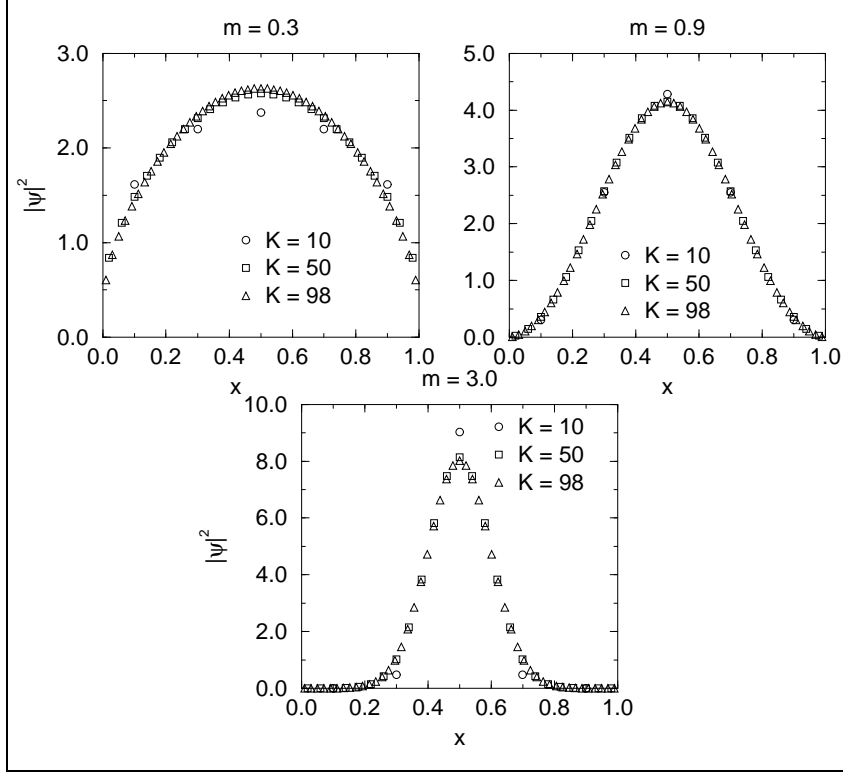


Figure 6.2: Quark distribution function $|\psi(x)|^2$ of the ground state in the $q\bar{q}$ approximation for three choices of quark masses with coupling constant $g = 1.0$.

6.5.2 Results of the one link approximation

We encountered logarithmic infrared divergences due to self energy corrections and, in Appendix J.5, we discuss the associated counterterms. In Fig. 6.3 we show the effect of self energy counterterms on the ground state energy in the two Hamiltonian cases we studied.

The convergence of lowest four eigenvalues with K for the Hamiltonian with forward-backward and symmetric lattice derivatives is shown in Table 6.2 for $m_f = 0.3$, $\mu_b = 0.2$. We also show the results extrapolated to $K \rightarrow \infty$. The convergence of the eigenvalues in K is very slow and one really needs to go for large K .

The quark distribution function for the ground state and the fifth state for the set of parameters $m_f = 0.3$, $\mu_b = 0.2$, $C_2 = 0.4$, $C_3 = 0.01$ and $K = 30$ is presented in Fig. 6.4. In this figure we also present separately the contribution from two particle and three particle states. As expected, the contribution from the three particle state peaks at smaller x compared to the two

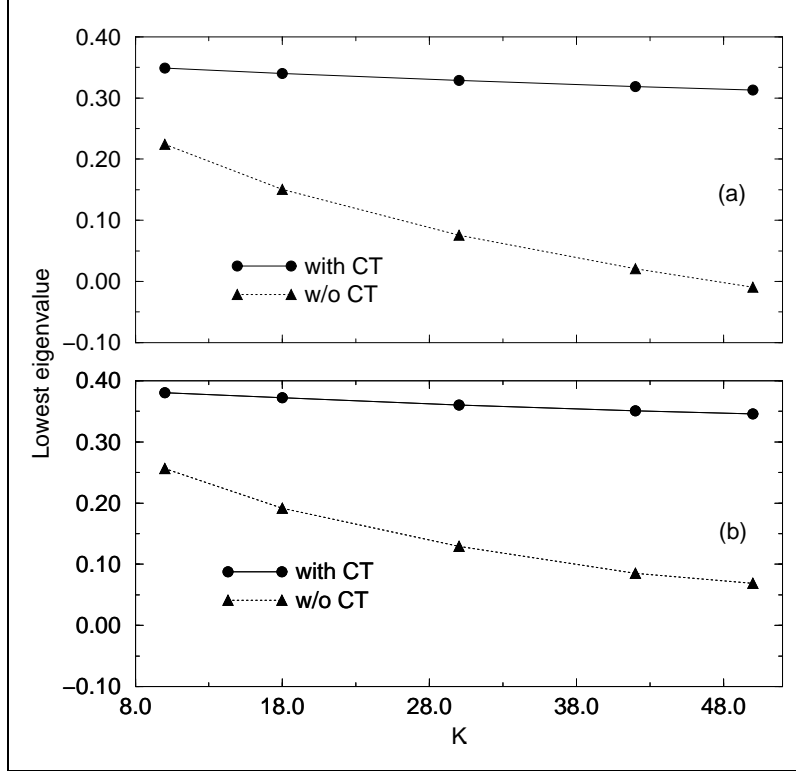


Figure 6.3: Effect of self energy counterterms on the ground state eigenvalue in the case of (a) symmetric derivative with $\tilde{C}_2 = 0.4$, $\tilde{C}_3 = 0.1$ and (b) forward-backward derivative with $C_2 = 0.4$, $C_3 = 0.01$. $m_f = 0.3$, $\mu_b = 0.2$ for both cases.

particle state. The exact location of this peak depends on the link mass. The ground state is dominated by two particle sector while the fifth state is dominated by three particle sector. We have shown only one of the first four states since they are similar looking states with different spin contents. Fig. 6.4 warns us that one link approximation is inadequate to study the excited states.

It is interesting to see the effect of fermion - link instantaneous interaction on the low lying eigenvalues. In its absence, there is no confining interaction in the longitudinal direction in the $q\bar{q}$ link sector. Furthermore, the mass of the lowest state in this sector corresponds to the threshold mass in this sector. Since its mass is lowered, it mixes more strongly with the $q\bar{q}$ sector in the ground state and from Fig. 6.5 we see that the ground state gets comparable

K	Forward-backward ($C_2 = 0.01, C_3 = 0.4$)				Symmetric ($\tilde{C}_2 = 0.1, \tilde{C}_3 = 0.4$)			
	\mathcal{M}_1^2	\mathcal{M}_2^2	\mathcal{M}_3^2	\mathcal{M}_4^2	\mathcal{M}_1^2	\mathcal{M}_2^2	\mathcal{M}_3^2	\mathcal{M}_4^2
10	0.38041	0.4800	0.4899	0.5996	0.3486	0.4507	0.4507	0.5980
18	0.3722	0.4968	0.5110	0.6447	0.3402	0.4673	0.4673	0.6409
30	0.3606	0.5027	0.5210	0.6680	0.3288	0.4702	0.4702	0.6620
42	0.3511	0.5029	0.5240	0.6765	0.3189	0.4677	0.4677	0.6682
50	0.3457	0.5019	0.5246	0.6790	0.3130	0.4651	0.4651	0.6693
$K \rightarrow \infty$	0.3243	0.5022	0.5313	0.6979	0.2913	0.4589	0.4589	0.6837

Table 6.2: Lowest four eigenvalues (in units of G^2) in one link approximation.

contribution from both sectors. The fifth state now corresponds to an almost free $q\bar{q}$ link state with infinitesimal $q\bar{q}$ component as shown in Fig. 6.5.

6.6 Summary and Discussion

We have performed an investigation of $q\bar{q}$ states using two different light front Hamiltonians in the one link approximation. The Hamiltonians correspond to two different ways of formulating fermions on the transverse lattice, namely, (a) forward and backward derivatives for ψ^+ and ψ^- respectively or vice versa and (b) symmetric derivatives for both ψ^+ and ψ^- . In the latter, fermion doubling is present which is removed by an addition of the Wilson term. In this case there is no interference between helicity flip hop and helicity non-flip hop and, as a result, the $q\bar{q}$ component of the ground state wavefunction which has helicity plus or minus one are degenerate. In the former case, interference between helicity flip and helicity non-flip leads to the absence of degeneracy in the low lying spectra. One can recover approximate degeneracy of helicity plus or minus one components only by keeping the strength of the helicity non-flip hopping very small.

Since the one link approximation is very crude and our motivation was to study and compare different fermions on the transverse lattice other than the assessment of the transverse lattice approach itself, we have not attempted a detailed fit to low lying states in the meson sector. Instead, we have explored the effects of various coupling strengths on the low lying spectra and

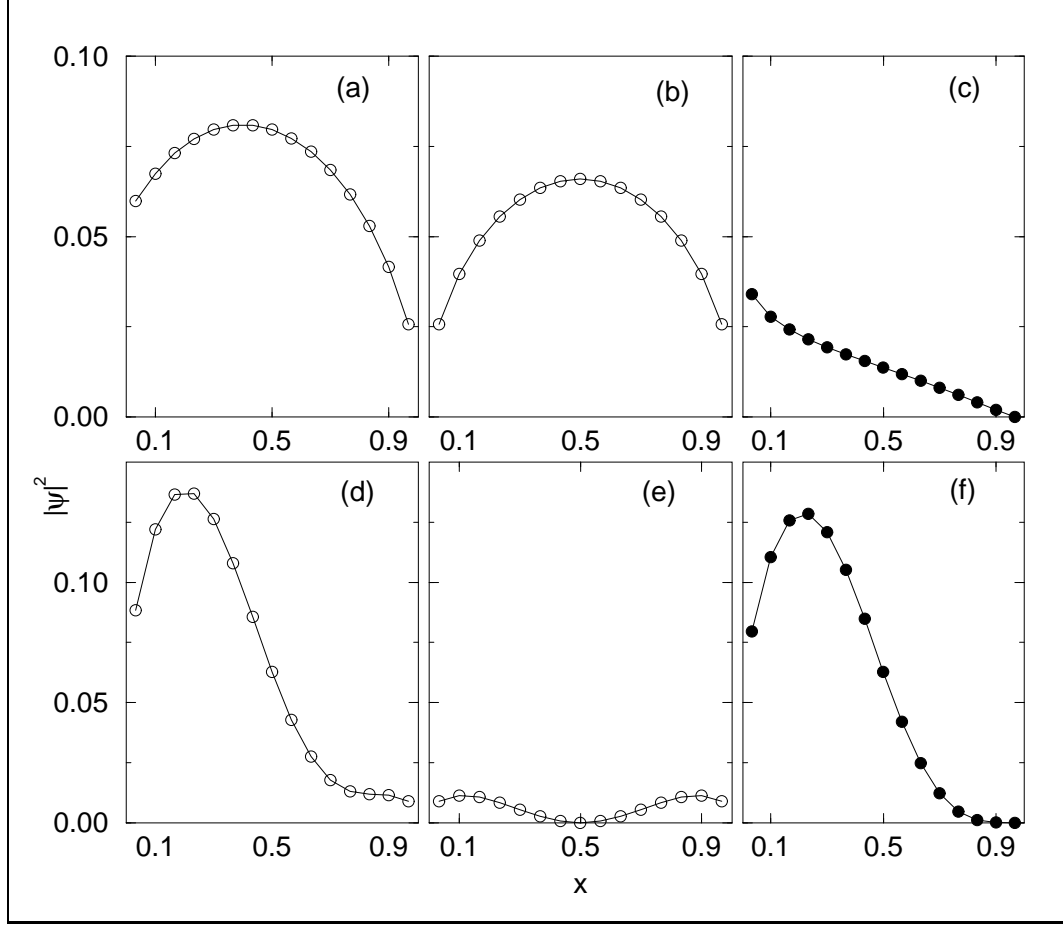


Figure 6.4: (a) Quark distribution function $|\psi(x)|^2$ of the ground state in the one link approximation, (b) $q\bar{q}$ contribution to the ground state, (c) $q\bar{q}$ link contribution to the ground state. (d) Quark distribution function $|\psi(x)|^2$ of the fifth eigenstate in the one link approximation, (e) $q\bar{q}$ contribution to the fifth eigenstate, (f) $q\bar{q}$ link contribution to the fifth eigenstate. The parameters are $m_f = 0.3$, $\mu_b = 0.2$, $C_2 = 0.4$, $C_3 = 0.01$ and $K = 30$.

associated wavefunctions. In this work, longitudinal dynamics is handled by DLCQ. We have performed a detailed study of various convergence issues in DLCQ using a wide range of K values.

We summarize our results as follows. We have shown the effectiveness of appropriate counterterms in the $q\bar{q}$ and $q\bar{q}$ link sector to regulate the instantaneous fermion and fermion - link interactions respectively. We have also checked the cancellation of logarithmic divergences due to self energy effects. In the limit where fermions are frozen on the transverse lattice but undergo instantaneous longitudinal interaction, we have studied the convergence of ground state

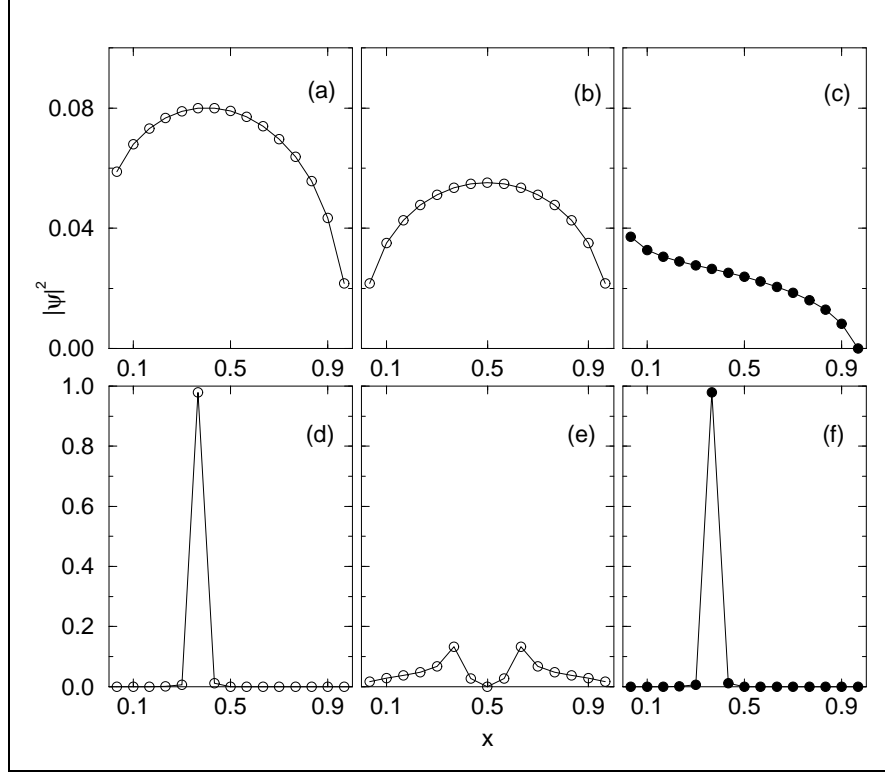


Figure 6.5: Without the fermion - link instantaneous interaction: (a) Quark distribution function $|\psi(x)|^2$ of the ground state in the one link approximation, (b) $q\bar{q}$ contribution to the ground state, (c) $q\bar{q}$ link contribution to the ground state. (d) Quark distribution function $|\psi(x)|^2$ of the fifth eigenstate in the one link approximation, (e) $q\bar{q}$ contribution to the fifth eigenstate multiplied by 10^4 , (f) $q\bar{q}$ link contribution to the fifth eigenstate. Parameters are the same as in Fig. 6.4.

wavefunction with respect to K for three typical values of the fermion mass. We have studied how the presence or absence of fermion - link instantaneous interaction in the $q\bar{q}$ link sector affects the wavefunction of low lying states. We have also studied the consequences of the interference of helicity flip and helicity non-flip hopping in the Hamiltonian with forward-backward derivatives. This interference is absent in the symmetric derivative case.

BIBLIOGRAPHY

- [1] M. Burkardt and H. El-Khozondar, Phys. Rev. D **60**, 054504 (1999), hep-ph/9805495.
- [2] D. Chakrabarti, A. K. De and A. Harindranath, Phys. Rev. D **67**, 076004 (2003), hep-th/0211145.
- [3] P. A. Griffin, Phys. Rev. D **47**, 3530 (1993), hep-th/9207083.
- [4] S. Dalley, Phys. Rev. D **64**, 036006 (2001), hep-ph/0101318.
- [5] M. Burkardt and S.K. Seal, Phys. Rev. D **65**, 034501 (2002), hep-ph/0102245; M. Burkardt and S. K. Seal, Phys. Rev. D **64**, 111501 (2001), hep-ph/0105109.
- [6] For a review, see, M. Burkardt and S. Dalley, Prog. Part. Nucl. Phys. **48**, 317 (2002), hep-ph/0112007.
- [7] S. Dalley and B. van de Sande, Phys. Rev. D **67**, 114507 (2003) hep-ph/0212086.
- [8] T. Maskawa and K. Yamawaki, Prog. Theor. Phys. **56**, 270 (1976); A. Casher, Phys. Rev. D **14**, 452 (1976); C. B. Thorn, Phys. Rev. D **17**, 1073 (1978); H.C. Pauli and S.J. Brodsky, Phys. Rev. D **32**, 1993, (1985); *ibid.*, 2001 (1985). For a review, see, S. J. Brodsky, H. C. Pauli and S. S. Pinsky, Phys. Rep. **301**, 299 (1998), hep-ph/9705477.
- [9] D. Chakrabarti, A. Harindranath and J. P. Vary, *A study of $q\bar{q}$ states in transverse lattice QCD using alternative fermion formulations*, hep-ph/0309317.
- [10] W. M. Zhang and A. Harindranath, Phys. Rev. D **48**, 4881 (1993), W. M. Zhang, Phys. Rev. D **56**, 1528 (1997), hep-ph/9705226.
- [11] W. A. Bardeen and R. B. Pearson, Phys. Rev. D **14**, 547 (1976).
- [12] W. A. Bardeen, R. B. Pearson and E. Rabinovici, Phys. Rev. D **21**, 1037 (1980).
- [13] J.P. Vary, The Many-Fermion-Dynamics Shell-Model Code, Iowa State University, 1992 (unpublished); J.P. Vary and D.C. Zheng, *ibid.*, 1994.

CHAPTER 7

Summary, Conclusions and Future Outlook

Hadronic bound state problem is one of the most challenging tasks in nonperturbative QCD. Since it is very important to have direct access to the bound state wavefunctions which is essential to calculate QCD observables, Hamiltonian approach is the most suitable candidate to address the problem of bound states. The simple structure of the vacuum in light-front QCD makes it possible to carry out a Hamiltonian analysis of the bound states in the Fock space language. In this thesis, we have investigated two nonperturbative techniques in light-front QCD, namely, similarity renormalization group (SRG) approach and light-front transverse lattice (LFTL) approach in the context of meson bound state problem. Unless and until we have complete control over the intricacies of the techniques in use, the dream to explore the nonperturbative QCD with full confidence will remain unrealized. In this work, we have performed a critical evaluation of the two nonperturbative approaches mentioned above and assessed them in terms of their strengths and weaknesses.

We have first investigated Bloch effective Hamiltonian in the context of meson bound states in (2+1) dimensional QCD. There we encounter infrared divergences due to vanishing energy denominators in the bound state equation and SRG becomes mandatory to get rid of the divergences. The investigation of the $q\bar{q}$ bound states with Bloch effective Hamiltonian serves as a benchmark for comparative study of the same problem with SRG generated effective Hamiltonian which is a modification over the Bloch Hamiltonian. Bound state equation in SRG scheme is free from the problem of uncanceled divergences coming from vanishing energy denominators. We have also compared three different choices for similarity factor. To have better understanding, we have performed analytic calculation in the lowest order with step function similarity factor which in (2+1) dimensions generates *linear confinement along the transverse*

direction (for large x^1 , $V(x^-, x^1) \sim x^1$) while only *square root confinement along the longitudinal direction* (for large x^- , $V(x^-, x^1) \sim \sqrt{x^-}$) and thus breaks the rotational symmetry. Here one should recall that in (3+1) dimensions, in the lowest order, SRG generates logarithmic confining potential which also violates rotational symmetry. If the confinement generated by similarity transformation of the Hamiltonian is not an artifact of the lowest order approximation, one might hope that the violation of the rotational symmetry will diminish with higher order corrections to the effective Hamiltonian. Higher order calculations are thus very important and illuminative in this context. It is also expected that higher order calculations in (2+1) dimensions will be much easier than in (3+1) dimensions due to simpler divergence structures and less demand of computing resources.

We have studied another nonperturbative approach, the light-front transverse lattice formulation in this thesis. It is still a developing subject and is a very potential tool for nonperturbative investigations. Only very recently efforts are being given to formulate fermions and to study meson bound states on the LFTL. Lattice formulation of fermions is complicated due to generation of extra species and needs special treatments to have a meaningful description of fermions in the discrete world. Thus it is very much important to know their origin and way(s) to overcome them before attempting any realistic QCD calculation on a lattice. We have shown that the origin of doublers on LFTL is completely different from usual lattice gauge theory. In the usual lattice gauge theory doublers come from the end of the Brillouin zone. But, when one uses symmetric lattice derivative to formulate fermions on a LFTL, doublers pop up due to decoupling of odd and even lattice points. We have also studied two different ways of removing doublers, namely, Wilson fermion and staggered fermion on LFTL. We have *proposed* another way of formulating fermions on LFTL by using forward and backward lattice derivatives in such a way that the Hermiticity of the Hamiltonian is preserved. In our method, *there is no generation of extra fermion species*. In this case, the helicity flip term proportional to fermion mass in full QCD becomes an irrelevant term in the free field limit.

To assess which one of these two fermion formulations is better than the other we have compared them in the context of the meson bound state problem in (3+1) dimensional QCD. In the zero link approximation i.e., when q and \bar{q} can sit only at the same transverse location, in the limit of large number of colors, it reduces to the 't Hooft model with linearly confining

instantaneous interaction along the longitudinal direction. In the one link approximation, q and \bar{q} can be separated at most by one lattice point. With this approximation, the major difference between these two methods (in the case of symmetric derivative we add a Wilson term to remove the doublers) is the interference between helicity flip and nonflip hopping in the case of Hamiltonian with forward and backward derivatives. As a consequence of this interference the degeneracy structure of the bound state spectrum of the Hamiltonian with forward and backward derivatives is different from that with symmetric lattice derivative.

Since this subject is still under development, there are many unresolved questions one need to answer. The transverse dynamics and the structure of the mesons are too constrained by the one link approximation and investigations are essential with more than one links. By construction, quarks in one link approximation are confined in the transverse directions. The true nature of confining potential in the transverse directions can only be realized when sufficient number of links will be included. These issues can be investigated as an extension of our work. A systemic study of the effects of sea quarks also need to be undertaken. In this thesis, all the studies are done with light quarks, it will also be highly interesting to address the problem of mesons containing one light and one heavy quark in the context of heavy quark effective theory on the transverse lattice.

A major unsettled issue in the transverse lattice formulation is the continuum limit of the theory when nonlinear link variables are replaced by linear link variables. The lack of well defined transformation rule between linear and nonlinear link variables makes it impossible to come back to nonlinear theory once the links are replaced by linear link variables and there is no straightforward way to take the continuum ($a \rightarrow 0$) limit. Thus, as an alternative on a coarse lattice, one needs to search for a trajectory in the parameter space with minimal violation of Lorentz invariance. Another disadvantage of linearization of the links is that one needs to include more and more terms in the effective potential when more and more links are include and calculations are viable only in the limit of large number of colors which suppress the higher order terms in the effective potential. It will be interesting to investigate the light-front quantization problem with non-linear constraints. The kinetic energy term of the nonlinear link variables is similar to the nonlinear σ model. In this respect, the study of nonlinear σ model on the light-front appears worthwhile.

APPENDIX A

Notations and Conventions

In this appendix we provide the notations and conventions used in different chapters of this thesis.

For completeness let us start from the definition of light-front coordinates. The light-front coordinates in (3+1) dimensions are defined by

$$x^\pm = x^0 \pm x^3, \quad x^\perp = \{x^1, x^2\} \quad (\text{A.1})$$

and any four vector in light-front is denoted as

$$V^\mu = (V^+, V^-, V^\perp). \quad (\text{A.2})$$

The metric tensors are as follows

$$g^{\mu\nu} = \begin{pmatrix} 0 & 2 & 0 & 0 \\ 2 & 0 & 0 & 0 \\ 0 & 0 & -1 & 0 \\ 0 & 0 & 0 & -1 \end{pmatrix}, \quad g_{\mu\nu} = \begin{pmatrix} 0 & \frac{1}{2} & 0 & 0 \\ \frac{1}{2} & 0 & 0 & 0 \\ 0 & 0 & -1 & 0 \\ 0 & 0 & 0 & -1 \end{pmatrix}, \quad (\text{A.3})$$

so that

$$x_- = \frac{1}{2}x^+, \quad x_+ = \frac{1}{2}x^- \quad (\text{A.4})$$

and the scalar product

$$x \cdot y = \frac{1}{2}x^+y^- + \frac{1}{2}x^-y^+ - x^\perp \cdot y^\perp. \quad (\text{A.5})$$

The light-front partial derivatives are

$$\partial^+ = 2\partial_- = 2\frac{\partial}{\partial x^-}. \quad (\text{A.6})$$

$$\partial^- = 2\partial_+ = 2\frac{\partial}{\partial x^+}. \quad (\text{A.7})$$

We define the integral operators

$$\frac{1}{\partial^+} f(x^-) = \frac{1}{4} \int dy^- \varepsilon(x^- - y^-) f(y^-), \quad (\text{A.8})$$

$$\left(\frac{1}{\partial^+}\right)^2 f(x^-) = \frac{1}{8} \int dy^- |x^- - y^-| f(y^-). \quad (\text{A.9})$$

The γ matrices are define as

$$\gamma^\pm = \gamma^0 \pm \gamma^3. \quad (\text{A.10})$$

We choose the representation for gamma matrices such that

$$\begin{aligned} \gamma^+ &= \begin{pmatrix} 0 & 0 \\ 2iI & 0 \end{pmatrix}, & \gamma^- &= \begin{pmatrix} 0 & -2iI \\ 0 & 0 \end{pmatrix}, \\ \gamma^r &= \begin{pmatrix} -i\hat{\sigma}^r & 0 \\ 0 & i\hat{\sigma}^r \end{pmatrix}, & \gamma^5 &= \begin{pmatrix} \sigma^3 & 0 \\ 0 & -\sigma^3 \end{pmatrix}, \end{aligned} \quad (\text{A.11})$$

$\hat{\sigma}^1 = \sigma^2$ and $\hat{\sigma}^2 = -\sigma^1$ where σ^r are Pauli matrices and I is a two component identity matrix.

The projection operators

$$\Lambda^\pm = \frac{1}{4} \gamma^\mp \gamma^\pm = \frac{1}{2} \gamma^0 \gamma^\pm \quad (\text{A.12})$$

in explicit form are

$$\Lambda^+ = \begin{pmatrix} I & 0 \\ 0 & 0 \end{pmatrix}, \quad \Lambda^- = \begin{pmatrix} 0 & 0 \\ 0 & I \end{pmatrix}. \quad (\text{A.13})$$

So, the fermionic fields

$$\psi^\pm = \Lambda^\pm \psi \quad (\text{A.14})$$

can be written as

$$\psi^+ = \begin{pmatrix} \eta \\ 0 \end{pmatrix} \quad \psi^- = \begin{pmatrix} 0 \\ \xi \end{pmatrix} \quad (\text{A.15})$$

where η and ξ are two component fields.

In (2+1) dimensions the light-front coordinates are defined as

$$x^\mu = (x^\pm = x^0 \pm x^2, x^1) \quad (\text{A.16})$$

and accordingly the γ matrices

$$\gamma^\pm = \gamma^0 \pm \gamma^2. \quad (\text{A.17})$$

We use the two component representation for γ matrices

$$\gamma^0 = \sigma_2 = \begin{pmatrix} 0 & -i \\ i & 0 \end{pmatrix}, \quad \gamma^1 = i\sigma_3 = \begin{pmatrix} i & 0 \\ 0 & -i \end{pmatrix}, \quad \gamma^2 = i\sigma_1 = \begin{pmatrix} 0 & i \\ i & 0 \end{pmatrix} \quad (\text{A.18})$$

so that

$$\gamma^\pm = \gamma^0 \pm \gamma^2, \quad \gamma^+ = \begin{pmatrix} 0 & 0 \\ 2i & 0 \end{pmatrix}, \quad \gamma^- = \begin{pmatrix} 0 & -2i \\ 0 & 0 \end{pmatrix}, \quad (\text{A.19})$$

and

$$\Lambda^\pm = \frac{1}{4} \gamma^\mp \gamma^\pm, \quad \Lambda^+ = \begin{pmatrix} 1 & 0 \\ 0 & 0 \end{pmatrix}, \quad \Lambda^- = \begin{pmatrix} 0 & 0 \\ 0 & 1 \end{pmatrix}. \quad (\text{A.20})$$

Fermion field operator $\psi^\pm = \Lambda^\pm \psi$. We have

$$\psi^+ = \begin{pmatrix} \xi \\ 0 \end{pmatrix}, \quad \psi^- = \begin{pmatrix} 0 \\ \eta \end{pmatrix} \quad (\text{A.21})$$

where ξ and η are single component fields.

APPENDIX B

Bloch Perturbation Theory for Effective Hamiltonian

Here, we present the detailed formalism of the Bloch perturbation theory¹ to calculate the effective Hamiltonian.

Consider a Hamiltonian H defined at a cutoff Λ . Let us try to lower the cutoff to λ . In general, the cutoff could be in energy and/or particle number. Let us denote by Q the operator that projects on to all of the states removed when the cutoff is lowered. Let $P = I - Q$. We have

$$Q^2 = Q, \quad P^2 = P, \quad PQ = QP = 0. \quad (\text{B.1})$$

Our purpose is to find an effective Hamiltonian H_{eff} that produces the same eigenvalues in the sub space P as the original Hamiltonian H .

Introduce an operator R that satisfies

$$Q | \psi \rangle = RP | \psi \rangle \quad (\text{B.2})$$

for all eigenstates of the Hamiltonian that have support in the subspace P . R gives the part of $| \psi \rangle$ outside the space projected by P in terms of the part of $| \psi \rangle$ inside the space. Require that R gives zero acting on states outside the subspace. This means $R = RP, R = QR, R^2 = 0$. From $R = QR$, we have, $PR = 0$. Note also that $R^\dagger \neq R$.

Start from the set of equations (projections² of Schrödinger equation by P and Q)

$$PHP | \psi \rangle + PHQ | \psi \rangle = EP | \psi \rangle, \quad (\text{B.3})$$

$$QHP | \psi \rangle + QHQ | \psi \rangle = EQ | \psi \rangle. \quad (\text{B.4})$$

¹C. Bloch, Nucl. Phys. **6**, 329 (1958). Here we follow the treatment of R. J. Perry, Ann. Phys. **232** (1994) 116 [hep-th/9402015] (reader can find here many examples of perturbative calculations); B. D. Jones and R. J. Perry, Phys. Rev. D **55**, 7715 (1997).

²In Bloch-Horowitz formalism [C. Bloch, J. Horowitz, Nucl. Phys. **8**, 91 (1958)] also, one has the same projection operators P and Q , but not R . Substitution of $Q | \psi \rangle$ from Eq. (B.4) into Eq. (B.3) gives the Bloch-Horowitz effective Hamiltonian.

From Eq. (B.3),

$$RPHP | \psi \rangle + RPHQRP | \psi \rangle = ERP | \psi \rangle. \quad (\text{B.5})$$

From Eq. (B.4),

$$QHP | \psi \rangle + QHQRP | \psi \rangle = ERP | \psi \rangle. \quad (\text{B.6})$$

Subtracting,

$$RH_{PP} - H_{QQ}R + RH_{PQ}R - H_{QP} = 0. \quad (\text{B.7})$$

We have introduced the notations, $PHP = H_{PP}$ and so on. Put $H = h + v$ with $[h, Q] = 0$. Then

$$Rh_{PP} - h_{QQ}R - v_{QP} + Rv_{PP} - v_{QQ}R + Rv_{PQ}R = 0 \quad (\text{B.8})$$

which shows that R starts first order in v .

We start from the eigenvalue equation,

$$H(P + Q) | \psi \rangle = E(P + Q) | \psi \rangle. \quad (\text{B.9})$$

i.e.,

$$H(P + R)P | \psi \rangle = E(P + R)P | \psi \rangle. \quad (\text{B.10})$$

Multiplying from the left by $(P + R^\dagger)$ we have,

$$(P + R^\dagger)H(P + R)P | \psi \rangle = E(P + R^\dagger)(P + R)P | \psi \rangle. \quad (\text{B.11})$$

Using $PR = 0$, $R^\dagger P = 0$, $(P + R^\dagger)(P + R) = P + R^\dagger R$. Thus we can rewrite the eigenvalue equation as

$$\begin{aligned} \left[\frac{1}{1 + R^\dagger R} \right]^{\frac{1}{2}} (P + R^\dagger)H(P + R) \left[\frac{1}{1 + R^\dagger R} \right]^{\frac{1}{2}} [1 + R^\dagger R]^{\frac{1}{2}} P | \psi \rangle \\ = E [1 + R^\dagger R]^{\frac{1}{2}} P | \psi \rangle. \end{aligned} \quad (\text{B.12})$$

i.e.,

$$H_{eff} | \phi \rangle = E | \phi \rangle \quad (\text{B.13})$$

where

$$|\phi\rangle = [1 + R^\dagger R]^{\frac{1}{2}} P |\psi\rangle \quad (\text{B.14})$$

and

$$H_{eff} = \left[\frac{1}{1 + R^\dagger R} \right]^{\frac{1}{2}} (P + R^\dagger) H (P + R) \left[\frac{1}{1 + R^\dagger R} \right]^{\frac{1}{2}}. \quad (\text{B.15})$$

Our next task is to generate a perturbative expansion. Denote free eigenstates in P by $|a\rangle$, $|b\rangle$, etc. Denote free eigenstates in Q by $|i\rangle$, $|j\rangle$, etc. Then

$$\begin{aligned} h_{PP} |a\rangle &= \varepsilon_a |a\rangle, \\ h_{QQ} |i\rangle &= \varepsilon_i |i\rangle. \end{aligned} \quad (\text{B.16})$$

Let us compute R to lowest orders in the perturbation theory. Let us write $R = R_1 + R_2 + \dots$ where the subscript denotes orders in v . A straightforward calculation leads to

$$\langle i | R_1 | a \rangle = \frac{\langle i | v_{QP} | a \rangle}{\varepsilon_a - \varepsilon_i}, \quad (\text{B.17})$$

$$\langle i | R_2 | a \rangle = - \sum_b \frac{\langle b | v | a \rangle \langle i | v | b \rangle}{(\varepsilon_a - \varepsilon_i)(\varepsilon_b - \varepsilon_i)} + \sum_j \frac{\langle i | v | j \rangle \langle j | v | a \rangle}{(\varepsilon_a - \varepsilon_i)(\varepsilon_a - \varepsilon_j)}. \quad (\text{B.18})$$

Note that the energy denominators in the matrix elements of R involve only the difference between free energies of states in P and Q subspaces. This difference may approach to zero and give rise the “vanishing energy denominator problem” discussed in chapter 3.

Our next task is to develop a perturbation theory expansion for the effective Hamiltonian to a given order.

We start from the expression for the effective Hamiltonian (B.15). Remember that $R_1 \sim O(v)$, $R_2 \sim O(v^2)$.

To order v , $H_{eff} = PHP$ and hence

$$\langle a | H_{eff} | b \rangle = \langle a | (h + v) | b \rangle. \quad (\text{B.19})$$

To second order in v , we have

$$H_{eff} = \left[1 - \frac{1}{2} R^\dagger R \right] [PHP + PHR + R^\dagger HP + R^\dagger HR] \left[1 - \frac{1}{2} R^\dagger R \right]. \quad (\text{B.20})$$

From $R^\dagger HR$ we get,

$$\langle a | R^\dagger HR | b \rangle = \sum_i \varepsilon_i \frac{\langle a | v | i \rangle \langle i | v | b \rangle}{(\varepsilon_a - \varepsilon_i)(\varepsilon_b - \varepsilon_i)}. \quad (\text{B.21})$$

From PHR and $R^\dagger HP$ terms we get

$$\sum_i \langle a | H | i \rangle \langle i | R_1 | b \rangle + \sum_i \langle a | R_1^\dagger | i \rangle \langle i | H | b \rangle \quad (\text{B.22})$$

$$= \sum_i \left[\frac{\langle a | v | i \rangle \langle i | v | b \rangle}{\varepsilon_a - \varepsilon_i} + \frac{\langle a | v | i \rangle \langle i | v | b \rangle}{\varepsilon_b - \varepsilon_i} \right]. \quad (\text{B.23})$$

Due to the normalization of the states, the effective Hamiltonian also gets contribution from the normalization factors. From the *normalization factors* we get

$$-\frac{1}{2}R^\dagger RPHP - \frac{1}{2}PHPR^\dagger R = -\frac{1}{2}(\varepsilon_a + \varepsilon_b) \sum_i \frac{\langle a | v | i \rangle \langle i | v | b \rangle}{(\varepsilon_a - \varepsilon_i)(\varepsilon_b - \varepsilon_i)} \quad (\text{B.24})$$

Adding everything, to second order, we have,

$$\langle a | H_{eff} | b \rangle = \frac{1}{2} \sum_i \langle a | v | i \rangle \langle i | v | b \rangle \left[\frac{1}{\varepsilon_a - \varepsilon_i} + \frac{1}{\varepsilon_b - \varepsilon_i} \right]. \quad (\text{B.25})$$

If $a = b$, this expression reduces to the familiar second order energy shift.

Why Bloch formalism is preferred over Bloch-Horowitz formalism?

In the former, eigenstates of the effective Hamiltonian are orthonormalized projections of the original eigenstates. In the latter, they are not. The Bloch wavefunctions are defined by Eq. (B.14) and the Bloch-Horowitz wavefunctions by $|\phi\rangle = P|\psi\rangle$. Consider two ortho normalized eigenstates of the original Hamiltonian $|\psi_1\rangle$ and $|\psi_2\rangle$ with $\langle\psi_1|\psi_2\rangle = 0$. However, $P|\psi_1\rangle$ and $P|\psi_2\rangle$ need not be orthogonal, i.e., $\langle\psi_1|PP|\psi_2\rangle = \langle\psi_1|P|\psi_2\rangle \neq 0$. Construct $|\tilde{\psi}_1\rangle = [1 + R^\dagger R]^{1/2}P|\psi_1\rangle$, $|\tilde{\psi}_2\rangle = [1 + R^\dagger R]^{1/2}P|\psi_2\rangle$. Then

$$\langle\tilde{\psi}_1|\tilde{\psi}_2\rangle = \langle\psi_1|P|\psi_2\rangle + \langle\psi_1|PR^\dagger RP|\psi_2\rangle = \langle\psi_1|(P+Q)|\psi_2\rangle = \langle\psi_1|\psi_2\rangle. \quad (\text{B.26})$$

APPENDIX C

Details of Numerical Procedure to Diagonalize the Effective Hamiltonian

We convert the bound state integral equation to a matrix eigenvalue equation by discretizing the integrations using Gauss quadrature points for both Bloch effective and similarity renormalized Hamiltonians. Here, we elaborate the parametrizations and diagonalization procedure we have used.

Parametrization: The light-front variables are parametrized in the following ways in our numerical calculations. The full k -interval is divided into n_1 quadrature points. k is defined by two different ways. One definition is

$$k = \frac{u\Lambda m}{(1-u^2)\Lambda + m}, \quad (\text{C.1})$$

where Λ is the ultraviolet cutoff and u 's are the quadrature points lying between -1 and $+1$, so that k goes from $-\Lambda$ to $+\Lambda$. The other definition is

$$k = \frac{1}{\kappa} \tan\left(\frac{u\pi}{2}\right), \quad (\text{C.2})$$

here κ is a parameter that can be tuned to adjust the ultraviolet cutoff. The second definition (C.2) of k is very suitable for weak coupling calculations where we need maximum points to be concentrated near $k = 0$ and get better convergence than the first definition (C.1).

The longitudinal momentum fraction x ranges from 0 to 1. We divide all x - integrations in our calculations into two parts, x ranging from 0 to 0.5 and x ranging from 0.5 to 1 and discretize each x -interval into n_2 quadrature points with the parametrization

$$x = \frac{1 + v + 2\varepsilon(1 - v)}{4}, \quad \varepsilon \leq x \leq 0.5, \quad (\text{C.3})$$

$$x = \frac{3 + v - 2\varepsilon(1 + v)}{4}, \quad 0.5 \leq x \leq 1 - \varepsilon, \quad (\text{C.4})$$

where v 's are the Gauss-quadrature points lying between -1 and $+1$ and $\varepsilon(\rightarrow 0)$ is introduced to handle end-point singularities in x as mentioned in the main text in Chapters 3 and 4.

To handle the infrared diverging terms we put the cutoff $|x - y| \geq \delta$ and at the end we take the limit $\delta \rightarrow 0$. Numerically, it means that the result should converge as one decreases δ if there is no net infrared divergence in the theory.

Diagonalization: After discretization, solving the integral equation becomes a matrix diagonalization problem. The diagonalization has been performed by using the packed storage *LAPACK*³ routines *DSPEVX* for the reduced model (real symmetric matrix) and *ZHPEVX* for the full Hamiltonian (Hermitian matrix).

³E. Anderson *et al.*, *LAPACK Users' Guide*, third edition (Society for Industrial and Applied Mathematics, Philadelphia, 1999). Available on the internet at the URL: <http://www.netlib.org/lapack/lug/index.html>.

APPENDIX D

Nonrelativistic Bound State Equation

In order to elucidate the implications of rotational symmetry in the (2+1) dimensional world, we review the nonrelativistic bound state equation in this appendix.

For clarity, in this appendix we restore the superscript to the transverse component, namely, $k = k^1$, $q = q^1$, etc. We also use the notation $\mathbf{k} = (k^1, k^2)$, etc. To discuss the nonrelativistic limit of the reduced model defined in Sec. 3.6, make the variable change, $x = \frac{1}{2} \left(1 + \frac{k^2}{E(k)} \right)$, $y = \frac{1}{2} \left(1 + \frac{q^2}{E(q)} \right)$, where $E(p) = \sqrt{m^2 + (p^1)^2 + (p^2)^2}$. So far, no approximations have been made. We have,

$$\begin{aligned}
 \frac{1}{x(1-x)} &= 4 \left[1 - \left(\frac{k^2}{E(k)} \right)^2 \right]^{-1} \approx 4 \left[1 + \left(\frac{k^2}{m} \right)^2 \right], \\
 m(x-y) &= \frac{m}{2} \left(\frac{k^2}{E(k)} - \frac{q^2}{E(q)} \right) \approx \frac{1}{2} (k^2 - q^2), \\
 ky - qx &= \frac{1}{2} (k^1 - q^1) + \frac{1}{2} \left(\frac{k^1 q^2}{E(q)} - \frac{q^1 k^2}{E(k)} \right) \approx \frac{1}{2} (k^1 - q^1), \\
 k(1-y) - q(1-x) &= \frac{1}{2} (k^1 - q^1) - \frac{1}{2} \left(\frac{k^1 q^2}{E(q)} - \frac{q^1 k^2}{E(k)} \right) \approx \frac{1}{2} (k^1 - q^1), \\
 \frac{\partial y}{\partial q^2} &= \frac{1}{2} \frac{(q^1)^2 + m^2}{[E(q)]^{\frac{3}{2}}} \approx \frac{1}{2E(q)}. \tag{D.1}
 \end{aligned}$$

The \approx equality holds in the nonrelativistic limit $|\mathbf{k}|, |\mathbf{q}| \ll m$. Introducing the binding energy \bar{B} by $M^2 = 4m^2(1 - \bar{B})$, the bound state equation in momentum space in the non-relativistic limit is given by

$$\left[\bar{B} + \frac{\mathbf{k}^2}{m^2} \right] \psi(\mathbf{k}) = \frac{g^2}{4\pi^2 m} C_f \int d\mathbf{q} \frac{\psi(\mathbf{q}) - \psi(\mathbf{k})}{(\mathbf{k} - \mathbf{q})^2}. \tag{D.2}$$

Fourier transforming to coordinate space, with the momentum in the self energy integral cutoff by fermion mass m , one arrives at the coordinate space bound state equation

$$\left\{ -\frac{1}{m} \frac{\partial^2}{\partial r^2} + \frac{4l^2 - 1}{4mr^2} + \frac{g^2}{2\pi} C_f [\gamma_E + \ln mr] \right\} \psi(r) = E \psi(r) \tag{D.3}$$

where $E = -m\bar{B}$ and $\psi(\mathbf{r}) = r^{-\frac{1}{2}}\psi(r)e^{\pm il\phi}$ and γ_E is the Euler constant. We note that rotational symmetry implies two-fold degeneracy for $l \neq 0$ states.

APPENDIX E

Similarity Renormalization Theory for the Effective Hamiltonian

As it was promised in chapter 4, we present the detailed derivation of the effective Hamiltonian using similarity renormalization group approach in this appendix.

Since the renormalization group transformation based on integrating out the high energy states encounters nearly degenerate states, an alternative way of calculating effective Hamiltonian was in demand. The solutions were proposed by Głazek and Wilson and Wegner independently⁴.

Starting from a cutoff Hamiltonian H_B which includes canonical terms and counterterms we wish to arrive at an effective Hamiltonian H_σ defined at the scale σ via a similarity transformation

$$H_\sigma = S_\sigma H_B S_\sigma^\dagger \quad (\text{E.1})$$

where S_σ is chosen to be unitary.

The boundary condition is $\text{Limit}_{\sigma \rightarrow \infty} H_\sigma = H_B$.

Introduce anti-Hermitian generator of infinitesimal changes of scale T_σ through

$$S_\sigma = \mathcal{T} e^{\int_\sigma^\infty d\sigma' T_{\sigma'}} \quad (\text{E.2})$$

where \mathcal{T} puts operators in order of increasing scale.

For infinitesimal change (lowering) of scale, $S_\sigma = 1 - T_\sigma d\sigma$ and $S_\sigma^\dagger = 1 + T_\sigma d\sigma$. Then we arrive at the infinitesimal form of the transformation

$$\frac{dH_\sigma}{d\sigma} = [H_\sigma, T_\sigma]. \quad (\text{E.3})$$

⁴S. D. Głazek and K. G. Wilson, Phys. Rev. D **48**, 5863 (1993); **49**, 4214 (1994); F. Wegner, Ann. Phys. (Leipzig) **3**, 77 (1994).

This equation which has been called the flow equation of the Hamiltonian is the starting point of the investigations.

The basic goal of the transformation S_σ is that H_σ should be band diagonal relative to the scale σ . Qualitatively this means that matrix elements of H_σ involving energy jumps much larger than σ should be zero. T_σ still remains arbitrary to a great extent. It is instructive to go through the steps of the derivation which leads to the Glazek-Wilson choice.

We write $H_B = H_{B0} + H_{BI}$ where H_{B0} is the free part and H_{BI} is the interaction part of the bare cutoff Hamiltonian. A brute force way of achieving our goal is to *define* the matrix elements $H_{I\sigma ij} = f_{\sigma ij} H_{BI ij}$ where we have introduced the function $f_{\sigma ij} = f(x_{\sigma ij})$ with x a function of σ^2 and ΔM_{ij}^2 . The function $f(x)$ should be chosen as follows:

$$\begin{aligned}
 & \text{when } \sigma^2 \gg \Delta M_{ij}^2, & f(x) &= 1 & (\text{near diagonal region}); \\
 & \text{when } \sigma^2 \ll \Delta M_{ij}^2, & f(x) &= 0 & (\text{far off diagonal region}); \\
 & \text{in between} & f(x) & \text{drops from 1 to 0} & (\text{transition region}). \quad (\text{E.4})
 \end{aligned}$$

Here $\Delta M_{ij}^2 (= M_i^2 - M_j^2)$ denotes the difference of invariant masses of states i and j . Because of the properties of f , $H_{I\sigma ij}$ is band diagonal. What is wrong with such a choice of inserting form factors by hand at the interaction vertices? First of all, we simply discard degrees of freedom above σ . Secondly, H_σ will have very strong dependence on σ . Thirdly, to ensure that H_σ has no ultraviolet cutoff dependence, H_B should contain canonical and counterterms. But, in light front Hamiltonian field theory, because of the complexities due to renormalization, a priori we do not know the structure of counterterms.

Note that in the definition of H_σ given in Eq. (E.3) the form of T_σ is still unspecified. In fact, a wide variety of choices are possible. In the following, we consider the choices made by Glazek and Wilson and Wegner. The price we have to pay for the use of flow equations is that it will generate complicated interactions even if the starting Hamiltonian has only simple interactions. For example, starting with a Hamiltonian which has only 2 particle interaction, the transformation will generate 3 particle interactions, 4 particle interactions, etc.

E.1 Głazek-Wilson Formalism

Writing $H_\sigma = H_0 + H_{I\sigma}$, noting that the free Hamiltonian H_0 does not depend on σ and taking matrix elements in free particle states, we have,

$$[H_\sigma, T_\sigma]_{ij} = (P_i^- - P_j^-)T_{\sigma ij} + [H_{I\sigma}, T_\sigma]_{ij} \quad (\text{E.5})$$

where $H_0 |i\rangle = P_i^- |i\rangle$, etc. . i.e.,

$$\frac{1}{f_{\sigma ij}} \frac{dH_{I\sigma ij}}{d\sigma} = \frac{1}{f_{\sigma ij}} [H_{I\sigma}, T_\sigma]_{ij} + \frac{1}{f_{\sigma ij}} (P_i^- - P_j^-)T_{\sigma ij}. \quad (\text{E.6})$$

Since we want $H_{I\sigma ij}$ to be band diagonal, it is advantageous to trade $\frac{1}{f_{\sigma ij}} \frac{dH_{I\sigma ij}}{d\sigma}$ for $\frac{d}{d\sigma} \left[\frac{1}{f_{\sigma ij}} H_{I\sigma ij} \right]$ which on integration has the chance to ensure that $H_{I\sigma ij}$ is band diagonal, we use

$$\frac{d}{d\sigma} \left[\frac{1}{f_{\sigma ij}} H_{I\sigma ij} \right] + \frac{1}{f_{\sigma ij}^2} \frac{df_{\sigma ij}}{d\sigma} H_{I\sigma ij} = \frac{1}{f_{\sigma ij}} \frac{dH_{I\sigma ij}}{d\sigma} \quad (\text{E.7})$$

and arrive at

$$\begin{aligned} \frac{d}{d\sigma} \left[\frac{1}{f_{\sigma ij}} H_{I\sigma ij} \right] &= \frac{1}{f_{\sigma ij}} (P_i^- - P_j^-) T_{\sigma ij} \\ &+ \frac{1}{f_{\sigma ij}} [H_{I\sigma}, T_\sigma]_{ij} - \frac{1}{f_{\sigma ij}^2} \frac{df_{\sigma ij}}{d\sigma} H_{I\sigma ij}. \end{aligned} \quad (\text{E.8})$$

Still $T_{\sigma ij}$ is not defined. We next convert this equation into two equations, one defining the flow of $H_{I\sigma ij}$ and other defining $T_{\sigma ij}$. Recalling the starting equation Eq. (E.3) we add and subtract $[H_{I\sigma}, T_\sigma]_{ij}$ to the r.h.s. and arrive at

$$\begin{aligned} \frac{d}{d\sigma} \left[\frac{1}{f_{\sigma ij}} H_{I\sigma ij} \right] &= [H_{I\sigma}, T_\sigma]_{ij} + \frac{1}{f_{\sigma ij}} (P_i^- - P_j^-) T_{\sigma ij} \\ &+ \frac{1}{f_{\sigma ij}} (1 - f_{\sigma ij}) [H_{I\sigma}, T_\sigma]_{ij} - \frac{1}{f_{\sigma ij}^2} \frac{df_{\sigma ij}}{d\sigma} H_{I\sigma ij}. \end{aligned} \quad (\text{E.9})$$

Głazek and Wilson choose T_σ to be

$$T_{\sigma ij} = \frac{1}{P_j^- - P_i^-} \left[(1 - f_{\sigma ij}) [H_{I\sigma}, T_\sigma]_{ij} - \frac{d}{d\sigma} (\ln f_{\sigma ij}) H_{I\sigma ij} \right]. \quad (\text{E.10})$$

Then from Eq. (E.9), we have,

$$\frac{d}{d\sigma} \left[\frac{1}{f_{\sigma ij}} H_{I\sigma ij} \right] = [H_{I\sigma}, T_\sigma]_{ij}. \quad (\text{E.11})$$

Integrating Eq. (E.11) from σ to ∞ , we arrive at,

$$H_{I\sigma ij} = f_{\sigma ij} \left[H_{IBij} - \int_{\sigma}^{\infty} d\sigma' [H_{I\sigma'}, T_{\sigma'}]_{ij} \right]. \quad (\text{E.12})$$

Note that $H_{I\sigma ij}$ is zero in the far off-diagonal region. This is clear from the solution given in Eq. (E.12) since $f(x)$ vanishes when $x \geq 2/3$.

$T_{\sigma ij}$ vanishes in the near diagonal region. When i is close to j , $f_{\sigma ij} = 1$ and both $(1 - f_{\sigma ij})$ and $\frac{d}{d\sigma} f_{\sigma ij}$ vanishes. It follows, then, from Eq. (E.10) that $T_{\sigma ij}$ vanishes in the near-diagonal region. This guarantees that a perturbative solution to $H_{I\sigma ij}$ in terms of H_{BIj} will never involve vanishing energy denominators.

The effective Hamiltonian can be calculated up to any order of perturbation theory from Eq. (E.12) by iterative method. Here, we derive the effective Hamiltonian to second order in perturbation theory. Using

$$H_{I\sigma ik}^{(1)} \simeq f_{\sigma ik} H_{BIk} \quad (\text{E.13})$$

and

$$T_{\sigma kj} \simeq \frac{1}{P_j^- - P_k^-} \left\{ -\frac{d}{d\sigma} (\ln f_{\sigma kj}) f_{\sigma kj} H_{BIkj} \right\} \quad (\text{E.14})$$

in Eq. (E.12), a straightforward calculation leads to

$$H_{I\sigma ij}^{(2)} = -\sum_k H_{BIik} H_{BIkj} \left[\frac{g_{\sigma ijk}}{P_k^- - P_j^-} + \frac{g_{\sigma jik}}{P_k^- - P_i^-} \right], \quad (\text{E.15})$$

where

$$\begin{aligned} g_{\sigma ijk} &= f_{\sigma ij} \int_{\sigma}^{\infty} d\sigma' f_{\sigma' ik} \frac{d}{d\sigma'} f_{\sigma' jk}, \\ g_{\sigma jik} &= f_{\sigma ij} \int_{\sigma}^{\infty} d\sigma' f_{\sigma' jk} \frac{d}{d\sigma'} f_{\sigma' ik}. \end{aligned} \quad (\text{E.16})$$

We find that the effective Hamiltonian in similarity perturbation theory is a modification of the effective Hamiltonian in Bloch perturbation theory⁵.

⁵Detail discussion of Bloch effective perturbation theory is given in Appendix B.

E.2 Wegner Formalism

In the Wegner formalism⁶, the flow equation is given by

$$\frac{dH(l)}{dl} = [\tau(l), H(l)]. \quad (\text{E.17})$$

Wegner chooses

$$\tau(l) = [H_d, H] = [H_d, H_r] \quad (\text{E.18})$$

where H_d is the diagonal part of the Hamiltonian and H_r is the rest, i.e., $H = H_d + H_r$. Here the word diagonal is used in the particle number conserving sense. It is important to note that H_d is not the free part of the Hamiltonian and both H_d and H_r depend on the length scale l .

The light front Hamiltonian has dimension of $(mass)^2$ and hence τ has the dimension of $(mass)^4$, l has dimension of $\frac{1}{(mass)^4}$.

Expanding in powers of the coupling constant,

$$H = H_d^{(0)} + H_r^{(1)} + H_d^{(2)} + H_r^{(2)} + \dots \quad (\text{E.19})$$

where the superscript denotes the order in the coupling constant,

$$\tau(l) = [H_d^{(0)}, H_r^{(1)}] + [H_d^{(0)}, H_r^{(2)}] + \dots \quad (\text{E.20})$$

Then, to second order,

$$\frac{dH}{dl} = [[H_d^{(0)}, H_r^{(1)}], H_d^{(0)}] + [[H_d^{(0)}, H_r^{(1)}], H_r^{(1)}] + [[H_d^{(0)}, H_r^{(2)}], H_d^{(0)}] + \dots \quad (\text{E.21})$$

Introduce the eigenstates of $H_d^{(0)}$,

$$H_d^{(0)} |i\rangle = P_i^- |i\rangle. \quad (\text{E.22})$$

Then, to second order,

$$\frac{dH_{ij}}{dl} = -(P_i^- - P_j^-)^2 H_{rij}^{(1)} + [\tau_l^{(1)}, H_r^{(1)}]_{ij} - (P_i^- - P_j^-)^2 H_{rij}^{(2)} + \dots \quad (\text{E.23})$$

⁶For applications of Wegner formalism in condensed matter physics and quantum field theory see F. J. Wegner, Nucl. Phys. Proc. Suppl. **90**, 141 (2000); E. L. Gubankova and F. Wegner, hep-th/9708054; E. L. Gubankova and F. Wegner, Phys. Rev. D **58**, 025012 (1998) [hep-th/9710233].

To first order in the coupling,

$$\frac{dH_{rij}}{dl} = -(P_i^- - P_j^-)^2 H_{rij}^{(1)} \quad (\text{E.24})$$

which on integration yields

$$H_{rij}^{(1)}(\sigma) = e^{-\frac{(P_i^- - P_j^-)^2}{\sigma^4}} H_{rij}^{(1)}(\Lambda) \quad (\text{E.25})$$

where we have introduced the energy scale σ via $l = \frac{1}{\sigma^4}$ and used the fact that $l = 0$ corresponds to the original bare cutoff. We notice the emergence of the similarity factor $f_{\sigma ij} = e^{-\frac{(P_i^- - P_j^-)^2}{\sigma^4}}$.

If we are interested only in particle number conserving (diagonal) part of the effective interaction, to second order we have,

$$\frac{dH_{lij}}{dl} = [\tau_l^{(1)}, H_r^{(1)}]_{ij} \quad (\text{E.26})$$

Using

$$\tau_{lij}^{(1)} = (P_j^- - P_i^-) H_{rij}^{(1)}, \quad (\text{E.27})$$

the effective interaction generated to second order in the diagonal sector is

$$H_{lij} = \sum_k H_{ik}^B H_{kj}^B \frac{(P_i^- - P_k^-) + (P_j^- - P_k^-)}{(P_i^- - P_k^-)^2 + (P_j^- - P_k^-)^2} \left[1 - e^{-\left\{ (P_i^- - P_k^-)^2 + (P_j^- - P_k^-)^2 \right\} / \sigma^4} \right]. \quad (\text{E.28})$$

Even though the second order formula is very similar to the one in Głazek-Wilson formalism when an exponential form is chosen for the similarity factor (see Sec. IV), we note a slight difference. In the Głazek-Wilson formalism, since the purpose is to bring the Hamiltonian into a band diagonal form, even in the particle number conserving sectors the large jumps in energies do not appear by construction. In the version of the Wegner formalism presented here the purpose is to bring the Hamiltonian in the block diagonal form in particle number sector so that large jumps in energies are allowed by the effective Hamiltonian. Note that small energy denominators do not appear in both formalisms.

APPENDIX F

Violations of Hypercubic Symmetry on Transverse Lattice

The canonical helicity non-flip interactions given in Eq. (6.23) for $r \neq s$ break the hypercubic symmetry on the transverse lattice. For interacting theory this is also true for the Hamiltonian with symmetric derivative. In the free field limit they do not survive for Hamiltonian with symmetric derivative but for forward-backward derivative they survive. In that case, in the free field limit they reduce to

$$\begin{aligned} \frac{1}{a^2} \int dx^- \sum_{\mathbf{x}} \sum_{r \neq s} \left[\eta^\dagger(\mathbf{x} + a\hat{\mathbf{r}}) \hat{\sigma}_r \hat{\sigma}_s \frac{1}{\partial_+} \eta(\mathbf{x}) \right. \\ \left. + \eta^\dagger(\mathbf{x}) \hat{\sigma}_r \hat{\sigma}_s \frac{1}{\partial_+} \eta(\mathbf{x} + a\hat{\mathbf{s}}) \right. \\ \left. - \eta^\dagger(\mathbf{x} + a\hat{\mathbf{r}}) \hat{\sigma}_r \hat{\sigma}_s \frac{1}{\partial_+} \eta(\mathbf{x} + a\hat{\mathbf{s}}) \right]. \end{aligned} \quad (\text{F.1})$$

Going to the transverse momentum space via

$$\eta(x^-, x^\perp) = \int d^2 k^\perp e^{ik^\perp \cdot x^\perp} \phi_{k^\perp}(x^-) \quad (\text{F.2})$$

we get

$$\begin{aligned} -\frac{2}{a^2} \int dx^- \int d^2 k^\perp \phi_{k^\perp}^\dagger(x^-) \sigma_3 \frac{1}{i\partial_+} \phi_{k^\perp}(x^-) \\ \left[\sin(k_y a) - \sin(k_x a) + \sin(k_x a - k_y a) \right]. \end{aligned} \quad (\text{F.3})$$

Thus the violations of hypercubic symmetry are of the order of the lattice spacing a . Sign in front of this term changes if we switch forward and backward derivatives.

In case of interacting theory with symmetric lattice derivative, these terms do not come in one link approximation but will come in if one considers more than one link. But in case of forward and backward derivative, they also appear in one link approximation. In our numerical studies presented in this work, we have set the coefficients of hypercubic symmetry violating terms to zero.

APPENDIX G

Fermions With Forward-Backward Derivatives in Conventional Lattice Theory

In chapter 5 we have discussed the light-front transverse lattice formulation of fermions with forward and backward lattice derivatives. Let us discuss the situation in conventional lattice gauge theory in this appendix.

In discretizing the Dirac action in conventional lattice theory the use of forward or backward derivative for ∂_μ leads to non-hermitian action. The hermiticity can be preserved in the following way ⁷.

In the chiral representation

$$\gamma^0 = \begin{bmatrix} 0 & -I \\ -I & 0 \end{bmatrix}, \quad \gamma^j = \begin{bmatrix} 0 & \sigma^j \\ -\sigma^j & 0 \end{bmatrix}, \quad \gamma^5 = \begin{bmatrix} I & 0 \\ 0 & -I \end{bmatrix}. \quad (\text{G.1})$$

The Dirac operator in Minkowski space

$$i\gamma^\mu \partial_\mu \equiv \begin{bmatrix} 0 & -i\sigma^\mu \partial_\mu \\ -i\bar{\sigma}^\mu \partial_\mu & 0 \end{bmatrix}, \quad (\text{G.2})$$

where, $\sigma^\mu = (I, \sigma)$, $\bar{\sigma}^\mu = (I, -\sigma)$. For massive Dirac fermions, this leads to the structure

$$-i\sigma^\mu \partial_\mu \psi_R - m\psi_L \quad (\text{G.3})$$

$$-i\bar{\sigma}^\mu \partial_\mu \psi_L - m\psi_R. \quad (\text{G.4})$$

For discretization we replace ∂_μ in Eq. (G.3) by forward derivative

$$\Delta_\mu^f = (\delta_{y,x+\mu} - \delta_{y,x})/a \quad (\text{G.5})$$

and in Eq. (G.4) by backward derivative

$$\Delta_\mu^b = (\delta_{y,x} - \delta_{y,x-\mu})/a. \quad (\text{G.6})$$

⁷In this appendix we follow the treatment of H. Banerjee and Asit K. De, Nucl. Phys. B (Proc. Suppl.) **53**, 641 (1997).

This leads to the structure

$$i\gamma^\mu \partial_\mu - m = i\gamma_\mu \Delta_\mu^s - i\gamma_\mu \gamma_5 \Delta_\mu^a - m \quad (\text{G.7})$$

which results in hermitian action. Here,

$$\begin{aligned} \Delta_\mu^s &= (\delta_{y,x+\mu} - \delta_{y,x-\mu})/2a \\ \Delta_\mu^a &= (\delta_{y,x+\mu} + \delta_{y,x-\mu} - 2\delta_{y,x})/2a. \end{aligned} \quad (\text{G.8})$$

Note that irrelevant helicity nonflip second order derivative term is produced in this method of discretization. In contrast, the corresponding term in the transverse lattice depends linearly on m and flips helicity. One can trace this difference to the presence of the constraint equation in the light front theory.

Writing lattice derivatives in this fashion in the conventional lattice theory eliminates the doublers from the edges of the Brillouin zone but some non-covariant doublers prop up from other places.

APPENDIX H

Mixed Covariant Derivative

Here we derive the form of mixed covariant derivative used in the transverse lattice formulation.

In a *local* field theory, we cannot simply compare objects at distances. As Feynman reminds us, “We must take into account of the rotation of the frame by transporting $U(x^\mu + \Delta x^\mu)$ back to x^μ before making a comparison”⁸. Hence the total change is given by

$$\begin{aligned}
 D^\mu U_r(x^\mu, \mathbf{x}) \Delta x_\mu &= R(\mathbf{x})^{-1} U_r(x^\mu + \Delta x^\mu, \mathbf{x}) R(\mathbf{x} + a\hat{\mathbf{r}}) - U_r(x^\mu, \mathbf{x}) \\
 &= [1 + A^\mu(\mathbf{x}) \Delta x_\mu] U_r(x^\mu + \Delta x^\mu, \mathbf{x}) [1 - A^\mu(\mathbf{x} + a\hat{\mathbf{r}}) \Delta x_\mu] - U_r(x^\mu, \mathbf{x}) \\
 &= U_r(x^\mu, \mathbf{x}) + \partial^\mu U_r(x^\mu, \mathbf{x}) \Delta x_\mu - U_r(x^\mu, \mathbf{x}) \\
 &\quad + A^\mu(\mathbf{x}) U_r(x^\mu, \mathbf{x}) \Delta x_\mu - U_r(x^\mu, \mathbf{x}) A^\mu(\mathbf{x} + a\hat{\mathbf{r}}) \Delta x_\mu \\
 &= \left\{ [\partial^\mu + A^\mu(\mathbf{x})] U_r(x^\mu, \mathbf{x}) - U_r(x^\mu, \mathbf{x}) A^\mu(\mathbf{x} + a\hat{\mathbf{r}}) \right\} \Delta x_\mu. \tag{H.1}
 \end{aligned}$$

⁸R. P. Feynman, in *Weak and Electromagnetic Interactions at High Energies*, (eds.) Roger Balian, Christopher H. Llewellyn Smith, (Elsevier North-Holland Pub. Co., Amsterdam 1977).

APPENDIX I

Transverse Gauge Invariance

Let us explicitly verify the transverse gauge invariance of the lattice theory. The theory is invariant under the gauge transformations

$$\eta(\mathbf{x}) \rightarrow \eta'(\mathbf{x}) = G^\dagger(\mathbf{x})\eta(\mathbf{x}) \quad (\text{I.1})$$

and

$$M_r(\mathbf{x}) \rightarrow M'_r(\mathbf{x}) = G^\dagger(\mathbf{x})M_r(\mathbf{x})G(\mathbf{x} + a\hat{\mathbf{r}}) \quad (\text{I.2})$$

where

$$G(\mathbf{x}) = e^{-iT^a\theta^a(\mathbf{x})}. \quad (\text{I.3})$$

For infinitesimal transformation,

$$G(\mathbf{x}) \approx 1 - iT^a\theta^a(\mathbf{x}) \quad (\text{I.4})$$

and

$$\eta(\mathbf{x}) \rightarrow \eta'(\mathbf{x}) = \eta(\mathbf{x}) + iT^a\theta^a(\mathbf{x})\eta(\mathbf{x}) \quad (\text{I.5})$$

and

$$M_r(\mathbf{x})_{pq} \rightarrow M'_r(\mathbf{x})_{pq} = M_r(\mathbf{x})_{pq} + iT_{pl}^a M_r(\mathbf{x})_{lq}\theta^a(\mathbf{x}) - iM_r(\mathbf{x})_{pl}T_{lq}^a\theta^a(\mathbf{x} + a\hat{\mathbf{r}}). \quad (\text{I.6})$$

In quantum theory the gauge transformations are generated by the operator

$$\mathcal{G} = e^{\frac{i}{2}\sum_{\mathbf{y}} Q^a(\mathbf{y})\theta^a(\mathbf{y})} \quad (\text{I.7})$$

with

$$Q^a(\mathbf{y}) = \int dy^- \left[Tr \left\{ T^a \sum_{r'} \left(M_{r'}(\mathbf{y}) i \overset{\leftrightarrow}{\partial}^+ M_{r'}^\dagger(\mathbf{y}) + M_{r'}^\dagger(\mathbf{y} - a\hat{\mathbf{r}}) i \overset{\leftrightarrow}{\partial}^+ M_{r'}(\mathbf{y} - a\hat{\mathbf{r}}) \right) \right\} - 2\eta^\dagger(\mathbf{y}) T^a \eta(\mathbf{y}) \right] \quad (\text{I.8})$$

so that

$$\eta(\mathbf{x}) \rightarrow \eta'(\mathbf{x}) = \mathcal{G} \eta(\mathbf{x}) \mathcal{G}^\dagger \quad (\text{I.9})$$

and

$$M_r(\mathbf{x}) \rightarrow M'_r(\mathbf{x}) = \mathcal{G} M_r(\mathbf{x}) \mathcal{G}^\dagger. \quad (\text{I.10})$$

For infinitesimal θ^a , using $[A, BC] = A\{B, C\} - \{A, C\}B$ and the canonical commutation relations for the fermion field operator, we readily verify Eq. (I.5). Using $[A, BC] = A[B, C] + [A, C]B$ and canonical commutation relation for the link field, we also verify Eq. (I.6).

Next we look at the behavior of fermion and link creation and annihilation operators under transverse gauge transformations in order to construct gauge invariant multiparticle states.

The gauge transformation on the link variable is

$$M_r(\mathbf{x}) \rightarrow M'_r(\mathbf{x}) = G^\dagger(\mathbf{x}) M_r(\mathbf{x}) G(\mathbf{x} + a\hat{\mathbf{r}}) \quad (\text{I.11})$$

where G belongs to $SU(N)$. Thus

$$A_r(\mathbf{x}) \rightarrow A'_r(\mathbf{x}) = G^\dagger(\mathbf{x}) A_r(\mathbf{x}) G(\mathbf{x} + a\hat{\mathbf{r}}), \quad B_r^\dagger(\mathbf{x}) \rightarrow B'^\dagger_r(\mathbf{x}) = G^\dagger(\mathbf{x}) B_r^\dagger(\mathbf{x}) G(\mathbf{x} + a\hat{\mathbf{r}}). \quad (\text{I.12})$$

Thus $Tr(A^\dagger B^\dagger)$, $Tr(AB)$, $Tr(A^\dagger A)$, $Tr(B^\dagger B)$ are locally gauge invariant operators. A locally gauge invariant two link state is $Tr(A^\dagger B^\dagger) | 0 \rangle$.

Recall that the current has the structure

$$J^{+a} \sim Tr(T^a M M^\dagger) \quad \text{with} \quad M \sim A + B^\dagger. \quad (\text{I.13})$$

The interaction term $J^{+a} (\frac{1}{\mathcal{F}})^2 J^{+a}$ has many terms. Consider one term

$$\begin{aligned} Tr(T^a A A^\dagger) Tr(T^a B^\dagger B) &= Tr((A^\dagger T^a A) Tr(B T^a B^\dagger)) = T_{mp}^a T_{st}^a A_{nm}^\dagger A_{pn} B_{rs} B_{tr}^\dagger \\ &\Rightarrow T_{mp}^a T_{st}^a \delta_{nr} \delta_{mt} \delta_{ps} \delta_{nr} = (T^a T^a)_{mm}. \end{aligned} \quad (\text{I.14})$$

On the other hand, consider the “pair creation term”

$$\begin{aligned}
Tr(T^a AB)Tr(T^a B^\dagger A^\dagger) &= Tr(BT^a A)Tr(A^\dagger T^a B^\dagger) \\
&= T_{mp}^a T_{st}^a B_{nm} A_{pn} A_{rs}^\dagger B_{tr}^\dagger \\
&\Rightarrow T_{mp}^a T_{st}^a \delta_{mp} \delta_{ts} = 0.
\end{aligned} \tag{I.15}$$

Thus pair creation or pair destruction terms (even if they conserve particle number) do not contribute if we restrict ourselves to a two link gauge invariant sector.

Next let us look at the two component fermion field $\eta(\mathbf{x})$. The transformation of $\eta(\mathbf{x})$ is

$$\eta(\mathbf{x}) \rightarrow \eta(\mathbf{x})' = G^\dagger(\mathbf{x})\eta(\mathbf{x}). \tag{I.16}$$

Since $\eta(\mathbf{x}) \approx b(\mathbf{x}) + d^\dagger(\mathbf{x})$, we have

$$b(\mathbf{x}) \rightarrow b(\mathbf{x})' = G^\dagger(\mathbf{x})b(\mathbf{x}) \text{ and } d^\dagger(\mathbf{x}) \rightarrow d^\dagger(\mathbf{x})' = G^\dagger(\mathbf{x})d^\dagger(\mathbf{x}). \tag{I.17}$$

Next consider how to form gauge invariant two-particle ($q\bar{q}$) and three-particle ($q\bar{q}$ link) states.

A gauge invariant $q\bar{q}$ state is $b^\dagger(\mathbf{x})d^\dagger(\mathbf{x}) | 0 \rangle$. Gauge invariant three particle states are $b^\dagger(\mathbf{x})B_r^\dagger(\mathbf{x})d^\dagger(\mathbf{x} + a\hat{\mathbf{r}}) | 0 \rangle$ and $b^\dagger(\mathbf{x} + a\hat{\mathbf{r}})A_r^\dagger(\mathbf{x})d^\dagger(\mathbf{x}) | 0 \rangle$ ($= b^\dagger(\mathbf{x} + a\hat{\mathbf{r}})B_{-r}^\dagger(\mathbf{x} + a\hat{\mathbf{r}})d^\dagger(\mathbf{x}) | 0 \rangle$).

APPENDIX J

Hamiltonian Matrix Elements in One Link Approximation

J.1 Structure of terms in DLCQ

We use DLCQ for the longitudinal dimension ($-L \leq x^- \leq +L$) and implement anti periodic boundary condition for the two component fermion field,

$$\eta_c(x^-, \mathbf{x}) = \frac{1}{\sqrt{2L}} \sum_{\lambda} \chi_{\lambda} \sum_{m=1,3,5,\dots} [b_c(m, \mathbf{x}, \lambda) e^{-i\pi m x^- / (2L)} + d_c^{\dagger}(m, \mathbf{x}, -\lambda) e^{i\pi m x^- / (2L)}] \quad (\text{J.1})$$

with

$$\{b_c(m, \mathbf{x}, \lambda), b_c^{\dagger}(m', \mathbf{x}', \lambda')\} = \{d_c(m, \mathbf{x}, \lambda), d_c^{\dagger}(m', \mathbf{x}', \lambda')\} = \delta_{mm'} \delta_{\mathbf{x}, \mathbf{x}'} \delta_{c,c'} \delta_{\lambda, \lambda'}. \quad (\text{J.2})$$

The link field has periodic boundary condition (with the omission of the zero momentum mode),

$$M_{r\ pq}(x^-, \mathbf{x}) = \frac{1}{\sqrt{4\pi}} \sum_{m=1,2,3,\dots} \frac{1}{\sqrt{m}} [B_{-r\ pq}(m, \mathbf{x} + a\hat{\mathbf{r}}) e^{-i\pi m x^- / L} + B_{r\ pq}^{\dagger}(m, \mathbf{x}) e^{i\pi m x^- / L}] \quad (\text{J.3})$$

with

$$[B_{r\ pq}(m, \mathbf{x}), B_{r'\ t s}^{\dagger}(m', \mathbf{x}')] = \delta_{mm'} \delta_{\mathbf{x}, \mathbf{x}'} \delta_{r,r'} \delta_{ps} \delta_{qt}. \quad (\text{J.4})$$

The Hamiltonian $P^- = \frac{L}{\pi} H$.

In the following subsection we give the explicit structure of terms in the Hamiltonian in the forward-backward case in DLCQ restricting to those relevant for the one link approximation.

Mass terms

Mass terms:

$$H_{f\ free} = m^2 \sum_{\mathbf{x}} \sum_c \sum_{\lambda} \sum_n \frac{1}{n} [b_c^{\dagger}(n, \mathbf{x}, \lambda) b_c(n, \mathbf{x}, \lambda) + d_c^{\dagger}(n, \mathbf{x}, \lambda) d_c(n, \mathbf{x}, \lambda)]. \quad (\text{J.5})$$

$$H_{LINK \text{ free}} = \frac{\mu^2}{2} \sum_{\mathbf{x}} \sum_{\hat{\mathbf{r}}} \sum_n \frac{1}{n} \left[B_r^\dagger(m, \mathbf{x}) B_r(m, \mathbf{x}) + B_{-r}^\dagger(m, \mathbf{x} + a\hat{\mathbf{r}}) B_{-r}(m, \mathbf{x} + a\hat{\mathbf{r}}) \right]. \quad (\text{J.6})$$

Four fermion instantaneous term

The four fermion instantaneous term which gives rise to a linear potential in the color singlet state

$$\begin{aligned} & 2 \frac{g^2}{\pi a^2} \sum_{cc'c''c'''} \sum_{\lambda\lambda'\lambda''\lambda'''} \sum_{\mathbf{x}} \delta_{\lambda\lambda'} \delta_{\lambda''\lambda'''} \sum_{m_1 m_2 m_3 m_4} \\ & \times b_c^\dagger(m_1, \mathbf{x}, \lambda) d_{c'''}^\dagger(m_4, \mathbf{x}, -\lambda''') b_{c'}(m_2, \mathbf{x}, \lambda') d_{c''}(m_3, \mathbf{x}, \lambda'') \\ & \times \frac{1}{(m_3 - m_4)^2} \delta_{m_1+m_4, m_2+m_3}. \end{aligned} \quad (\text{J.7})$$

Helicity flip terms

Particle number conserving terms:

$$\begin{aligned} & \frac{mg}{a} \sum_r \sum_{\mathbf{x}} \sum_{\lambda_1, \lambda_2} \chi_{\lambda_1}^\dagger \hat{\sigma}_r \chi_{\lambda_2} \sum_{m_1} \frac{1}{m_1} \\ & \left[b_c^\dagger(m_1, \mathbf{x}, \lambda_1) b_c(m_1, \mathbf{x}, \lambda_2) + d_c^\dagger(m_1, \mathbf{x}, -\lambda_2) d_c(m_1, \mathbf{x}, -\lambda_2) \right]. \end{aligned} \quad (\text{J.8})$$

Particle number non conserving terms: a typical term is

$$\begin{aligned} & \frac{mg}{a} \frac{1}{\sqrt{4\pi}} \sum_r \sum_{\mathbf{x}} \sum_{\lambda_1, \lambda_2} \chi_{\lambda_1}^\dagger \hat{\sigma}_r \chi_{\lambda_2} \sum_{m_1 m_2 m_3} \frac{1}{\sqrt{m_3}} \frac{1}{2m_3 + m_2} \delta_{m_1 - m_2, 2m_3} \\ & b_c^\dagger(m_1, \mathbf{x}, \lambda_1) B_{-rc'}(m_3, \mathbf{x} + a\hat{\mathbf{r}}) b_{c'}(m_2, \mathbf{x} + a\hat{\mathbf{r}}, \lambda_2). \end{aligned} \quad (\text{J.9})$$

Helicity non flip terms

Two operators:

$$\frac{2}{a^2} \sum_{\mathbf{x}} \sum_{\lambda} \sum_n \frac{1}{n} \left[b_c^\dagger(n, \mathbf{x}, \lambda) b_c(n, \mathbf{x}, \lambda) + d_c^\dagger(n, \mathbf{x}, \lambda) d_c(n, \mathbf{x}, \lambda) \right]. \quad (\text{J.10})$$

Three operators:

A typical term is

$$\begin{aligned} & -g \frac{1}{a^2} \frac{1}{\sqrt{4\pi}} \sum_r \sum_{\mathbf{x}} \sum_{\lambda} \sum_{m_1 m_2 m_3} \frac{1}{\sqrt{m_3}} \frac{1}{2m_3 + m_2} \delta_{m_1 - m_2, 2m_3} \\ & b_c^\dagger(m_1, \mathbf{x}, \lambda) B_{-rc'}(m_3, \mathbf{x} + a\hat{\mathbf{r}}) b_{c'}(m_2, \mathbf{x} + a\hat{\mathbf{r}}, \lambda). \end{aligned} \quad (\text{J.11})$$

Fermion - link instantaneous term

A typical term is

$$\begin{aligned}
& 2 \frac{g^2}{4\pi a^2} \sum_{\mathbf{x}} \sum_r \sum_{cc'} \sum_{d'd''} T_{cc'}^\alpha T_{d'd''}^\alpha \sum_{m_1 m_2 m_3 m_4} \frac{1}{\sqrt{m_3}} \frac{1}{\sqrt{m_4}} \\
& b_d^\dagger(m_1, \mathbf{x}, \lambda_1) b_{d'}(m_2, \mathbf{x}, \lambda_2) B_{-rc'e''}(m_3, \mathbf{x} + a\hat{\mathbf{r}}) B_{-rc'd}^\dagger(m_4, \mathbf{x} + a\hat{\mathbf{r}}) \\
& (-)(m_3 + m_4)/(m_1 - m_2)^2 \delta_{m_1 - m_2, 2m_3 - 2m_4} .
\end{aligned} \tag{J.12}$$

J.2 States in DLCQ

We will consider states of zero transverse momentum. In the one - link approximation, the gauge invariant states are $q\bar{q}$ state

$$\begin{aligned}
|2\rangle &= \frac{1}{\sqrt{N}} \frac{1}{\sqrt{V}} \sum_d \sum_{\mathbf{y}(q)} \sum_{\mathbf{y}(\bar{q})} \delta_{\mathbf{y}(q), \mathbf{y}(\bar{q})} \\
& b_d^\dagger(n_1, \mathbf{y}(q), \sigma_1) d_d^\dagger(n_2, \mathbf{y}(\bar{q}), \sigma_2) |0\rangle
\end{aligned} \tag{J.13}$$

and the $q\bar{q}$ link states

$$\begin{aligned}
|3a\rangle &= \frac{1}{N} \frac{1}{\sqrt{V}} \frac{1}{\sqrt{2}} \sum_{dd'} \sum_s \sum_{\mathbf{y}(q)} \sum_{\mathbf{y}(\bar{q})} \sum_{\mathbf{y}(l)} \delta_{\mathbf{y}(l), \mathbf{y}(q)} \delta_{\mathbf{y}(q), \mathbf{y}(\bar{q}) - a\hat{\mathbf{s}}} \\
& b_d^\dagger(n_1, \mathbf{y}(q), \sigma_1) B_{sdd'}^\dagger(n_3, \mathbf{y}(l)) d_{d'}^\dagger(n_2, \mathbf{y}(\bar{q}), \sigma_2) |0\rangle
\end{aligned}$$

and

$$\begin{aligned}
|3b\rangle &= \frac{1}{N} \frac{1}{\sqrt{V}} \frac{1}{\sqrt{2}} \sum_{dd'} \sum_s \sum_{\mathbf{y}(q)} \sum_{\mathbf{y}(\bar{q})} \sum_{\mathbf{y}(l)} \delta_{\mathbf{y}(l), \mathbf{y}(q)} \delta_{\mathbf{y}(q), \mathbf{y}(\bar{q}) + a\hat{\mathbf{s}}} \\
& b_d^\dagger(n_1, \mathbf{y}(q), \sigma_1) B_{-sdd'}^\dagger(n_3, \mathbf{y}(l)) d_{d'}^\dagger(n_2, \mathbf{y}(\bar{q}), \sigma_2) |0\rangle .
\end{aligned} \tag{J.14}$$

We shall consider transition from these initial states to the following final states: The $q\bar{q}$ state

$$\begin{aligned}
\langle 2' | &= \frac{1}{\sqrt{N}} \frac{1}{\sqrt{V}} \sum_e \sum_{\mathbf{z}(q)} \sum_{\mathbf{z}(\bar{q})} \delta_{\mathbf{z}(q), \mathbf{z}(\bar{q})} \\
& \langle 0 | d_e(n'_2, \mathbf{z}(\bar{q}), \sigma'_2) b_e(n'_1, \mathbf{z}(q), \sigma'_1)
\end{aligned} \tag{J.15}$$

and the $q\bar{q}$ link states

$$\begin{aligned}
\langle 3a' | &= \frac{1}{N} \frac{1}{\sqrt{V}} \frac{1}{\sqrt{2}} \sum_{ee'} \sum_t \sum_{\mathbf{z}(q)} \sum_{\mathbf{z}(\bar{q})} \sum_{\mathbf{z}(l)} \delta_{\mathbf{z}(l), \mathbf{z}(q)} \delta_{\mathbf{z}(q), \mathbf{z}(\bar{q}) - a\hat{\mathbf{t}}} \\
& \langle 0 | d_e(n'_2, \mathbf{z}(\bar{q}), \sigma'_2) B_{tee'}(n'_3, \mathbf{z}(l)) b_{e'}(n'_1, \mathbf{z}(q), \sigma'_1)
\end{aligned} \tag{J.16}$$

and

$$\begin{aligned} \langle 3b' | &= \frac{1}{N} \frac{1}{\sqrt{V}} \frac{1}{\sqrt{2}} \sum_{ee'} \sum_t \sum_{\mathbf{z}(q)} \sum_{\mathbf{z}(\bar{q})} \sum_{\mathbf{z}(l)} \delta_{\mathbf{z}(l), \mathbf{z}(q)} \delta_{\mathbf{z}(q), \mathbf{z}(\bar{q}) + \hat{a}} \\ &\langle 0 | d_e(n'_2, \mathbf{z}(\bar{q}), \sigma'_2) B_{-tee'}(n'_3, \mathbf{z}(l)) b_{e'}(n'_1, \mathbf{z}(q), \sigma'_1) \end{aligned} \quad (\text{J.17})$$

J.3 Forward-backward derivatives: Matrix Elements in DLCQ

J.3.1 Transitions from two particle state

To two particle state

Let us consider transitions to the two particle state: We have, from the free particle term,

$$\langle 2' | H_{f \text{ free}} | 2 \rangle = m^2 \left(\frac{1}{n_1} + \frac{1}{n_2} \right) \mathcal{N}_2 \quad (\text{J.18})$$

where

$$\mathcal{N}_2 = \delta_{n_1, n'_1} \delta_{\sigma_1, \sigma'_1} \delta_{n_2, n'_2} \delta_{\sigma_2, \sigma'_2}. \quad (\text{J.19})$$

From the four fermion instantaneous term we get

$$\begin{aligned} \langle 2' | H_{qqc} | 2 \rangle &= -2 \frac{g^2}{\pi a^2} C_f \delta_{n_1+n_2, n'_1+n'_2} \frac{1}{(n_1 - n'_1)^2} \\ &\delta_{\sigma_1, \sigma'_1} \delta_{\sigma_2, \sigma'_2} \end{aligned} \quad (\text{J.20})$$

where $C_f = \frac{N^2-1}{2N}$.

To implement the regulator prescription for $\frac{1}{(k^+)^2}$, we add the counterterm matrix elements

$$\langle 2' | H_{CT} | 2 \rangle = 2 \frac{g^2}{\pi a^2} C_f \delta_{n_1+n_2, n'_1+n'_2} \sum_{n_{loop}=1}^K \frac{1}{(n_1 - n_{loop})^2} \delta_{\sigma_1, \sigma'_1} \delta_{\sigma_2, \sigma'_2}. \quad (\text{J.21})$$

Here the term $n_{loop} = n_1$ is dropped from the sum.

From the helicity flip term we get

$$\langle 2' | H_{hf1} | 2 \rangle = -2 \frac{1}{a} \sum_s \left[\frac{m}{n_1} \chi_{\sigma'_1}^\dagger \hat{\sigma}_s \chi_{\sigma_1} \delta_{\sigma_2, \sigma'_2} + \frac{m}{n_2} \chi_{-\sigma_2}^\dagger \hat{\sigma}_s \chi_{-\sigma'_2} \delta_{\sigma_1, \sigma'_1} \right] \mathcal{N}_{hf} \quad (\text{J.22})$$

with

$$\mathcal{N}_{hf} = \delta_{n_1, n'_1} \delta_{n_2, n'_2}. \quad (\text{J.23})$$

From the helicity non-flip term we get

$$\langle 2' | H_{hnf}(1) | 2 \rangle = 2 \frac{1}{a^2} \left(\frac{1}{n_1} + \frac{1}{n_2} \right) \mathcal{N}_2. \quad (\text{J.24})$$

To three particle state

To the state $|3a\rangle$

From the helicity flip term we get

$$\begin{aligned} \langle 3a' | H_{hf2} | 2 \rangle &= \frac{mg}{a} \sqrt{N} \frac{1}{V} \frac{1}{\sqrt{2}} \frac{1}{\sqrt{4\pi}} \sum_t \chi_{\sigma_1'}^\dagger \hat{\sigma}_t \chi_{\sigma_1} \delta_{\sigma_2, \sigma_2'} \\ &\delta_{n_2, n_2'} \frac{\delta_{n_1' + 2n_3', n_1}}{n_1'} \frac{1}{\sqrt{n_3'}} \sum_{\mathbf{z}(q)} \sum_{\mathbf{y}(q)} \delta_{\mathbf{z}(q), \mathbf{y}(q) - \hat{a}} \\ &+ \frac{mg}{a} \sqrt{N} \frac{1}{V} \frac{1}{\sqrt{2}} \frac{1}{\sqrt{4\pi}} \sum_t \chi_{-\sigma_2}^\dagger \hat{\sigma}_t \chi_{-\sigma_2'} \delta_{\sigma_1, \sigma_1'} \\ &\delta_{n_1, n_1'} \frac{\delta_{n_2' + 2n_3', n_2}}{n_2} \frac{1}{\sqrt{n_3'}} \sum_{\mathbf{z}(\bar{q})} \sum_{\mathbf{y}(\bar{q})} \delta_{\mathbf{z}(\bar{q}), \mathbf{y}(\bar{q}) + \hat{a}}. \end{aligned} \quad (\text{J.25})$$

From the helicity non-flip term we get

$$\begin{aligned} \langle 3a' | H_{hnf}(2) | 2 \rangle &= -g \frac{1}{a^2} \sqrt{N} \frac{1}{V} \frac{1}{\sqrt{2}} \frac{1}{\sqrt{4\pi}} \delta_{\sigma_1, \sigma_1'} \delta_{\sigma_2, \sigma_2'} \\ &\delta_{n_2, n_2'} \frac{\delta_{n_1' + 2n_3', n_1}}{n_1'} \frac{1}{\sqrt{n_3'}} \sum_t \sum_{\mathbf{z}(q)} \sum_{\mathbf{y}(q)} \delta_{\mathbf{z}(q), \mathbf{y}(q) - \hat{a}} \\ &-g \frac{1}{a^2} \sqrt{N} \frac{1}{V} \frac{1}{\sqrt{2}} \frac{1}{\sqrt{4\pi}} \delta_{\sigma_2, \sigma_2'} \delta_{\sigma_1, \sigma_1'} \\ &\delta_{n_1, n_1'} \frac{\delta_{n_2' + 2n_3', n_2}}{n_2} \frac{1}{\sqrt{n_3'}} \sum_t \sum_{\mathbf{z}(\bar{q})} \sum_{\mathbf{y}(\bar{q})} \delta_{\mathbf{z}(\bar{q}), \mathbf{y}(\bar{q}) + \hat{a}}. \end{aligned} \quad (\text{J.26})$$

To the state $|3b\rangle$

From the helicity flip term we get

$$\begin{aligned} \langle 3b' | H_{hf2} | 2 \rangle &= \frac{mg}{a} \sqrt{N} \frac{1}{V} \frac{1}{\sqrt{2}} \frac{1}{\sqrt{4\pi}} \sum_t \chi_{\sigma_1'}^\dagger \hat{\sigma}_t \chi_{\sigma_1} \delta_{\sigma_2, \sigma_2'} \\ &\delta_{n_2, n_2'} \frac{\delta_{n_1' + 2n_3', n_1}}{n_1'} \frac{1}{\sqrt{n_3'}} \sum_{\mathbf{z}(q)} \sum_{\mathbf{y}(q)} \delta_{\mathbf{z}(q), \mathbf{y}(q) + \hat{a}} \\ &+ \frac{mg}{a} \sqrt{N} \frac{1}{V} \frac{1}{\sqrt{2}} \frac{1}{\sqrt{4\pi}} \sum_t \chi_{-\sigma_2}^\dagger \hat{\sigma}_t \chi_{-\sigma_2'} \delta_{\sigma_1, \sigma_1'} \\ &\delta_{n_1, n_1'} \frac{\delta_{n_2' + 2n_3', n_2}}{n_2'} \frac{1}{\sqrt{n_3'}} \sum_{\mathbf{z}(\bar{q})} \sum_{\mathbf{y}(\bar{q})} \delta_{\mathbf{z}(\bar{q}), \mathbf{y}(\bar{q}) - \hat{a}}. \end{aligned} \quad (\text{J.27})$$

From helicity non-flip term we get

$$\begin{aligned}
\langle 3b' | H_{hmf}(3) | 2 \rangle &= -g \frac{1}{a^2} \sqrt{N} \frac{1}{V} \frac{1}{\sqrt{2}} \frac{1}{\sqrt{4\pi}} \delta_{\sigma_1, \sigma'_1} \delta_{\sigma_2, \sigma'_2} \\
&\delta_{n_2, n'_2} \frac{\delta_{n'_1+2n'_3, n_1}}{n_1} \frac{1}{\sqrt{n'_3}} \sum_t \sum_{\mathbf{z}(q)} \sum_{\mathbf{y}(q)} \delta_{\mathbf{z}(q), \mathbf{y}(q)+\mathbf{a}\hat{t}} \\
&-g \frac{1}{a^2} \sqrt{N} \frac{1}{V} \frac{1}{\sqrt{2}} \frac{1}{\sqrt{4\pi}} \delta_{\sigma_2, \sigma'_2} \delta_{\sigma_1, \sigma'_1} \\
&\delta_{n_1, n'_1} \frac{\delta_{n'_2+2n'_3, n_2}}{n'_2} \frac{1}{\sqrt{n'_3}} \sum_t \sum_{\mathbf{z}(\bar{q})} \sum_{\mathbf{y}(\bar{q})} \delta_{\mathbf{z}(\bar{q}), \mathbf{y}(\bar{q})-\mathbf{a}\hat{t}}. \quad (J.28)
\end{aligned}$$

J.3.2 Transitions from three particle ($q \bar{q}$ link) state $|3a\rangle$

To three particle state

From the free particle term, we get

$$\langle 3a' | H_{free} | 3a \rangle = \left(m^2 \left(\frac{1}{n_1} + \frac{1}{n_2} \right) + \frac{1}{2} \mu^2 \frac{1}{n_3} \right) \mathcal{N}_3 \quad (J.29)$$

with

$$\mathcal{N}_3 = \delta_{n_1, n'_1} \delta_{n_2, n'_2} \delta_{n_3, n'_3} \delta_{\sigma_1, \sigma'_1} \delta_{\sigma_2, \sigma'_2}. \quad (J.30)$$

Diagonal contribution from the four fermion instantaneous term to the three particle state vanishes due to the vanishing trace of the generators of $SU(N)$.

Contribution from the fermion - link instantaneous term

$$\begin{aligned}
\langle 3a' | H_{qgc}(1) | 3a \rangle &= -\frac{g^2}{\pi} \frac{1}{a^2} C_f \delta_{n_1+2n_3, n'_1+2n'_3} \delta_{n_2, n'_2} \\
&\frac{1}{\sqrt{n_3} \sqrt{n_1 - n'_1 + 2n_3}} \frac{(n_1 - n'_1 + 4n_3)}{(n_1 - n'_1)^2} \frac{1}{\sqrt{2}} \delta_{\sigma_1, \sigma'_1} \delta_{\sigma_2, \sigma'_2} \\
&-\frac{g^2}{\pi} \frac{1}{a^2} C_f \delta_{n_2+2n_3, n'_2+2n'_3} \delta_{n_1, n'_1} \\
&\frac{1}{\sqrt{n_3} \sqrt{n_2 - n'_2 + 2n_3}} \frac{(n_2 - n'_2 + 4n_3)}{(n_2 - n'_2)^2} \frac{1}{\sqrt{2}} \delta_{\sigma_1, \sigma'_1} \delta_{\sigma_2, \sigma'_2}. \quad (J.31)
\end{aligned}$$

Counterterm matrix elements in DLCQ to implement the regulated prescription for $\frac{1}{(k^+)^2}$

$$\langle 3a' | H_{CT}(1) | 3a \rangle = \frac{g^2}{\pi} \frac{1}{a^2} C_f \delta_{n_1+2n_3, n'_1+2n'_3} \delta_{n_2, n'_2} \delta_{\sigma_1, \sigma'_1} \delta_{\sigma_2, \sigma'_2}$$

$$\left[\sum_{n_{loop}=1}^{n_{1max}} \frac{1}{\sqrt{n_3}\sqrt{n_1-n_{loop}+2n_3}} \frac{(n_1-n_{loop}+4n_3)}{(n_1-n_{loop})^2} \frac{1}{\sqrt{2}} \right. \\ \left. + \sum_{n_{loop}=1}^{n_{2max}} \frac{1}{\sqrt{n_3}\sqrt{n_2-n_{loop}+2n_3}} \frac{(n_2-n_{loop}+4n_3)}{(n_2-n_{loop})^2} \frac{1}{\sqrt{2}} \right], \quad (J.32)$$

where $n_{1max} < n_1 + 2n_3$ and $n_{2max} < n_2 + 2n_3$.

The contribution from the helicity flip term that conserves particle number is

$$\langle 3a' | H_{hf}(1) | 3a \rangle = -2 \frac{m}{a} \delta_{n_1, n'_1} \delta_{n_2, n'_2} \delta_{n_3, n'_3} \\ \left[\frac{1}{n_1} \sum_r \chi_{\sigma'_1}^\dagger \hat{\sigma}_r \chi_{\sigma_1} \delta_{\sigma_2, \sigma'_2} + \frac{1}{n_2} \sum_r \chi_{-\sigma_2}^\dagger \hat{\sigma}_r \chi_{-\sigma'_2} \delta_{\sigma_1, \sigma'_1} \right]. \quad (J.33)$$

The contribution from the helicity non-flip term that conserves particle number is

$$\langle 3a' | H_{hnf}(1) | 3a \rangle = \frac{2}{a^2} \left(\frac{1}{n_1} + \frac{1}{n_2} \right) \mathcal{N}_3. \quad (J.34)$$

To two particle state

From the helicity flip term we get

$$\langle 2' | H_{hf2} | 3a \rangle = \frac{mg}{a} \sqrt{N} \frac{1}{V} \frac{1}{\sqrt{2}} \frac{1}{\sqrt{4\pi}} \sum_s \chi_{\sigma'_1}^\dagger \hat{\sigma}_s \chi_{\sigma_1} \delta_{\sigma_2, \sigma'_2} \\ \delta_{n_2, n'_2} \frac{\delta_{n'_1, n_1+2n_3}}{n_1} \frac{1}{\sqrt{n_3}} \sum_{\mathbf{z}(q)} \sum_{\mathbf{y}(q)} \delta_{\mathbf{z}(q), \mathbf{y}(q)+a\hat{s}} \\ + \frac{mg}{a} \sqrt{N} \frac{1}{V} \frac{1}{\sqrt{2}} \frac{1}{\sqrt{4\pi}} \sum_s \chi_{-\sigma_2}^\dagger \hat{\sigma}_s \chi_{-\sigma'_2} \delta_{\sigma_1, \sigma'_1} \\ \delta_{n_1, n'_1} \frac{\delta_{n'_2, n_2+2n_3}}{n'_2} \frac{1}{\sqrt{n_3}} \sum_{\mathbf{z}(\bar{q})} \sum_{\mathbf{y}(\bar{q})} \delta_{\mathbf{z}(\bar{q}), \mathbf{y}(\bar{q})-a\hat{s}}. \quad (J.35)$$

From the helicity non-flip term we get

$$\langle 2' | H_{hnf} | 3a \rangle = -g \frac{1}{a^2} \sqrt{N} \frac{1}{V} \frac{1}{\sqrt{2}} \frac{1}{\sqrt{4\pi}} \delta_{\sigma_1, \sigma'_1} \delta_{\sigma_2, \sigma'_2} \\ \delta_{n_2, n'_2} \frac{\delta_{n'_1, n_1+2n_3}}{n_1} \frac{1}{\sqrt{n_3}} \sum_s \sum_{\mathbf{z}(q)} \sum_{\mathbf{y}(q)} \delta_{\mathbf{z}(q), \mathbf{y}(q)+a\hat{s}} \\ -g \frac{1}{a^2} \sqrt{N} \frac{1}{V} \frac{1}{\sqrt{2}} \frac{1}{\sqrt{4\pi}} \delta_{\sigma_2, \sigma'_2} \delta_{\sigma_1, \sigma'_1}$$

$$\delta_{n_1, n'_1} \frac{\delta_{n'_2, n_2 + 2n_3}}{n'_2} \frac{1}{\sqrt{n_3}} \sum_{\mathbf{z}(\bar{q})} \sum_{\mathbf{y}(\bar{q})} \delta_{\mathbf{z}(\bar{q}), \mathbf{y}(\bar{q}) - a\hat{s}}. \quad (\text{J.36})$$

J.3.3 Transitions from three particle ($q \bar{q}$ link) state $|3b\rangle$

To three particle state

From the free particle term, we get

$$\langle 3b' | H_{free} | 3b \rangle = \left(m^2 \left(\frac{1}{n_1} + \frac{1}{n_2} \right) + \frac{1}{2} \mu^2 \frac{1}{n_3} \right) \mathcal{N}_3 \quad (\text{J.37})$$

with

$$\mathcal{N}_3 = \delta_{n_1, n'_1} \delta_{n_2, n'_2} \delta_{n_3, n'_3} \delta_{\sigma_1, \sigma'_1} \delta_{\sigma_2, \sigma'_2}. \quad (\text{J.38})$$

The diagonal contribution from the four fermion instantaneous term to the three particle state vanishes due to the vanishing trace of the generators of $SU(N)$.

The contribution from the fermion - link instantaneous term is

$$\begin{aligned} \langle 3b' | H_{qgc}(1) | 3b \rangle &= -\frac{g^2}{\pi} \frac{1}{a^2} C_f \delta_{n_1 + 2n_3, n'_1 + 2n'_3} \delta_{n_2, n'_2} \\ &\quad \frac{1}{\sqrt{n_3} \sqrt{n_1 - n'_1 + 2n_3}} \frac{(n_1 - n'_1 + 4n_3)}{(n_1 - n'_1)^2} \frac{1}{\sqrt{2}} \delta_{\sigma_1, \sigma'_1} \delta_{\sigma_2, \sigma'_2} \\ &\quad - \frac{g^2}{\pi} \frac{1}{a^2} C_f \delta_{n_2 + 2n_3, n'_2 + 2n'_3} \delta_{n_1, n'_1} \\ &\quad \frac{1}{\sqrt{n_3} \sqrt{n_2 - n'_2 + 2n_3}} \frac{(n_2 - n'_2 + 4n_3)}{(n_2 - n'_2)^2} \frac{1}{\sqrt{2}} \delta_{\sigma_1, \sigma'_1} \delta_{\sigma_2, \sigma'_2} \quad (\text{J.39}) \end{aligned}$$

Here also we have the counterterm matrix elements given in Eq. (J.32).

The contribution from the helicity flip term that conserves particle number is

$$\begin{aligned} \langle 3b' | H_{hf}(1) | 3b \rangle &= -2 \frac{m}{a} \delta_{n_1, n'_1} \delta_{n_2, n'_2} \delta_{n_3, n'_3} \\ &\quad \left[\frac{1}{n_1} \sum_r \chi_{\sigma'_1}^\dagger \hat{\sigma}_r \chi_{\sigma_1} \delta_{\sigma_2, \sigma'_2} + \frac{1}{n_2} \sum_r \chi_{-\sigma_2}^\dagger \hat{\sigma}_r \chi_{-\sigma'_2} \delta_{\sigma_1, \sigma'_1} \right]. \quad (\text{J.40}) \end{aligned}$$

The contribution from the helicity non-flip term that conserves particle number is

$$\langle 3b' | H_{hnf}(1) | 3b \rangle = \frac{2}{a^2} \left(\frac{1}{n_1} + \frac{1}{n_2} \right) \mathcal{N}_3. \quad (\text{J.41})$$

To the two particle state

From the helicity flip term we get

$$\begin{aligned}
\langle 2' | H_{hf2} | 3b \rangle &= \frac{mg}{a} \sqrt{N} \frac{1}{V} \frac{1}{\sqrt{2}} \frac{1}{\sqrt{4\pi}} \sum_s \chi_{\sigma'_1}^\dagger \hat{\sigma}_s \chi_{\sigma_1} \delta_{\sigma_2, \sigma'_2} \\
&\delta_{n_2, n'_2} \frac{\delta_{n'_1, n_1 + 2n_3}}{n'_1} \frac{1}{\sqrt{n_3}} \sum_{\mathbf{z}(q)} \sum_{\mathbf{y}(q)} \delta_{\mathbf{z}(q), \mathbf{y}(q) - a\hat{s}} \\
&+ \frac{mg}{a} \sqrt{N} \frac{1}{V} \frac{1}{\sqrt{2}} \frac{1}{\sqrt{4\pi}} \sum_s \chi_{-\sigma_2}^\dagger \hat{\sigma}_s \chi_{-\sigma'_2} \delta_{\sigma_1, \sigma'_1} \\
&\delta_{n_1, n'_1} \frac{\delta_{n'_2, 2n_3 + n_2}}{n_2} \frac{1}{\sqrt{n_3}} \sum_{\mathbf{z}(\bar{q})} \sum_{\mathbf{y}(\bar{q})} \delta_{\mathbf{z}(\bar{q}), \mathbf{y}(\bar{q}) + a\hat{s}} . \tag{J.42}
\end{aligned}$$

From the helicity non-flip term we get

$$\begin{aligned}
\langle 2' | H_{mf} | 3b \rangle &= -g \frac{1}{a^2} \sqrt{N} \frac{1}{V} \frac{1}{\sqrt{2}} \frac{1}{\sqrt{4\pi}} \delta_{\sigma_1, \sigma'_1} \delta_{\sigma_2, \sigma'_2} \\
&\delta_{n_2, n'_2} \frac{\delta_{n'_1, n_1 + 2n_3}}{n'_1} \frac{1}{\sqrt{n_3}} \sum_s \sum_{\mathbf{z}(q)} \sum_{\mathbf{y}(q)} \delta_{\mathbf{z}(q), \mathbf{y}(q) - a\hat{s}} \\
&- g \frac{1}{a^2} \sqrt{N} \frac{1}{V} \frac{1}{\sqrt{2}} \frac{1}{\sqrt{4\pi}} \delta_{\sigma_2, \sigma'_2} \delta_{\sigma_1, \sigma'_1} \\
&\delta_{n_1, n'_1} \frac{\delta_{n'_2, n_2 + 2n_3}}{n_2} \frac{1}{\sqrt{n_3}} \sum_s \sum_{\mathbf{z}(\bar{q})} \sum_{\mathbf{y}(\bar{q})} \delta_{\mathbf{z}(\bar{q}), \mathbf{y}(\bar{q}) + a\hat{s}} . \tag{J.43}
\end{aligned}$$

J.4 Symmetric derivatives and Wilson term: Matrix elements in DLCQ

In this section, we list only those matrix elements that differ from the forward-backward case.

J.4.1 Transitions from the two particle state

To the state $|3a\rangle$

Helicity flip:

$$\begin{aligned}
\langle 3a' | P_{whf}^- | 2 \rangle &= \left(m + 4\frac{\kappa}{a}\right) \frac{1}{2a} \sqrt{N} \frac{1}{V} \frac{1}{\sqrt{2}} \frac{1}{\sqrt{4\pi}} \sum_t \chi_{\sigma'_1}^\dagger \hat{\sigma}_t \chi_{\sigma_1} \delta_{\sigma_2, \sigma'_2} \\
&\sum_{\mathbf{y}(q)} \sum_{\mathbf{z}(q)} \delta_{\mathbf{z}(q), \mathbf{y}(q) - a\hat{t}} \\
&\frac{1}{\sqrt{n'_3}} \left(\frac{1}{n_1} - \frac{1}{n'_1}\right) \delta_{n_2, n'_2} \delta_{n'_1 + 2n'_3, n_1}
\end{aligned}$$

$$\begin{aligned}
& + \left(m + 4\frac{\kappa}{a}\right) \frac{1}{2a} \sqrt{N} \frac{1}{V} \frac{1}{\sqrt{2}} \frac{1}{\sqrt{4\pi}} \sum_t \chi_{-\sigma_2}^\dagger \hat{\sigma}_t \chi_{-\sigma_2'} \delta_{\sigma_1, \sigma_1'} \\
& \sum_{\mathbf{y}(\bar{q})} \sum_{\mathbf{z}(\bar{q})} \delta_{\mathbf{z}(\bar{q}), \mathbf{y}(\bar{q}) + \hat{a}} \\
& \frac{1}{\sqrt{n_3'}} \left(\frac{1}{n_2'} - \frac{1}{n_2} \right) \delta_{n_1, n_1'} \delta_{n_2' + 2n_3', n_2} .
\end{aligned} \tag{J.44}$$

Helicity non-flip:

$$\begin{aligned}
\langle 3a' | P_{wmf1}^- | 2 \rangle & = - \left(m + 4\frac{\kappa}{a}\right) \frac{\kappa}{a} \sqrt{N} \frac{1}{V} \frac{1}{\sqrt{2}} \frac{1}{\sqrt{4\pi}} \delta_{\sigma_2, \sigma_2'} \delta_{\sigma_1, \sigma_1'} \\
& \sum_t \sum_{\mathbf{y}(q)} \sum_{\mathbf{z}(q)} \delta_{\mathbf{z}(q), \mathbf{y}(q) - \hat{a}} \\
& \frac{1}{\sqrt{n_3'}} \left(\frac{1}{n_1} + \frac{1}{n_1'} \right) \delta_{n_2, n_2'} \delta_{n_1' + 2n_3', n_1} \\
& - \left(m + 4\frac{\kappa}{a}\right) \frac{\kappa}{a} \sqrt{N} \frac{1}{V} \frac{1}{\sqrt{2}} \frac{1}{\sqrt{4\pi}} \delta_{\sigma_2, \sigma_2'} \delta_{\sigma_1, \sigma_1'} \\
& \sum_t \sum_{\mathbf{y}(\bar{q})} \sum_{\mathbf{z}(\bar{q})} \delta_{\mathbf{z}(\bar{q}), \mathbf{y}(\bar{q}) + \hat{a}} \\
& \frac{1}{\sqrt{n_3'}} \left(\frac{1}{n_2'} + \frac{1}{n_2} \right) \delta_{n_1, n_1'} \delta_{n_2' + 2n_3', n_2} .
\end{aligned} \tag{J.45}$$

To the state $|3b\rangle$

Helicity flip:

$$\begin{aligned}
\langle 3b' | P_{whf}^- | 2 \rangle & = \left(m + 4\frac{\kappa}{a}\right) \frac{1}{2a} \sqrt{N} \frac{1}{V} \frac{1}{\sqrt{2}} \frac{1}{\sqrt{4\pi}} \sum_t \chi_{\sigma_1'}^\dagger \hat{\sigma}_t \chi_{\sigma_1} \delta_{\sigma_2, \sigma_2'} \\
& \sum_{\mathbf{y}(q)} \sum_{\mathbf{z}(q)} \delta_{\mathbf{z}(q), \mathbf{y}(q) + \hat{a}} \\
& \frac{1}{\sqrt{n_3'}} \left(-\frac{1}{n_1} + \frac{1}{n_1'} \right) \delta_{n_2, n_2'} \delta_{n_1' + 2n_3', n_1} \\
& + \left(m + 4\frac{\kappa}{a}\right) \frac{1}{2a} \sqrt{N} \frac{1}{V} \frac{1}{\sqrt{2}} \frac{1}{\sqrt{4\pi}} \sum_t \chi_{-\sigma_2}^\dagger \hat{\sigma}_t \chi_{-\sigma_2'} \delta_{\sigma_1, \sigma_1'} \\
& \sum_{\mathbf{y}(\bar{q})} \sum_{\mathbf{z}(\bar{q})} \delta_{\mathbf{z}(\bar{q}), \mathbf{y}(\bar{q}) - \hat{a}} \\
& \frac{1}{\sqrt{n_3'}} \left(-\frac{1}{n_2'} + \frac{1}{n_2} \right) \delta_{n_1, n_1'} \delta_{n_2 + 2n_3, n_2'} .
\end{aligned} \tag{J.46}$$

Helicity non-flip:

$$\begin{aligned}
\langle 3a' | P_{wnf1}^- | 2 \rangle &= - \left(m + 4 \frac{\kappa}{a} \right) \frac{\kappa}{a} \sqrt{N} \frac{1}{V} \frac{1}{\sqrt{2}} \frac{1}{\sqrt{4\pi}} \delta_{\sigma_2, \sigma_2'} \delta_{\sigma_1, \sigma_1'} \\
&\quad \sum_t \sum_{\mathbf{y}(q)} \sum_{\mathbf{z}(q)} \delta_{\mathbf{z}(q), \mathbf{y}(q) + a\hat{t}} \\
&\quad \frac{1}{\sqrt{n_3'}} \left(\frac{1}{n_1} + \frac{1}{n_1'} \right) \delta_{n_2, n_2'} \delta_{n_1' + 2n_3', n_1} \\
&- \left(m + 4 \frac{\kappa}{a} \right) \frac{\kappa}{a} \sqrt{N} \frac{1}{V} \frac{1}{\sqrt{2}} \frac{1}{\sqrt{4\pi}} \delta_{\sigma_1, \sigma_1'} \delta_{\sigma_2, \sigma_2'} \\
&\quad \sum_t \sum_{\mathbf{y}(\bar{q})} \sum_{\mathbf{z}(\bar{q})} \delta_{\mathbf{z}(\bar{q}), \mathbf{y}(\bar{q}) - a\hat{t}} \\
&\quad \frac{1}{\sqrt{n_3'}} \left(\frac{1}{n_2'} + \frac{1}{n_2} \right) \delta_{n_1, n_1'} \delta_{n_2' + 2n_3', n_2} .
\end{aligned} \tag{J.47}$$

J.4.2 Transitions from three particle state $|3a\rangle$ to two particle state

Helicity flip:

$$\begin{aligned}
\langle 2' | P_{whf}^- | 3a \rangle &= \left(m + 4 \frac{\kappa}{a} \right) \frac{1}{2a} \sqrt{N} \frac{1}{V} \frac{1}{\sqrt{2}} \frac{1}{\sqrt{4\pi}} \sum_s \chi_{\sigma_1'}^\dagger \hat{\sigma}_s \chi_{\sigma_1} \delta_{\sigma_2, \sigma_2'} \\
&\quad \sum_{\mathbf{z}(q)} \sum_{\mathbf{y}(q)} \delta_{\mathbf{z}(q), \mathbf{y}(q) + a\hat{s}} \\
&\quad \frac{1}{\sqrt{n_3}} \left(\frac{1}{n_1'} - \frac{1}{n_1} \right) \delta_{n_2, n_2'} \delta_{n_1 + 2n_3, n_1'} \\
&+ \left(m + 4 \frac{\kappa}{a} \right) \frac{1}{2a} \sqrt{N} \frac{1}{V} \frac{1}{\sqrt{2}} \frac{1}{\sqrt{4\pi}} \sum_s \chi_{-\sigma_2}^\dagger \hat{\sigma}_s \chi_{-\sigma_2'} \delta_{\sigma_1, \sigma_1'} \\
&\quad \sum_{\mathbf{z}(\bar{q})} \sum_{\mathbf{y}(\bar{q})} \delta_{\mathbf{z}(\bar{q}), \mathbf{y}(\bar{q}) - a\hat{s}} \\
&\quad \frac{1}{\sqrt{n_3}} \left(\frac{1}{n_2} - \frac{1}{n_2'} \right) \delta_{n_1', n_1} \delta_{n_2' + 2n_3', n_2} .
\end{aligned} \tag{J.48}$$

Helicity non-flip:

$$\begin{aligned}
\langle 2' | P_{wnf1}^- | 3a \rangle &= - \left(m + 4 \frac{\kappa}{a} \right) \frac{\kappa}{a} \sqrt{N} \frac{1}{V} \frac{1}{\sqrt{2}} \frac{1}{\sqrt{4\pi}} \delta_{\sigma_2, \sigma_2'} \delta_{\sigma_1, \sigma_1'} \\
&\quad \sum_s \sum_{\mathbf{z}(q)} \sum_{\mathbf{y}(q)} \delta_{\mathbf{z}(q), \mathbf{y}(q) + a\hat{s}} \\
&\quad \frac{1}{\sqrt{n_3}} \left(\frac{1}{n_1} + \frac{1}{n_1'} \right) \delta_{n_2, n_2'} \delta_{n_1 + 2n_3, n_1'}
\end{aligned}$$

$$\begin{aligned}
& - \left(m + 4\frac{\kappa}{a}\right) \frac{\kappa}{a} \sqrt{N} \frac{1}{V} \frac{1}{\sqrt{2}} \frac{1}{\sqrt{4\pi}} \delta_{\sigma_2, \sigma_2'} \delta_{\sigma_1, \sigma_1'} \\
& \sum_{\mathbf{z}(\bar{q})} \sum_{\mathbf{y}(\bar{q})} \delta_{\mathbf{z}(\bar{q}), \mathbf{y}(\bar{q}) + a\hat{s}} \\
& \frac{1}{\sqrt{n_3}} \left(\frac{1}{n_2'} + \frac{1}{n_2} \right) \delta_{n_1, n_1'} \delta_{n_2 + 2n_3, n_2'}.
\end{aligned} \tag{J.49}$$

J.4.3 Transitions from three particle state $|3b\rangle$ to two particle state

Helicity flip:

$$\begin{aligned}
\langle 2' | P_{whf}^- | 3b \rangle & = \left(m + 4\frac{\kappa}{a}\right) \frac{1}{2a} \sqrt{N} \frac{1}{V} \frac{1}{\sqrt{2}} \frac{1}{\sqrt{4\pi}} \sum_s \chi_{\sigma_1'}^\dagger \hat{\sigma}_s \chi_{\sigma_1} \delta_{\sigma_2, \sigma_2'} \\
& \sum_{\mathbf{z}(q)} \sum_{\mathbf{y}(q)} \delta_{\mathbf{z}(q), \mathbf{y}(q) - a\hat{s}} \\
& \frac{1}{\sqrt{n_3}} \left(\frac{1}{n_1} - \frac{1}{n_1'} \right) \delta_{n_2, n_2'} \delta_{n_1 + 2n_3, n_1'} \\
& + \left(m + 4\frac{\kappa}{a}\right) \frac{1}{2a} \sqrt{N} \frac{1}{V} \frac{1}{\sqrt{2}} \frac{1}{\sqrt{4\pi}} \sum_s \chi_{-\sigma_2}^\dagger \hat{\sigma}_s \chi_{-\sigma_2'} \delta_{\sigma_1, \sigma_1'} \\
& \sum_{\mathbf{z}(\bar{q})} \sum_{\mathbf{y}(\bar{q})} \delta_{\mathbf{z}(\bar{q}), \mathbf{y}(\bar{q}) + a\hat{s}} \\
& \frac{1}{\sqrt{n_3}} \left(\frac{1}{n_2'} - \frac{1}{n_2} \right) \delta_{n_1, n_1'} \delta_{n_2 + 2n_3, n_2'}.
\end{aligned} \tag{J.50}$$

Helicity non-flip:

$$\begin{aligned}
\langle 2' | P_{whf}^- | 3b \rangle & = - \left(m + 4\frac{\kappa}{a}\right) \frac{\kappa}{a} \sqrt{N} \frac{1}{V} \frac{1}{\sqrt{2}} \frac{1}{\sqrt{4\pi}} \delta_{\sigma_2, \sigma_2'} \delta_{\sigma_1, \sigma_1'} \\
& \sum_s \sum_{\mathbf{z}(q)} \sum_{\mathbf{y}(q)} \delta_{\mathbf{z}(q), \mathbf{y}(q) - a\hat{s}} \\
& \frac{1}{\sqrt{n_3}} \left(\frac{1}{n_1} + \frac{1}{n_1'} \right) \delta_{n_2, n_2'} \delta_{n_1 + 2n_3, n_1'} \\
& - \left(m + 4\frac{\kappa}{a}\right) \frac{\kappa}{a} \sqrt{N} \frac{1}{V} \frac{1}{\sqrt{2}} \frac{1}{\sqrt{4\pi}} \delta_{\sigma_2, \sigma_2'} \delta_{\sigma_1, \sigma_1'} \\
& \sum_s \sum_{\mathbf{z}(\bar{q})} \sum_{\mathbf{y}(\bar{q})} \delta_{\mathbf{z}(\bar{q}), \mathbf{y}(\bar{q}) + a\hat{s}} \\
& \frac{1}{\sqrt{n_3}} \left(\frac{1}{n_2'} + \frac{1}{n_2} \right) \delta_{n_1, n_1'} \delta_{n_2 + 2n_3, n_2'}.
\end{aligned} \tag{J.51}$$

J.5 Self energy counterterms

In this section we list the self energy counterterms.

Symmetric derivatives case

The counterterm for self energy for a quark or an antiquark with longitudinal momentum n_1 due to double helicity flip hops

$$CT_1 = \frac{2}{n_1} \sum_{n'_1=1}^{n_1} \frac{1}{n'_1} \frac{(n_1 - n'_1)^2}{\mu^2 n_1 n'_1 + m^2 (n_1 - n'_1)^2}. \quad (\text{J.52})$$

The counterterm for self energy for a quark or an antiquark with longitudinal momentum n_1 due to double helicity non-flip hops

$$CT_2 = \frac{2}{n_1} \sum_{n'_1=1}^{n_1} \frac{1}{n'_1} \frac{(n_1 + n'_1)^2}{\mu^2 n_1 n'_1 + m^2 (n_1 - n'_1)^2}. \quad (\text{J.53})$$

Forward and backward derivative case

In this case we have three types of contributions: (1) helicity flip acting twice, (2) helicity non-flip acting twice and (3) interference of helicity flip and helicity non-flip hops. The first two are diagonal in helicity space but the last one is off-diagonal in helicity space.

The transition from state $|2\rangle$ to state $|3a\rangle$ and back due to a quark hop gives rise to longitudinal infrared divergence. In this case the counterterm due to double helicity flip is

$$CT_3 = 2 \sum_{n'_1=1}^{n_1} \frac{1}{n'_1} \frac{n_1}{\mu^2 n_1 n'_1 + m^2 (n_1 - n'_1)^2}. \quad (\text{J.54})$$

The counterterm due to double helicity non-flip is the same without the factor of 2. The transition from state $|2\rangle$ to state $|3b\rangle$ and back due to a quark hop does not give rise to longitudinal infrared divergence. Similarly the transition from state $|2\rangle$ to state $|3a\rangle$ and back due to an antiquark hop does not give rise to longitudinal infrared divergence. The transition from state $|2\rangle$ to state $|3b\rangle$ and back due to an antiquark hop gives rise to longitudinal infrared divergence which requires counterterms the explicit forms of which are the same as in the quark case for the transition from $|2\rangle$ to state $|3a\rangle$. Lastly we consider counterterms for self energy contributions arising from the interference of helicity flip and helicity non-flip hopping. The counterterms

have the same structure as in the case of helicity non-flip transitions accompanied by the following extra factors. Since we have two possibilities namely helicity flip followed by helicity non-flip and vice versa and these two contributions are the same, we get a factor of two. We also get a factor $\chi_{s'}^\dagger \hat{\sigma}^\perp \chi_s$ where $s(s')$ is the initial (final) helicity and $\hat{\sigma}^1 = \sigma^2$, $\hat{\sigma}^2 = -\sigma^1$.

List of Publications

1. **Ab initio results for the broken phase of scalar light front field theory**

Dipankar Chakrabarti, A. Harindranath, L. Martinovič, G. B. Pivovarov and J. P. Vary
hep-th/0310290, submitted for publication.

2. **Kinks in discrete light cone quantization**

Dipankar Chakrabarti, A. Harindranath, L. Martinovič and J. P. Vary
hep-th/0309263, submitted for publication.

☞ 3. **A study of $q\bar{q}$ states in transverse lattice QCD using alternative fermion formulations**

Dipankar Chakrabarti, A. Harindranath and J. P. Vary
hep-ph/0309317, to be published in Phys. Rev. D.

☞ 4. **Fermions on the light front transverse lattice**

Dipankar Chakrabarti, Asit K. De and A. Harindranath
Phys. Rev. D67(2003), 076004; hep-th/0211145.

☞ 5. **Mesons in (2+1) dimensional light front QCD. II. Similarity renormalization approach**

Dipankar Chakrabarti and A. Harindranath
Phys. Rev. D65(2002), 045001; hep-th/0110156.

☞ 6. **Mesons in (2+1)-dimensional light-front QCD: Investigation of a Bloch effective Hamiltonian**

Dipankar Chakrabarti and A. Harindranath
Phys. Rev. D64(2001), 105002; hep-th/0107188.

7. **Quark transversity distribution in perturbative QCD: light-front Hamiltonian approach**

Asmita Mukherjee and Dipankar Chakrabarti
Phys. Lett. B506(2001), 283; hep-ph/0102003.

8. A numerical experiment in DLCQ: microcausality, continuum limit and all that

Dipankar Chakrabarti, Asmita Mukherjee, Rajen Kundu, A. Harindranath

*Phys. Lett. B*480(2000), 409; *hep-th/9910108*.

☞ included in the thesis⁹.

⁹Though the *official* spelling of my name is **Dipankar Chakravorty**, the papers are published with the spelling **Dipankar Chakrabarti**.

